Experiments and numerical simulations of interactions between transverse acoustic modes and cryogenic flames

Franck Richecoeur

CENTRALE
P A R I S

Ecole Centrale Paris

THESE

présentée par

Franck Richecoeur

pour l'obtention du

GRADE de DOCTEUR

Formation doctorale : Energétique

Laboratoire d'accueil : Laboratoire d'Énergétique Moléculaire et Macroscopique, Combustion (EM2C) du CNRS et de l'ECP

Expérimentations et simulations numériques des interactions entre modes acoustiques transverses et flammes cryotechniques

Soutenue le 28 Novembre 2006

Composition du jury :

MM	Candel	S.	Directeur de thèse
	Caries	L.	
	Champion	M.	Président
	Ducruix	S.	
	Poinsot	T.	Rapporteur
	Searby	G.	Rapporteur

Ecole Centrale des Arts et Manufactures
Grand Établissement sous tutelle
du Ministère de l'Éducation Nationale
Grande Voie des Vignes
92295 Châtenay-Malabry Cedex
Tél : 33 (1) 41 13 10 00
Télex : 634 991 F EC PARIS

Laboratoire d'Énergétique Moléculaire et Macroscopique, Combustion (E.M2.C.)
UPR 288, CNRS et Ecole Centrale Paris
Tél : 33 (1) 41 13 10 31
Fax : 33 (1) 47 02 80 35

2006 - 25

Résumé

L'objectif général de cette recherche est de contribuer à la compréhension des mécanismes fondamentaux conduisant à des instabilités de combustion dans les moteurs fusées à propulsion liquides. Le processus implique un couplage fort entre la combustion et les modes acoustiques transverses de la chambre. Le problème est analysé au moyen d'une combinaison d'outils expérimentaux, numériques et de modélisation. Les expériences sont réalisées sur une chambre équipée de plusieurs injecteurs coaxiaux placés en ligne et alimentés en oxygène liquide et méthane gazeux. On recrée ainsi au moins partiellement les conditions qui prévalent dans les moteurs fusées. Le système a été conçu pour permettre une nette séparation entre les fréquences des modes longitudinaux et transverses. Le foyer est équipé de hublots donnant un accès optique à la zone de flamme et de capteurs de pression détectant les fluctuations de cette variable dans la chambre et dans le circuit d'alimentation en ergols. Un modulateur comportant une roue dentée tournant à grande vitesse et bloquant de façon périodique une tuyère auxiliaire permet d'injecter des perturbations acoustiques dans le système. Des méthodes d'imagerie numérique sont utilisées pour examiner la dynamique des flammes. Des essais systèmatiques ont été réalisés à basse (0.9 MPa), moyenne (3 MPa) et haute pression (6 MPa) pour déterminer les conditions dans lesquelles la flamme est la plus sensible aux modulations acoustiques transverses. Un niveau de réponse remarquable a été observé dans les expériences à basse pression. Le niveau d'oscillation était dans ce cas de 8% de la pression moyenne. La flamme est fortement modifiée lorsque le couplage est réalisé avec le premier mode acoustique transverse, son taux d'expansion est augmenté et la luminosité s'accroît sensiblement. La vitesse de convection des structures émissives observées par caméra rapide montre une réduction assez surprenante. Les relations de phase établies entre les preturbations de pression et de dégagement de chaleur dans la chambre montrent que ces deux quantités sont caractérisées par des distributions spatiales assez semblables. Les essais à pression intermédiaire réalisés avec un nouveau dispositif comportant 5 injecteurs induisant un dégagement de chaleur plus important montrent que la résonance est moins marquée, un phénomène qui est lié à un niveau de fluctuations de température plus élévé dans les nouvelles conditions de ces essais. Des expériences sont menées à froid par injection d'oxygène liquide et d'azote gazeux pour examiner le mouvement induit par une excitation acoustique transverse. Ces expériences sont complétées par des calculs numériques réalisés dans le cadre des simulations aux grandes échelles (SGE). Ces méthodes sont utilisées pour analyser le mouvement de jets coaxiaux en présence d'une modulation acoustique transverse imposée dans le domaine de calcul. L'oscillation induit un mouvement collectif et le mélange est intensifié. Un modèle est développé pour le taux de réaction filtré permettant une description des flammes non prémélangées contrôlant la combustion cryotechnique. Des calculs initiaux sont effectués dans une configuration réaliste d'injecteurs multiples, alimentés en ergols gazeux. Deux problèmes sont envisagés au niveau de la modélisation. Le premier traite de la relation entre les fluctuations de dégagement de chaleur et les perturbations de vitesse transverses. Une expression est proposée qui

dépend de ces perturbations et du signe du gradient de vitesse transverse. Les conséquences de ce modèle sont examinées et il est notamment montré que l'on peut retrouver la structure du dégagement de chaleur observée dans des travaux antérieurs. Le second modèle traite de l'influence de fluctuations de température sur les caractéristiques de résonance d'un système. La simulation directe et une analyse fondée sur la méthode des moyennes indique que l'amplitude de la résonance et la finesse de la réponse sont diminuées en présence de fluctuations, un phénomène qui semble avoir été négligé mais qui peut avoir des conséquences pratiques. Les connaissances acquises dans ces études peuvent servir de guide à des développements de méthodes de calcul destinées à prévoir les instabilités. Elles peuvent aussi servir à développer des méthodes de conception permettant d'éviter le phénomène.

Summary

The general objective of this research is to contribute to the understanding of fundamental mechanisms leading to high frequency instabilities in liquid rocket engines. The process involves a tight coupling between combustion and transverse acoustic modes of the thrust chamber. This problem is investigated with a combination of experimental, numerical and modeling tools. Experiments are carried out on a model scale combustor comprising multiple coaxial injection units placed in a row and fed with liquid oxygen and gaseous methane. This experiment recreates some of the conditions prevailing in liquid rocket engines. The combustor was designed to allow a clear separation between the longitudinal and tranverse resonant modes. It is equipped with large windows providing optical access to the flames and with pressure transducers detecting fluctuations of this quantity in the chamber and in the propellant injection manifold. A toothed wheel modulator is used to periodically block an auxiliary nozzle and inject acoustic perturbations in the system. Digital imaging techniques are used to examine the flame dynamics. Systematic hot fire tests have been carried out at low (0.9 MPa), intermediate (3 MPa) and high pressure (6 MPa) to determine conditions where the flame is the most receptive to transverse acoustic modulations. A remarkable level of response was observed in the low pressure experiments. The level of oscillation was in that case around 8 % of the mean pressure. The flame is strongly modified when the coupling takes place with the first transverse mode of the cavity, its spreading rate is augmented and its luminosity is increased. An intriguing reduction of the axial convection velocity is also observed with the high speed camera. Phase relations established between the pressure perturbations and the heat release in the chamber indicate that these two quantities feature similar spatial distributions. The intermediate pressure experiments carried out with a new injection head comprising 5 injectors at a higher rate of heat release indicate that the sharpness of resonance is reduced and that this can be attributed to a more intense level of temperature fluctuations in the system. Cold flow experiments were also carried out to examine the motion of injected streams of liquid oxygen and gaseous nitrogen when they are submitted to a resonant transverse acoustic excitation. These experiments are complemented with numerical calculations carried out in the large eddy simulation (LES) framework. LES is used to examine the motion of multiple cold jets submitted to a transverse modulation. The oscillation induces a collective motion and mixing is intensified. A model is developed to represent the filtered rate of burning allowing a description of nonpremixed flames controlling cryogenic combustion. Initial calculations are carried out in a realistic multiple injector configuration fed with gaseous reactants. Two problems are envisaged on the modeling level. The first aims at describing how heat release fluctuations can be generated by tranverse velocity perturbations. An expression is devised which depends on the transverse velocity perturbation and on the sign of its gradient and its consequences are investigated. It is shown in particular that the model retrieves the pattern of heat release observed in some early experiments. The second model deals with the influence of temperature fluctuations on the resonance characteristics of a system. Direct

simulation and analysis based on the method of averaging indicates that the response amplitude and the resonance sharpness are diminished in the presence of fluctuations, a phenomenon which seems to have been overlooked in the past but may have practical consequences. The knowledge gathered in these studies is intended to provide guidelines for further developments of computational tools aimed at the prediction of instabilities. It can also serve to develop design methods which would avoid the phenomenon.

Contents

List of Figures

List of Tables

Introduction

Introduction et état de l'art

Les instabilités de combustion haute fréquence ont été observées pour la première fois dans les années 40 lors du développement des premiers moteurs de fusées à propulsion liquide. Ces oscillations de pression ont parfois eu des conséquences désastreuses. Les moteurs étaient endommagés et rapidement détruits par l'intensité des flux de chaleur induits par les fortes fluctuations de pression dans la chambre de combustion, ce qui entraîna des échecs de lancement spectaculaires. Des tests en grandeur réelle ou à échelle réduite ont été menés depuis pour comprendre l'origine de ces instabilités et essayer de les supprimer. Des capteurs de pression, montés directement sur les moteurs, ont permis d'observer les amplitudes et les fréquences des oscillations, et d'identifier les modes acoustiques mis en jeu. Ces expériences ont permis de montrer que les instabilités se développaient dans les hautes fréquences et qu'elles étaient dues à un couplage entre la combustion et les modes propres de la chambre de combustion. Le processus peut être représenté sous la forme du boucle mettant en jeu les phénomènes liés à l'injection, la combustion et les modes acoustiques tel que présentés sur la Figure 1.

Il fut cependant difficile d'obtenir des informations fondamentales sur les mécanismes à l'origine de ce phénomène. Durant les développements de moteurs suivants, beaucoup d'efforts et d'argent ont été nécessaires pour tenir compte des risques d'instabilités hautes fréquences en modifiant la forme des moteurs, en ajoutant des séparateurs, des résonateurs ou bien des cavités afin d'atténuer le problème et de vérifier que les moteurs fonctionnaient de façon stable. L'historique des difficiles recherches effectuées lors du développement du moteur F1 est résumé dans un article de Oefelein and Yang (1993). Ces tests, coûteux et longs, ont fourni des informations pratiques pour le contrôle des instabilités et la mise en place d'outils de prédiction de ce phénomène. Des séparateurs ont été ajoutés sur le fond de chambre afin de réduire les vitesses transverses associées aux mode azimutaux et radiaux; des résonateurs quart d'onde ont été placés autour de la chambre de combustion pour amortir les oscillations; la géométrie des injecteurs a été modifiée pour réduire l'amplitude de leur réponse aux perturbations. La plupart des systèmes utilisés pour supprimer les oscillations ont rendu la conception des moteurs plus complexes et les ont sensiblement alourdis.

Au milieu des années 50, les premières expériences en laboratoire ont été mises en place afin d'étudier le problème des instabilités à un niveau plus fondamental. Des moteurs à ergols liquides de petites dimensions ont été testés dans des conditions réalistes. Le résultat de l'un de ces tests apparaît sur la Figure 2 qui montre une tête d'injection après le déclenchement des instabilités. Le fond de chambre est initialement muni d'injecteurs coaxiaux standards semblables à ceux utilisés dans les moteurs réels.

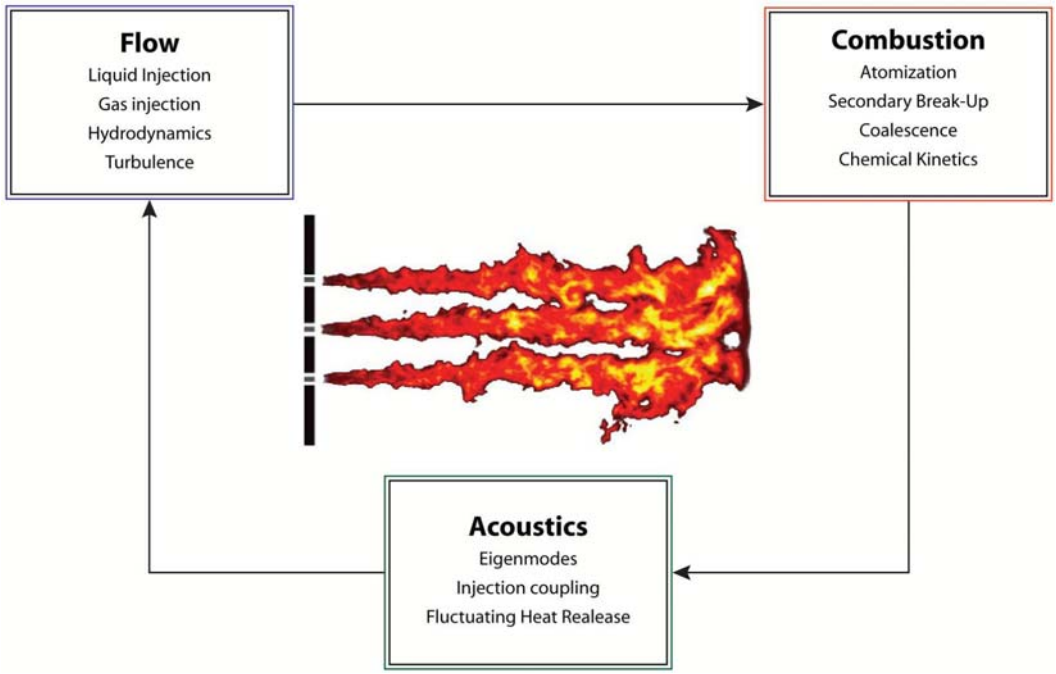

Fig. 1: Les différentes étapes mises en jeu dans le déclenchement des instabilités haute fréquence. Tous ces phénomènes sont couplés et peuvent s'amplifier.

La Figure 2 montre clairement les dégâts irrémédiables provoqués par les instabilités. De nombreux tests en laboratoire ont été menés sur des systèmes ne fournissant que de très petits accès visuel voire aucun ce qui ne permet pas de comprendre la dynamique et la structure des flammes.
Quelques expériences ont cependant été menées sur des systèmes avec hublots ou bien comprenant de petites ouvertures pour observer le phénomène de combustion. Des films à grande vitesse ont été enregistrés pour obtenir des images instantanées de la lumière émise par la flamme. Ces films ont montré une modification profonde de la combustion lorsque la chambre devient instable. Les expériences de Tischler et Male (1956) ou de Lawhead (1961) mettent en évidence ces modifications. Barrère et Corbeau (1963) fournissent également quelques exemples de visualisations instantanées. D'autres exemples peuvent être trouvés chez Fisher et al. (1995). Les films rapides fournissent des informations intéressantes mais limitées dans le temps et l'espace.
Du point de vue théorique, le problème des instabilités a fait l'objet de modèles analytiques allant du plus simple au plus élaboré. La plupart des travaux reposent sur le concept de délai sensible, introduit dans les années 40. La combustion instable est caractérisée par un terme de délai τ et un terme d'interaction n (Crocco and Cheng 1954; Barrère and Corbeau 1963). Le délai est induit par les processus d'injection, d'atomisation, de mélange et de combustion, et représente le délai entre le moment où les fluides sont injectés dans la chambre et le moment où ils sont consommés dans la flamme. Ceci pour des conditions de température et de pression données. Ce concept a été largement utilisé pour la modélisation et l'analyse de données, car il est relativement simple et rend compte du délai de combustion des réactifs. Les modèles basés sur ce concept ont été développés et utilisés de façon efficace dans les outils de conception mais ils ont tendance à masquer la nature première du phénomène. Les délais basés sur le délai de combustion ne fournissent pas une description des

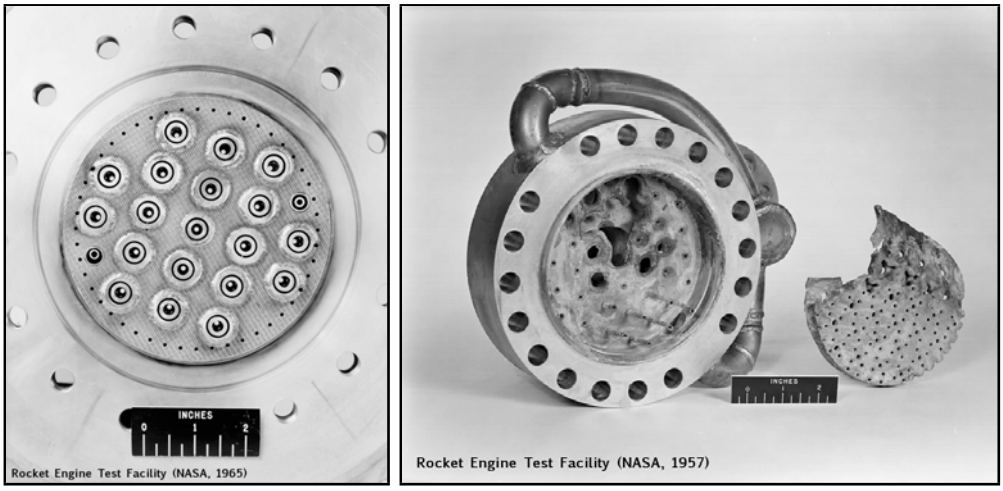

(a) (b)

Fig. 2: Vue d'une tête d'injection utilisée pour l'étude des instabilités de combustion haute fréquence. A gauche, la photo d'une tête saine représentative d'une tête d'injection réelle et à droite une tête d'injection endommagée par des instabilités de combustion. (Credits NASA)

mécanismes physiques contrôlant les instabilités mais rend compte d'un des aspects de la combustion : le délai entre l'injection et la réaction.

Les recherches effectuées durant les années 60 et au début des années 70 sont rassemblées dans un manuel édité par Harrje and Reardon (1972) et bien connu sous le nom de rapport NASA SP-194. Ce document contient une quantité intéressante d'informations, des sous-modèles utilisés pour décrire quelques-unes des nombreuses facettes du problème. Il y a cependant des points manquant concernant principalement les mécanismes à l'origine du déclenchement des instabilités.

Dernièrement, les recherches concernant les instabilités de combustion ont concerné d'autres domaines d'applications. Les problèmes rencontrés dans la combustion prémélangée pauvre ont été largement étudiés pour développer des brûleurs à faible émission de NOx et la plupart de ces recherches ont concerné les instabilités basse fréquence couplées aux modes acoustiques longitudinaux. Les travaux concernant la dynamique de combustion et son contrôle ont été rassemblés par Candel (1992, McManus et al. (1993, Candel (2003). Ces articles contiennent un grand nombre de références récentes et montrent que les dernières recherches ont principalement concerné les instabilités basse fréquence. Un chapitre du livre de Poinsot et Veynante traite de ce problème en se concentrant principalement sur les instabilités longitudinales qui sont également le sujet d'un ouvrage récent édité par Lieuwen et Yang (2005).

Dernièrement, les instabilités haute fréquence dans les moteurs à propulsion liquide ont causé de nouveaux échecs importants. Les instabilités haute fréquence constituent toujours un obstacle majeur dans le développement des moteurs à propulsion liquide mais la quantité d'études dans ce domaine a dans l'ensemble diminué. L'état de l'art au début des années 90 est rapporté dans l'ouvrage édité par

Anderson et Yang (1995).

Alors que les recherches sur les instabilités de combustion haute fréquence diminuaient, de considérables progrès ont été accomplis dans la compréhension fondamentale des flammes cryotechniques utilisées dans les moteurs fusées. Des recherches conséquentes ont été menées en France durant les années 90 dans le cadre d'un groupement de recherche incluant ONERA, les laboratoires du CNRS, SNECMA et CNES dans une collaboration étroite. Des efforts similaires ont été accomplis en Allemagne, principalement au DLR. Le laboratoire EM2C s'est engagé dans ces recherches et a contribué au développement d'expériences et de modèles théoriques et numériques. Les connaissances sur la combustion ont été approfondies grâce à l'utilisation de nouveaux bancs d'essais comme Mascotte en France ou le micro moteur et le banc P8 au DLR. Des diagnostics modernes ont fourni des informations sur les phénomènes de stabilisation, d'injection et de dispersion de jet liquide, de structure de flamme ainsi que les effets de la pression et de l'état transcritique de fluides. La plupart de ces études ont été réalisées avec de l'oxygène liquide et de l'hydrogène gazeux (Herding et al. 1996; Snyder et al. 1997; Herding et al. 1998; Kendrick et al. 1998; Candel et al. 1998; Kendrick et al. 1999; Juniper et al. 2000), et des études plus récentes ont permis de tester des flammes d'oxygène et méthane liquide (Singla et al. 2005). La majorité de ces travaux sont rassemblés dans un article récent de Candel et al. (2006).

La fluorescence induite par laser utilisée dans ces expériences a fourni des informations uniques sur la structure de flamme. Les expériences à basse pression menées par Snyder et al. (1997) ont été récemment étendues à la haute pression par Singla et al. (2006a) et Singla et al. (2006). Des images uniques de fluorescence ont été enregistrées à haute pression (6 MPa) pour le couple LOx/GH_2 et à une pression intermédiaire de 2 MPa pour le couple LOx/GCH_4.

Ces données constituent la base des études menées sur les instabilités haute fréquence dans le présent rapport. Les connaissances accumulées dans le domaine de la combustion cryotechnique sont essentielles pour l'étude des instabilités. Elles permettent de mettre en place les expériences et de proposer des modèles théoriques. Ces connaissances représentaient un manque évident pour les recherches précédentes et expliquent en partie pourquoi les avancées ont été difficiles dans le domaine des instabilités haute fréquence. Les autres difficultés sont à mettre au compte des moyens de diagnostic limités en matière de visualisations, d'acquisition de données et de traitement des signaux. Des améliorations considérables ont été réalisées dans ces différents domaines ouvrant ainsi de nouvelles perspectives. De même, les efforts de modélisation passés se sont restreints à des méthodes analytiques du fait des ressources informatiques limitées. La situation a radicalement évolué en matière d'équipement matériel, de logiciel et de moyens numériques. Dans le domaine de la simulation numérique des fluides, les méthodes moyennées ont laissé place aux simulations aux grandes échelles (SGE). La simulation numérique de la combustion suit la même tendance. En SGE, les grandes échelles sont résolues tandis que les petites sont modélisées. Cette approche est particulièrement bien adaptée à la simulation de problèmes où la turbulence et les phénomènes instationnaires jouent un rôle essentiel. Les simulations aux grandes échelles font l'objet d'intenses efforts de développement principalement dans le cadre des problèmes d'instabilités rencontrés en combustion prémélangée. Des modèles dédiés ont également été développés pour la combustion cryotechnique, comme le montrent les exemples présentés par Oefelein

et Yang (1998).

Le programme de recherche sur les instabilités haute fréquence, initié en 2000, a été mis en place pour améliorer la compréhension du problème en utilisant les connaissances nouvelles, les diagnostics modernes, les bancs d'essais récents et les idées et outils modernes en simulation numérique. La conviction est née à cette période que des expériences menées en laboratoire pouvaient apporter les informations manquantes sur les mécanismes fondamentaux des instabilités. Ces réflexions ont conduit à la création d'une chambre de recherche commune (CRC) exploitée à l'IRPHE par Cheuret (2005) et par le DLR, ainsi qu'une chambre de combustion à injecteurs multiples (MIC), conçue au laboratoire EM2C, dessinée par l'ONERA et mise en place sur le banc d'essai Mascotte de l'ONERA. Il est également à noter qu'un programme similaire a été mis en place aux Etats-Unis où la collaboration entre plusieurs universités et groupements de recherche a pour objectif d'apporter des informations expérimentales et numériques sur cette question.

Le travail présenté dans ce document a été réalisé dans le cadre du groupement de recherche franco-allemand sur les instabilités haute fréquence. Le groupe fut créé en 2000 en définissant des projets à la fois théoriques, numériques et expérimentaux. Les travaux réalisés au laboratoire EM2C ont été initiés par Rey et sont rapportés dans différents articles ou communications en conférences (Rey et al. 2002; Rey et al. 2002; Rey et al. 2004; Rey et al. 2005). Ces études concernaient le rôle des interactions collectives dans les instabilités haute fréquence. Les premières expériences ont été réalisées dans la chambre à injecteurs multiples avec le couple oxygène liquide/hydrogène gazeux. Les dimensions de la chambre de combustion ont été définies afin que les modes propres longitudinaux et transverse soient clairement séparés. Certaines caractéristiques des moteurs fusées ont été reprises. Ainsi trois injecteurs coaxiaux permettent d'observer les interactions de front de flammes. L'objectif de ces recherches étaient de fournir des informations expérimentales sur le couplage entre ondes acoustiques et combustion cryotechnique. Pour cela, les flammes étaient soumises à des oscillations acoustiques transverses générées par un modulateur externe constitué d'une roue dentée en rotation, obstruant périodiquement la sortie d'un tuyère secondaire située sur le dessus de la chambre. En ce qui concerne les simulations numériques, des conditions aux limites fluctuantes ont été mises en place afin de générer des ondes acoustiques dans un domaine de calcul. Des simulations aux grandes échelles de configurations prémélangées et nonprémélangées ont été réalisées avec le code AVBP et les résultats ont pu être comparés à des expériences dans lesquelles une excitation transverse était utilisée pour modulée des flammes de prémélange (Zikikout et al. 1986). Les travaux de Rey ont fourni de solides fondements aux travaux expérimentaux et numériques présentés ici.

Les recherches actuelles font suite à cet effort initial. L'objectif global est d'apporter une contribution à la compréhension des mécanismes fondamentaux conduisant aux instabilités de combustion. On cherche spécifiquement à guider la mise en place d'outils de prédiction des instabilités haute fréquence. Les aspects numériques et expérimentaux sont développés en parallèle car il semble évident qu'ils fournissent des informations complémentaires. Les expériences permettent de comprendre la physique des phénomènes mais il est également nécessaire d'essayer de modéliser les mécanismes pour tirer au maximum profit d'expériences coûteuses. Les outils numériques sont dans tous les cas nécessaires pour

accomplir un travail de conception des moteurs et leur mise au point ne peut s'effectuer sans les expériences. On essaiera de montrer dans ce document que les simulations numériques nécessitent des expériences pour la validation et qu'en retour elles fournissent des informations importantes pour l'amélioration des expériences. Elles permettent en outre de balayer un plus grand nombre de conditions qui ne sont pas accessibles expérimentalement, car elles mettent en danger l'intégrité du banc.

Organisation et contenu

Ce documents est divisé en six chapitres. Les trois premiers concernent principalement les études et les résultats expérimentaux tandis que les trois derniers chapitres rassemblent les travaux de simulation et de modélisation. Ce découpage est également présenté sous la forme de six illustrations (Figure 3) caractéristiques des questions abordées dans chaque chapitre. Le contenu est décrit plus en détail dans la suite.

Expériences

Les trois premiers chapitres décrivent principalement les aspects expérimentaux. Les expériences réactives sont réalisées sur le banc d'essais Mascotte pour observer les oscillations de combustion à l'aide de diagnostics optiques et de capteurs de pression. Etant donnée la complexité des moteurs fusées, seuls les phénomènes cruciaux sont recréés à échelle réduite. L'objectif est d'observer les interactions les plus fortes possibles entre les ondes de pression acoustiques et la combustion dans des conditions les plus réalistes possibles.

Dans les années 50, les expériences étaient menées sur des moteurs naturellement instables avec un nombre limité de diagnostics. L'avantage était que les conditions expérimentales étant quasiment identiques à celles d'un moteur réel mais les diagnostics se résumaient à quelques capteurs de pression et les données devaient être collectées avant la destruction du moteur. Les visualisations étaient extrêmement limitées et étaient matérialisées par des films rapides au travers de petits hublots.

Dans le travail présenté ici, les techniques modernes de visualisation sont mises en place pour examiner la dynamique de flamme. La chambre de combustion est munie de large fenêtres en quartz permettant un accès visuel aisé. La combustion étant naturellement stable dans cette configuration, l'énergie acoustique doit être artificiellement apportée au système pour destabiliser les flammes. L'avantage d'une telle configuration est que la modulation est bien contrôlée et la combustion facilement observable, l'inconvénient étant qu'une grande quantité d'énergie acoustique est nécessaire pour perturber la combustion et que les conditions expérimentales diffèrent des conditions présentes dans les moteurs.
La combustion cryotechnique met en jeu une multitude de phénomènes fortement couplés présentés sur la Figure 1. La combustion est corrélée en temps et en espace à la modulation acoustique transverse qui peut être amplifiée déclenchant ainsi des instabilités. Il est alors naturel d'explorer différentes conditions expérimentales pour trouver dans quelques situations, les flammes sont sensibles aux perturbations. L'idée est de faire varier les paramètres d'injection pour générer le plus fort couplage possible entre les flammes et les ondes acoustiques.

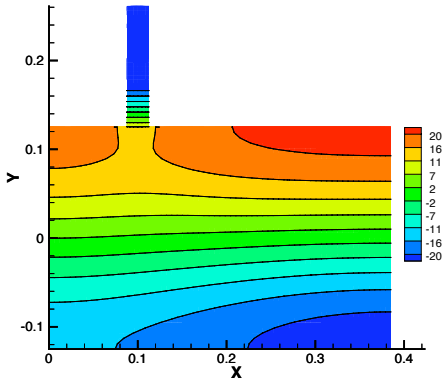

Chapitre I : Champ de pression numérique correspondant au premier mode transverse.

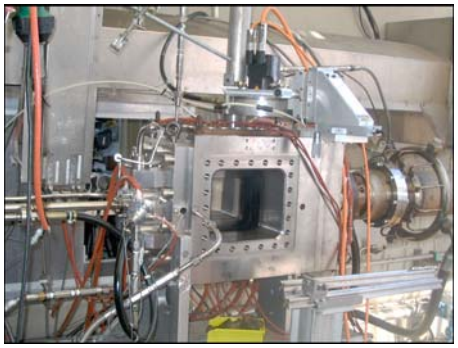

Chapitre II : Photo de la chambre de combustion installée sur le banc d'essai Mascotte.

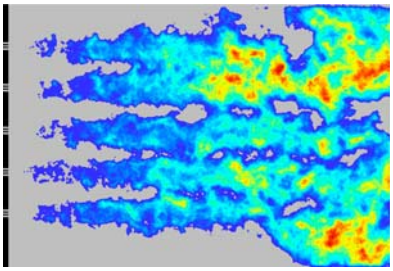

Chapitre III : Emission instantanée du radical OH issu de cinq flammes LOx/Méthane.*

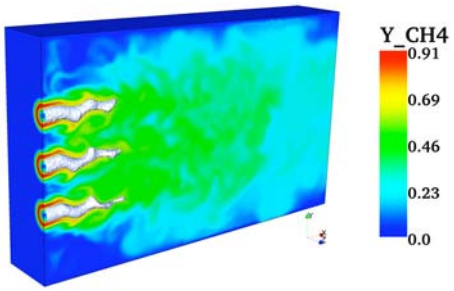

Chapitre IV : LES de trois jets coaxiaux oxygène/méthane modulés transversalement.

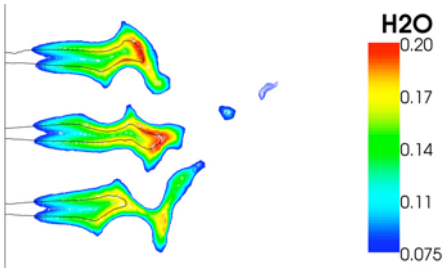

Chapitre V : Champ de vapeur d'eau obtenu par LES à l'aide du modèle de flamme nonprémélangée RBR.

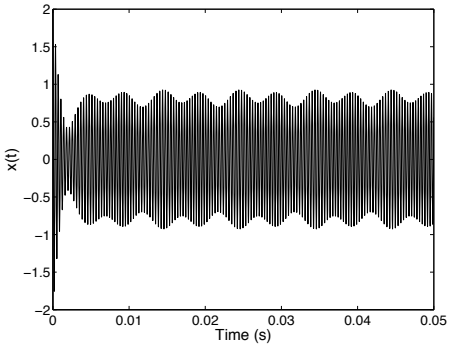

Chapitre VI : Réponse acoustique d'un système du second ordre à fréquence propre oscillante.

Fig. 3: Illustrations des études présentées dans chaque chapitre du document.

Le banc d'essais "Mascotte" est utilisé car il permet de travailler avec des fluides cryotechniques réels qui peuvent être injectés à travers des injecteurs coaxiaux. Le système est dimensionné pour supporter de très hautes pressions. Les expériences précédentes conduites par Rey sur ce banc ont montré que le modulateur externe et la chambre de combustion étaient des outils bien adaptés à l'étude des instabilités haute fréquence, des interactions entre combustion et ondes acoustiques étant observables. La conclusion de ces travaux initiaux étaient que l'énergie acoustique dans le système devait être la plus grande possible pour générer de fortes interactions.

Pour amplifier le niveau d'excitation dans la chambre, deux moyens sont utilisés. Premièrement, on essaie d'amplifier la modulation acoustique. Le modulateur est constitué d'une tuyère secondaire située sur le dessus de la chambre et d'une roue dentée obstruant périodiquement la sortie de la tuyère. Les fluctuations de débit génère des ondes acoustiques dans la chambre. il est alors possible d'augmenter le niveau de fluctuations en ajustant au mieux, la position relative de la roue dentée et de la tuyère. Ceci nécessite un mécanisme d'ajustement fin permettant des déplacements relatifs millimétriques.

Dans un second temps, le couplage entre les flammes et l'acoustique peut être renforcé en augmentant la sensibilité des flammes aux perturbations. Ceci passe par une étude systématique de l'influence des paramètres d'injection sur la structure de flamme. Les flammes cryotechniques stabilisées sur des injecteurs coaxiaux sont communément caractérisées par deux nombres sans dimension, le rapport de quantité de mouvement $J = \rho_{CH_4} v_{CH_4}^2 / \rho_{LOx} v_{LOx}^2$ et le rapport de mélange $E = \dot{m}_{LOx} / \dot{m}_{CH_4}$. Ces paramètres ont une forte influence sur la structure des flammes ainsi que sur la réponse global du système aux perturbations acoustiques. Il est donc naturel d'étudier l'influence de ces paramètres sur le comportement acoustique de la chambre de combustion et la stabilité naturelle des flammes.
Tous les couples E-J ne peuvent être testés du fait du nombre limité d'essais et des risques que certains points de fonctionnement font courir à l'installation. L'utilisation d'outils numériques et analytiques permet d'explorer une large gamme de paramètres et de comprendre l'influence des conditions d'injection sur la combustion.

Le premier chapitre du document contient essentiellement les études analytiques, numériques et expérimentales de l'acoustique de la chambre de combustion. Ces études sont menées en amont des essais pour préparer au mieux les campagnes expérimentales. La principale nouveauté ici est que le méthane remplace l'hydrogène qui fut utilisé précédemment, l'oxygène liquide restant l'oxydant. Ceci modifie les fréquences propres du système et a une influence directe sur la réponse acoustique de la chambre. Ce chapitre aborde également la stabilité hydrodynamique des jets de réactifs. Les fréquences propres et les champs de pression correspondants sont prédits analytiquement et numériquement en fonction des conditions d'injection. L'influence des paramètres E et J sur la réponse du système est étudiée afin de choisir les points de fonctionnement offrant les flammes les plus sensibles aux perturbations acoustiques. Les instabilités de combustion mettent également en jeu des phénomènes non linéaires, il est donc intéressant de soumettre le système à différents types de modulations. Le chapitre I étudie cet aspect puisque des systèmes de génération de train d'ondes et d'impulsion laser sont expérimentés, l'excitation laser étant mis en oeuvre dans une chambre à échelle réduite.

Le second chapitre présente les résultats de la première campagne d'essais réalisés à des pressions voisines de 0.9 MPa. L'objectif est d'explorer expérimentalement différentes conditions d'injection pour trouver celles qui permettront un fort couplage entre la combustion et l'acoustique. Les conditions expérimentales sont caractérisées par des vitesses et températures de méthane différentes, les conditions d'injection de l'oxygène étant maintenues constantes. Les diagnostics optiques sont utilisés pour rendre compte de la structure et de la dynamique des flammes avec et sans modulations acoustiques. 24 tests de 30 secondes sont réalisés à 0.9 MPa avec trois injecteurs coaxiaux. Le modulateur externe a été considérablement amélioré.

Le troisième chapitre décrit les tests réalisés à 3 MPa avec cinq injecteurs. Les débits sont également augmentés afin d'augmenter la puissance globale du banc. L'augmentation des pressions contribue à rapprocher les expériences des conditions rencontrées dans les moteurs fusées (la pression étant supérieure à 10 MPa dans un moteur type Vulcain). Il est aussi supposé qu'une augmentation de la puissance de la réaction génère des interactions renforcées entre l'acoustique et la combustion. La puissance reste cependant bien en dessous de ce qui est produit dans un moteur (de l'ordre de 50 GW m^{-3}). Cette valeur extrême ne peut pas être atteinte en laboratoire mais l'influence de l'augmentation de puissance et de pression demeure un élément intéressant à étudier. Le chapitre III présente les résultats obtenus durant la campagne d'essais à haute pression dans une chambre équipée d'une nouvelle tête d'injection à cinq injecteurs. L'influence des paramètres E et J sur les structures de flamme est étudiée.

Des tests supplémentaires ont été réalisés à 1 MPa avec uniquement deux injecteurs. La dispositions des injecteurs est telle que les interactions collectives entre les front de flammes et quasiment impossible. Ce test a pour but l'observation des effets d'une modulation acoustique sur une flamme isolée. Enfin, trois essais à 6 MPa sont réalisés. A cette pression, l'oxygène est injecté dans un état transcritique, la température étant inférieure à la température critique ($T_c(LOx) = 154$ K) tandis que la pression est au-delà de la pression critique (p_c=5.04 MPa). L'influence de l'état transcritique de l'oxygène sur les flammes est étudiée.

Simulations numériques et modélisations

Les chapitres IV et V concernent principalement les simulations numériques des oscillations de combustion à haute fréquence dans le cadre des simulations aux grandes échelles (SGE). Ce type de modélisation est choisi car il est parfaitement adapté à la description numérique des processus faisant intervenir la turbulence et les phénomènes instationnaires. Les simulations RANS, où les valeurs sont moyennées, ne sont pas adaptées à ces études de stabilité. Les simulations aux grandes échelles étant le cadre de notre étude, il est important de rappeler les principales difficultés qui résident dans la simulation de la combustion dans les moteurs fusées :

- L'un des réactifs est injecté sous forme liquide (dans des conditions sous critiques) ou bien dans un état très dense. Les simulations aux grandes échelles d'écoulements diphasiques ou transcritiques sont actuellement en voie de développement et l'approche choisie n'est pas encore complètement prouvée ni validée. Les très forts gradients de densité rencontrés en pratique

représentent une grande difficulté pour la plupart des outils numériques.

- La combustion met en jeu des réactifs cryotechniques. Elle est principalement nonprémélangée et se déroule à très haute pression. Le dégagement de chaleur est contrôlé par le transport turbulent des réactifs vers le front de flamme et le taux de consommation local est déterminé par la turbulence. La description des instabilités de combustion passe nécessairement par une description correcte du taux de réaction. Il est également primordial que l'effet de la pression soit correctement reproduit.

- Plusieurs injecteurs doivent être représentés (un moteur réel en comprend plus de 500). Des moyens importants sont nécessaires pour simuler une chambre de combustion entière. Même une expérience à échelle réduite nécessite un maillage raffiné pour représenter trois injecteurs et la chambre.

- Une modulation transverse doit être générée pour étudier les cas où la combustion est perturbée par une excitation acoustique. Les méthodes de modulation acoustiques ont été développées mais des améliorations peuvent encore être réalisées.

- La réponse acoustique d'une chambre doit être correctement simulée. Les dissipations ne doivent pas être trop importantes pour éviter que les instabilités acoustiques ne soient trop fortement atténuées et ainsi réduire l'intérêt prédictif des simulations.

- Les impédances du fond de chambre et de la tuyère doivent être correctement représentées car elles jouent un rôle fondamental dans les phénomènes d'instabilité.

Ces nombreux aspects peuvent seulement être traités dans le cadre d'un programme global de développement d'outils numériques. Les études rapportées dans ce document ont des objectifs plus limités mais apportent des éléments essentiels. Les simulations sont menées avec des réactifs gazeux pour s'affranchir des problèmes d'injection liquide ou transcritique. Des recherches sont cependant en cours grâce à une collaboration du laboratoire EM2C et du CERFACS pour mettre en place les outils LES nécessaires à la description de la combustion transcritique.

Cette forte simplification autorise néanmoins à étudier l'effet d'une modulation acoustique transverse sur plusieurs jets coaxiaux nonréactifs et à s'intéresser au mélange et à la dynamique des écoulements dans ces conditions.

Les résultats d'une telle simulation sont décrits dans le chapitre IV où la LES est utilisée pour simuler la réponse dynamique de trois jets coaxiaux constitués d'oxygène gazeux entouré de méthane. Dans un premier temps, le système est laissé libre puis il est forcé acoustiquement. Ce chapitre présente également des données expérimentales obtenues au cours d'essais nonréactifs sur le banc Mascotte. L'oxygène liquide, entouré d'azote à grande vitesse, est introduit à basse vitesse dans la chambre à travers cinq injecteurs coaxiaux. L'expérience est réalisée à 3 MPa et le rétro éclairage est utilisé pour observer le comportement des jets avec et sans modulation acoustique. L'étude porte principalement sur l'effet collectif de la modulation sur les jets. Une caméra rapide est utilisée pour obtenir une résolution temporelle permettant de suivre le mouvement des jets.

La simulation numérique et l'expérience ne sont pas réalisées dans des conditions identiques mais elles ont toutes les deux comme objectif d'observer l'influence d'une onde de pression sur le comportement collectif de jets coaxiaux.

Le chapitre V concerne le problème fondamental qui consiste à modéliser le taux de réaction dans des conditions d'injection proches de celles rencontrées dans les moteurs. Une première partie permet de détailler et de décrire le mode de combustion mis en jeu dans les moteurs cryotechniques. L'objectif est de mettre en place un modèle simple, intégrable dans le schéma de résolution LES, applicable sur des maillages classiques des grandes échelles et qui puisse fournir directement le taux de réaction. Le dégagement de chaleur obtenu avec ce modèle devra être positionné autour du front de flamme tout en étant suffisamment distribué sur le maillage pour être résolu. Pour modéliser la combustion, il serait possible d'utiliser des méthodes existantes, basées sur la fraction de mélange associée à des fonctions de densités de probabilités. Seulement ces méthodes ne permettent pas d'obtenir directement le taux de réaction qui joue un rôle fondamental dans l'étude des instabilités de combustion. On préférera extraire le taux de réaction volumique du taux de réaction par unité de surface pour pouvoir ensuite le distribuer autour du front de flamme et ainsi obtenir le taux de consommation local par unité de surface. Avec un tel modèle, il est possible de tenir compte des réactions ayant lieu en sous-maille. Ce modèle de reconstruction du taux de réaction (Reconstructed Burning Rate Model, RBRM) semble plus physique que le modèle de fonction de probabilités où le taux de réaction est masqué. Ce modèle permet de localiser le front de flamme et d'observer ses interactions avec les modes acoustiques. Ainsi, la relation entre fluctuations de pression et de dégagement de chaleur peut-être obtenue numériquement, à l'image de ce qui est fait expérimentalement. La démarche présentée au chapitre V suppose une chimie infiniment rapide, ce qui est le cas lors de réactions réalisées avec l'oxygène pur. Des simulations de la configuration à trois jets coaxiaux sont utilisées pour mettre en place le modèle et observer l'effet d'une modulation acoustique sur les fronts de flammes.

Le chapitre VI présente deux modèles issus des observations expérimentales. Le premier a pour objectif de décrire comment les fluctuations de dégagement de chaleur peuvent être générées par un mouvement transverse. Cette question est apparue lors de la mise en place du programme de recherche. Les premiers travaux ont été initiés par Rey et sont poursuivis ici. Une expression est proposée pour modéliser les fluctuations de dégagement de chaleur mises en jeu lors de mouvement oscillatoires transverses. La direction de la vitesse est un paramètre important et est prise en compte dans ce modèle. Le dégagement de chaleur dépend du gradient de vitesse transverse et de son signe. Ce modèle fournit une interprétation réaliste des comportements de flammes observés lors d'expériences antérieures réalisées par Tischler et Male.

Le second modèle rend compte de l'influence des fluctuations turbulentes de la température sur les capacités résonantes d'un système. Précédemment des travaux ont été menés par Clavin et Williams ou encore Burnley et Culick sur l'influence d'une perturbation stochastique sur la stabilité acoustique d'un système, mais ces travaux ne considèrent pas l'effet de la turbulence sur la résonance du système. L'analyse décrite dans ce dernier chapitre est issue d'observations expérimentales réalisées lors de la seconde campagne d'essais à 3 MPa. Il a été observé que la résonance du système n'était

pas aussi fine qu'espérée. Il semble que le facteur de qualité du système ait été modifié par les conditions de l'écoulement. L'idée mise en place dans ce modèle est que des fluctuations basse fréquence de la température peuvent modifier les capacités de résonance d'une système acoustique. Une simulation est réalisée et montre des phénomènes proches de ceux observés expérimentalement. Le modèle est également développé grâce à la méthode des moyennes décrite par Bogolioubov (1962). Les conséquences pratiques d'un tel phénomène sont discutées dans ce chapitre.

Publications

Les différentes parties de ces travaux ont été publiées dans des articles ou bien présentées lors de conférences :

C. Rey, S. Ducruix, F. Richecoeur, P. Scouflaire, L. Vingert and S. Candel (2004) High frequency combustion instabilities associated with collective interactions in liquid propulsion. AIAA Paper 2004-3518. *Joint Propulsion Conference*, Fort Lauderdale, Florida.

F. Richecoeur, S. Ducruix, P. Scouflaire and S. Candel (2005) Experimental investigation of interactions between acoustics and combustion in liquid rocket engines. *40e colloque d'Aérodynamique Appliquée : Aérodynamique instationnaire*. Toulouse 21-23 mars 2005.

F. Richecoeur, P. Scouflaire, S. Ducruix and S. Candel (2005) Experimental investigation of high frequency combustion instabilities in liquid rocket engine. *52nd International Astronautical Congress*. Fukuoka, Japan.

F. Richecoeur, P. Scouflaire, S. Ducruix and S. Candel (2005) Experiments on high frequency combustion oscillations induced by transverse acoustic modulations. *20th ICDERS*, Montreal, Canada.

F. Richecoeur, P. Scouflaire, S. Ducruix and S. Candel (2005) Experimental investigation of high-frequency instabilities in liquid rocket engine. *Proceedings of INCA colloquium*. S. Candel, M. Cazalens and F. Hirsinger, eds. pp. 229-237.

F. Richecoeur, P. Scouflaire, S. Ducruix and S. Candel (2006) Interactions between propellant jets and acoustic modes in liquid rocket engines : experiments and simulations. *AIAA Joint Propulsion Conference*, AIAA Paper 2006-4397. July 9-12, 2006 Sacremento, California.

F. Richecoeur, S. Ducruix, P. Scouflaire and S. Candel (2006) High frequency transverse acoustic coupling in a multiple injector cryogenic combustor. *Journal of Propulsion and Power 22 (4)* 790-799.

Introduction

Introduction and background

High frequency combustion instabilities were observed for first time during the early development of liquid rocket engines (LRE) in the 40's. These oscillations had in most cases fatal consequences. Engines were damaged and quickly destroyed by the intensified heat fluxes induced by the large amplitude pressure oscillations developing in the thrust chamber. This led to many spectacular rocket failures. Full scale tests and smaller scale experiments were carried out over an extended period of time to investigate the sources of these instabilities and find ways to suppress their occurrence. Pressure transducers were directly mounted on real engines and allowed observations of the frequencies and amplitudes of the oscillations and an identification of the acoustic modes involved in the process. It soon became clear that these instabilities were associated in most cases with high-frequency, high amplitude pressure oscillations resulting from a coupling between combustion and acoustic modes of the thrust chamber. The process could be represented schematically in the form of a closed loop involving the injected flow, combustion in the chamber and acoustic modes as illustrated in Figure 1.

It was however difficult to obtain fundamental information on the driving mechanisms. A substantial experimental effort and a considerable amount of money were spent during most of the developments of high performance liquid rocket engines to deal with instabilities by modifying the engine design, adding baffles, resonators and cavities to reduce the problem and verify that the system would operate in a stable manner. The history of the painstaking trial and error process which was defined to suppress instabilities in the F1 engine is summarized in a remarkable article by Oefelein and Yang (1993). Such costly and time consuming tests provided practical solutions for instability control and advanced to a lesser extent the state of knowledge required to predict the development of these dynamical phenomena. Baffles were added to the chamber backplane to reduce transverse velocity perturbations associated with the azimuthal and radial modes, quarter wave cavities were placed around the chamber to damp oscillations, different injector geometries were investigated to reduce their dynamical response to perturbations. Many of the systems used to eliminate oscillations like baffles, cavities or resonators increased the design complexity and the engine weight.

In the mid-fifties, the first laboratory scale experiments were designed to study the instability problem on a more fundamental level. Small scale liquid rocket engines were tested under realistic conditions. The result of one of these tests appears in Figure 2 which shows a view of the injection head before and after an unstable hot fire run. The backplane is initially equipped with standard coaxial elements similar to those found in real engines. Figure 2 clearly shows the irreversible damage associ-

ated with a high amplitude instability observed during the experiment. Many of the small scale tests were carried out in blind systems providing no optical access to the combustion chamber with the consequence that not much could be learned about the driving mechanisms and the dynamics of the flame.

Some experiments were however carried out in transparent systems or in systems comprising a thin slit providing a limited access to the combustion process. High speed films were used to obtain streak images of the light emitted by the flame. These films revealed fundamental modification of the combustion process when the chamber became unstable. This is exemplified in the experiments of Tischler and Male (1956) or in those carried out by Lawhead (1961) in a two-dimensional thrust chamber. Barrère and Corbeau (1963) also give some examples of these streak visualizations. Examples can also be found in Fisher et al. (1995). The streak film method provided interesting but limited information on the space time distribution of heat release in unstable rocket engines.

On the theoretical side, the instability problem was the subject of simplified or more elaborate analytical investigation. Much of the work was founded on the sensitive time lag (STL) concept introduced in the late 1940's in which the nonsteady combustion process is characterized in terms of a time lag τ and an interaction index n (Crocco and Cheng 1954; Barrère and Corbeau 1963). The time lag is induced by processes of injection, atomization, mixing and combustion and represents the delay between injection of reactants and their conversion into products. This time lag is a function of local conditions and in particular of pressure and temperature. The concept has been extensively used in modeling, and data reduction and interpretation activities because it is relatively simple and reflects the time delayed burning of propellants. Models based on this concept have been extensively developed and implemented in useful engineering tools but they have tended to hide the physical nature of the phenomena. The time lag models do not provide a detailed description of the driving mechanisms but represent at least one of the aspects of the phenomena which is the inherent delay between injection and combustion.

Research carried out during the 1960's and early 1970's is summarized in a highly cited handbook edited by Harrje and Reardon (1972) and known as the NASA SP-194 report. This document contains a valuable amount of information, many of the submodels used to describe the many facets of the problem and much of the know-how in this field. There are also some weak points and in particular those pertaining to the processes, which act as driving mechanisms.

In the more recent period research on combustion instabilities has concerned other application areas. Problems encountered in lean premixed combustion have been extensively investigated in relation with low NOx gas turbine combustors and most of this work has focused on low frequency oscillations coupled by plane acoustic modes. Much of the work on combustion dynamics and control is reviewed by Candel (1992, McManus et al. (1993, Candel (2003). These articles contain a large number of references to the recent literature and show that much of the recent work has mainly concerned low frequency system instabilities. A chapter in the book by Poinsot and Veynante (2005) also deals with the problem but mainly discusses low frequency longitudinal instabilities and this is also the subject of a recent book edited by Lieuwen and Yang (2005).

During the more recent period, problems of high frequency instability in liquid rocket engines have continued to arise in various systems causing some important failures. High frequency instabilities still form a major obstacle in the development of liquid rocket motors but the level of research in this area had generally diminished. The state of the art in the early 1990's is reviewed in an edited book (Anderson and Yang 1995).

While this reduction of scientific activity on HF instabilities was taking place, much progress was accomplished on the fundamental understanding of cryogenic flames of the type used in high performance LRE. An important research program was carried out in France during the 1990's in the framework of a research group (GDR) associating ONERA, CNRS Laboratories, SNECMA and CNES with a close collaboration with similar efforts undertaken in Germany most notably by DLR. EM2C was heavily engaged in this research and contributed to the development of experiments, theory and numerical modeling. Knowledge has been accumulated on the combustion process by making use of new experimental testbeds like Mascotte in France or the microcombustor and P8 at DLR. Modern optical diagnostics have provided unique data on the process. This research has concerned many aspects of stabilization, injection and liquid jet break-up, flame structure, high pressure and transcritical effects. Most of the studies have been carried out with liquid oxygen and gaseous hydrogen by Herding et al. (1996, Snyder et al. (1997, Herding et al. (1998, Kendrick et al. (1998, Candel et al. (1998, Kendrick et al. (1999, Juniper et al. (2000), and more recent experiments have used liquid oxygen and gaseous or liquid methane (Singla et al. 2005). Much of this work is reviewed in a recent article by Candel et al. (2006).

Laser induced fluorescence used in these experiments has provided some unique information on the flame structure. The low pressure experiments carried out by Snyder et al. (1997) were extended more recently by Singla et al. (2006a, Singla et al. (2006) to the high pressure range. Some remarkable instantaneous images have been recorded for high pressure (6.3 MPa) LOx/GH2 combustion and intermediate pressure (2.0 MPa) LOx/GCH4 flames providing essential indications on the mode of combustion.

This data set forms a basis for the HF instability analysis carried out in the present investigation. The knowledge accumulated on cryogenic combustion is in the present context essential. It serves to guide experimentation and it can be used to orient modeling and simulation. This knowledge was essentially lacking in the earlier experimental work and this explains in part why progress was relatively slow. Other difficulties were associated with the limited capabilities of experimental diagnostics, imaging equipment, digital data acquisition and processing systems. Considerable progress has been made in these various areas and this has opened new perspectives. Similarly, much of the early modeling effort had to rely on analytical methods because the computational resources were extremely limited. The situation has changed quite drastically with progress made in hardware, software and computational science. In computational fluid dynamics, the emphasis has shifted from Reynolds average Navier-Stokes (RANS) methods to large eddy simulations (LES). Current effort in numerical combustion has followed similar trends. In LES the large scales are resolved while the small scales are modeled

and these methodologies are well adapted to the calculation of problems where turbulence and unsteadiness play central roles. LES is now actively developed in numerical combustion in particular to deal with instability problems mostly those encountered in premixed combustion instabilities. LES of transcritical combustion of cryogenic propellants has also been developed and it is exemplified by Oefelein and Yang (1998).

At the beginning of the High Frequency program in the year 2000, it was clear that the state of the art could be seriously advanced by making use of recent knowledge, advanced diagnostics, new testbeds and modern computational ideas and tools. It was also believed that laboratory experiments could provide the missing pieces of information on the mechanisms driving instabilities. This led to the development of the Common Research Chamber (CRC) exploited at IRPHE (Cheuret 2005) and at DLR and to the Multiple Injector Combustor (MIC) conceived at EM2C (Rey 2004) designed by ONERA and exploited on the Mascotte facility of ONERA. It is worth noting that a program on LRE combustion instabilities has also been set-up in the United-States, involving several universities and organization in a collaborative experimental and numerical effort.
The work reported in the present document has been accomplished in the framework of the French-German Research Initiative on High Frequency Instabilities. The group was put together in the year 2000. A roadmap was defined with a variety of theoretical, numerical and experimental projects. The work at EM2C was first carried out by Rey and it was reported in various conference papers and articles (Rey et al. 2002; Rey et al. 2002; Rey et al. 2004; Rey et al. 2005). These studies were focused on collective interactions. The multiple injector combustor (MIC) operating with liquid oxygen and gaseous hydrogen was used in a set of initial experiments. The geometry was defined to allow a good separation between longitudinal and transverse acoustic modes. It had some of the features of a rocket engine and in particular included three coaxial injectors to allow interactions between multiple flames. The objective of this experimental investigation was to generate data on the coupling between acoustics and combustion. To this purpose, the system was excited by an external toothed wheel modulator (TWM) using a periodically blocked auxiliary nozzle to induce acoustic tranverse modes in the chamber. In parallel, simulation of transverse acoustic modulation was initiated and a method was developed to this purpose. Calculations of premixed and nonpremixed configurations were carried out in the large eddy simulations framework using the AVBP code and some results of calculations were found to be in agreement with early experiments in which a transverse mode was used to modulate a set of premixed flames (Zikikout et al. 1986). The work of Rey provided a solid basis for the present experimental and numerical investigations.

The present investigation continues this initial effort. The general objective is to contribute to the understanding of the fundamental mechanisms leading to high frequency combustion instabilities. It is also hoped that the knowledge generated could be used to guide the development of computational tools for the prediction of instabilities and could be used to control instabilities. Experimental and numerical modeling efforts are developed in parallel because they provide complementary information. It is important to understand the physics of the phenomenon with detailed experiments but it is as crucial to model the mechanisms in order to interpret what is being observed. It is also clear that computational tools are needed for engineering purposes but their development will not be possible

without validation and fine tuning using experimental data. We try to show in the present document that numerical simulations need experiments for validation and that in turn simulations provide information, which may be used to improve experiments. Simulations will eventually be capable to extend the range of conditions, which can be explored.

Organization and contents

This document is organized in six chapters. The first three chapters mainly focus on experimental issues and results while the last three chapters describe simulations and modeling. This organization is also shown in the form of a diagram in Figure 3 which gathers a set of figures typifying what is done in each chapter. Contents are described in what follows in further details.

Experimentation

The first three chapters mainly describe experimental aspects. Hot-fire experiments are carried out on the model scale testbed Mascotte to generate and observe combustion oscillations with optical diagnostics in combination with pressure transducers. Due to the complexity of liquid rocket engines, only the key phenomena can be recreated on the test facility. The challenge is to observe the strongest possible interactions between pressure fluctuations and combustion under conditions as close as possible to real engines.

In the 50's, experiments were carried out on naturally unstable engines, with a limited amount of diagnostics. This had the advantage that the operating conditions were close to the real ones but only a few pressure transducers could be set on the experimental devices and data had to be recorded before the deterioration of the system. Visualization was quite limited and essentially relied on streak films obtained through thin transparent slits.

In the present work, modern imaging techniques are set up to examine the dynamics of the process. The chamber is equipped with large windows providing an excellent optical access. Since combustion is stable, pressure fluctuations are artificially generated in the chamber to destabilize the system. The advantage of this configuration is that the modulation is well controlled and the combustion area is easily observable. The drawback is that high acoustic energy has to be injected in the system and operating conditions are not quite similar to those found in practice.
Cryogenic combustion involves a wide range of phenomena represented in Figure 1 which are all strongly coupled. If combustion becomes correlated in space and time with the transverse acoustic modulation, the oscillation can be amplified and will lead to instability. It is then natural to explore the range of operating parameters and find when the flames become more sensitive to external modulation. The idea is to vary the parameters to generate a strong coupling with the external modulation.

The "Mascotte" testbed is used for this experimental research because it operates with real cryogenic fluids injected through coaxial injectors. The system is designed to sustain high chamber pressures and this feature is extremely useful. Previous experiments on high frequency combustion instabilities

carried out by Rey showed that the external modulator and the combustion chamber were adapted to this investigation, and interactions were observed between combustion and transverse acoustic modes. The conclusion of this initial work was that the acoustic energy provided to the system had to be increased to the highest possible amplitude to observe interactions of the kind found in unstable engines.

To increase the level of fluctuations in the chamber one may first try to amplify the acoustic modulation. The external modulator comprises an auxiliary nozzle located on the top of the chamber and a toothed wheel periodically blocking the nozzle throat. The fluctuating mass flow rate generates acoustic waves in the chamber. It is then possible to augment the level of fluctuations by carefully matching the nozzle and the rotating wheel. This requires an improved mechanical adjustment of this device and of its coupling with the chamber. It is therefore important to carefully optimize this system to increase its efficiency.

The pressure fluctuation amplitude may also be augmented by finding the parameters, which yield flames that are most receptive to external modulation. Cryogenic flames formed by coaxial injectors are usually characterized by two dimensionless numbers, the momentum flux ratio $J = \rho_{CH_4} v_{CH_4}^2 / \rho_{LOx} v_{LOx}^2$ and the mixture ratio $E = \dot{m}_{LOx}/\dot{m}_{CH_4}$. These parameters have a strong influence on the flame structure but also on the global response of the system to acoustic perturbations. It is then logical to investigate the influence of these parameters on the acoustic behavior of the combustion chamber and on the natural stability of the flames.
All the parameters cannot be systematically tested because the number of experiments is limited and also because not all operating conditions can be reached safely. Analytical and numerical tools can help to understand the influence of these parameters on the acoustic behavior and the system stability.

The first chapter of this document essentially contains analytical, numerical and experimental studies of the acoustics of the multiple injector combustor. This work is carried out to prepare hot fire tests. The main difference with previous experiments is that gaseous methane replaces hydrogen while liquid oxygen is still used as oxidizer. This changes the eigenfrequencies and directly influences the acoustic response of the chamber. This chapter also discusses some the natural hydrodynamic instabilities of the propellant streams. Eigenfrequencies and corresponding pressure distributions are predicted with respect to the injection conditions. The influence of the methane injection velocity and temperature on the system response is investigated to determine injection conditions which might generate sensitive flames. Combustion instabilities feature nonlinear phenomena so it may be relevant to study the response of the system to different types of modulation. Chapter I also deals with this topic. A wave train modulation is defined and an impulsive excitation system based on laser break-down is considered. This last method is tested in a small scale laboratory chamber.

The second chapter presents an initial set of experiments carried out in the low pressure range $p = 0.9$ MPa. The objective is to explore different operating points to find the most resonant operating conditions. Operating points are characterized by different methane injection velocities and temperatures. It is known that these two parameters strongly modify the flame structure. Hot-fire tests aim at investigating their influence on combustion receptivity to external excitation. Optical imaging is used

to examine the flame structure and dynamics in the absence or in the presence of modulation. Strong interactions were not observed previously and it is therefore interesting to see how the flame structure is influenced by the transverse acoustic mode. Twenty four tests of 30 seconds are carried out at 0.9 MPa with three coaxial injection elements. The acoustic modulator has been notably improved and methane is used as fuel. Digital data processing is used to characterize the modifications induced on the flames and specifically examine possible coupling between the pressure and heat release fluctuations.

The third chapter describes tests carried out at intermediate and high pressures and the number of injectors is changed from three to five. The mass flow rates are also increased in the same proportions and correspondingly the power level is augmented. These pressures are closer to those prevailing in real devices (in excess of 10 MPa in the Vulcain engine). It was also reasoned that the augmented power level could lead to a stronger response of the flame to the imposed perturbations. The power density remains however much lower than that found in the real engine which is typically of the order of 50 GW m^{-3}. This extreme value cannot be reached in laboratory scale facilities but the influence of the pressure and the global power on the acoustics and flame stability is a field of interest. Chapter III describes results obtained during the high pressure hot fire tests with a new injection head equipped with five coaxial elements, and the chamber pressure is increased to 3 MPa. The influence of the mixture ratio E and the momentum flux ratio J on the flame structure and on its sensitivity to external acoustic modulation is investigated.

A few tests are also carried out at 1 MPa with only two injectors. These injectors are separated by a large distance and do not interact. This test is used to see if flame interactions intervene in the coupling process or if the coupling can be observed when the transverse mode interacts with an isolated flame. All the previous tests have been carried out with at least three flames as close as possible from each other. The modulation effect on isolated flame has never been observed.
The high end of the pressure range is also explored in Chapter III with a few hot fire runs at 6 MPa. This pressure exceeds the critical value for oxygen which is 5.04 MPa. Injection conditions are in this case transcritical because the injection temperature of oxygen of 80 K is below critical ($T_c(LOx) = 154$ K) while pressure is above critical. The influence of the transcritical oxygen on the flame structure is investigated.

Simulations and modeling

Chapters IV and V are essentially concerned with the numerical simulation of high frequency combustion oscillations. This is envisaged in the framework of LES. This choice is made because LES is well suited to the numerical description of processes in which turbulence and unsteadiness play a major role. The problem at hand cannot be considered with RANS methods which essentially provide steady average fields of the flow variables. This is clearly inadequate in problems where the nonsteady combustion process constitutes the driving mechanism.
In LES, the large scales are resolved while the small scales are modeled. This constitutes a compromise between the cost in terms of computational resources and precision of the simulation. While LES is the

appropriate framework for the numerical investigation of combustion instabilities, it is important to acknowledge the many difficulties which will have to be overcome to obtain a high fidelity description of the process in the case at hand. At this point, it is sufficient to underline some of the main issues :

- One of the propellants is injected in a liquid form (under subcritical conditions) or in very dense form under transcritical conditions. LES of such two-phase or trancritical state injection is still in an early state of development and the methodologies are not yet proven and validated. The very large density gradients found in practice constitute a serious difficulty for most of the numerical tools.

- The combustion process in cryogenic propellant combustion is essentially nonpremixed and it takes place at very high pressure. Heat release is governed by the turbulent transport of reactants to the flame and the local rate of burning is dominated by the turbulent motion. The description adopted for this quantity is essential to the description of combustion instabilities. It will be specifically important to make sure that the model also correctly represents the effect of pressure.

- Typical situations involve multiple injectors (a real engine features more than 500 units). Very large resources will be needed for direct descriptions of full thrust chambers. Even the small laboratory scale experiment will need some fairly large discrete meshes to accomodate three injectors and their environment.

- External modulation in the transverse direction is required to examine cases where combustion is perturbed by an imposed excitation. Methods allowing this excitation have been developed but there is room for improvement.

- The acoustic response of the chamber has to be correctly simulated. It will be important to make sure that the computational method will not induce an excessive level of dissipation which could damp oscillations and deteriorate the predictive capability of the simulation.

- Impedance of the injection plane and of the exhaust nozzle have to be well described because they are directly involved in the process.

These many points can only be treated by a large scale program on the development of simulation tools. Research carried out in the present project is more limited but addresses some of the central issues. The developments are carried out by assuming gaseous injection to avoid the fundamental difficulties associated with the description of the liquid or transcritical phase. It is worth noting that an effort is now underway at CERFACS and EM2C to develop LES tools for transcritical combustion. Having made this important choice, it is nevertheless possible to look at cold flow configurations including multiple coaxial jets and use an external modulation to see how these jets respond to a transverse mode of oscillation. One may observe in this way effects of transverse acoustic modulation and study the influence of the modulation on mixing and motion.

Results of such simulations are reported in chapter IV where LES is used to calculate the dynamical response of three coaxial jets of gaseous oxygen surrounded by gaseous methane. The system is either modulated at the first transverse eigenfrequency or it develops freely. Chapter IV also includes

experimental results generated on the Mascotte facility under cold flow conditions (in the absence of combustion). Liquid oxygen is injected at low speed and is surrounded by a high speed stream of gaseous nitrogen. The experiment uses the new injection head equiped with five coaxial units. Experiments carried out at 3 MPa are used to obtain views of the five jets modulated transversally to investigate the effect of the acoustic perturbations on the multiple injection of coaxial streams. The study is specifically focused on the collective effect of the modulation on this configuration. The jet motion is investigated by backlighting the chamber and recorded with a high speed camera.
Simulations and experiments correspond to different operating conditions but have some common features explaining why they are reported in the same chapter.

Chapter V addresses the central problem of defining a model for the burning rate. The mode of combustion and modeling issues are first described. It is shown that the model should be designed to deal with nonpremixed combustion. The objective is to develop a simple model which can be integrated in the LES methodology, operate on a coarse grid and provide reasonable values of the volumetric rate of reaction. The heat release distribution obtained with this model should be concentrated around the flame position but needs to be sufficiently distributed to be computable on coarse grids which are typically used in LES. It would be possible to use methods based on the mixture fraction in combination with a probability density function to model combustion without an explicit expression for the burning rate. Since this quantity plays a central role in combustion instability, it has been found preferable to extract the volumetric reaction rate from the reaction rate per unit surface. The burning rate is then given explicitely and may be distributed around the flame. When the volumetric rate is integrated in the direction normal to the front one retrieves the local rate of combustion per unit surface. With this model, it is possible to account for combustion taking place at the subgrid level. This reconstructed burning rate model (RBRM) is perhaps more physical than the probability density function approach in which the reaction rate is a hidden variable. The RBRM may be used to locate the flame front and observe the flame interactions with the transverse acoustic mode. The relation between heat release and pressure fluctuations can be numerically investigated in a configuration close to that explored in the experiments. The derivation in chapter V relies on the assumption that chemistry is infinitely fast, an assumption which is fairly reasonable in the present context where burning takes place with pure oxygen. Calculations of a multiple jet configuration is used for illustrative purposes. Interaction with a transverse acoustic wave is also exemplified.

Chapter VI focuses on modeling issues. Analytical developments are motivated by experimental observations. The first model aims at describing how heat release fluctuations can be generated by the tranverse motion. This question was raised at the beginning of the High Frequency program and has been addressed by the team led by M. Habiballah at ONERA. This was also considered by Rey (2004). This issue is advanced in this chapter. An expression is proposed for the nonsteady heat release which involves the transverse velocity. It is argued that the direction of the velocity is also important and has to be included in this expression. The heat release thus also depends on the transverse velocity gradient and its spatial distribution is reversed every half period. This model provides a plausible interpretation of the behavior observed in the streak films reported in earlier works on high frequency instability (e.g. Tischler and Male or Barrère and Corbeau).

The second model deals with the influence of turbulent temperature fluctuations on the resonance sharpness of the system. There is some work in the previous literature on the influence of random excitations on acoustic instabilities by Clavin et al. (1994, Burnley and Culick (2000) but these do not deal with the influence of turbulence on the system resonance characteristics. The present analysis is motivated by observations made during the second set of experiments at 3 MPa. It was found that resonance was much weaker than under cold flow conditions. The system acts as if its quality factor were modified under hot flow conditions. It was then reasoned that this could be related to the temperature fluctuations in the system. These low frequency fluctuations may directly influence the eigenfrequencies. A model problem is devised to study this possibility. A direct simulation is carried out which shows trends similar to those found in the experiments. The model is also analyzed with the method of averaging described by Bogolioubov and Mitropolski (1962) and it is shown that in the presence of fluctuations the response amplitude is diminished. Some of the practical implications are discussed in this chapter.

Various parts of this work have been presented as conference papers or published as an article :

C. Rey, S. Ducruix, F. Richecoeur, P. Scouflaire, L. Vingert and S. Candel (2004) High frequency combustion instabilities associated with collective interactions in liquid propulsion. AIAA Paper 2004-3518. *Joint Propulsion Conference*, Fort Lauderdale, Florida.

F. Richecoeur, S. Ducruix, P. Scouflaire and S. Candel (2005) Experimental investigation of interactions between acoustics and combustion in liquid rocket engines. *40e colloque d'Aérodynamique Appliquée : Aérodynamique instationnaire*. Toulouse 21-23 mars 2005.

F. Richecoeur, P. Scouflaire, S. Ducruix and S. Candel (2005) Experimental investigation of high frequency combustion instabilities in liquid rocket engine. *52nd International Astronautical Congress*. Fukuoka, Japan.

F. Richecoeur, P. Scouflaire, S. Ducruix and S. Candel (2005) Experiments on high frequency combustion oscillations induced by transverse acoustic modulations. *20th ICDERS*, Montreal, Canada.

F. Richecoeur, P. Scouflaire, S. Ducruix and S. Candel (2005) Experimental investigation of high-frequency instabilities in liquid rocket engine. *Proceedings of 1st INCA colloquium*. S. Candel, M. Cazalens and F. Hirsinger, eds. pp. 229-237.

F. Richecoeur, P. Scouflaire, S. Ducruix and S. Candel (2006) Interactions between propellant jets and acoustic modes in liquid rocket engines : experiments and simulations. *AIAA Joint Propulsion Conference*, AIAA Paper 2006-4397. July 9-12, 2006 Sacramento, California.

F. Richecoeur, S. Ducruix, P. Scouflaire and S. Candel (2006) High frequency transverse acoustic coupling in a multiple injector cryogenic combustor. *Journal of Propulsion and Power 22 (4)* 790-799.

Part 1 : High frequency instability experiments

Chapter I

Combustion acoustics for LOx/GCH$_4$ operation

Abstract

Analytical and numerical analysis of the multiple injector combustor (MIC) acoustics are carried out. Previous experiments indicated that the MIC was a well suited tool to studies of high frequency combustion instabilities. It was however found important to replace the LOx/GH$_2$ fuel couple by LOx/GCH$_4$. The use of methane modifies the flame stability characteristics and changes the combustor acoustics. The acoustic eigenmodes of the combustor are predicted in this case by making use of analytical estimates and numerical simulation. A first approximation of the eigenfrequencies is provided by replacing the geometry by a rectangular box. Three dimensional solutions of the Helmholtz equation are used to take into account coupling effects associated with the auxiliary nozzle to obtain the pressure distribution in the chamber and accurate prediction of the eigenfrequencies. These results are compared with experimental data obtained in a previous test and are found to be in good agreement with measurements. Different types of modulation are theoretically and experimentally tested to generate a continuous modulation, a wave train or an impulsive excitation.

Résumé

L'acoustique du brûleur multi-injecteur (MIC) est étudié analytiquement et numériquement. Les campagnes d'essais précédentes ont indiqué que le MIC était un outil bien adapté à l'étude des instabilités de combustion haute-fréquence. Cependant il s'est révélé nécessaire de remplacer le couple oxygène liquide / hydrogène gazeux par oxygène liquide / méthane gazeux. L'utilisation du méthane influe sur la stabilité de la flamme et modifie le comportement acoustique de la chambre. Les modes propres du système sont prédits de façons analytique et numérique. Une première approximation des fréquences propres est obtenue en réduisant la chambre de combustion à une boîte rectangulaire. Numériquement, les solutions de l'équation de Helmholtz en trois dimensions sont utilisées pour obtenir une estimation plus précise des fréquences propres ainsi que le champ de pression associé. Ces résultats sont comparés avec les mesures expérimentales et sont en bon accord. Différentes sortes de modulations acoustiques sont testées théoriquement et expérimentalement pour générer successivement une modulation continue, un train d'ondes ou une impulsion.

I.1 Introduction

Previous experiments carried out by Rey (2004) to investigate high frequency instabilities relied on liquid oxygen and gaseous hydrogen combustion. A few final tests were performed with gaseous methane and were sufficiently conclusive to pursue high frequency (HF) instability studies with this new couple of propellants (LOx/CH_4). Three reasons motivate the switch from hydrogen to methane.
(1) With methane the chemical time is significantly increased. The corresponding flames are less stable because the reaction rate per unit is lower. Since chemical time is longer, combustion is more sensitive to external perturbations.
(2) With methane the gas phase density is increased. For the same oxygen quantity, the mass flow rate of gaseous fuel is reduced. At low injection speed, the hydrodynamic frequency, determined by a characteristic Strouhal number, is reduced. Under these conditions, the natural jet oscillation frequency, due to the high injection velocity, decreases to become of the same order of magnitude as the chamber eigenfrequency. The effect of external acoustic modulations may then be amplified by the natural jet dynamics.
(3) Fundamental studies carried out by Singla (2005) provide a good basis on cryogenic oxygen/methane flames at high pressure. This couple is envisaged for future launcher systems because it yields specific impulse values of the order of 350 s with a notably reduced tank volume for liquid methane storage. The possibilities of LOx/Methane engines are documented for example by Tamura et al. (1987), Kalmykov and Mossolov (2000), Pempie et al. (2001). Many studies have concerned injector design (Philippart and Moser 1988; Zurbach et al. 2002) and stability properties (Breisacher and Priem 1988; Jensen et al. 1990; Tamura et al. 1995; Takahashi and Katta 1999). In this context fundamental studies on the combustion stability of liquid oxygen and methane at high pressure are of industrial interest.

This chapter describes preliminary studies carried out before the hot fire test series. Analytical models are used to determine the order of magnitude of the main operating parameters and eigenmodes of the combustion chamber. Numerical simulations are carried out to obtain precise pressure field distribution and accurate eigenfrequencies. A set of experiments is then carried out in the laboratory to test the modulation system and study the possibilities of external excitation with high power laser pulses.
This chapter is divided in two main parts. The first deals with the acoustic characterization of the combustion chamber. The second describes results obtained in the laboratory experiments.

I.2 Multiple injector combustor eigenmodes for LOx/GCH_4 combustion

In the high frequency instability experiments to be carried out on the Mascotte facility operating with liquid oxygen and gaseous methane, the eigenmodes are determined by the chamber dimensions and sound velocity. It is first interesting to estimate the resonant frequencies analytically and then calculate more accurate estimates numerically. Results are then compared with the experimental data collected during the last tests of the last hot fire experiments carried out by Rey (2004).

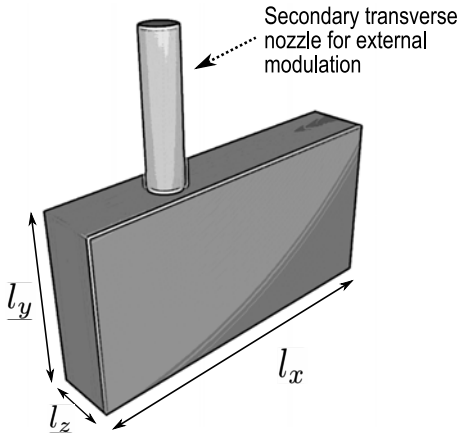

Fig. I.1: Schematic representation of the rectangular combustion chamber with the top modulation nozzle.

I.2.1 Theoretical estimates

This first basic analysis uses simplifying assumptions but aims at obtaining an order of magnitude of the eigenfrequencies. Experiments have to be carried out in the high frequency range, meaning that the transverse eigenfrequencies have to be above 1 kHz. In the present analysis the system features three injector elements and the mean chamber pressure is nominally set at 1 MPa.
The multiple element combustor is considered as a closed rectangular chamber without gas flow. Assuming that temperature in the chamber is uniform, the resonant modes of this cavity are determined by the standard relation:

$$f_{n_x,n_y,n_z} = \frac{\overline{c}}{2}\sqrt{\left(\frac{n_x}{l_x}\right)^2 + \left(\frac{n_y}{l_y}\right)^2 + \left(\frac{n_z}{l_z}\right)^2} \tag{I.1}$$

where n_x, n_y, n_z are modal integers and l_x, l_y, l_z represent the axial and transverse dimensions of the combustion chamber (Figure I.1). Sound velocity depends on the burnt gas composition and temperature through the relation

$$\overline{c} = (\gamma r T)^{1/2}$$

where γ is a function of temperature and composition, and $r = R/W$ is a function of composition. These parameters are calculated at equilibrium using the CHEMKIN library. It is assumed in what follows that the gas temperature is uniform inside the chamber.

I.2.1.1 Mixing temperature

The burnt gas composition depends strictly on the mixing temperature. As a first approximation, the mixing temperature is considered to be uniform in the chamber. Initially, n_{LOx} moles of liquid oxygen are introduced at a temperature $T_{LOx} = 85$ K, n_{CH_4} moles of gaseous methane are injected at a temperature $T_{CH_4} = 288$ K. n_{He} moles of helium are also introduced at a temperature $T_{He} = 288$ K to cool the lateral windows. The chamber pressure $p_c = 1$ MPa. Chemical conversion in the chamber takes place at constant enthalpy. It is first convenient to determine a mixture temperature

Test	m_{CH_4} (g.s^{-1})	U_{CH_4} (m.s^{-1})	n_{CH_4} (mol.s^{-1})	m_{LOx} (g.s^{-1})	U_{LOx} (m.s^{-1})	n_{LOx} (mol.s^{-1})	m_{He} (g.s^{-1})	J	E	n_{CH_4}/n_{LOx}	Tm (K)
1	60.7	100.4	3.79	61.6	2.7	1.92	7.5	7.88	0.99	1.97	198.98
2	61.7	102	3.86	63.3	2.8	1.98	7.4	7.56	0.98	1.95	197.49
3	61.6	106.5	3.85	60.1	2.8	1.88	7.5	8.24	1.03	2.05	201.28
4	60.4	104.9	3.78	61.6	2.8	1.93	7.5	8.00	0.98	1.96	198.76

Tab. I.1: Injection characteristics of oxygen and methane for the hot fire tests carried out by Rey (June 2003)

before chemical conversion.

$$\begin{aligned}(n_{LOx})_0\, H_{LOx}(T_{LOx},p_c) + (n_{CH_4})_0\, H_{CH_4}(T_{CH4},p_c) + (n_{He})_0\, H_{He}(T_{He},p_c)\\ = (n_{O_2})_m\, H_{O_2}(T_m,p_c) + (n_{CH_4})_m\, H_{CH_4}(T_m,p_c) + (n_{He})_m\, H_{He}(T_m,p_c)\end{aligned} \tag{I.2}$$

where H_k is the molar enthalpy of the k-th species.

The molar enthalpies of LOx and helium can be found in the tables compiled by Air Liquide (2002) :

$$H_{LOx}(85\,\mathrm{K}, 10\,\mathrm{bar}) = -13.179\,\mathrm{kJ\ mol^{-1}}$$

$$H_{He}(288\,\mathrm{K}, 10\,\mathrm{bar}) = -0.20768\,\mathrm{kJ\ mol^{-1}}$$

Equation (I.2) may be rearranged as follows :

$$\begin{aligned}&n_{LOx}H_{LOx}(T_{LOx},p_c) + n_{CH_4}H_{CH_4}(T_{CH4},p_c) + n_{He}H_{He}(T_{He},p_c)\\ &= \int_{T_{ref}}^{T_m}(n_{LOx}C_{p_{O_2}} + n_{H_2}C_{p_{CH_4}} + n_{He}C_{p_{He}})dT + n_{CH_4}H_{f_{CH_4}}(T_{ref})\end{aligned}$$

with

$$C_{p_{O_2}} = 33.464\,\mathrm{J\ mol^{-1}K^{-1}}$$

$$C_{p_{CH_4}} = 35.7\,\mathrm{J\ mol^{-1}K^{-1}}$$

$$C_{p_{He}} = 20.768\,\mathrm{J\ mol^{-1}K^{-1}}$$

Calculations are carried out under conditions used in the last four tests described by Rey (2004). The experimental conditions are summarized in table III.3. Temperatures are given in the last column of this table. The runs were carried out under similar conditions generating nearly similar mixing temperatures. In what follows, the initial mixture temperature is taken equal to 200 K.

n_{CH_4} (mol)	n_{O_2} (mol)	T_m (K)	p_c (MPa)
2	1	200	1

Tab. I.2: Initial conditions for equilibrium calculations.

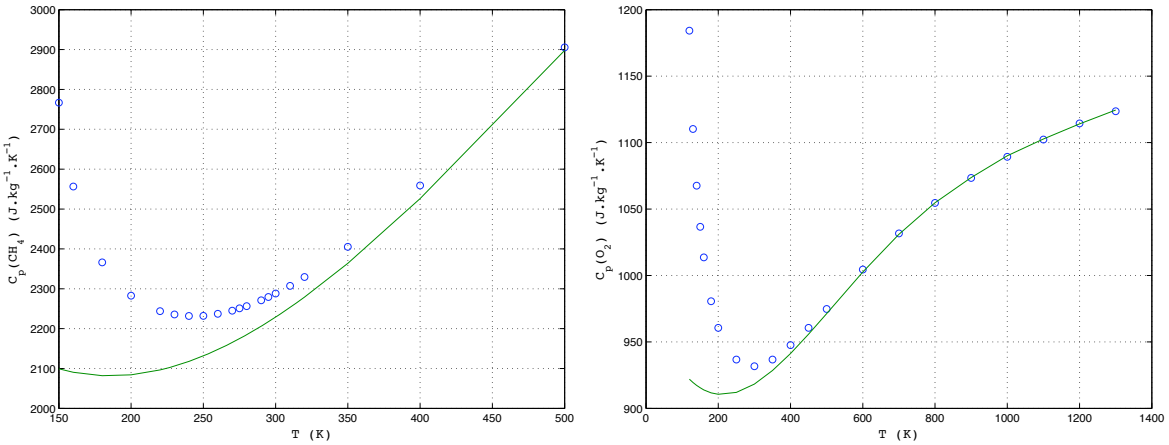

Fig. I.2: Methane (left) and oxygen (right) specific heats versus temperature (o : Air Liquide data, - : Imperial College table).

W (g mol^{-1})	γ	T_{ad} (K)	c (m s^{-1})	n_{CH_4} (mol)	n_{H_2} (mol)	n_{H_2O} (mol)	n_H (mol)	n_{CO} (mol)	n_{CO_2} (mol)
12.33	1.29	1164	1007	0.4	2.91	0.28	1.21 10^{-7}	1.48	0.12

Tab. I.3: Burnt gas characteristics calculated with the Imperial College thermodynamic tables

I.2.1.2 Burnt gas composition

The temperature of burnt gases at equilibrium is calculated with CHEMKIN. Thermodynamic functions for the various species are obtained from a table compiled at Imperial College for methane/oxygen mixtures.

Figure I.2 shows specific heats for methane and oxygen as a function of temperature. Data are well correlated in the high temperature range but there are some differences in the lower end of the temperature range. The effect of pressure is not taken into account and the specific heats are under-estimated in the low temperature range.
The values obtained with the Imperial College table are displayed in table I.3. Only the main species are included in this table and the adiabatic temperature is

$$T_{ad} = 1164 \text{ K}$$

The calculated sound velocity $c = 1007$ m s^{-1} is also close to that obtained by Rey ($c = 1018$ m s^{-1}).

The adiabatic temperature and gas composition are not measured in the hot fire experiments. There is a single thermocouple which measures the wall temperature during each run. It is only possible to compare the eigenfrequencies deduced from the adiabatic temperature and the measured resonant frequencies. Considering the assumptions used in the previous calculations, it is clear that (1) the temperature in the chamber is over-estimated. The heat losses are neglected and the specific heats are underestimated in the low temperature range. The adiabatic temperature probably overestimates the

l_y (cm) / Modes	16	17	18	19	20	21	22	23	24	25
1L (Hz)	1500	1500	1500	1500	1500	1500	1500	1500	1500	1500
2L (Hz)	3000	3000	3000	3000	3000	3000	3000	3000	3000	3000
1T (Hz)	3187	3000	2833	2684	2550	2428	2318	2217	2125	2038
2T (Hz)	6375	6000	5666	5368	5100	4857	4636	4434	4250	4080
1T1L (Hz)	3522	3354	3205	3074	2958	2854	2761	2677	2601	2532
1T2L (Hz)	4377	4242	4126	4025	3937	3859	3791	3730	3676	3627
2T1L (Hz)	6549	6184	5861	5574	5316	5083	4872	4681	4506	4347
2T2L (Hz)	7045	6708	6411	6149	5916	5708	5522	5354	5202	5064

Tab. I.4: Eigenfrequencies for LOx/GCH$_4$ combustion and l_x = 34 cm. The height of the test chamber l_y is varied between 16 and 25 cm.

burnt gas temperature by about 5%. (2) The spatial temperature variations in the chamber are not taken into account. The flames are stabilized in the center of the chamber and a temperature gradient is established in the cross flow direction. This will not strongly modify the eigenfrequencies but the spatial distributions of pressure eigenmodes will be influenced to a greater extent. (3) The external modulator, which comprises a secondary transverse nozzle located on the top of the chamber, is not taken into account. This changes the geometry, introducing additional modes and modifying those associated with the main chamber.
The previous analysis is only used to estimate the range of frequencies which have to be considered in the hot fire experiments.

I.2.1.3 Resonant frequencies

The resonant frequencies of the closed chamber are given by equation I.1. The chamber height l_y and length l_x are respectively 25 cm and 34 cm. Since the eigenmodes of the cavity depend on the geometry (more specifically the transverse modes depend on the height of the chamber), it is relevant to examine the influence of this dimension on the resonant frequencies. The values included in table I.4 correspond to l_x = 34 cm and l_y varying between 16 and 25 cm.
Two points may be examined : (1) The eigenfrequency of the first transverse mode has to be in the range accessible with the toothed wheel modulatior (TWM), and (2) The different modes must be clearly separated. The first two transverse modes are designated as 1T and 2T, and their frequency is compared with that of other eigenmodes in Tab.I.4 for different values of l_y. These frequencies may be compared to those which can be reached by the modulator which is equipped with a fifty tooth wheel. At 3600 rpm it generates a 3 kHz excitation. This constitutes a maximum frequency for safe operation of the modulator. The frequency of the second transverse mode 2T is twice that of the first transverse mode and cannot be reached with the TWM but the frequency is too close to the 1T1L mode which couples transverse and longitudinal oscillations. With the current dimensions of the test chamber (l_x = 34 cm, l_y = 25 cm), the first transverse mode is easily excited and its frequency remains relatively far from other eigenfrequencies. The separation between different eigenfrequencies is of the order of 500 Hz. The previous estimates of eigenfrequencies serve as guidelines. A more precise determination

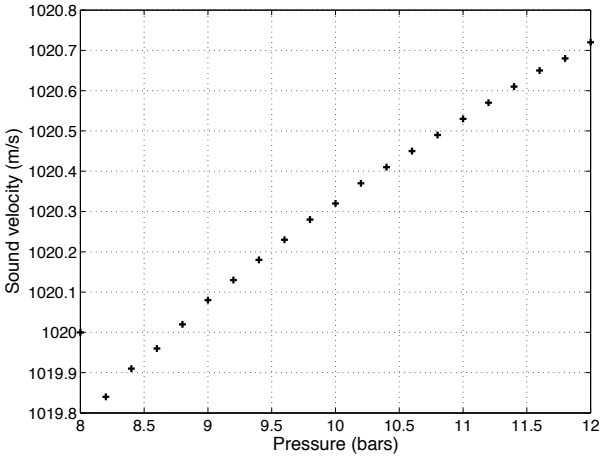

Fig. I.3: Influence of the chamber pressure on the sound velocity in the hot gases. As pressure increases, the equilibrium composition is shifted to a more complete state of reaction and the temperature increases.

of these frequencies will be obtained experimentally by submitting the chamber to a linear frequency ramp.

I.2.2 Effect of operating parameters on eigenfrequencies

I.2.2.1 Influence of the chamber pressure

Due to the secondary nozzle of the MIC and the fluctuation of flow rate imposed by the TWM, the mean pressure in the chamber cannot be accurately determined but takes values between 0.9 and 1 MPa. The eigenfrequencies are calculated by making use of the speed of sound in the hot gases which depends weakly on the pressure. It is relevant to examine the influence of a mean pressure variation around 1 MPa. This effect is illustrated in Fig.I.3 which indicates that the influence of pressure on the sound velocity is negligible with a variation of less than one meter per second for a pressure variation of 0.4 MPa. Even if the chamber parameters are slightly different from one run to the other, the sound speed will be nearly constant and the resonant frequencies will be essentially unchanged.

I.2.2.2 Influence of the mixture ratio

The mixture ratio E is conventionally defined as the ratio of the oxidizer to fuel mass flow rates : $E = \dot{m}_{LOx}/\dot{m}_{CH_4}$. The influence of this quantity on the adiabatic temperature and on the sound speed is shown in Fig.I.4. Previous experiments were carried out for $E = 1$ at 1 MPa (Rey 2004), the eigenfrequencies obtained are presented in Fig.I.5(b). They can be correlated with the analytical estimates shown in Fig.I.5(a). Theoretical and experimental results are in good agreement in this case.

The first peak obtained analytically corresponds to the first longitudinal mode which is also the first eigenmode since the length l_x is the largest of the chamber dimensions. The corresponding eigenfre-

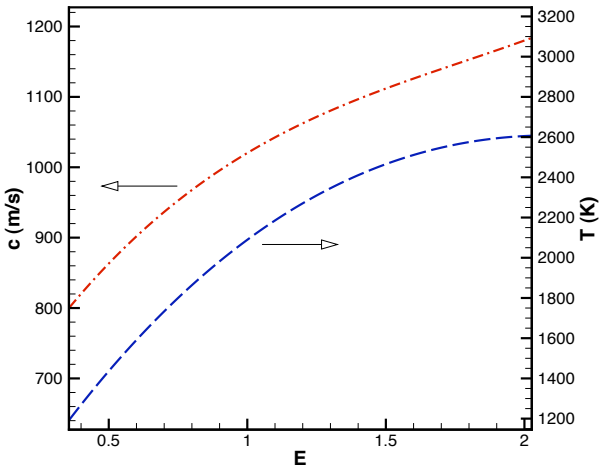

Fig. I.4: Sound velocity and equilibrium temperature calculate for different mixture ratios.

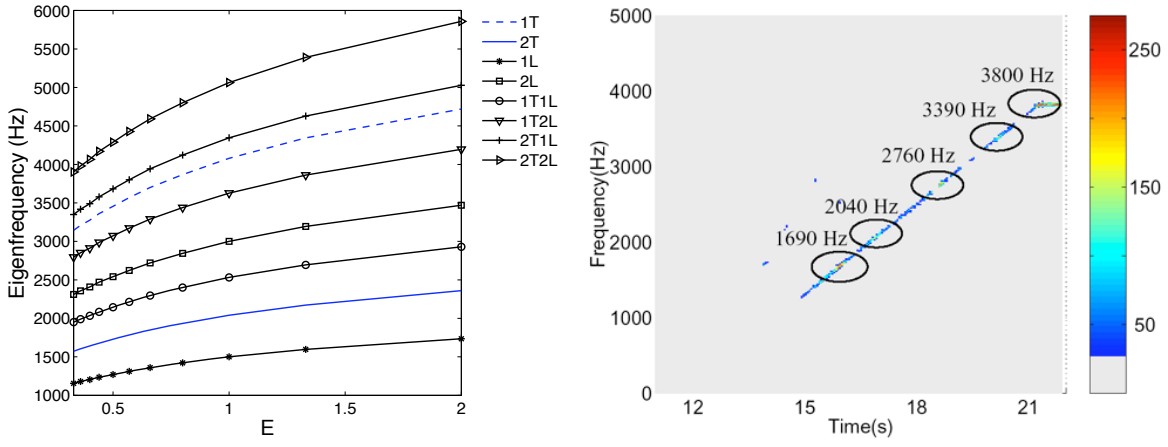

(a) (b)

Fig. I.5: Eigenfrequencies of the multiple injector combustion (MIC) for LOx/GCH$_4$ operation : (a) Analytically determined eigenfrequencies versus the mixture ratio E, (b) Experimental eigenfrequencies for $J = 8$ and $E = 1$.

quency estimate is 1.5 kHz. The experiment shows that the first peak is located at 1680 Hz. While some error can be expected from the analytical model, the difference of 180 Hz between theory and experiment is relatively large. Further numerical calculations presented in the next section indicate that the 1680 Hz eigenmode cannot be determined analytically without considering the secondary transverse nozzle. This resonance corresponds to a coupling between the combustion chamber and the auxiliary nozzle. Analytically, no peak can be found between the first longitudinal and the first transverse modes whereas experimentally, an additional eigenmode is detected at 1680 Hz. The intensity of the first longitudinal mode is significantly lower than that of the transverse modes due to the modulator position. It does not appear in the spectral map displayed in Fig.I.5(b) but is probably present around 1.5 kHz. Numerical simulation will be used to confirm this point.

Experimentally the first transverse mode is found at 2040 Hz. The analytical model predicts a frequency of 2038 Hz. Considering the strong assumptions used in the model, the small difference between predicted and measured values is extremely good. The adiabatic temperature calculated with a detailed equilibrium model provides suitable estimates of the sound speed and reasonable eigenfrequencies. The temperature gradient in the chamber only weakly changes these values. The main factor influencing the eigenmode structure is the chamber geometry and specifically the presence of an auxiliary nozzle. This will be taken into account in what follows.

I.2.2.3 First conclusions

Estimates obtained previously were deduced by considering that the multiple injector combustor MIC behaves like a closed cavity without any gas flow. The real system differs from this idealized description on the following points:

1. A mixture of gases flow in the chamber
2. Viscosity and heat conductivity have finite values and they affect to some extent the propagation of acoustic perturbations
3. The exhaust nozzle has a finite impedance
4. Temperature is not uniform

All these parameters were studied by Rey in his thesis and it was concluded that :

- Gas flow had a Mach number of 0.05 at 1 MPa and that its influence was negligible
- Viscosity and heat conductivity have a minor influence
- The nozzle output impedance does not influence the transverse mode and can be modeled by adding a virtual length to the chamber of a few centimeters to take into account the dynamics of the nozzle
- Three dimensional simulations including a nonuniform temperature field showed that the values of resonant frequencies were close to those calculated by assuming a uniform temperature field.

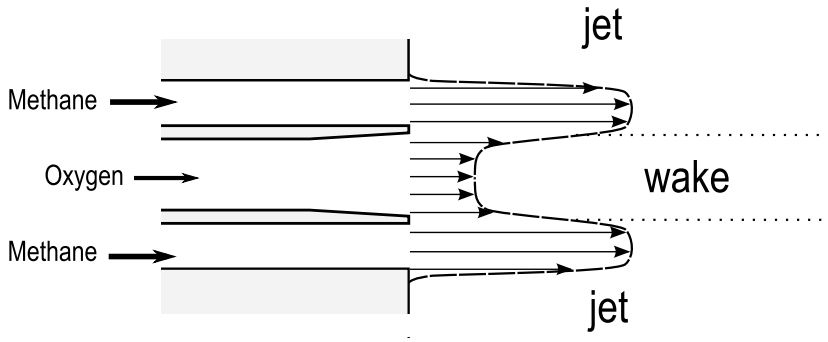

Fig. I.6: Flow velocity profile induced by a single injection element.

The eigenmodes of the test chamber were determined analytically for LOx/CH$_4$ propellants and for a range of frequencies between 1 to 6 kHz. It is found that the first transverse eigenmode can be easily excited around 2 kHz. This value was confirmed by previous experiments carried out in June 2003 by Rey. It is also found that the other modes feature eigenfrequencies far removed from those corresponding to the first transverse modes. This will greatly facilitate the identification of the transverse mode resonance.

The use of methane as propellant instead of hydrogen allows a decrease in the injection velocity for the same mixture ratio and correspondingly a reduction of the preferred hydrodynamic instability frequency of the gaseous jet. It will be possible to examine the expected coupling between hydrodynamic instabilities and acoustic modes in the test chamber, a point which is examined further in the next section.

I.2.3 Hydrodynamic instabilities and their coupling with acoustic eigenmodes

Hydrodynamic instabilities have been studied extensively in the case of non reactive shear flows in relation with observations of large-scale vortices. Fundamental experiments were carried out by Crow and Champagne (1971). Reviews of this topic are due to Ho and Huerre (1984) and Ongoren and Rockwell (1988). An initial velocity difference between two fluid streams produces a shear layer in which inflectional velocity profile gives rise to instabilities. This phenomenon appears for example in the case of a free jet or in the wake flow behind bluff bodies. It is logical to ask whether this type of instabilities can couple with the acoustic eigenmodes of the system inducing sustained oscillations of the flow. This question can be examined by considering the flow induced by each individual injector.

In the cryogenic combustion experiments, liquid oxygen injected by the central tube acts like a solid body due to its high density and low velocity. The methane stream injected in an annular fashion around the liquid oxygen shear behaves like a jet with respect to the outer region and features an internal wake constituted by the low speed liquid oxygen stream (Fig.I.6).

In the experiment of Crow and Champagne (1971) on air jets at Reynolds numbers between 100 and 10^4, it was shown that the amplitude of the hydrodynamic instabilities reaches its highest value for a Strouhal number ($St = fd/U$) equal to 0.3. This defines the preferred mode of instability of free jets.

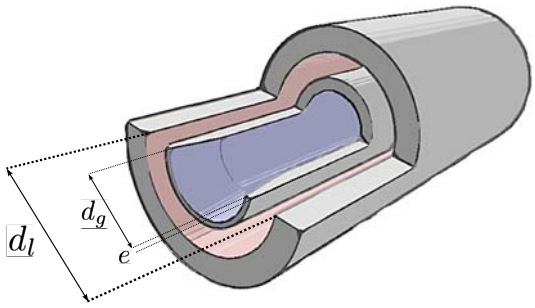

d_g (mm)	d_l (mm)	e (mm)
2.9	7	0.3

Fig. I.7: Geometrical characteristics of a typical injector used in the low pressure (p = 1 MPa) experiments.

Instability	Experimental Strouhal	f_p (Hz)
Jet	0.3	4660
Wake	0.194	3017

Tab. I.5: Theoretical frequencies of hydrodynamic instabilities of a methane jet introduced at U = 100 m s^{-1} (E=1) trough a nozzle of hydraulic diameter d_h = 6.43.

In the case of wakes behind various type of bluff bodies Ongoren and Rockwell (1988) indicate that the characteristic Strouhal number of such flows is around 0.194. Effects of sub-harmonic, harmonic and super-harmonic excitations of the flow are also examined in the same reference. These references and many others indicate that the Strouhal numbers takes values between 0.1 and 0.5. It is natural to examine possible hydrodynamic instabilities of the cryogenic propellant jets by considering jet and wake flow instabilities of the compound stream formed by the coaxial injection represented schematically in Fig.I.6. This yields an interval of sensitive frequencies and makes the predictions somewhat uncertain.

The geometry of a single element injector is given in Fig.I.7. Using a jet Strouhal number of 0.3 to determine jet mode instabilities and a value of 0.194 for the internal wake instability one finds the frequencies gathered in Table I.5. The liquid phase is considered to form a solid body surrounded by a stream of methane having a hydraulic diameter d_h such that $d_h = \sqrt{d_g^2 - d_{liq}^2}$.

The estimated frequencies are not far from those of transverse acoustic modes. One may try to refine the Strouhal number values by taking into account the strong variations in density in the vicinity of the propellant jet as was done by Trouvé et al. (1988). However, this will not be pursued here because the information on compound flows of the type envisaged in his study is incomplete.

This short analysis of the hydrodynamic instability of the injected propellant stream is aimed at examining if there is a possibility of coupling hydrodynamic instabilities and acoustic eigenmodes. A hydrodynamic oscillation may arise at one eigenfrequency and contribute significantly to the unstable behavior of the system. When E decreases, the eigenfrequencies increase and hydrodynamic frequencies decrease which make this coupling likely as shown in Fig.I.8. The transverse acoustic eigenfrequencies and the wake and jet preferred mode frequencies are plotted as a function of the

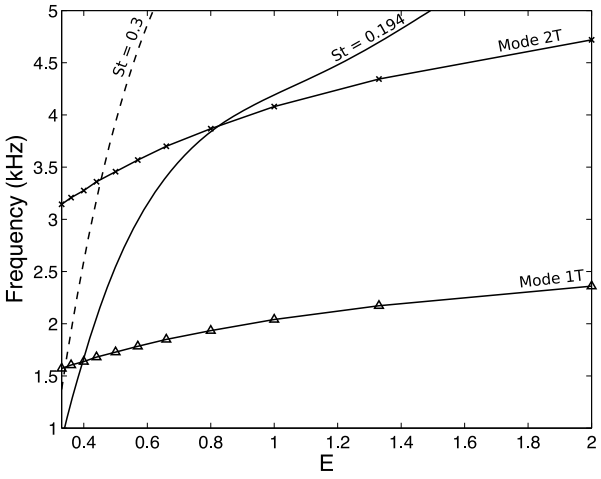

Fig. I.8: 1T and 2T eigenfrequencies and hydrodynamic instability frequencies calculated for a Strouhal number of 0.194 (preferred oscillation mode of a wake) and a Strouhal number of 0.3 (preferred oscillation mode of a jet) versus the mixture ratio for LOx/CH_4 combustion.

mixture ratio E. Strong coupling can be expected at the crosspoints of these two families of curves. Considering the preferred mode of oscillation in a wake ($St = 0.194$), the two types of instabilities may couple to enhance unstable behavior of the chamber for $E \simeq 0.4$ (1T acoustic eigenmode) and for $E \simeq 0.8$ (2T acoustic eigenmode). This analysis indicates that it may be useful to vary the methane injection velocity keeping the oxygen velocity constant in order to increase or decrease the mixture ratio E. However, a variation of E induces a variation of the total flow rate and corresponding a change in the chamber pressure. The experiment will be carried out with always the same output nozzle so E can only vary in a limited range of values to maintain the chamber pressure around the nominal value. One may choose to scan a mixture ratio of 0.5 to 2 so that the pressure in the chamber will only change from 0.85 to 1.1 MPa.

I.2.4 Numerical analysis of the chamber acoustics

I.2.4.1 Objectives

The analytical model exploited previously has provided reasonable estimates of the transverse mode eigenfrequencies. It has however two limitations.

First, the geometry of the chamber is simplified and the presence of the auxiliary nozzle is not taken into account. The coupled acoustics of this element when it is connected to the main combustor cavity can be analyzed with some standard analytical methods as illustrated by Candel and Poinsot (1987) and exploited by Rey (2004) to optimize the secondary nozzle length. Work along these lines has also been carried out by Cheuret (2005). Analytical results can be used to show that the most effective acoustic coupling between these two cavities occurs when the auxiliary nozzle dimension is half of

the combustor height. A strong coupling between the chamber and the nozzle is required to generate high amplitude pressure waves in the chamber but this coupling also modifies the eigenmodes. The coupling between the cavities is studied in this section by three dimensional numerical calculations of the system eigenmodes.

Second, the analytical model gives accurate eigenfrequencies but the corresponding pressure distributions are approximate. The 3D simulation provides the exact pressure maps corresponding to different eigenmodes. This can be used to understand how the coupling between the chamber and the transverse nozzle modifies the pressure distribution. This information will be essential in the interpretation of experimental data.

I.2.4.2 Simulations

The calculations are based on a finite element method discretizating the Helmholtz equation

$$\boldsymbol{\nabla} \cdot (c^2 \boldsymbol{\nabla} p') + \omega^2 p' = 0$$

together with homogeneous boundary conditions such as a null acoustic pressure or a null acoustic normal velocity. This eigenvalue problem is treated with the MESA-3D code developed at EM2C (Nottin 2002). The nozzle is treated as a rigid wall because it was shown previously (Rey 2004) that this has only a minor effect on the transverse mode eigenfrequencies and pressure distribution.

The mesh includes the chamber and the secondary nozzle. The boundaries are treated as rigid walls with null velocity. The temperature is considered to be uniform and equal to the previously calculated adiabatic values (Fig.I.4). The calculated frequencies are shown in Fig.I.9 for different mixture ratios E and the pressure distribution corresponding to the three first modes are plotted in Fig.I.10 for one value of the mixture ratio (E=0.6).

As observed experimentally, an additional mode is generated between the first longitudinal and first transverse modes. Its structure is quite similar to that of the first transverse mode. It involves the side nozzle and the main chamber and features a coupled motion in these two cavities. The frequency of this mode is slightly overestimated compared to the experimental result. The difference is probably due to the simplified boundary condition at the output of the secondary nozzle. Simulations without the secondary nozzle do not feature this mode. The first longitudinal and transverse modes have standard structures. Experimentally, strong interactions have been observed between acoustics and combustion for the intermediate and first transverse modes.

I.3 External excitation systems

It would be interesting to trigger a high frequency instability in the multiple injector combustor (MIC) and analyze natural oscillations but this could not be obtained. This is so because the power density in the test chamber is much lower than that characterizing the real engine. The test chamber also features larger acoustic losses associated with the large lateral wall areas. In a relatively thin rectangular chamber of the type used in the present experiments the lateral surface to volume ratio $S/V \sim 2/e$

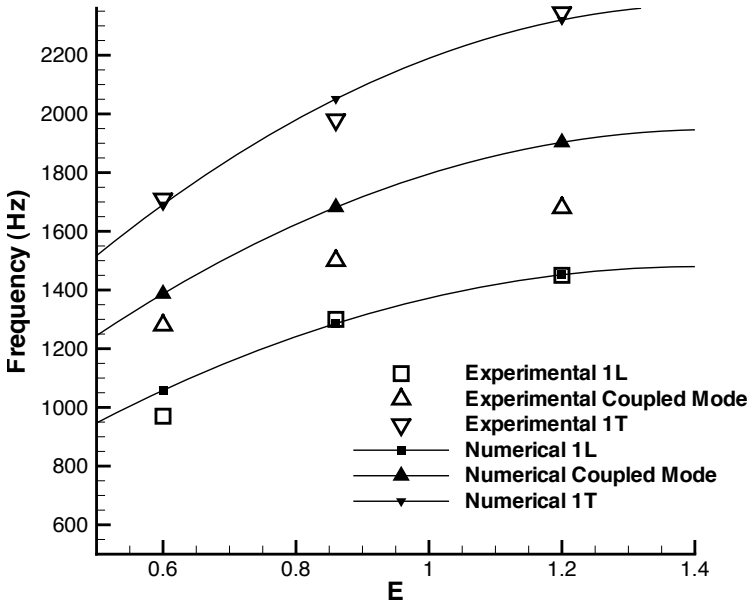

Fig. I.9: Experimental and numerical eigenfrequencies of the Mascotte combustion chamber. Experiments carried out in September 2004 (presented in the next chapter) correspond to three different operating points featuring three different values of E. Numerical simulations have been carried out for the same values of E. In each case, the three first eigenfrequencies are included in the diagram.

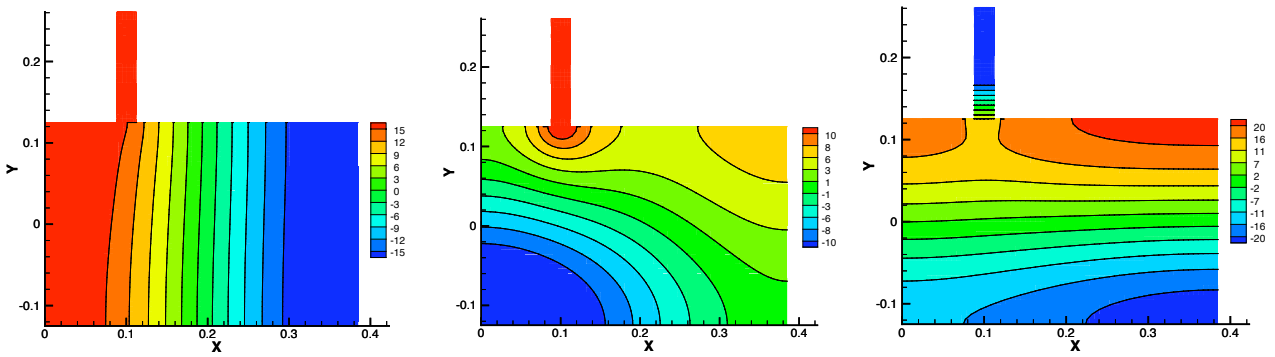

(a) (b) (c)

Fig. I.10: Structures of the three first acoustic modes in the combustion chamber calculated numerically for E=0.6 : (a) first longitudinal mode at 1452 Hz, (b) coupled mode at 1903 Hz, (c) first transverse mode at 2320 Hz.

where e is the distance between the lateral walls. In a cylindrical chamber this ratio is $S/V \sim 4/D$ where D is the chamber diameter. Since e is much smaller than D the surface to volume ratio is much larger on the model scale and the viscous losses at the lateral walls are augmented. Under these circumstances, one has to use external perturbations and examine the combustion response to these modulations. This may be achieved in various ways. One may try to disturb the combustion process in a linear way or to trigger a nonlinear response. It is here worth briefly considering these two types of excitations.

On one side, linear oscillations are characterized by a slow evolution and a relatively slow growth rate from an initially stable situation with no oscillation to an unstable operation where the oscillation amplitude reaches several percents of the mean pressure. In this situation, the system acts like a forced oscillator and its behavior may be roughly described by a second order equation

$$\frac{d^2p'}{dt^2} + 2\alpha\frac{dp'}{dt} + \omega_0^2 p' = f(t)$$

The system transfer function may be defined as the ratio of pressure to the external forcing. One objective in this case is to find conditions under which a linearly stable system may become unstable. One necessary condition is that the energy gain must exceed the energy losses. Examples of such instabilities observed in real engine studies are discribed by Culick and Yang (1995).

Non-linear oscillations are usually triggered by a brief and intense perturbation generated in an initially stable engine. The amplitude of this type of perturbation may reach twice the mean pressure. If an oscillation arises the system is said to be dynamically unstable and safe operation is not guaranteed. One usually requires that the engine should be dynamically stable and this is verified by performing bomb tests. Linear and nonlinear instabilities may be observed in rocket motors and may be envisaged in the experimental program using two types of perturbation generators.

I.3.1 Continous wave modulation

Linear oscillations may be obtained by applying a constant excitation at the first transverse (1T) eigenfrequency of the cavity. A secondary nozzle is set at the top of the test chamber and is periodically opened by a rotating toothed wheel. A schematic representation of the set-up is shown in Fig.I.11. The rotation of the wheel is assured by a *Kollmorgen* synchronous motor which may operate at constant speed or may be accelerated at a constant rate. The position of the wheel relative to the secondary nozzle is given by a photodiode output square wave signal (0-5 V) indicating the presence of a tooth in front of the secondary nozzle output.
The excitation system was validated by Rey (2004). It was shown that the system could be used to generate oscillations with an amplitude of a few percent of the mean pressure in the chamber. It was found however that some design improvements were needed to get higher modulation levels. These improvements are considered in what follows.

The auxiliary nozzle comprises a converging section and a throat to maintain a pressure difference between the chamber and the atmosphere. Previous experiments on Mascotte showed that a significant amount of gas had to be evacuated by the secondary output in order to get a visible effect on the

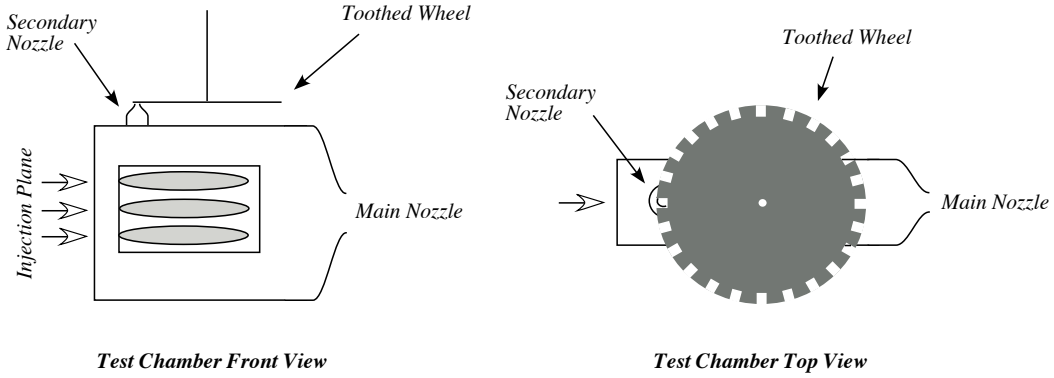

Fig. I.11: Lateral and top schematic views of the test chamber equipped with the toothed wheel modulator (TWM).

$\dot{m}_s/\dot{m}_m$ %	A_s^* (mm^2)	d_s^* (mm)	A_{s_e} (mm^2)	d_{s_e} (mm)
14	24.64	5.60	289.80	19.21
15	26.4	5.80	310.5	19.88
16	28.16	5.99	331.2	20.54
18	31.68	6.35	372.6	21.8

Tab. I.6: Secondary nozzle dimensions for different values of the mass flow ratio $\dot{m}_s/\dot{m}_m$.

flames in the chamber. The secondary nozzle inlet exhaust section areas (A_{s_e} and A_s^*) are designed to eject 15% of the main flow rate. Considering that the nozzle is blocked (the inside pressure is eight times the outside pressure)and operates in a quasi-steady regime the mass flow rate has the expression

$$\dot{m} = \Gamma \frac{p_c A^*}{(rT_c)^{1/2}}$$

where p_c and T_c are the pressure and temperature in the chamber respectively, A^* the throat area and Γ depends on the specific heat ratio γ of the gases flowing through the nozzle. Assuming that the gases exhausted through this element are similar in composition and temperature to those ejected trough the main nozzle, the ratio of the secondary over the primary flow rate is given by $\dot{m}_s/\dot{m}_m = A_s^*/A_m^*$. One may deduce A_s^* from A_m^*. Knowing the Mach number at the input of the secondary nozzle ($M_e = v/c = 0.05$), the secondary nozzle inlet area may be deduced from

$$\frac{A_{s_e}}{A_s^*} = \frac{1}{M_e}\left[\frac{2}{\gamma+1}\left(1+\frac{\gamma-1}{2}M_e^2\right)\right]^{\frac{\gamma+1}{2(\gamma-1)}} \tag{I.3}$$

Table I.6 gathers the dimensions of the secondary nozzle determined with $\gamma = 1.27$ (previously calculated with CHEMKIN for the burnt gases) for different values of the ratio $\dot{m}_s/\dot{m}_m$.
The toothed wheel was manufactured with 6-mm large teeth a size determined to accommodate the number of teeth (fifty) on a wheel with a reasonable diameter. The output diameter of the secondary nozzle is limited by this dimension. It was decided to use a nozzle evacuating 15% of the main mass flow rate.

The toothed wheel is used to generate a significant level of excitation in the test chamber. If the teeth are distributed over the whole circumference this will produce, a sinusoidal wave train and the system will be submitted to a permanent oscillation. If only a part of the circumference has teeth, the excitation is produced during a finite time and the system will be submitted to a finite duration wave train. A second wheel has been manufactured to test this type of excitation. The optimal number of teeth makes a compromise between the number of teeth required to bring the system to a sufficient amplitude of oscillation and the time required to dissipate the perturbation (assuming that the perturbation is attenuated by the system and not amplified). This may be examined by considering that the system reacts like an oscillator governed by a second order differential equation :

$$\frac{d^2x}{dt^2} + 2\zeta\omega_0\frac{dx}{dt} + \omega_0^2 x = F(t) \tag{I.4}$$

The system is excited at a frequency close to $f_e = 2$ kHz and the maximum number of teeth is $N = 50$. One rotation is executed in 25 ms. If the wheel has n teeth, the excitation time during one rotation will be n/f_e. The excitation function $F(t)$ is then defined by

$$\begin{cases} F(t) = A\sin(\omega_e t) & \text{for } 0 < t < \dfrac{n}{f_e} \\ \\ F(t) = 0 & \text{for } \dfrac{n}{f_e} < t < \dfrac{N}{f_e} \end{cases} \tag{I.5}$$

For a second order system, the resonance bandwidth Δf (typically of the order of 60 Hz in the present system) is linked to the damping coefficient α by the relation $\Delta f = \alpha/\pi$. In this specific case, $\alpha = 2\omega_0\zeta$ which yields

$$\zeta = \frac{\Delta f \pi}{2\omega_0} = \frac{\Delta f}{4 f_0}$$

Equation I.4 can be solved numerically by replacing the second order differential equation by a first order system. If a new vector (X, Y) is defined such that $X = x$, the second order equation I.4 is similar to the first order system

$$\begin{cases} \dfrac{dX}{dt} = Y \\ \\ \dfrac{dY}{dt} = -2\zeta\omega_0 Y - \omega_0^2 X + F(t) \end{cases} \tag{I.6}$$

with $X(0) = 0$ and $Y(0) = 0$. This system is solved numerically for increasing values of the number of teeth n. The response of the system changes with n. For $n \leqslant 6$, the excitation does not reach a suitable level and the oscillation amplitude drops quickly. For $n \geqslant 6$, the level of excitation is sufficient but the perturbation does not completely vanish after one rotation of the wheel. Figure I.12 shows the excitation and response signals simulated for the duration of one rotation of the wheel (i.e. 0.025 s for a 2000 Hz excitation) with $n = 6$. The excitation function is given by Eq. I.5 which generate a sinusoidal signal during six periods before vanishing. In the response signal, the oscillation amplitude increases while the excitation is on and then decreases exponentially. A wheel with $n = 6$ constitutes a compromise between the duration of modulation and the time left to dissipate the perturbation.

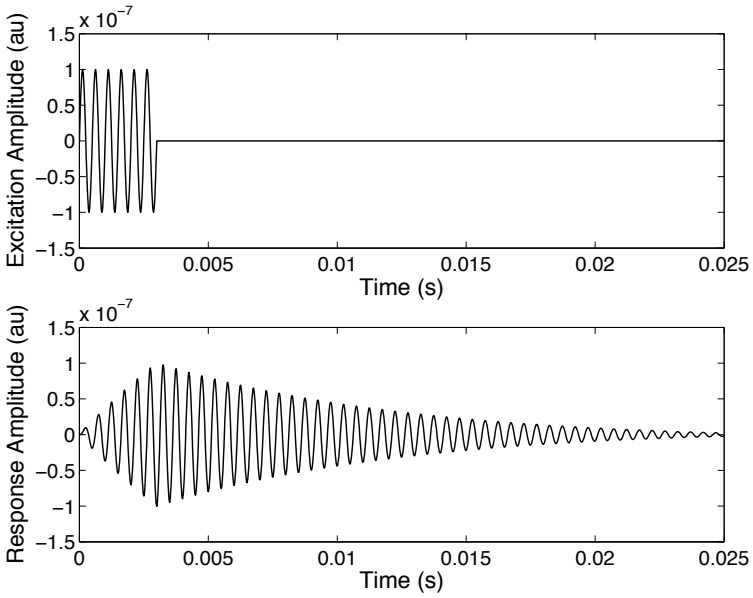

Fig. I.12: Numerical determination of the optimum number of teeth for the partially toothed wheel : excitation signal for one rotation (top), second order system response for one rotation (bottom).

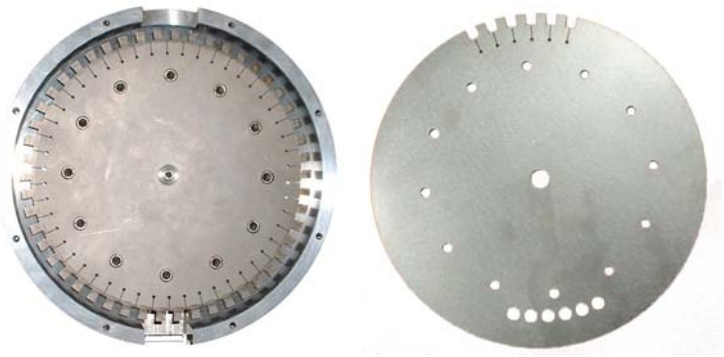

Fig. I.13: The fifty-tooth wheel (Ø185 mm, left) and the six-tooth wheel (Ø185mm, right)

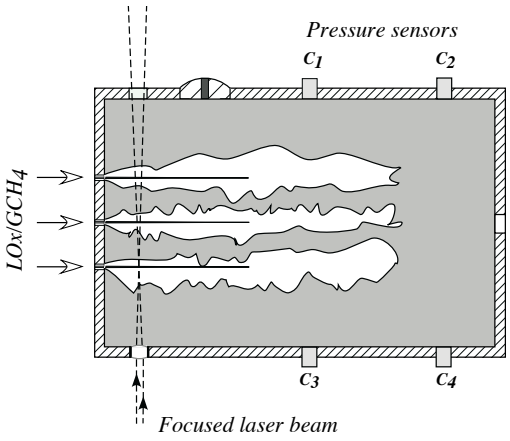

Fig. I.14: Mascotte test chamber designed for laser beam spark perturbation. The laser beam coming from the bottom is focused on the LOx nozzle to generate a shock wave and induce oxygen vaporization.

I.3.2 Impulsive excitation

Nonlinear instabilities appear when a brief and intense pulse drives an initially stable system into sustained oscillations. The sudden release of energy associated with a bomb explosion generates a high amplitude pressure wave required to induce such phenomena. Bomb tests are used in practice to rate the stability of real engines and verify that they are dynamically stable. Because of safety constraints, it is difficult to envisage bomb tests in the Mascotte facility. One may however use an optical access to bring energy locally by focusing a laser beam and induce a pressure pulse. If the laser beam is focused on the oxygen jet, vaporization of a small amount of LOx may also increase the local combustion rate. The large amount of energy released in a short amount of time (10 ns) generates a shock wave in the near vicinity of the focal point and this may be sufficient to perturb the system impulsively. These two possibilities are considered successively.

I.3.2.1 Enhancement of combustion by LOx vaporization

A laser pulse is provided by a Nd:YAG laser tuned at 532 nm. This system delivers an energy of 250 mJ/pulse at a frequency of 10 Hz. Figure I.14 shows how the laser beam is focused in the lower part of the test chamber in order to vaporize an amount of liquid oxygen. A 125-mm focal lens protected by a quartz window is set up in the bottom wall to focus the laser in front of the first injector. A second window on the opposite wall is used to evacuate the the beam.
An elementary analysis may be used to estimate the amount of energy released by the growth of the combustion rate due to the laser beam energy. At a pressure of 1 MPa the vaporization of oxygen takes place at 90.2 K, the vaporization enthalpy of liquid oxygen is $h_{vap}(O_2)_{90.2\,\mathrm{K}} = 12.16\,\mathrm{kJ\ kg^{-1}}$ and the specific heat is $c_p(LOx) = 95.5\,\mathrm{J\ kg^{-1}K^{-1}}$ at 80 K and 1 MPa. So the enthalpy variation from

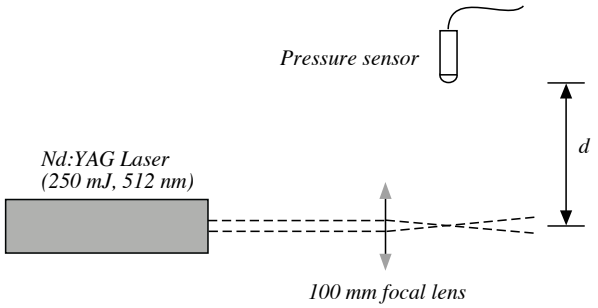

Fig. I.15: Schematic view of the laboratory laser beam focusing experiments (the distance d is varied from 40 to 100 cm).

the injection temperature (80 K) to 90.2 K may be estimated by the relation

$$\begin{aligned} \Delta h &= c_p(T_v - T_0) + h_{vap}(O_2) \\ &= 13.13\,\text{kJ kg}^{-1} \end{aligned}$$

Assuming that all the energy delivered by the laser pulse is absorbed by liquid oxygen, the mass vaporized by the energy E is $E/\Delta h$. The oxygen mass vaporized by the focused laser beam is $m_{vap} = 1.9\,10^{-5}$ kg. The energy released by combustion of 1 kg of oxygen reacting with methane generates $1.5\,10^7$ J, the energy released by the combustion of the extra vaporized oxygen is $E_{comb} = 285$ J. Since this amount of energy is released near one of the propellant jets (i.e. not on the symmetry axis of the chamber) it may be sufficient to trigger a transverse oscillation.

I.3.2.2 Energy released by a focused laser beam

When a pulsed laser beam is focused, a plasma is created near the focal point and a shock wave generated by the sudden energy deposition propagates outwards. Laboratory tests were carried out to determine the pressure amplitude which can be reached and its evolution with the mean pressure. A Nd:YAG beam tuned at 532 nm was focused by a 100 mm focal lens in ambient air, and a pressure sensor (*Kistler 701 A*) was positioned at different distances from the focal point to measure the overpressure generated by the spark (Fig.I.15).
The pressure signal recorded at an ambient temperature and pressure for several distances d between the focal point and the pressure sensor are plotted in Fig.I.16.
As expected the pressure amplitude decreases when the distance increases. For a distance from the focal point from 40 to 110 cm the pressure evolution can be fitted by a hyperbolic function "$1/x$" (Fig.I.17). Closer to the spark, the intensity of the pressure is so high that the sensor tends to oscillate at its eigenfrequency (70 kHz) making the measurement inaccurate.

I.4 Conclusion

The main part of this chapter deals with the acoustics of the multiple injector combustor fed with liquid oxygen and gaseous methane. The eigenfrequencies are calculated with analytical and numerical methods and compared with experimentally determined values. Results of simulations based on a

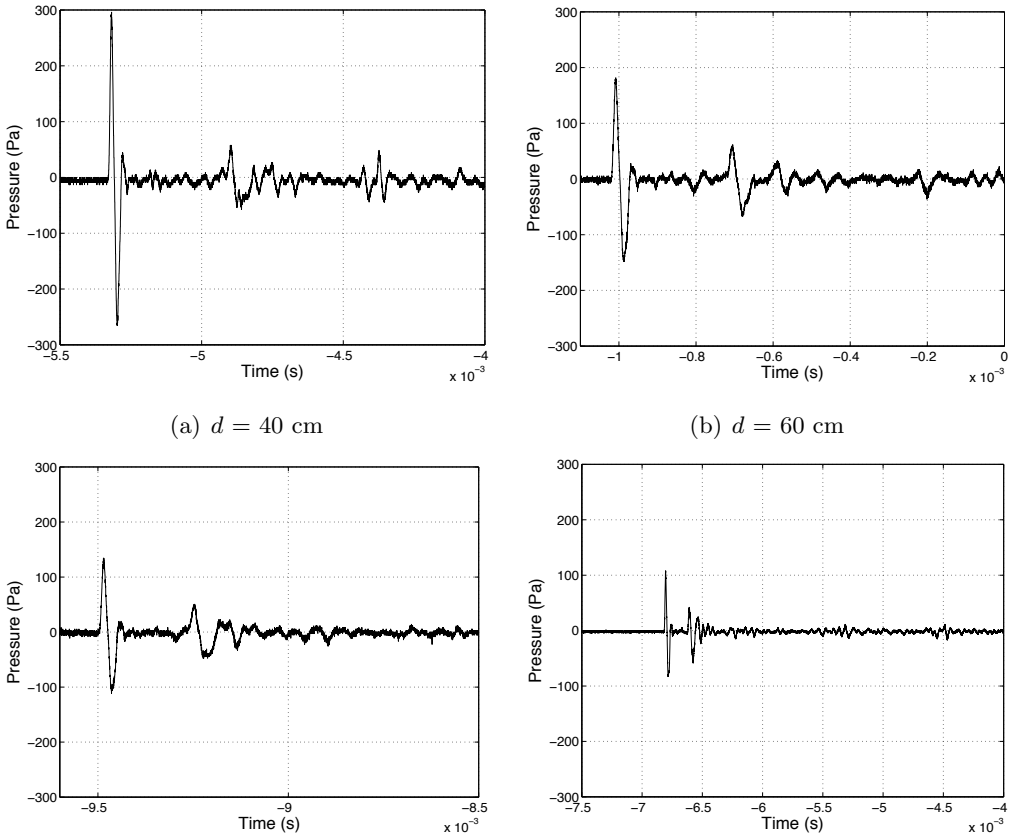

(a) $d = 40$ cm

(b) $d = 60$ cm

(c) $d = 80$ cm

(d) $d = 100$ cm

Fig. I.16: Pressure signals induced by a focused laser beam (Nd:YAG, at 532 nm releasing 250 mJ) in ambient air for different distances from the focal point

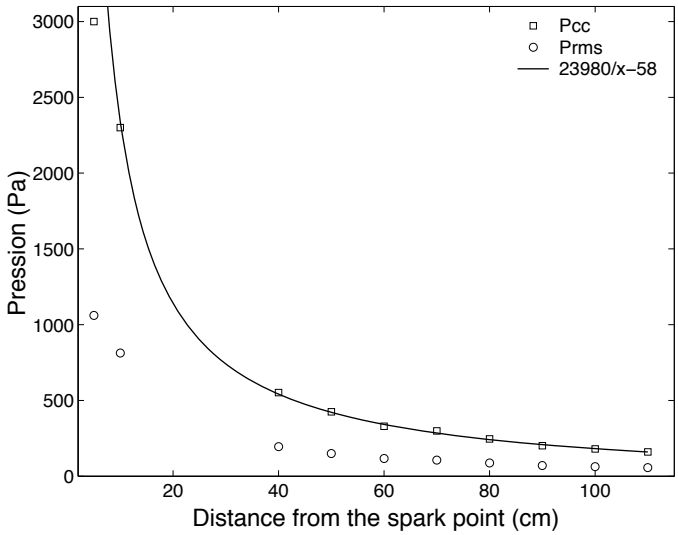

Fig. I.17: Peak intensity of the pressure wave generated by a focused laser beam as a function of distance from the spark. □ Peak to peak pressure, ○ Root mean square pressure, - hyperbolic curve fit.

three dimensional solution of the Helmholtz equation for a simplified geometry including the auxiliary nozzle are used to identify the various modes and determine the corresponding distributions of pressure. The chapter also contains a brief analysis of the possible coupling between acoustic resonances and hydrodynamic instability modes of the flow formed by a coaxial injector. It is shown that this possibility exists and that it may be investigated by changing the methane injection velocity. The external modulation of the multiple injector combustor is envisaged in the last part of this chapter. The toothed wheel modulator is presented and its characteristics are discussed. A novel method for inducing an impulsive excitation is explored. The method relies on a focused laser beam which is transmitted into the chamber through a taleral wall. This produces a short pulse of energy and induces a pressure perturbation which could be used to trigger instabilities.

Chapter II

Low pressure hot fire experiments

Résumé

Les instabilités de combustion haute-fréquence sont étudiées expérimentalement. La chambre de combustion fonctionne à une pression moyenne égale à 0.9 MPa et est alimentée en oxygène liquide et méthane gazeux à travers trois injecteurs coaxiaux. Les paramètres d'injection sont du même ordre de grandeur que ceux utilisés dans les moteurs fusée. Un modulateur externe est utilisé pour produire des fluctuations de pression dans la chambre. La résonance, obtenue pour des fréquences supérieures à 1 kHz, est caractérisée par une forte réponse en pression. Le système est ensuite modulé à la fréquence propre du premier mode transverse, précédemment identifié. La réponse des flammes et leurs structures sont observées à l'aide d'une caméra rapide et deux caméras intensifiées sensibles à la phase de la modulation. Lors d'une première série d'essais, les conditions d'injection sont systématiquement changées pour déterminer le point de fonctionnement générant les flammes les plus sensibles aux perturbations acoustiques. Un fort couplage est observé pour des conditions d'injection précises se traduisant par une spectaculaire modification de l'expansion de la flamme. L'émission naturelle des flammes augmente significativement lors du couplage et les thermocouples placés dans les parois de la chambre traduisent d'une forte augmentation de température. L'intensité de l'émission du radical OH* oscille transversalement, en phase avec les signaux de pression. Le comportement oscillatoire est également observé à l'aide de la caméra rapide qui met également en évidence la convection à basse fréquence de tourbillons réactifs en aval de l'écoulement.

Abstract

High frequency combustion oscillations are investigated experimentally. The combustor operates under moderately high pressure conditions (p_c = 0.9 MPa) and is equipped with three coaxial injectors fed by liquid oxygen and gaseous methane. Injection parameters are in the typical range used in rocket engines. An external modulator is used to generate pressure oscillations in the chamber. A strong pressure response is obtained when the process is resonant at frequencies above 1 kHz. The combustor is then excited at the first transverse eigenfrequency identified in a first step. The flame motion and response is observed with a high speed camera and two intensified CCD cameras recording phase conditioned images. In a set of experiments carried out on the multiple injector combustor, operating conditions were changed systematically to determine parameter ranges leading to combustion sensitivity to transverse excitation. Strong coupling is observed in this way with a spectacular modification of the flame spread. Emission from the three flames is notably intensified when this coupling occurs while thermocouples placed on the lateral walls detect a rapid increase in temperature. The OH* emission intensity which can be linked to the heat release rate is increased. A phase analysis indicates that the pressure and OH* emission oscillate transversally and in phase at the modulation frequency. This behavior is also observed with the high speed camera which also features enhanced reactive vortices convected in the downstream direction at a lower frequency.

II.1 Introduction

The previous chapter has focused on the multiple injector combustor acoustics and on the determination of resonant frequencies and modal structure when this device is fed with LOx and methane. The tools presented in the previous chapter are used in the present chapter to perform hot fire experiments at a moderately high level of pressure ($\sim$ 0.9 MPa). It is first worth giving some brief comments on the state of art in the field and explain the strategy adopted in the present investigation. We have already indicated in the general introduction that a substantial research effort has focused on instability mechanisms. Investigations have concerned fundamental instabilities of flames and combustion dynamics phenomena encountered in practical devices. Recent work has mainly focused on gas turbines of the premixed type with an emphasis on low frequency oscillations coupled by plane acoustic modes of the system. Model scale experiments have provided a large amount of data leading to a good understanding of the fundamental processes. In parallel, large eddy simulations have been developed to represent dynamical combustion effects and devise predictive tools. Less experimental work has been carried out on high frequency oscillations. Such instabilities are most often observed in rocket engines where they are coupled by transverse chamber modes but they also appear in annular gas turbine combustors. Most of the data in this frequency range were generated during the early development of rocketry where instability problems were continuously encountered and hampered many projects inducing serious development problems and some spectacular failures. Laboratory scale experiments date back to the late 60's and early 70's but a detailed characterization of the driving and coupling phenomena could not be carried out to completion because of limitations in experimentation, diagnostics and digital data processing.

Little progress has been made in this field because of a lack of fundamental information. It iss therefore timely to take a new look at the problem and use state of the art experimental tools in well controlled model scale experiments. It is sometimes felt that one cannot study high frequency instabilities outside real engines because engine conditions cannot be reproduced in model scale experiments. This mismatch between real and laboratory scale systems has been one important difficulty of experimental research and it is not overcome in the present study. One may however envisage to study some of the fundamental processes by suitably designing the experiment and properly choosing operating conditions and injection parameters. It is not possible to reproduce all the complexity of rocket motors but some of the essential aspects are conserved. To this purpose, the model scale combustion chamber is fed with real cryogenic propellants, it operates at an elevated pressure, injection conditions are in the range characterizing real engines. The injector elements are similar to those used in engines. The combustor geometry features well separated resonant modes and characteristic eigenfrequencies in the standard range where high frequency instabilities usually occur ($f > 1$ kHz). The present experimental design relies heavily on recent knowledge gathered on the processes of cryogenic propellant combustion. Operating conditions are deduced from those determined from these studies. The momentum flux ratio between gaseous methane and liquid oxygen is in the range corresponding to real engines. The flame lengths are typical of those found in practice ($l/d_{LOx} \simeq 50$ where l is the length and d is the LOx post diameter).

One idea explored in the present work is that collective interactions constitute a fundamental source of combustion instability. This is supported by recent experiments on premixed flames which indicate that strong sources of instability are most often related to interactions. It has been shown for example that flames interacting with walls can become a powerful source of instability (Schuller et al. 2002). Other experiments on flame/flame interactions indicate that mutual flame annihilation can also constitute a strong source of self induced oscillations. One particular characteristic of rocket engines is their showerhead arrangement of reactant jets. The closely packed flame geometry produces interactions in the vicinity of the chamber back plane. Collisions between adjacent streams may enhance turbulence and augment the volumetric rate of reaction. There is a natural delay in this process and a possibility of tuning the collision process with one of the acoustic resonances. This is why one should examine collective effects involving more than a single jet. These fundamental effects have not been extensively investigated in the past or at least no conclusions were given on the possible collective effects of such arrangements of closely packed highly reactive jets.

Experiments are carried out on a multiple injector combustor (MIC) on the Mascotte test bench operated by ONERA. The combustor has been designed and manufactured in the year 2000 and was first used by Rey (2004) during his thesis.
The MIC backplane geometry takes into account the key parameters in multiple flame combustion. The distance between the injector elements has been minimized to increase interaction effects. Dimensions of the chamber have been chosen to dissociate the eigenmodes and locate the first transverse eigenfrequency around 3 kHz with GH_2 and 2 kHz with GCH_4. The combustor is equipped with pressure sensors, and large quartz windows have been incorporated to allow optical diagnostics. The toothed wheel modulator (TWM) was first tested during the two experiment sets conducted by Rey and proved to be a very efficient tool to generate high amplitude and well controlled pressure waves. The first experiments have been carried out with LOx/GH_2 and a three coaxial element injector. Various diagnostics were implemented and the data were extensively analyzed. Knowledge from these initial experiments has provided a basis for further investigations of high frequency instabilities in the multiple injector combustor. From these experiments it was possible to propose a mechanism leading to the instabilities (Rey et al. 2004). Conclusion of this work have been taken into account to modify and improve further experiments.

This has led to four main changes in the set up and in its operations. These modifications aim at increasing the pressure wave amplitude to observe stronger interactions between combustion and acoustics, and to enhance the flame sensitivity to external perturbations.

(1) Previous experiments showed that very high pressure amplitude fluctuations were needed to disturb the combustion process. It was concluded that the pressure level of oscillation had to reach 10% of the mean chamber pressure to generate strong modifications of combustion. The modulator operates most effectively when the relative position of the toothed wheel and the exit of the transverse nozzle are in close contact. To improve this point it was necessary to design a new wheel holder allowing high precision displacement with respect to the nozzle. A displacement of a few tenth of a millimeter of the relative position may compromise the level of modulation as demonstrated in what follows and

a careful control of this distance is essential.
(2) Hydrogen was changed to methane. Compared to hydrogen, methane is injected at a lower speed while keeping the mixture ratio in the same range. A lower injection velocity enhances the flame sensitivity to external perturbations and a coupling with hydrodynamic instabilities is possible as discussed in chapter I.
(3) Different injection conditions are tested in a systematic way to determine optimal conditions where the sensitivity is maximized. The corresponding effect is investigated by operating at three different injection velocities. The injection temperature may also modify the flame response to acoustic perturbation. Its influence on the response is also examined.
(4) The present investigation relies on some new optical diagnostics to describe the flame behavior under acoustic oscillations. A high speed camera and two photo multipliers give additional information on the flow dynamics and oscillatory motion of the flames. These diagnostics are used to increase the spatial or temporal resolution of the analysis. The intensified cameras provide high spatial resolution of the instantaneous flame structure but a limited time resolution. On the other hand the high speed films yield useful dynamic information on the evolution of the larger structures in the combustion region but small scale structures are not precisely described. The various diagnostics employed in the hot fire experiments provide complementary data which are globally analyzed to understand the dynamics of the combustion process.

The first section of this chapter describes the combustor and the external modulator. Geometrical dimensions, characteristic operating parameters, pressure sensors and optical diagnostics are described in detail.
Results of the first set of experiments are reported in the third section. The purpose of this study is to systematically investigate the effect of the injection parameters on the flame sensitivity. Three different injection velocities and two different injection temperatures are examined.
One operating point has been chosen to investigate the effect of a strong pressure modulation on the flame dynamics. Three tests are carried out in each case. A linear frequency sweep is aimed at identifying the first transverse eigenfrequency. A modulation free test provides a reference. A steady modulation is then used to study the coupling process.
Experimental data are discussed in the last section.

II.2 Experimental configuration

The experimental set-up involves three main elements :

- A combustion chamber and a cryogenic feed system
- An injector comprising three coaxial elements forming interacting jet flames inside the chamber
- An external source of modulation to excite one of the chamber transverse modes (the toothed wheel modulator, TWM)

The chamber has a rectangular section. Dimensions are $35\times25\times5$ cm^3. The upper and lower walls are respectively equipped with three and two cooled pressure transducers. The lateral side walls comprise

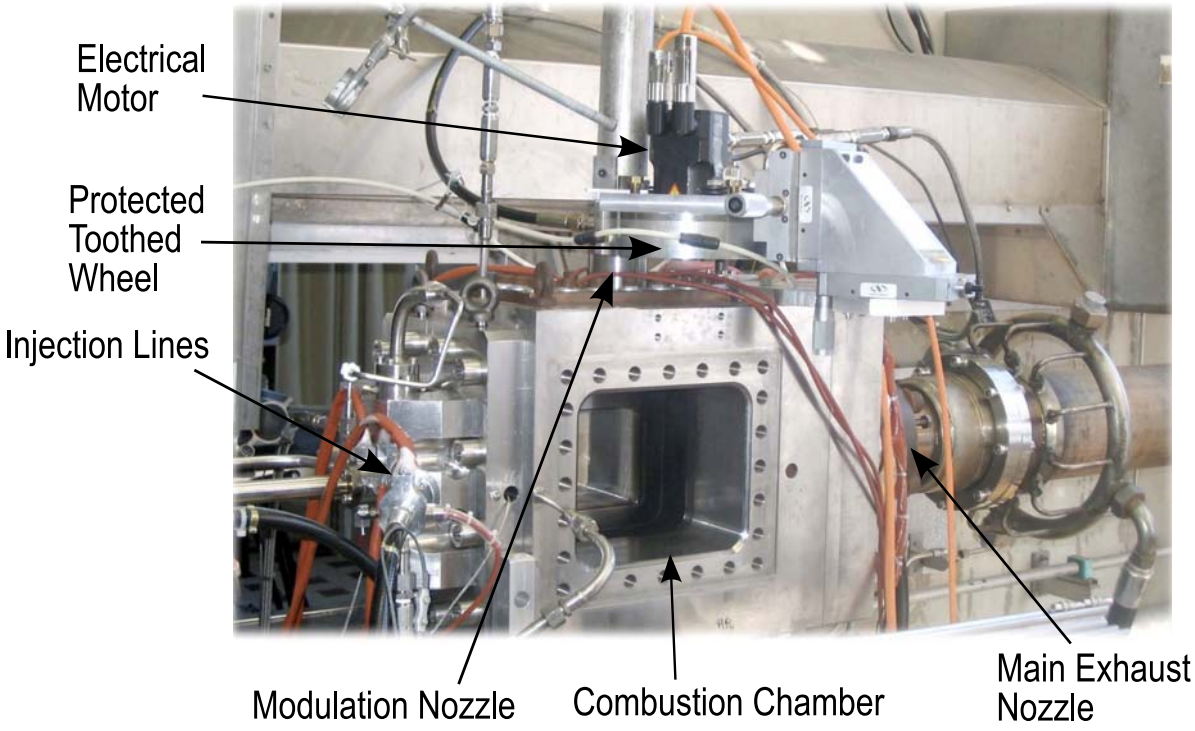

Fig. II.1: Photography of the Mascotte test bench.

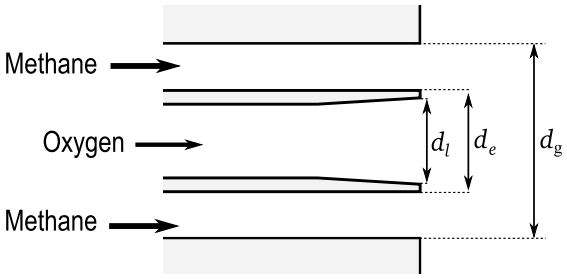

Methane injection temperature	d_l (mm)	d_e (mm)	d_g (mm)
280 K	2.9	3.5	7.0
180 K	2.9	3.5	6.5

Fig. II.2: Schematic of a coaxial element and characteristic dimensions with respect to the operating point.

transparent quartz windows (15×10 cm^2) allowing direct observation of the three flames in the visible and near UV range. The chamber ends with a sonic nozzle. The nozzle diameter is adjusted to reach the expected chamber pressure for the prescribed mass flow rates of oxygen and methane.
The chamber volume is relatively large to obtain a transverse mode in the proper frequency range (i.e. around 2 kHz). The power density is therefore not equal to that found in a practical devices but it is already sizable (see Chapter I). This could be augmented by increasing the number of elements and the mass flow rate of oxygen. This aspect is investigated in the next chapter with higher pressure and augmented mass flow rates and heat release.

The injector comprises three coaxial elements. Dimensions and schematic representation of these devices are given in the previous chapter. The distance separating adjacent elements is 17 mm. One would like to diminish the injector spacing to pack these elements more closely and reduce the inter-

action distance but there are mechanical constraints which could not be overruled. The methane flow velocity varies from 100 to 200 m s^{-1}. The momentum flux ratio between the gas and liquid streams is chosen in a range which is typical of real engines. Velocities outside the jets are admittedly lower than those found in practical systems because the available cross section is larger. However, the flame is located between the inner oxygen stream and the co-annular methane jet and it is only weakly influenced by the outer flow, at least close to the injector plane.

The modulation system is an essential element in this investigation. Combustion in the chamber is naturally stable. To observe combustion oscillations, the system has to be forced externally and a sufficient level of modulation is required to obtain an observable interaction with combustion. The modulator is used to identify the eigenmodes under hot fire operation (by exciting the system at different frequencies and observing the resonance) and it is then exploited to excite the system at a constant frequency.
The modulator comprises an auxiliary nozzle placed at 100 mm from the injection plate. The total size of this unit is 14 centimeter. This forms a cylindrical cavity which crosses the top wall and ends with a sonic throat. The nozzle throat is periodically blocked by a rotating toothed wheel. The modulation frequency is adjusted with the rotation speed between 0 and 4800 rotations per minute. This gives rise to mass flow rate fluctuations which constitute an intense source of sound. The gases exhausted from this nozzle are diluted by injecting nitrogen at the output to avoid a possible external combustion. The modulator design used in the previous experiments has been improved to increase the modulation amplitude. The wheel has now 50 six millimeter large square teeth and its diameter is 185 millimeters. The secondary nozzle is designed to extract 15% of the main flow rate. In practice, the secondary flow rate corresponds to 7.5% of the main flow since the the secondary nozzle is blocked half of the time.

II.3 Diagnostics

II.3.1 Sensors

High frequency Kistler pressure transducers (Type 701A) are used to record the pressure fluctuations. Five sensors are flush mounted the combustion chamber walls, three on the top, two on the bottom (Fig.II.4). Two other sensors are situated respectively in the oxygen and methane feeding lines. The signals are acquired at 40 kHz. All signals are recorded simultaneously by making use of sample and hold units. A thermocouple is set up in the bottom wall to record the temperature variations in the chamber. This signal is acquired at 1 kHz but the thermocouple response time is approximately 100 ms and this sensor yields a low pass average of the temperature during the test.

The heat release rate is characterized with two photomultipliers. Their aperture are vertically aligned in front of the windows at the end of the observable part of the chamber where the flames interact strongly with the acoustic modulation. A spatial filter is fitted on the photo multipliers (PM) to reduce the observable area. The first PM records the light emission in the top part of the chamber while the second, vertically aligned, detects light emitted from the lower part of the chamber (Fig.II.4(a)). The cross spectral analysis of the signals delivered by the two PM provides the phase between the light

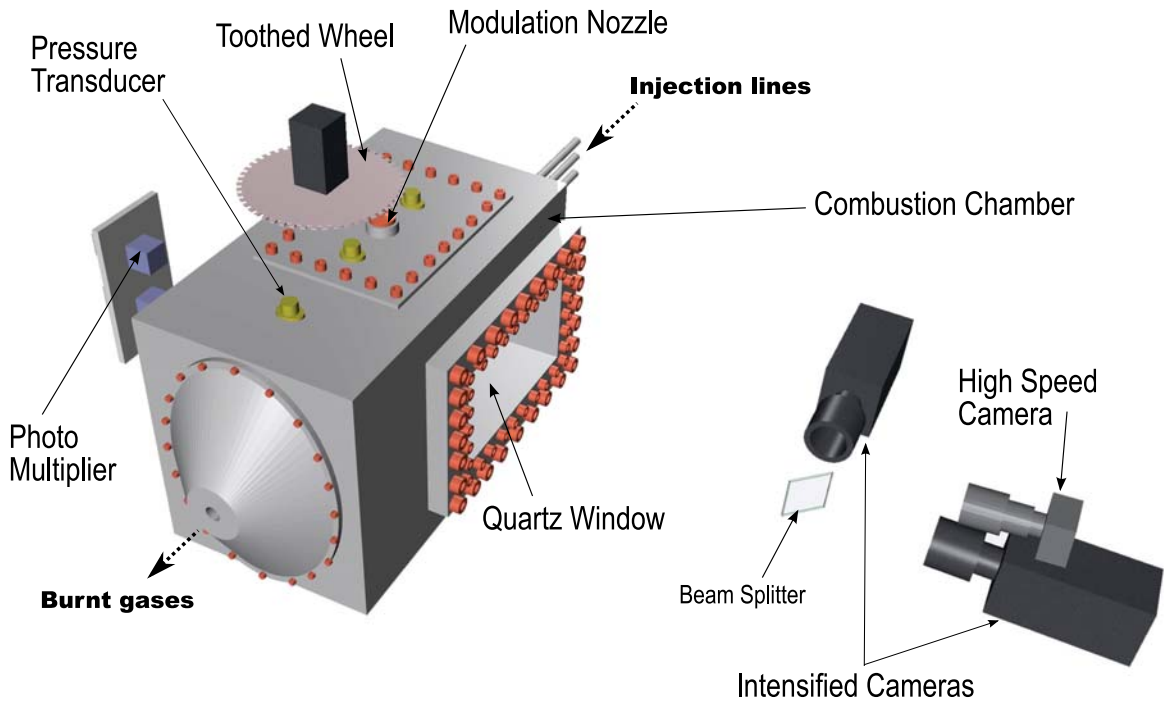

Fig. II.3: Schematic of MASCOTTE combustion chamber with the diagnostics set up for the hot fire tests.

emitted in the top part of the chamber and the light originating from the bottom of the combustor. This phase highlights the transverse motion of the flames submitted to transverse acoustic perturbations.

Photomulipliers do not provide a quantitative measure of the heat release in the combustion chamber. It is known that OH* or CH* emission can be used to quantify the integrated rate of heat release in premixed flames operating at a fixed equivalence ratio. However, the present combustion process is essentially nonpremixed and the relation between OH* or CH* and heat release does not apply. One may however consider that the light intensity associated with OH* emission is related monotonically to heat release. The dynamic information in the PM signals is used (1) to observe the vertical oscillating motion of the flame and (2) to link the pressure oscillation with the heat release. The phase between the two PM defines the dynamics of reactive zones while the phase between the PM and the pressure signals may be used to see if a region contributes positively to the oscillation. Combustion instabilities are amplified when heat release and pressure perturbations are in phase. Processing of the signals will specifically consider the phase relation between these two signals.

II.3.2 Optical diagnostics

Two intensified cameras are used to observe the instantaneous reaction zone. The cameras focus on the same area but observe different radicals. Emission trough the whole quartz window (15×10 cm^2) is recorded with a resolution of 3.4 pixels per millimeter.
The emission of the vibrationally excited hydroxyl radical (OH*) is mainly used to observe the flame front and the burnt gases originating from the flame. OH* is the most intense radical and its radiation

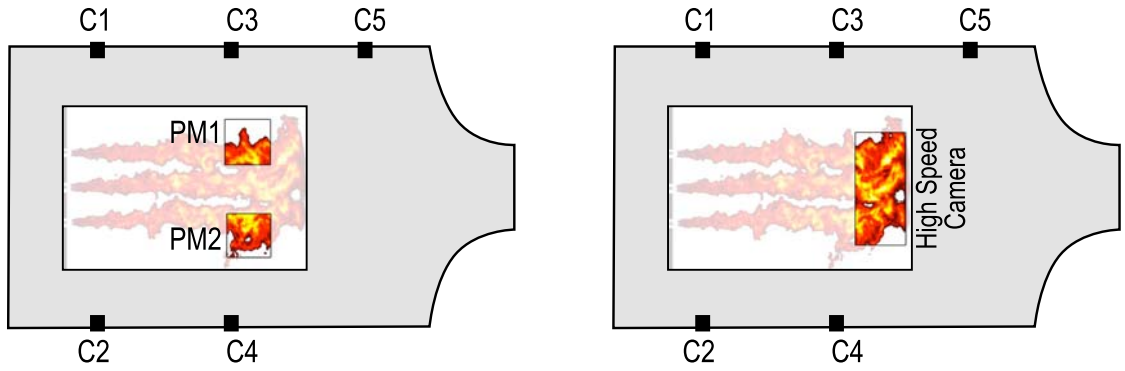

(a) Photo-multipliers focus zone. (b) High speed camera focus zone.

Fig. II.4: Schematic side views of the combustion chamber with the pressure transducers (C1 to C5).

can be observed in the close UV range around 300 nm. A combination of two optical filters (UG-11 and WG 305) are placed on the ICCD1 camera to select the appropriate band of wavelengths.
Combustion of methane generates another interesting radical CH*. Emission of CH* is less intense than that originating from OH* but it may be considered as a better tracer of the flame front. To compare the information delivered by this radical compared to that of OH*, the second camera ICCD2 is equipped with a combination of two optical filters (431AF20 and SWP 604).
A beam splitter separates the emission signal in two beams of equal intensity. The two cameras are equipped with Nikon^{TM}optics UV Glass 105mm/f4. The typical exposure time is around 10 μs but its value is varied by a few microseconds as a function of experimental conditions. This exposure time is short enough to freeze the flow and obtain spatially resolved frames. It is important to remember that the cameras detect light emitted over the line of sight.

The relatively high frame rate of the high speed camera does not allow to focus over the same viewing area. Because of the two intensified cameras it is necessary to place the high speed camera slightly outside the horizontal plane of the chamber. The camera is set-up above the intensified camera ICCD1 and its axis forms an angle of 12° with respect to the horizontal plane containing the burner axis. This displacement from the optical axis is quite small and does not change the imaging quality. Among the configurations tested for the position and viewing area for the high speed camera that adopted here constitutes a compromise between spatial and time resolution.
To get a well defined temporal resolution, at least 10 frames should be recorded for each modulation cycle. The acoustic modulation frequency is around 2 kHz so that the recording frame rate should be at least 20 000 frames per second. At this frequency, the dynamics of combustion can only be recorded in a small frame including 256×128 pixels. This corresponds to the selected band area of 3×6 cm^2 which is located as shown in Fig.II.4(b). The observation area is situated at the end of the visible part of the chamber where the flames interact and the effect of the acoustic perturbations is most pronounced.
A second high speed camera was also available during the first hot fire test series. Its field of observation was extended to the entire window by decreasing the framing rate to 4000 images per second. This sampling rate was however too slow to follow the vortex formation in the flow and their convection in

Points	$\dot{m}_{CH_4}$ (g s^{-1})	U_{CH_4} (m s^{-1})	T_{CH_4} (K)	$\dot{m}_{LOx}$ (g s^{-1})	U_{LOx} (m s^{-1})	T_{LOx} (K)	E	J
F50-T280	50	90	280	60	2.8	80	1.2	5.4
F70-T280	70	115	280	60	2.8	80	0.85	12
F100-T280	100	150	280	60	2.8	80	0.6	20
F50-T180	50	65	180	60	2.8	80	1.2	4.6

Tab. II.1: Operating points tested during the hot fire test series. The tests are identified by the methane mass flow rate and injection temperature.

the chamber.

II.4 Operating points

II.4.1 Introduction

Previous experiments were carried out with liquid oxygen and gaseous hydrogen (Rey et al. 2004) but the resulting flames were stable and the modulation system generated insufficient levels of pressure oscillations. Modifications of the flames were observed but the amplitude was too low to detect a profound change in the flame expansion rate and dynamics.

The purpose of the present set of experiments was to explore combustion sensitivity to acoustic perturbations by improving the modulator capabilities and decreasing the flame stability. Efforts have been done to increase the modulator efficiency by modifying the auxiliary nozzle geometry and introducing an accurate adjustment of the relative position between the wheel and the nozzle. On the other hand, the flame stability has been reduced by playing with three different parameters.
(1) Hydrogen has been replaced by methane keeping liquid oxygen at 80K as oxidizer. With methane, it is possible to reduce the injection speed keeping a momentum flux ratio J in a realistic range (between 4 and 30). In this way the frequency of the natural hydrodynamic instability of the jet is of the order of magnitude of the modulation frequency. Hydrodynamic and forced modulation may couple to increase the perturbation.
(2) Systematic tests have been carried out to evaluate the flame sensitivity to external modulation as a function of the injection speed. An important conclusion is obtained on this point and the effect of the injection velocity will be discussed in the next section.
(3) Hot fire tests on real engines show that high frequency combustion instabilities often develop during transients when the gaseous propellant temperature has low values. The effect of the temperature on the flame stability and sensitivity to external perturbations is investigated.

Twenty-four hot fire experiments were planned and operating points are chosen to test all these parameters. The runs were carried out with the chamber pressure stabilized at 0.9 MPa. The oxygen injection parameters were kept constant while the methane injection velocity and temperature were changed. Table III.3 summarizes the different operating conditions.

II.4.2 Test procedure

For each operating point, three runs are required to investigate the acoustic response and the flame behavior. Each run lasts 35 seconds with 20 seconds of stabilized conditions. The changing parameter between the three runs is the external modulation applied to the system. The configuration is naturally stable and the first test is carried out without external modulation and serves as a reference.

The second run serves to identify the resonant frequencies by submitting the system to a linear frequency sweep. This is used to locate the eigenfrequencies by short time Fourier transform. The modulation frequency is swept linearly from 0 to 3.5 kHz at a rate of 150 Hz s^{-1}. The rate of change of this linear sweep was selected by taking into account the frequency response of the system or equivalently the damping characteristics of the system as determined from previous experiments.
Using a wave train modulation it was found that the pressure signal decayed like $A\exp(-\alpha t)\cos(2\pi f t)$ where f is the modulation frequency, A the amplitude, t the time and α the damping coefficient. Data fitting provided a value $\alpha = 200$ s^{-1}. This was used to estimate the resonance bandwidth Δf of a second order system representing the chamber response $\Delta f = \alpha/\pi$. Using this result, it was possible to determine the system bandwidth : $\Delta f \simeq 60$ Hz. This gives the typical spectral width of the combustor resonant modes. The frequency ramp at 150 Hz s^{-1} is slow enough to obtain a suitable system response.
Short time Fourier transform analysis of one of the pressure signals provides the modal eigenfrequencies. For each of these frequencies, the phase difference between the pressure transducers is calculated in order to determine the modal structure.

In the last run the system is excited at the first transverse eigenfrequency deduced from the second test. During this procedure, the first and last runs are used to compare the flame structure without and with modulation, the intermediate test provides the acoustic response in the range of frequencies traversed by the linear sweep.

II.4.3 Influence of injection parameters

II.4.3.1 Influence of the methane injection flow rate

Three different injection points are considered. Methane is injected at flow rates equal to 50, 70 and 100 g s^{-1} at a temperature equal to the ambient (288K) while keeping the oxygen mass flow rate equal to 60 g s^{-1} at 80 K. This corresponds to injection velocities equal to 90, 150 and 200 m s^{-1} for methane and 2.8 m s^{-1} for oxygen.

The instantaneous OH* emission recorded during the three different tests are displayed in figure II.5. The ICCD cameras are focused on the vertical mid-chamber plane. The optical field depth is minimized, by using a large diaphragm aperture, to avoid any three dimensional disturbance of the signal. However the light intensity is integrated over the line of sight which artificially increases the intensity of the flame downstream. The most intense spots (red color) appear only in the second part of the chamber (where the flame is thicker) whereas all the flame should have nearly similar levels of reaction. This disturbs the interpretation of the images obtained in the modulated tests since the volumetric

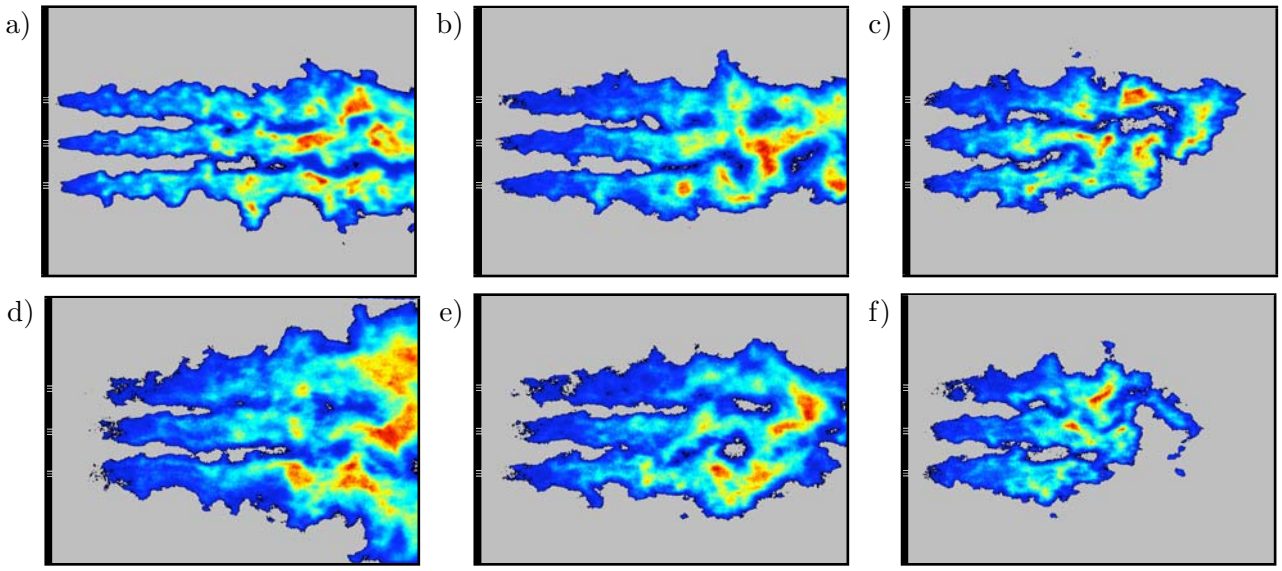

Fig. II.5: Instantaneous OH emission for non-modulated tests (a,b,c), modulated tests at the first transverse eigenfrequency (d,e,f) and different methane flow rates : 50 g s^{-1} (a, d), 70 g s^{-1} (b, e) and 100 g s^{-1} (c, f)*

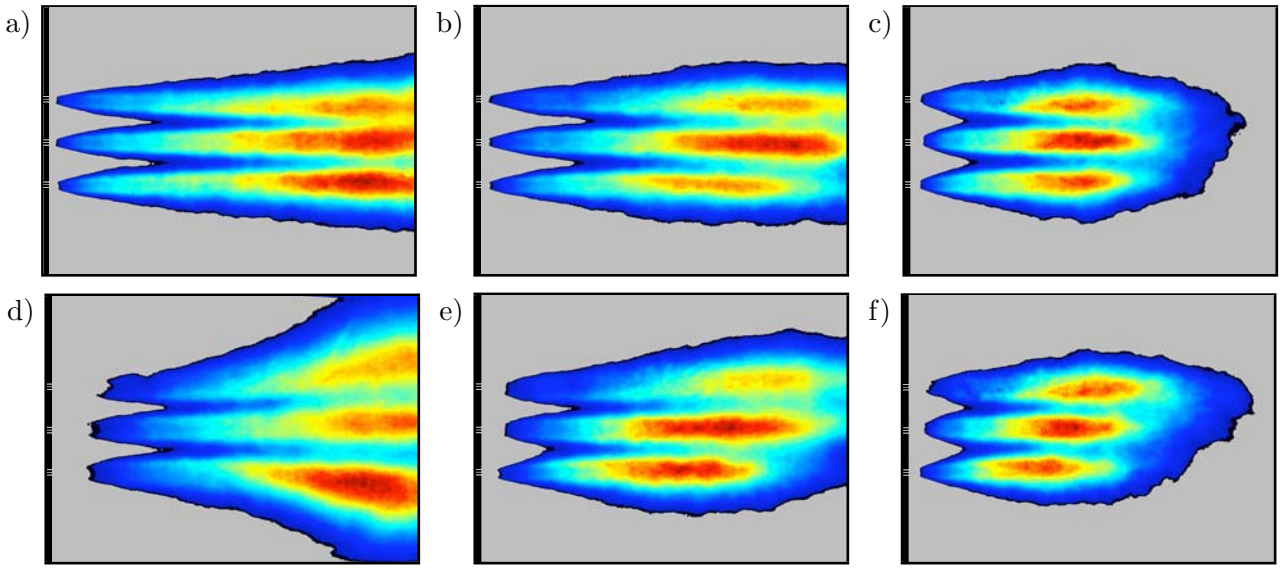

Fig. II.6: Average OH emission (over 200 instantaneous frames) for non-modulated tests (a,b,c), modulated tests (d,e,f) and different methane flow rates : 50 g s^{-1} (a, d), 70 g s^{-1} (b, e) and 100 g s^{-1} (c, f)*

reaction rate is increased by the external excitation giving the wrong feeling that the flame is lifted. This artifact is due to the intense reaction zone created downstream and the limited dynamic range of the CCD camera. In fact the flame is always attached to the injector lips and the anchor point is very close to the injector. The flame edge is always at the same location as shown by Singla et al. (2006b), but the reaction layer is situated between the oxidizer and fuel streams. There is no premixing in the first millimeters after injection. This is confirmed in the second test series where specific imaging diagnostics have been implemented to investigate this point.

Instantaneous frames reveal the complex geometry of the multiple jet flames. The average emission intensity can be used to compare the various configurations. Figures II.6(a) to II.6(c) show average emission images of OH* radicals for tests carried out *without external modulation* at three different methane flow rates. This set of figures shows the effect of the injection velocity on the flame structure. The flame is obviously longer when the methane flow rate is decreased. For low mass flow rates, the ratio of methane velocity to oxygen injection velocity is diminished. When this ratio is small, the velocity differential is reduced and, atomization is less effective producing larger droplet sizes which in turn require more time to vaporize. Burning then takes place on a longer distance. From a temporal point of view, the combustion characteristic time is increased when the velocity ratio is reduced. One possible mechanism which can give rise to combustion instabilities is a match between a fluid mixing and acoustic characteristic times. When the injection velocity is high the fluid mixing time is shorter than the modulation time. By reducing the methane injection velocity, the two times become closer and the effect of the acoustic modulation on the flames may be amplified.

Figures II.6(d) to II.6(f) tend to confirm this possible scenario. They show the average OH* radical emission when the flames are externally modulated at the eigenfrequency of the first transverse mode for different flow rates. A visible effect of the external perturbation is the expansion of the reactive zone. The flame expansion rate is more important in the case of low injection velocity. When the methane flow rate equals 50 g s^{-1}, the mean flame angle is 18° while it is only 9° for the highest injection speed. The change in expansion rate indicates that the system is sensitive to external perturbations. Flames stabilized at low methane injection velocities are clearly more sensitive to the external modulation. At the same time the amplitude of the pressure oscillations level is doubled. This indicates that the flames are sensitive to acoustics but that a feedback process also occurs in which the perturbed flames generate pressure waves.

At least three explanations can justify the strong coupling observed at the low methane injection velocity.
(1) The hydrodynamic instability frequencies are reduced and come closer to the acoustic frequencies giving rise to a possible coincidence. This can be discussed in terms of a Strouhal number defined by $St = fd/U$ where f is the hydrodynamic frequency, d the hydraulic diameter of the methane annular injector and U the injection velocity. If the Strouhal number St and the injection diameter d remain constant, when the injection velocity decreases the hydrodynamic frequency decreases by the same order of magnitude. Considering that the mean injection velocity between oxygen and methane is 50 m s^{-1} and the external diameter of the jet is 7 mm and taking a Strouhal value of 0.3 for the preferred

hydrodynamic instability mode. One finds a frequency of 2142 Hz. The eigenfrequency of the chamber at low methane injection velocity is 2345 Hz. These two frequencies are close and their matching may amplify the flame response.
(2) The flame length increases due to a slower atomization of the liquid oxygen when the shear rate decreases. The level of pressure fluctuations may be significant enough to improve the atomization process. The external modulation generates transverse velocities which can accelerate the jet break-up. A strong transverse dispersion can be produced compared to the case where atomization is only controlled by the natural shear between the reactants streams.
(3) The pressure differential in the injector decreases with methane injection velocity. This could lead to a coupling of the combustion chamber with the injection lines. Pressure transducers are placed on the LOx and methane manifolds but they are relatively distant from the injection plane. The corresponding data do not provide reliable indications on the dynamics taking place in the chamber and it is not possible to conclude at this stage on a possible coupling between the combustion chamber and the injection lines.

The physical parameter leading to the strong interaction between combustion and pressure fluctuation is not precisely determined but the hot fire tests already indicate that at low injection velocities the flames are more receptive to external modulation. This occurs for the operating point F50-T280 (Tab.III.3).

II.4.3.2 Influence of the methane injection temperature

The reduction of the methane injection temperature may also influence the flame response to acoustic perturbations. Two main effects can be expected. (1) When methane is injected at low temperature, the liquid oxygen will need a longer time to atomize and vaporize and its gas phase reaction will be delayed. (2) The chemical time may also be increased under lower temperature conditions. Tests have been carried out at low velocity and low injection temperature (operating point F50-T180). Methane is still gaseous but its temperature is 180 K.

Figure II.7 displays the instantaneous OH* emission as a function of the methane injection temperature and external modulation. Without modulation (Figs.II.7(a) and II.7(b)), low temperature injection induces an expansion of the emission region. The angle is equal to 9° for ambient injection temperature. At a low injection temperature, the angle takes a larger value of 15° and the instantaneous distributions are more ragged. A higher variability between successive snapshots is also observed. The reactive zone oscillates showing an unstable behavior of combustion, meaning that the flame is less stable when methane is injected at low temperature. The effect of modulation is visible in the average emission images presented in Fig.II.8. When the modulation is on, the expansion rate under low injection temperature changes to a lesser extent when compared to the ambient injection conditions (Figs.II.8(c) and II.8(d)). This modification in expansion rate is also apparent in the instantaneous images (Figs.II.7(c) and II.7(d)). This indicates that the natural jet flames obtained under low injection temperature are less stable but also less sensitive to external modulations.

The effect of a reduced methane injection temperature has complex consequences which would require

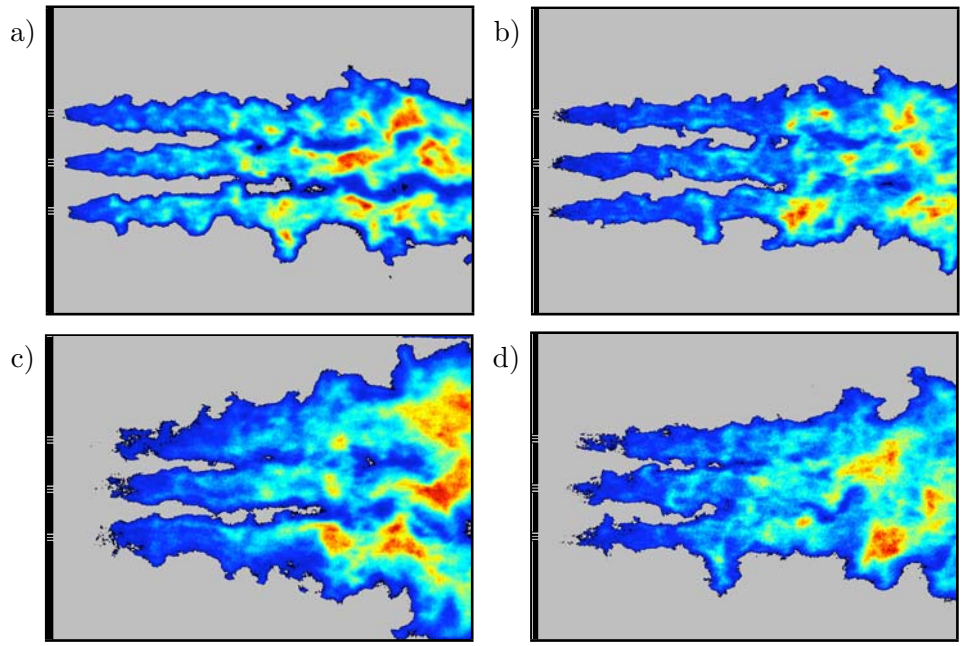

Fig. II.7: Instantaneous OH emission for non-modulated tests (a, b), transversally modulated tests (c, d) and different methane injection temperature : 280 K (a, c) and 180 K (b, d). The modulation frequency corresponds to the 1T mode.*

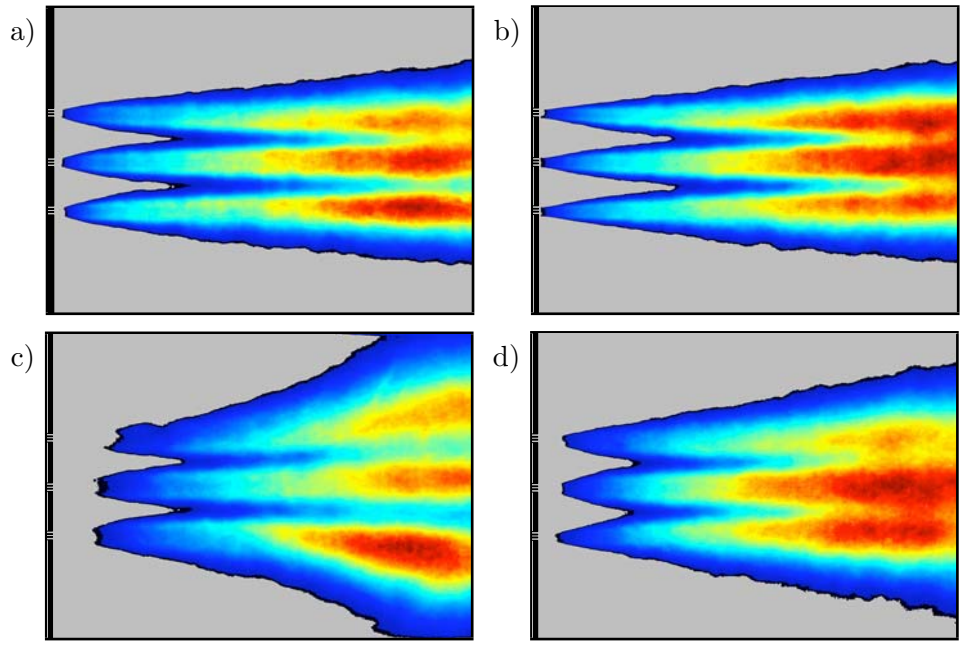

Fig. II.8: Average OH emission for non-modulated tests (a, b), transversally modulated tests (c, d) and different methane injection temperature : 280 K (a, c) and 180 K (b, d). The modulation frequency corresponds to the 1T mode.*

Points	p_{ch}	$\dot{m}_{CH_4}$	U_{CH_4}	T_{CH_4}	$\dot{m}_{LOx}$	U_{LOx}	T_{LOx}	E	J
F50-T280	0.9 MPa	50 g s^{-1}	90 m s^{-1}	280 K	60 g s^{-1}	2.8 m s^{-1}	80 K	1.2	5.4

Tab. II.2: Experimental conditions

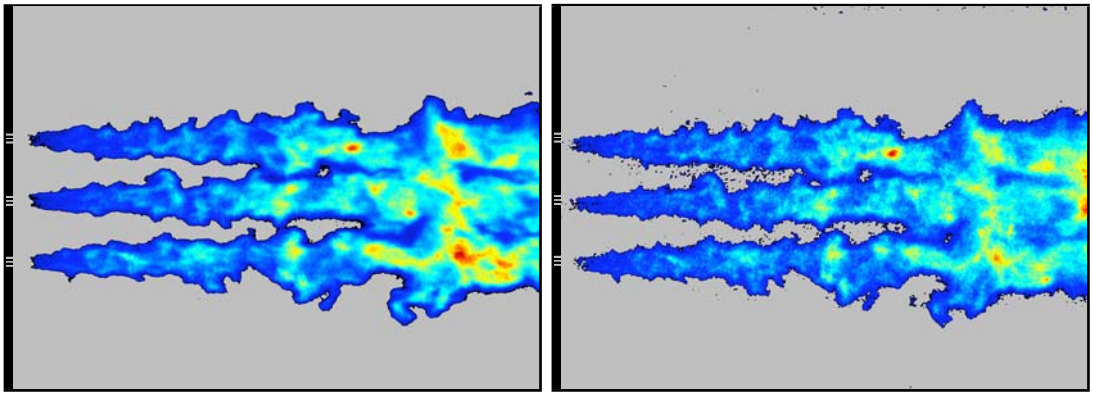

(a) OH* spontaneous emission field (b) CH* spontaneous emission field

Fig. II.9: Chemiluminescence emission of the two radical OH and CH* for* F50-T280 *operating point. Frames are recorded with an exposure time equal to 10 μs which provided instantaneous field.*

further systematic tests currently not available (The number of tests is limited). In what follows we will only examine experiments carried out with methane injected at ambient temperature. These tests may be used to determine the parameters which yield a stable flame in the absence of excitation and a flame sensitive to external modulations. The injection parameters used for the systematic study correspond to the operating point F50-T280.

II.5 Results

II.5.1 Modulation free run

Operating conditions chosen for the following analysis are gathered in table II.2. Reaction is ignited by a LOx/Hydrogen torch placed in the top wall, in the middle of the chamber, the flames are stabilized close to the injector lip and the test lasts 20 seconds.

Instantaneous OH* and CH* radical emissions are displayed in Fig.II.9 for this operating point. The instantaneous images show spatial distribution of light intensity originating from the flame. The two frames are recorded simultaneously with the same exposure time. The emission of the two radicals OH* and CH* are quite similar and feature the same patterns of interactions between the flame fronts. These two radicals show similar structures with some minor differences in amplitudes. The OH* fields which are more intense and more precisely defined will be used in what follows.

Well localized reactive spots can be identified and large scale eddies are observed. The maximum combustion intensity appears in the second part of the combustion chamber. The flame seems to be lifted from the coaxial injectors. This is due to the integration of emission over the line of sight. The

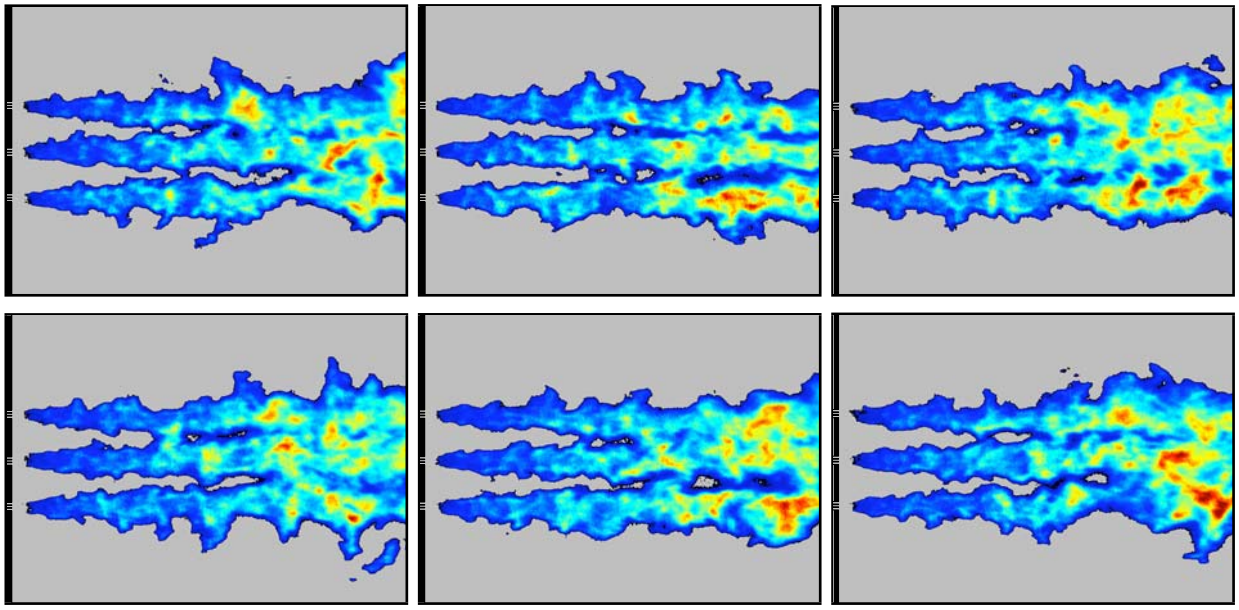

Fig. II.10: Set of instantaneous OH emission fields for non-modulated tests at operating point* F50-T280.

projection of radiation on the camera induces an artificial enhancement of the intensity in the downstream region. The intensity scale is then displaced towards the largest values and the low intensity close to the injector apparently vanish. The Abel transform is not applicable in such configurations because they are not symmetric. This effect is amplified in the modulated hot fire experiments where the reaction rate increases and the light intensity in the downstream region is augmented. When examining intensity maps this should be kept in mind.

II.5.2 Linear frequency sweep experiments

During the 20 seconds of the hot fire test, a linear frequency modulation is applied between 0 and 3.5 kHz. The pressure signals are numerically high-pass filtered with a cut-off frequency of 1 kHz and analyzed with the Short Time Fourier Transforms to identify the eigenfrequencies of the system.
Figure IV.2 shows the pressure signal recorded during a typical test (this signal was recorded by sensor C3 in Fig.II.4). Three resonant peaks can be distinguished in the time-frequency plot displayed in Fig.II.11. The color scale gives the most amplified pressure fluctuations as a function of time (horizontal axis) and frequency (vertical coordinate). The three peaks observed in the pressure signal may be linked in this way to the modal eigenfrequencies.

The peaks correspond to 1450 Hz, 1680 Hz and 2345 Hz. As expected from the theoretical reasoning developed in the previous chapter, an additional mode at 1680 Hz is detected between the first longitudinal and the first transverse modes. To check these conclusions it is interesting to examine the pressure signals simultaneously. After bandpass filtering around the resonant frequency the signals are plotted as a function of time and the phase difference between the sensors is determined to identify the modal structure.

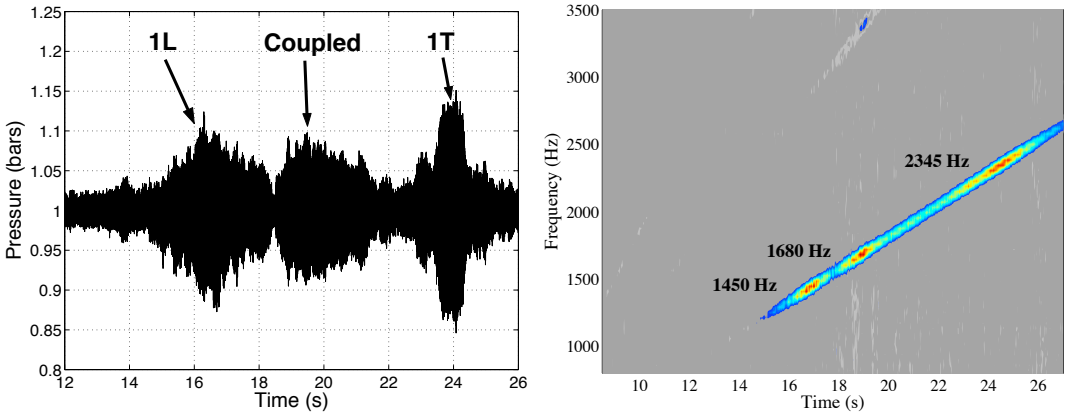

(a) (b)

Fig. II.11: Pressure variation during a frequency sweep modulation at 100 Hz.s^{-1} (a) and its Fast Fourier Transform (b)

The first resonant peak corresponds to the first longitudinal mode. This mode is characterized by a phase difference of 180° between the upstream (C1 and C2) and downstream sensors (C3, C4 and C5) as shown in figure II.12(a). Longitudinal modes are usually involved in low frequency instabilities. In the high frequency range these modes are governed by the output impedance imposed by the critical nozzle. Longitudinal instabilities will not be considered in the present context because they are less intense than transverse instabilities and also less destructive when they occur in real engines.

The second peak defines the coupled mode involving the chamber and the secondary nozzle. Figure II.12(b) shows the five pressure signals at the time corresponding to this resonance. The phase relations between the sensors is close to that of the first transverse mode and this could have been confusing without the numerical simulation carried out in the previous ch apter indicating the existence of a coupled mode in this intermediate frequency range. The two bottom sensors are in phase and the phase difference with the top downstream sensor (C5) is almost 180° as for the first transverse mode. The first two top sensors placed near the modulation nozzle record signals which are less easy to interpret. This might be due to the rapid evolution of the pressure distribution near the cavity junction as observed numerically.

The third eigenfrequency characterizes the first transverse mode. Fig.II.12(c) shows the filtered signals recorded by the five sensors. The odd numbered sensors (solid lines) correspond to the three top transducers while the even numbered sensors (dashed lines) are located on the lower wall of the combustion chamber. The top sensors are exactly out of phase by 180° with respect to the bottom units. This situation corresponds to the first transverse mode.

Because the spanwise dimension of the chamber is quite small the eigenfrequency of the first mode in the third direction is well above the frequencies of interest and only longitudinal and transverse modes may readily appear. Data accumulated over many years of research indicate that high frequency com-

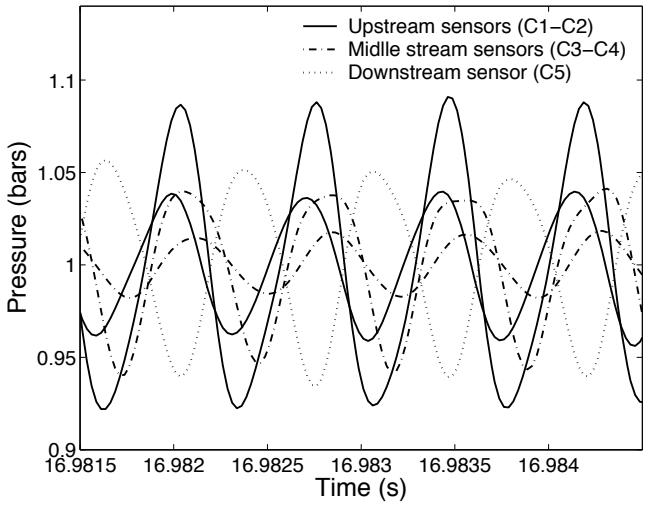

(a) Pressure sensors at the first longitudinal eigenfrequency (1450 Hz)

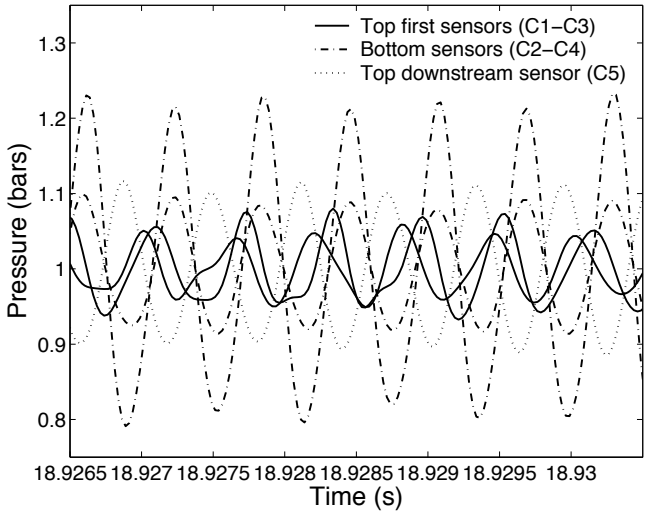

(b) Pressure sensors at the coupled eigenfrequency (1680 Hz)

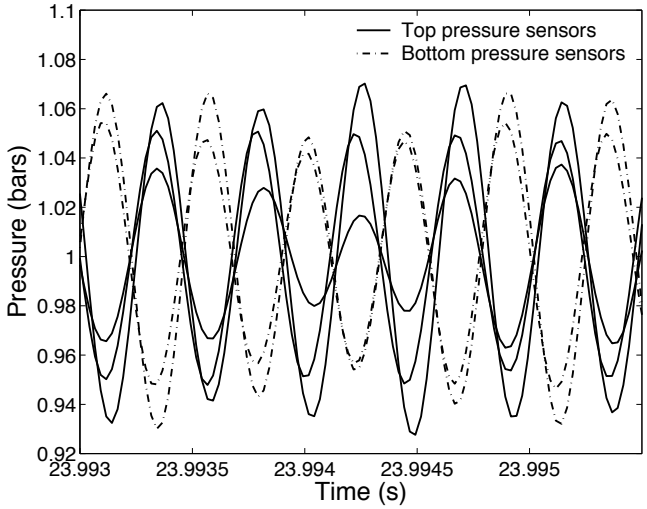

(c) Pressure sensors at the first transverse eigenfrequency (2345 Hz)

Fig. II.12: Five pressure sensors at different eigenfrequencies.

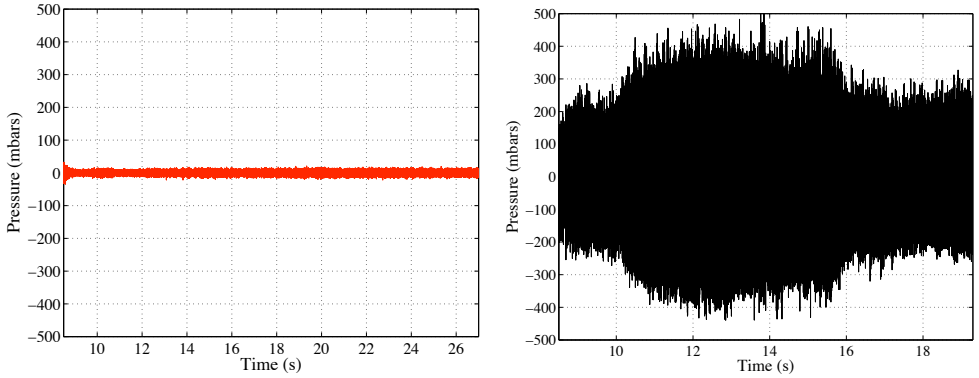

(a) Pressure signal without modulation (b) Pressure signal with modulation

Fig. II.13: Pressure signal recorded by sensor 3 with and without the modulator activation.

bustion instabilities are mostly coupled by transverse sloshing modes. It is then logical to modulate the combustion chamber at the eigenfrequency corresponding to this transverse mode (2345 Hz) and see how the jet flames respond to this external forcing.

II.5.3 Modulation at the first transverse eigenfrequency

II.5.3.1 Pressure signals

When the chamber is externally modulated at the first transverse mode frequency, the pressure transducers confirm that the system resonates. In the absence of modulation, the peak to peak pressure reaches 30 mbar. This quantity equals 650 mbar when the modulator is operating which corresponds to 7% of the average chamber pressure. The coupling between acoustic modulation and combustion amplifies the pressure oscillations by a factor of 20.

The pressure wave amplitude modifies the flame dynamics. It was shown in previous studies that the toothed wheel could generate pressure waves of a reasonable amplitude when the system was tuned on a resonant frequency (Rey, Ducruix, Richecoeur, Scouflaire, Vingert, and Candel 2004). This is however the first test where the amplitude of oscillations is so high. One of the challenges in this study of high frequency instabilities in a laboratory scale experiment is to generate a strong external modulation and the modified TWM serves this purpose well. It provides a precise frequency control and a good level of excitation.

II.5.3.2 Instantaneous radical emission

A set of instantaneous frames of the OH* spontaneous emission is presented in figure II.14. The intensified cameras show the interactions between pressure waves and cryogenic flames. The modulation has two main effects on the flames : the expansion angle is increased and the volumetric heat release is amplified.

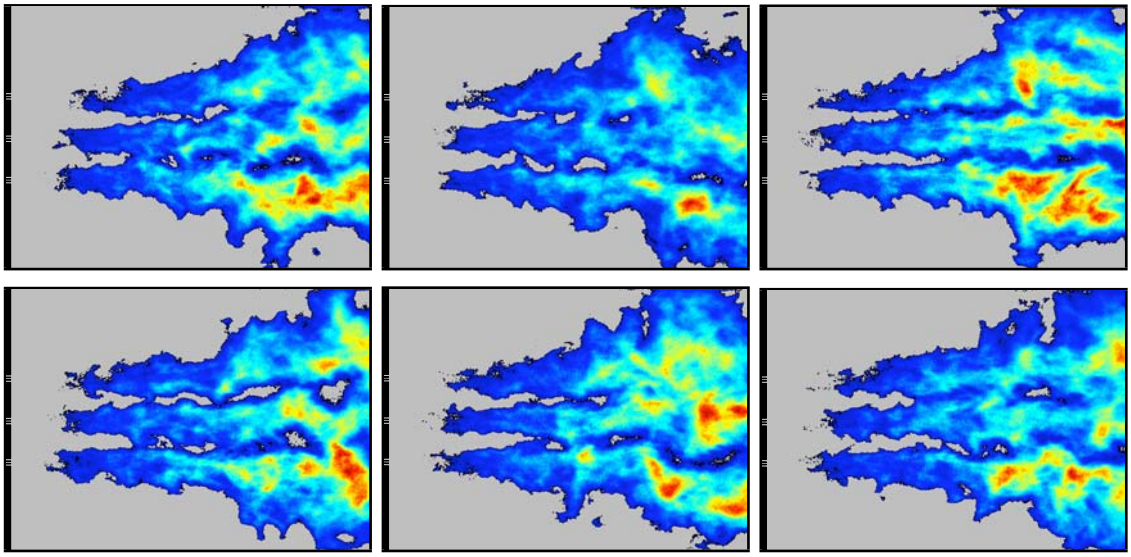

Fig. II.14: Set of instantaneous frames of the OH emission when modulated at 2345 Hz for operating point F50T280.*

Typical instantaneous images of OH* emission without modulation (Fig.II.15(a)) may be compared to images recorded with external modulation (Fig.II.15(b)). Emission images are plotted on the same intensity scale. They feature fundamental modifications in the flame structures. Without excitation the three flames spread as classical turbulent jet flames, with a small expansion angle. Turbulent structures are convected without significant interactions. The external modulation intensifies the level of fluctuation. The flame expansion angle is augmented and the size of the convected reactive vortices increases. The transverse velocity generates larger structures which lead to flame interactions and collision of adjacent shear regions.

Modification of the flame expansion rate appear when acoustic energy is introduced by the modulator. This may not be the only parameter leading to an augmented expansion rate. This effect is more pronounced in the present case than what might happen in a real configuration because the distance between adjacent injectors is larger and because the fresh propellants are injected in the middle of the chamber, far from the top and bottom walls. This geometry differs from that of real engines where the injection plane features closely packed injection units. This induces at least three distortions with respect to LRE configurations: (1) A recirculation region of fresh methane may develop in the upper and lower sides of the chamber above and below the injector group, (2) Effects of heat losses at the walls are minimized, (3) Interaction between the transverse mode and the flames takes place over a limited region. This affects the flame expansion rate which is a visible effect of the coupling between the transverse acoustic mode and combustion. The change in spreading rate may not be as strong in real engines. However, the comparison between the two tests (modulation free and modulated) gives relevant information on the flame motion and on the interaction process.

The image presented in Fig.II.15(b) corresponds to an instant in the modulation period, when the

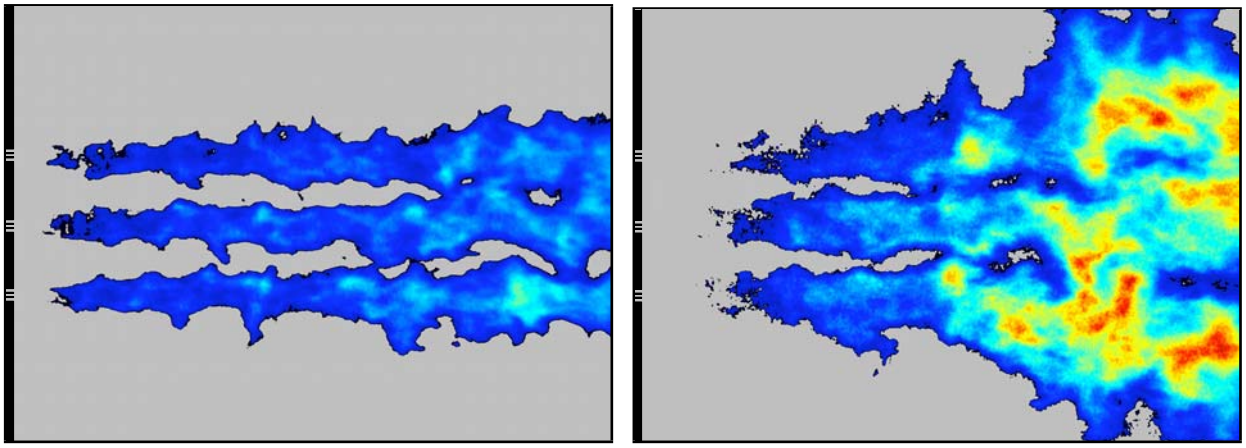

(a) (b)

Fig. II.15: Instantaneous OH emission (exposure time is 2µs) without modulation (a) and with modulation at 2345 Hz (b) represented with the same intensity scale (arbitrary units)*

pressure field is uniform in the chamber. A direct correlation between the pressure phase and the position of the flames was expected but not obtained. Frames in figure II.14 have been taken at different phase values and no noticeable displacement of the flames could be observed. This is probably due to the fact that the fluctuation levels associated with acoustic (coherent) modulations is important but still not high enough compared to turbulent (random) fluctuations. The second explanation is that the displacement induced by the modulation is not large enough to be easily observed. Modulation occurs at high frequency so the duration of the gas displacement is too short. Even if the induced transverse velocity is large, the motion does not last long enough to induce a large scale flame displacement. This is clearly observed on high speed films where the structures can be followed visually and observed as they evolve in time.

The average light emission level (roughly corresponding to the reaction rate) is also increased with the modulation. The large reactive structures generated by the external modulation improve the mixing process and presumably the liquid jet atomization. This has direct consequences on combustion intensity. A thermocouple located in the lower chamber wall (not in direct contact with the hot gases) features a sizable increase of the wall temperature when the system is modulated at the frequency of the first transverse mode. The photomultipliers also witness this phenomenon. The gain of these units had to be significantly reduced when the system was modulated. The camera optical aperture had to be reduced to avoid saturation. The strong change in luminosity is demonstrated in figure II.15 by plotting images of the flames with the same color scale. This clearly shows that light intensity from the flames changes markedly when the modulator operates.

II.5.3.3 Dynamics of the modulated combustion

The dynamical behavior of heat release is conveniently analyzed by the two photomultipliers (PM) in figure II.16(a). These sensors measure the OH* light emission from the reactive regions. Figure II.16(b) shows the power spectral density of the bottom PM signal with and without modulation.

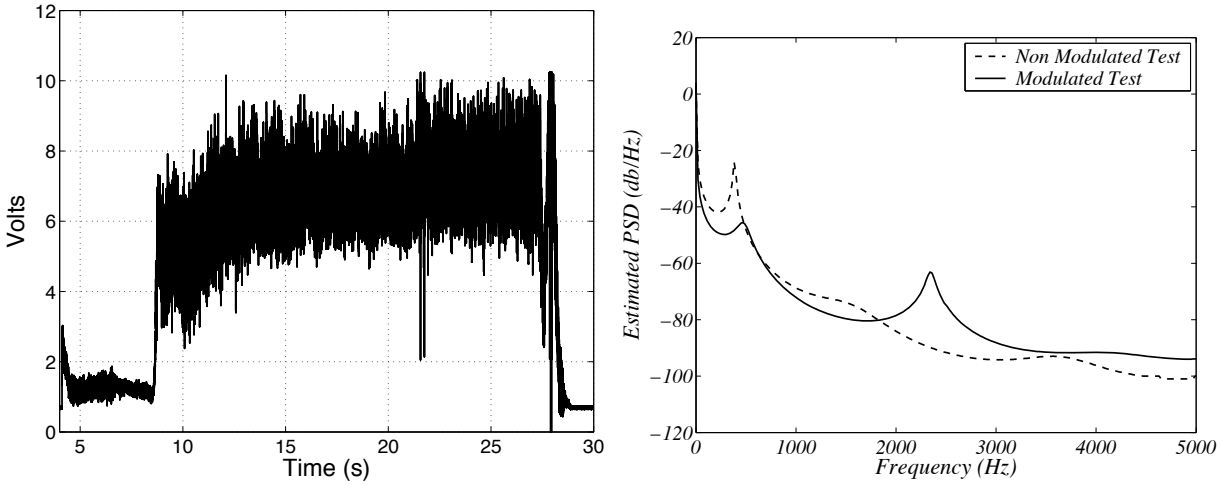

(a) Bottom Photo-Multiplier signal

(b) Prony Spectral Analysis of the PM signall

Fig. II.16: Bottom Photo Multiplier signal recorded when modulated at 2345 Hz (the nine first seconds are before the ignition) and the Prony spectral analysis of the PM signals with and without modulation.

The average shape of the power spectral density features a strong low frequency component detected around 400 Hz (exactly 360 Hz for the naturally evolving flames and 450 Hz for the modulated test). This frequency corresponds to the turbulent combustion process. The spectral density also features a peak at the modulation frequency indicating that light intensity oscillation occurs at the excitation frequency. The pressure fluctuations generated by the rotating wheel have a direct influence on light emission and disturb the heat release rate.
This shows that acoustic energy injected by the modulator modifies the combustion process. A coupling between the pressure fluctuations and heat release fluctuations is observed which is a necessary condition to develop combustion instabilities.

The pressure transducer and the photo-multiplier locations are shown in Fig.II.4(a). The odd numbered sensors and photomultiplier are in the top part of the chamber while the even numbered probes are located in the bottom part. Using these elements it is possible to examine the phase difference between the signals collected from the upper and lower parts of the chamber. As previously shown in Fig.II.12, the top pressure transducers are out of phase by 180° with respect to the bottom ones at the modulation frequency (2345 Hz) indicating that the pressure field corresponds to the first transverse eigenmode.

Similarly, the photomultipliers phase difference is 180° at the forcing frequency (Figure III.10). The cross spectral density diagram shows that the low-frequency perturbations are uncorrelated, natural combustion fluctuations of the top and bottom parts are not linked. In contrast, at the modulation frequency, the coherence of the two PM is close to 1 and light emission in the combustion chamber oscillates between top and bottom parts of the chamber with nearly equal signal amplitudes.

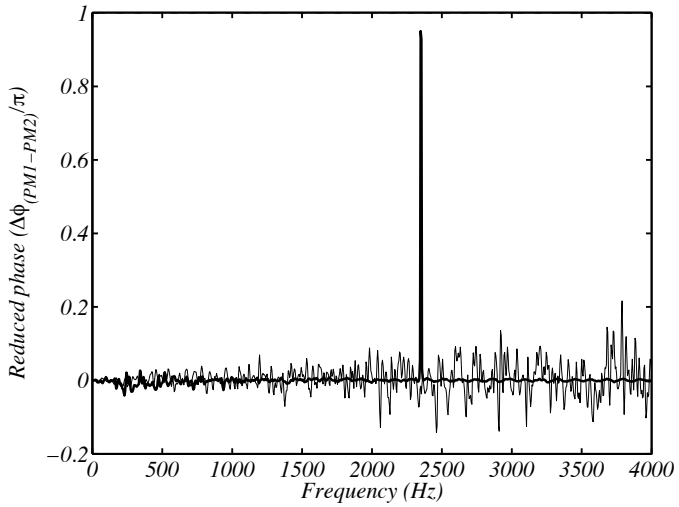

Fig. II.17: Non dimensional phase difference between the two PM without modulation (thin line) and with 2345 Hz modulated (bold line).

II.5.3.4 Heat release and pressure fluctuations

To see if the coupling process corresponds to a gain, it is important to examine the phase difference between the fluctuating heat release rate q' and the pressure fluctuations p'. These two quantities oscillate at the modulation frequency and their magnitude squared coherence, displayed in Fig.II.18(a) and II.18(b), is high enough ($\simeq 0.7$) to prove that heat release and pressure fluctuations are strongly correlated. The phase difference between the PMs and the pressure sensors have been calculated for all the possible combinations. Figure II.19 gathers the reduced phases between the two PMs and the five pressure transducers at the modulation frequency (2345 Hz). The sensor numbers are placed below the horizontal axis and the corresponding value of the reduced phase differences between each sensor and the two PMs are plotted as bars in this diagram. PM1 is in phase with pressure transducers C1, C3 and C5 while PM2 is out of phase with these same sensors. In contrast, PM2 is in phase with C2 and C4 while PM1 is out of phase with them. In other words, the PMs and the pressure transducers are not only strongly correlated but the top and bottom PMs are respectively in phase with the top and bottom sensors.

This indicates that the fundamental mechanism leading to combustion oscillation which involves a strong and coherent coupling between the heat release and pressure fluctuations is operating and that the flames are directly sensitive to the excitation frequency.

However, low frequency perturbations still dominate the motion in the high speed film images. The camera sampling rate is set to 20000 frames per second with a window of 256×128 pixels. The flame motion is observed at the end of the chamber, where the flames interact. The high speed film features the oscillating transverse motion of the flames at 2345 Hz but lower frequencies corresponding to convection of reactive vortices are quite visible, indicating that the high frequency excitation enhances to a great extent low frequency ($\sim$ 400 Hz) vortices. The coupling between the high frequency

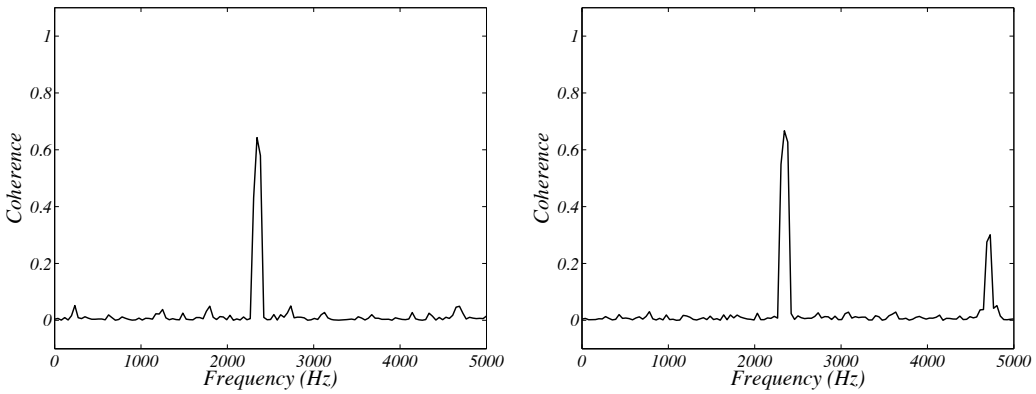

(a) (b)

Fig. II.18: Magnitude squared coherence ($|S_{xy}|^2/S_{xx}S_{yy}$) between PM 1 and C5 (a) then between PM 2 and C5 (b). c: Reduced phase difference between the two PM and the five pressure transducers at the modulation frequency (2345 Hz).

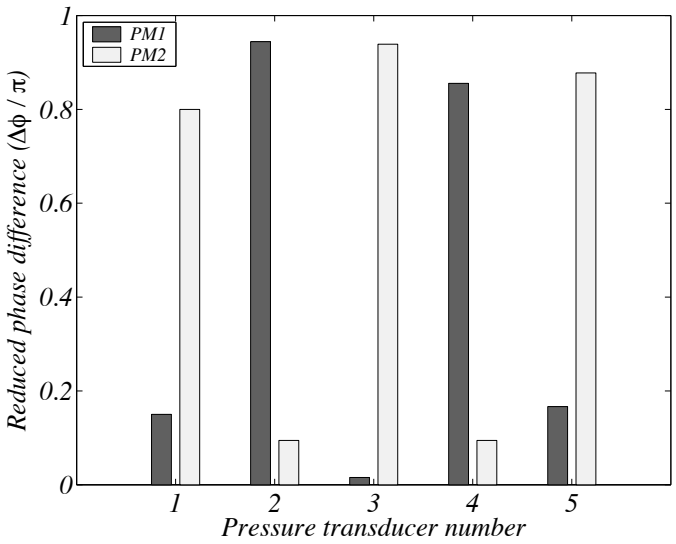

Fig. II.19: Reduced phase difference between the two PM and the five pressure transducers at the modulation frequency (2345 Hz).

transverse motion and the low frequency longitudinal convection appears to be an important feature of the phenomenon.

II.6 Discussion

The data reported in the previous section may now be used to discuss the following aspects :

1. Coupling observed at the modulation frequency between the photo-multipliers and the different pressure transducers.
2. Similarities and differences between the present externally induced oscillations and self-sustained high frequency instabilities.
3. Link between the imposed high-frequency modulation and the low frequency turbulent fluctuations.

These three points are considered successively. High frequency combustion oscillations are induced in the present experiments by imposing a large amplitude transverse mode with a pressure fluctuation of the order of 7% of the mean pressure. A coupling between combustion and the first transverse mode is indeed obtained and leads to enhanced acoustic fluctuations.

The data indicate that heat release fluctuations take a spatial structure which resembles that of the transverse mode and oscillates in phase with the pressure. This could lead to self sustained oscillations but this does not happen here because the losses exceed the gain associated with this coupling.

Consequently, the flame response differs from what is observed from earlier experiments. This can be seen by examining some of the initial experiments on self-sustained high frequency instability. One may use for example model scale investigations providing high speed records like those of Tischler and Male (1956) or Barrère and Corbeau (1963) to compare the present data with earlier observations. Tischler and Male (1956) used a 10-cm diameter 1-m long model scale rocket engine is equipped with a slit extending over part of the circumference of the system. A video camera records the light intensity through the transverse slit located at 14 cm from the injection plane. Figure II.20 shows the light observed when a 6000 Hz azimuthal mode is set-up in the chamber. A luminous zone moves across the chamber in a helical way and this is recorded by the camera as a periodic energy release in the upper and lower sides of the chamber. The frequency of positive excursions of heat release in the upper and lower parts of the chamber coincides with the oscillation frequency. It is then natural to infer that positive heat release fluctuations occur at the same frequency as the transverse velocity fluctuations.

Similar phenomena have been identified in the present experiments. Light emission, recorded by the photo-multipliers, features the same frequency as the first transverse mode, indicating that the periodic heat release is coupled to this mode. The most intense reaction rate position in the chamber also oscillates between the top and bottom sides of the combustion chamber. From the high speed camera it is possible to create numerically a virtual slit similar to the real aperture used by Tischler and Male (1956). In each frame, a one-pixel column is extracted and placed next to the same column from the

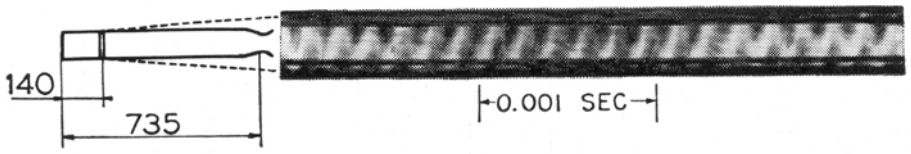

Fig. II.20: Streak photograph of rotary screaming waves in a cross section at 14 cm from the injection plane

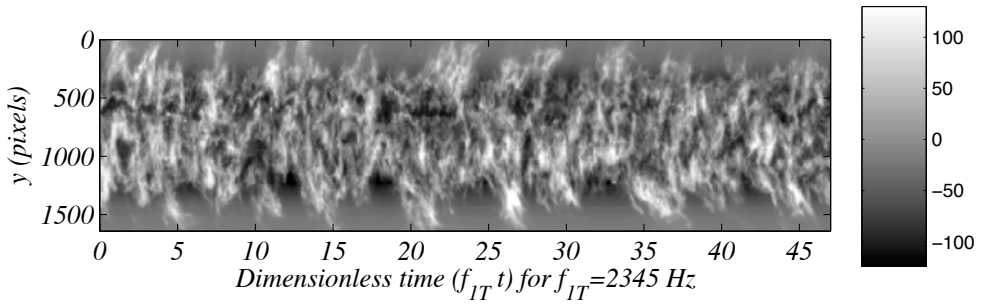

(a)

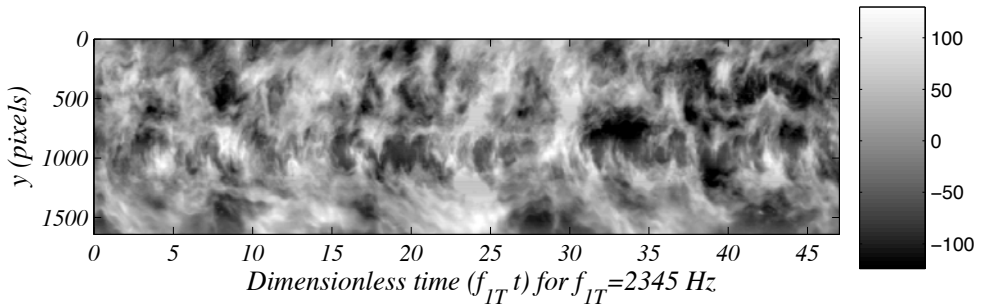

(b)

Fig. II.21: Temporal evolution of the flame light emission in a cross section at 12 cm from the injection plane for non-modulated (a) and modulated test (b).

previous frame. The temporal evolution of light intensity in a given cross section can be retrieved in this way.

Figure II.21 displays this type of data for natural and modulated hot fire tests. The oscillations of the modulation free combustor appears clearly around 400 Hz. When modulated, the combustion zone is enlarged and more intense but no regular pattern can be observed at the modulation frequency. This is so because two competing phenomena generate perturbations in the flow field. The first is shear flow turbulence, the second is the fluctuating acoustic field. An order of magnitude analysis indicates that the displacement induced by the acoustic field is largely inferior to that related to turbulence. The average pressure fluctuations generated by the rotating wheel are $p' \simeq 700$ mbars providing velocity fluctuation $v' \simeq p'/\rho_0 c \simeq 37$ m s^{-1} considering $c = 1000$ m s^{-1} and $\rho_0 = 1.87$ kg m^{-3}, this yields a maximum displacement of 1.5 cm during each period of modulation. This transverse displacement is observable in the high speed film but it remains small compared to the chamber dimensions. The

transverse oscillations are still too small to be observed independently from the low-frequency motion around 400 Hz.

A different view of this issue may be obtained by comparing the induced transverse velocity v' with typical turbulent fluctuations v'_t existing in the present configurations. The turbulence level in the jet flames is typically of about 15% of the mean injection velocity difference between the methane and oxygen streams (Hussein et al. 1994; Wygnanski and Fiedler 1969). This gives rise to turbulent fluctuations of the order of 15 m s^{-1} in the F50-T280 test case and the ratio v'/v'_t is of about 2. It appears that this value is already sufficient to modify the flame dynamics but is too low to have the flow switch from an essentially turbulence controlled organization to a high frequency nearly periodic motion.

Having established that the situation at hand is intermediate in the sense that it is controlled by competing phenomena (high-frequency oscillation, low frequency fluctuations) one may now discuss the coupling observed in such circumstances. Indeed, one unusual feature is that the high frequency modulation also enhances the low frequency motion. The flow is dominated by natural instabilities but the transverse perturbations enhance the rate of entrainment of reactive material in the larger scale vortex patterns.
The instantaneous OH* emission images show that combustion becomes more intense, that the spatial distribution is changed and that sizes of the turbulent burning structures are augmented. The flame expansion and the emission amplitude increase drastically under external modulation. Reaction spreads over a wider region in the chamber which corresponds to an improved and more homogeneous atomization than without modulation. The eddy sizes are also increased by the external modulation. The reactive spots observed with the ICCD cameras are larger and their convection in the downstream direction is more easy to detect.
An examination of the time evolution of burning spots also indicates that the local reactive layers are submitted to an augmented strain rate which in turn increases the local reaction rates.

II.7 Conclusion

The dynamics of a multiple injector combustor is investigated under high frequency transverse excitation. The study is carried out on a rectangular cross section system featuring three coaxial injectors fed with cryogenic propellants. A modulation system is used for external excitation. The system eigenmodes are first identified by performing a linear frequency sweep. Injection parameters are varied to determine conditions under which combustion becomes sensitive to external oscillations. Such conditions are observed when the methane stream velocity is relatively low. Pressure sensors provide the acoustic response of the system to the external modulation and clearly indicate that the spatial distribution is that expected for the 1T mode. The eigenfrequencies of the combustion chamber are determined numerically and identified experimentally.

When modulated at the first transverse frequency, the pressure amplitude oscillation reaches 7% of the average chamber pressure which is significant enough to induce a strong coupling between acoustics

and combustion. This coupling manifests itself as a visible enhancement of flame spread, radiation from the flame is augmented by a large factor while thermocouples placed on the lateral walls detect a rapid increase in temperature. The OH* emission intensity which can be linked to the heat release rate increases significantly. Photo-multipliers indicate that the most intense emission area in the chamber oscillates transversally at the modulation frequency. A phase analysis carried out at that frequency indicates that the pressure and OH* emission have similar spatial distributions and oscillate in phase. This behavior has also been observed with the high speed camera which also features enhanced reactive vortices convected in the downstream direction at a lower frequency.

The experimental improvements of the combustor allowed to generated a strong coupling between the combustion process and acoustics. The external modulation induces large modification of the flame behavior but only a small feedback effect has been observed. The combustion does amplify the acoustic fluctuations in the chamber but this do not lead to self-sustained oscillations. When the modulator is deactivated, the pressure fluctuations drops and the combustion runs normally. One of the challenges for the next experiments is still to increase the pressure fluctuation amplitude to generate self-sustained oscillations. Novel modifications have been tested in the next set of experiments.

Chapter III

High Pressure Hot Fire Experiments with a Five Element Injector

Résumé

On s'intéresse maintenant à une configuration haute pression comportant cinq injecteurs. Cinq flammes cryotechniques coaxiales sont formées dans la chambre. Les vingt-quatre tirs de la campagne d'essais ont permis de faire varier les paramètres et les configurations de fonctionnement. On a ainsi pu explorer le domaine des hautes pressions jusqu'à des valeurs de 6 MPa. La structure des flammes est étudiée à l'aide de trois caméras intensifiées enregistrant l'émission instantanée du radical OH*. Des capteurs de pression, des photomultiplicateurs et une caméra rapide sont utilisés pour analyser la dynamique de l'écoulement et des flammes. Pour chaque condition expérimentale, trois tirs sont effectués, le premier en l'absence de modulation sert de référence, le second avec une modulation linéaire de la fréquence a pour objectif l'identification des modes et enfin le troisième avec une modulation continue monofréquentielle permet l'étude de la réponse des flammes pour l'une des fréquences identifiées au cours du deuxième essai. Dans un premier temps, la pression chambre a été fixée à une valeur intermédiaire de 3 MPa et l'influence du rapport de mélange E et du rapport de quantité de mouvement J sur la sensibilité des flammes à la modulation externe est étudiée. J et E ont une forte influence sur la structure et la réponse dynamique des flammes. La pression de la chambre est ensuite augmentée et fixée à 6 MPa pour explorer le domaine transcritique. Le jet d'oxygène est injecté à une température inférieure à la température critique mais à une pression supérieure à la pression critique $p_c(LOx) = 5.04$ MPa. Les mêmes diagnostics sont mis en place montrant une structure de flamme différente. Enfin, une étude fondamentale sur l'effet d'une modulation acoustique transverse sur deux flammes cryotechniques isolées l'une de l'autre est conduite à 1 MPa. Ces essais n'ont pas permis de trouver une réponse aussi marquée que celle observée à plus basse pression. Cela est peut être du au faible nombre d'essais disponible pour explorer une large gamme de paramètres. On observe aussi qu'il est plus difficile d'obtenir une résonance prononcée dans la nouvelle configuration. D'une part, le niveau des fluctuations de pression mesuré en absence de modulation est plus élevé indiquant que le bruit associé à la combustion turbulente est plus important. D'autre part, les fluctuations de température couvrent un volume plus large de la cavité et leur niveau est plus élévé car la puissance dégagée a été augmentée. Dans cette situation, la résonance est moins nette et les modes sont perturbés. Ces observations conduisent à étudier les effets des fluctuations turbulentes de température sur le facteur de qualité du système, un aspect peu traité dans la littérature mais dont l'impact peut être important en pratique. Une modélisation théorique de cet aspect est développée au Chapitre VI.

Abstract

High frequency combustion oscillations are investigated experimentally with a new five element injector operating at high pressure. The 24 hot fire tests carried out with this new system correspond to different operating configurations and parameters. It has been possible to explore the high pressure range up to a value of 6 MPa. Three intensified cameras record the instantaneous OH* emission to study the flame geometry. Pressure transducers, photomultipliers and a high speed camera are used to investigate the flame dynamics and the coupling between heat release and pressure fluctuations. For each operating point, three tests are carried out, the first without modulation serves as a reference, the second with a linear frequency sweep is used for modal identification and finally the third hot fire test with a continuous modulation at one of the frequencies determined during the second test, provides the system response. First, the chamber pressure is set at an intermediate value of 3 MPa and the influence of the mixture ratio E and the momentum flux ratio J on the flame sensitivity to external acoustic modulation is investigated. Results show large difference in the structure and response of the flames. Experiments are then carried out at a transcritical pressure of 6 MPa. The oxygen jet is injected at a temperaure which is below the critical temperature but at a pressure which exceeds the critical value $p_c = 5.04$ MPa. Results obtained with the same optical diagnostics indicate that the flame geometry differs from that observed at the subcritical pressure of 3 MPa. Finally, a fundamental investigation is carried out on the effect of the acoustic modulation on isolated flames at 1 MPa. These various tests have not allowed to find a coupled response as strong as that observed at low pressure. This could be due to the limited number of tests available to scan a broad range of operating conditions. One also observes that it is more difficult to observe a pronounced resonance in the new configuration. On one hand the level of pressure fluctuation in the absence of modulation is higher indicating that the noise radiated by the turbulent combustion process is more intense. On the other hand, the temperature fluctuations cover a broader volume of the cavity and their level is higher because the power release has been augmented. Under these circumstances the system resonance is less pronounced and the normal modes are perturbed. These observations indicate that one should study the effect of turbulent fluctuations on the quality factor of the system, an aspect which is not well documented in the literature but which may have important consequences in practice. A theoretical modeling is developed in chapter VI.

III.1 Introduction

Experimental investigations are essential to a better understanding of the dynamics of cryogenic flames of the type used in liquid rocket engines. Various modes of interactions including collective effects can be studied in a multiple injector combustor (MIC) and a wide range of parameters can be explored to determine the mechanisms and key parameters governing the development of combustion oscillations. The Mascotte facility equipped with a new MIC is used to advance the state of the art in this are area and specifically to develop experiments at intermediate and high pressures up to 6 MPa. The new configuration features five injectors instead of the three elements used previously and the mass flow rates have been augmented to reach the new pressure values. The study relies on the modulator wheel and optical diagnostics used at low pressure.

The experimental investigation described in this chapter was designed on the basis of the findings of the tests carried out at low pressure. These were carried out with three injection elements operating at 1 MPa. It was found that strong interactions could be induced between combustion and pressure fluctuations (Richecoeur et al. (2006) and chapter II). Systematic experiments were carried out by varying the methane injection velocity and temperature. These variations induced important modifications in the flame structure and dynamics. Low injection velocity led to long flames which were the most receptive to external modulation. Coherence between the pressure and heat release fluctuations occured when the level of oscillation was high. The low pressure experiments indicated that the toothed wheel modulator could induce strong acoustic perturbations in phase with the flame response.
A strong coupling between heat release and pressure oscillations could be observed but the acoustic energy provided by the external modulator was still not quite sufficient to reach a situation where acoustic perturbations dominate turbulent fluctuations. It was thus believed that by increasing the operating pressure one would be able to augment the level of pressure oscillation. This increased pressure would also more closely reflect conditions prevailing in real engines. It would also be possible to operate in the transcritical range by setting the pressure at a value exceeding $p_c(LOx) = 5.04$ MPa. At the end of the low pressure tests, the injection plane had burned up and there was an opportunity to design a new injector with a number of units larger than that used previously. It was then decided to design a new backplane with five units to come closer to the practical case where injectors are arranged like a showerhead. The five injectors constitute a finite row which is somewhat more realistic than the three injector set-up used previously.

The set of experiments described in this chapter aim at increasing the modulation level to obtain a system dominated by acoustics and perhaps trigger self-sustained instabilities. For this, it was important to increase the power release in the chamber and distribute this power over a larger volume. This was done by increasing the number of injection units. The new backplane comprises five coaxial elements. With this new arrangement it was reasoned that collective interactions could become more effective. It was also decided to increase the chamber pressure. The nominal pressure was set at an intermediate value of 3 MPa but several tests have been performed at a relatively high value of 6 MPa. By increasing the pressure chamber, the amplitude of the modulation is increased because the mass

flux exiting the chamber through the secondary top nozzle is augmented.
Twenty four hot fire tests were planned and executed to explore the domain of operation including variations in chamber pressures, momentum flux ratio J, and mixture ratio E. Changes of the last two parameters were made to find regions where combustion is more receptive to external modulations and study the dynamics of the system in those regions.
Two additional configurations were also defined to obtain fundamental information. In the first case the central three injectors were blocked with the two outer units operating. In this situation the distance between the two elements is large and the flames are sufficiently far from each other to avoid interactions. This is a complementary study to the first set of experiments. This is used to study the effect of acoustic modulation on non interacting flames. These tests were carried out at 1 MPa. Second, liquid oxygen and gaseous nitrogen were injected at a pressure of 3 MPa chamber and the jet dynamics was observed in the absence or in the presence of a transverse modulation. This cold flow experiment is used to examine the collective coaxial jet motion when they are submitted to strong acoustic perturbations. It will be described in the following chapter together with numerical simulations.

The next section describes the new MIC and the experimental instrumentation. The test bench and the modulator were modified again to reduce some of the problems observed in the previous set of experiments. The diagnostics are the same as those used previously but improvements have been made to increase the accuracy. These modifications are also presented in section III.2.
Section III.3 gathers operating conditions. Their selection is based on information from previous experiments and takes into account the objectives defined previously.
Experiments carried out at 3 MPa are described in Section III.4. The hot fire tests were aimed at investigating the influence of the momentum flux and mixture ratio. Results corresponding to three operating points are presented together with a comparison between the various tests.
The fifth and sixth sections respectively present tests results obtained at a pressure of 6 MPa corresponding to a transcritical operation and in the case of two isolated flames at a low pressure of 1 MPa. The number of experiments in these two ranges is too small to allow systematic analysis. It is however possible to conclude that further experiments should be carried out in the higher pressure range.

III.2 Experimental configuration and diagnostics

III.2.1 The combustion chamber

In the new multiple injector combustor, the downstream part of the chamber remains unchanged and its dimensions are those given previously ($35\times25\times5$ cm^3). This unit is equipped with two 15×10 cm^2 quartz windows located on the lateral sides of the chamber. A new injection head has been designed and built to bring the number of injection elements to five and to place dynamic pressure sensors in the injection cavities.

With this new injection plane it is possible to increase the power released by keeping the same mass flow rates per coaxial injector (i.e. around 20 g s^{-1} for oxygen and 17 g s^{-1} for methane per element).

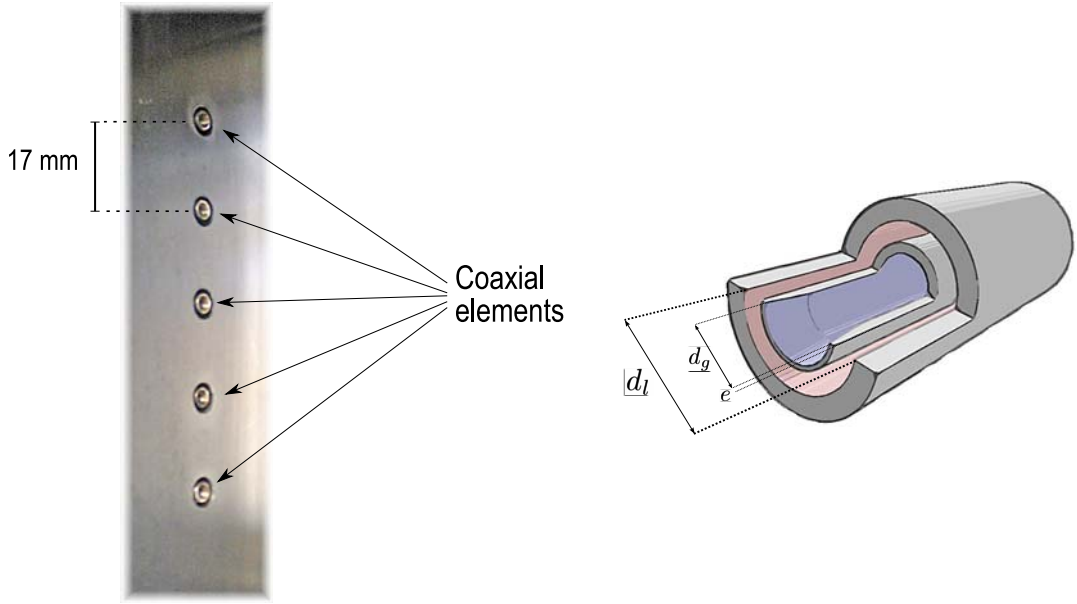

Fig. III.1: General view of the new injection head used at 3 and 6 MPa for the high pressure hot fire experiments and schematic representation of a single injector element.

The total mass flow rate delivered to the system is 100 g s^{-1} of liquid oxygen and 85 g s^{-1} of gaseous methane. A view of the injection head with its five elements is presented in Fig.III.1. The liquid oxygen injection diameter (d_l) is constant during the test series and its value is equal to 2.9 mm. The lip thickness is equal to 0.3 mm. The oxygen is injected at a temperature of 80 K.
The gaseous methane injection diameter (d_g) can be easily changed to adapt injection conditions to the targeted operating point. The values of the available diameters are shown in table III.1 associated with the corresponding operating point characteristics. With the smallest value $d_g = 4.95$ mm, the external surface of the oxygen element and the methane channel inner surface are only separated by 0.72 mm. This is the minimum gap which can be used reliably. Below this value, the relative position of the two parts composing each injection element cannot be set up accurately and this may lead to fatal damage to the injection head.

As already indicated most of the hot fire tests have been performed at 3 MPa. Exploratory tests have been carried out at 6 MPa and some experiments correspond to a low pressure of 1 MPa. The pressure in the chamber is controlled by a balance between the total mass flow rate entering the chamber and the discharge characteristics of the exhaust nozzle. The operating pressure is obtained by changing the throat diameter (d_c) of the main exhaust nozzle. Table III.1 gathers the different values of d_c used as a function of the operating points.

It is known from some experimental investigations of liquid rocket engine instabilities that the chamber and the injection lines may couple, giving rise to large amplitude pressure fluctuations. This occurs when the head loss in the injector element is too small giving rise to low frequency instabilities. One may wonder if this type of coupling may also appear in the high frequency range. This question is less well documented and there are no clear measurements indicating that this can happen. It is therefore interesting to see if such a coupling can be observed in the present experiments. This is accomplished

Operating point	I2-P10	I5-P30-A to D	I5-P60
Chamber pressure (MPa)	1	3	6
Main nozzle diameter, d_c (mm)	12.25	11	6.5
Secondary nozzle diameter (mm)	5.8	5.8	3.5
Percentage of mass flow rate	11 %	18.5 %	14.5 %

Tab. III.1: Diameter of the main and auxiliary nozzles, and the corresponding percentage of mass flow rate exiting the chamber through the auxiliary nozzle, depending on the operating point. The percentage is the square ratio of the secondary diameter over the main nozzle diameter divided by 2 (gases are ejected through the secondary nozzle only during half of the time).

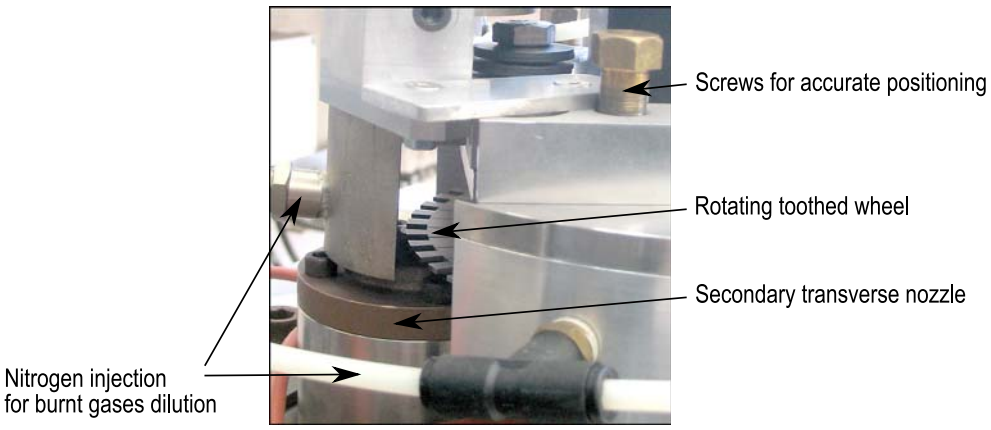

Fig. III.2: View of the modulation toothed wheel periodically blocking the secondary transverse nozzle on the top wall of the combustor. A rigid casing confines the system to protect operators and equipment in case of rupture of the high speed rotating wheel.

by placing two dynamic pressure sensors in the oxygen and methane cavities. These transducers will detect the pressure fluctuation on the upstream side of the injection elements. It will be possible to see if the pressure waves generated in the chamber can be measured in the cavities used to distribute the propellants. The positioning of these transducers is not easy but the information provided by these probes could be extremely relevant.

III.2.2 Evolution of the modulation wheel

Suitable operation of the modulation system is critical in the present experiments. The modulator comprises a toothed rotating wheel which periodically blocks a secondary nozzle plugged on the upper wall of the chamber. The modulation of the mass flow rate exiting the chamber through the auxiliary nozzle generates acoustic waves in the chamber at a frequency depending on the rotation speed. Figure III.2 shows a view of the modulator installed on the MIC.

The toothed wheel has a total diameter of 185 mm and it comprises fifty 6-millimeter square teeth. The thickness of the wheel is 2 mm. This wheel was used during the first hot fire tests and proved

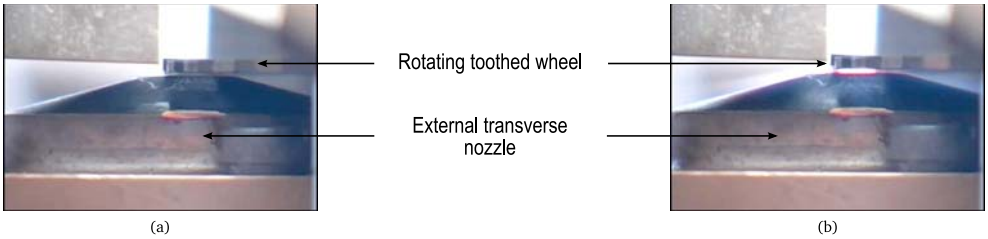

Fig. III.3: Position of the 2 millimeter thick toothed wheel relatively to modulation nozzle without pressure in the chamber (a) and during the hot fire experiment at 3 MPa (b).

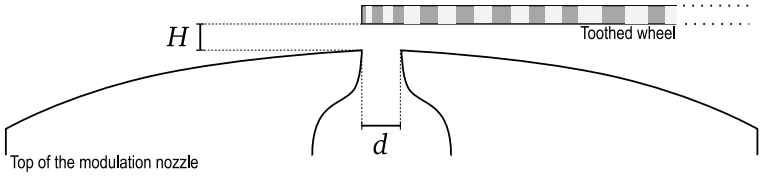

Fig. III.4: Schematic of the relative position of the toothed wheel and the secondary transverse nozzle. The optimized position of the wheel is obtained for $H = 0$.

to be well-adapted to the generation of acoustic modulations. Here, the chamber pressure has been augmented initially by a factor of 3 and later by a factor of 6. This induces larger loads on the wheel and correspondingly an augmented deflection. This is not negligible and may deteriorate the modulator performance and reduce the level of oscillation which can be obtained with the system. The teeth are bent by the impinging jet and this has been observed during the high pressure tests. A digital camera was focused on the secondary nozzle to track the wheel location relative to the nozzle (Figure III.3). The chamber pressure generates a force which is strong enough to displace the wheel almost 2 mm away from the top of the nozzle. The negative impact of this deflection on the modulation can be deduced from simple geometrical considerations.

The system operates like a nozzle with a double throat. The first throat is that of the auxiliary nozzle. Its diameter is d. The second throat corresponds to the area of a cylinder of diameter d and height H which corresponds to the gap between the nozzle and the wheel (Figure III.4). The areas of these two throats can be compared. The first area S_1 is the exit area when the wheel does not block the nozzle : $S_1 = \pi d^2/4$. The second area S_2 is the area available when the wheel is supposed to block the nozzle : $S_2 = \pi dH$. Hence, the ratio of these two areas is $\Sigma = S_2/S_1 = 4H/d$. To generate a strong acoustic modulation, this ratio Σ should be as small as possible ($H \sim 0$) and at least smaller than unity. If the second throat is larger than the first, the mass flow rate is governed by the nozzle throat diameter which is fixed and the mass flow rate will not oscillate. With $H = 2$ mm and $d = 5.8$ mm (like in the I5-P30-A test case), $\Sigma = 1.38$ and this means that the rotating wheel does not modulate the secondary flow.

A precise positioning of the wheel relative to the nozzle is critical for the modulator efficiency. It is

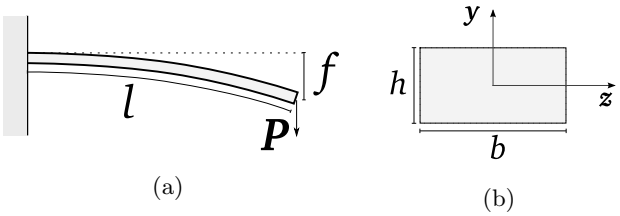

Fig. III.5: Schematic side (a) and front (b) views of a single tooth attached to the wheel and characteristic dimensions.

$b = 5$ mm	$h = 2$ mm	$l = 20$ mm
E = 2.10^{11} N m^{-2}	$\rho = 7.8\ 10^3$ kg m^{-3}	P = 50 N

Tab. III.2: Dimensions and mechanical characteristics of one tooth of the modulation wheel.

therefore interesting to estimate the deflection induced in the steady state and also examine a possible resonance mechanism of the teeth composing the wheel. Assuming that an isolated tooth can be assimilated to a rectangular beam, the deflection f is given by

$$f = \frac{Pl^3}{3EI} \tag{III.1}$$

where l is the tooth length, P the vertical force acting on the tooth when it is fully exposed to the jet (Figure III.2.2), E the Young modulus and I the moment of inertia given by

$$I = \int_{-h/2}^{h/2} y^2 dz dy$$

where y and z are the cross section axes, h and b are respectively the thickness and width of a tooth as shown in figure III.2.2. Thus I can be calculated as:

$$I = \frac{bh^3}{12} \tag{III.2}$$

Using equations III.1 and III.2,

$$\boxed{f = \frac{P}{3E}\left(\frac{l}{h}\right)^3} \tag{III.3}$$

one finds that by doubling the tooth thickness h, the deflection can be divided by 8.

Using the same simplifying assumptions it is possible to estimate the eigenfrequencies of each tooth. The eigenmodes of each element treated as a cantilevered beam are defined by

$$\lambda_n l = (2n-1)\frac{\pi}{2}$$

with

$$\lambda_n^4 = \frac{\rho bh\omega_n^2}{EI}$$

for n = 1, $\lambda = \pi/2$ so

$$\omega^2 = \frac{EI}{\rho bh}\lambda^4$$

which leads to

$$\boxed{\omega = \left(\frac{E}{12\rho}\right)^{1/2} \left(\frac{\pi}{2l}\right)^2 h} \tag{III.4}$$

Using the actual dimensions, one finds a first eigenfrequency of 2870 Hz. This value is in the range of frequencies swept by the modulator and this could induce a resonance and modify the level of excitation. There is a linear relation between the thickness of a single tooth h and its eigenfrequencies. By doubling the thickness, the eigenfrequency is multiplied by 2. The eigenfrequencies also scale like the inverse square of the beam length l. When the length is divided by 2, the eigenfrequency is multiplied by 4.

Both the deflection and the eigenfrequency can be modified by changing the length and thickness of each tooth. When it became clear that the wheel thickness was insufficient, a new toothed wheel was designed and quickly manufactored. this set of experiments with a doubled thickness ($h = 4$ mm) and a length divided by 2 ($l = 10$ mm). In this way, the deflection was divided by 8 and the eigenfrequencies were multiplied by 8. The new wheel was used during most of the hot fire tests and it notably improved the modulator effectiveness.

III.2.3 Diagnostics

Five pressure transducers (Kistler^{TM}) are plugged on the combustion chamber as in previous experiments. Three sensors are placed in the top wall, the two others are in the bottom wall. The pressure signals delivered by these transducers are sampled at a rate of 40 kHz and they are recorded in a dynamic way meaning that the continuous component of the pressure is not recorded. All the sensors are cooled down, there is no filtering and the range is adapted to the typical amplitude of the signals.

A thermocouple is set in the bottom wall of the chamber. The sampling rate is only equal to 1 kHz since the response time of the thermocouple is relatively slow compared to the characteristic time of the acoustic phenomena. This sensor cannot portray the dynamic behavior of the temperature at the wall but it gives an average evolution which can be used to see if the heat flux to the wall is augmented during modulated tests.

The flame behavior is characterized with two intensified cameras equipped with optical filters focusing on the central plane of the chamber. The two cameras have an UV optics (Nikon^{TM}105 mm f/2.8) with the same couple of filters, UG-11 and WG 305, to isolate the wavelength corresponding to the OH* radical emission. The data acquisition rate is 18 Hz with frame dimensions equal to 512×330 pixels (i.e. about 3 pixels per millimeter). A beamsplitter divides the incoming light into two equally intense beams captured by the two cameras. Images are recorded exactly out of phase to improve the statistics. The exposure time varies significantly with the operating point but remains around 1 μs which is small enough to freeze the flow.

A key factor in the study of combustion instabilities is the coupling between pressure and heat release fluctuations. Pressure fluctuations are measured by the pressure transducers while two photo-

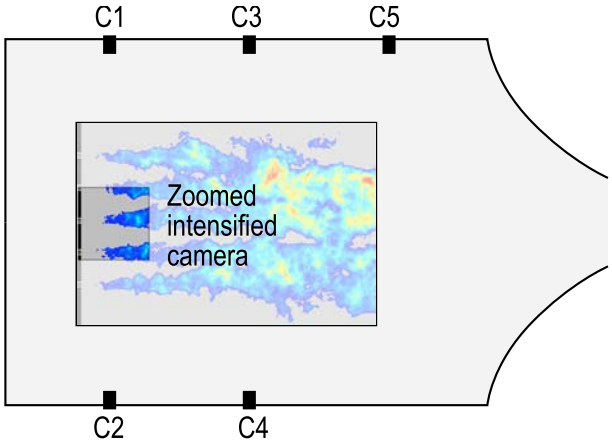

Fig. III.6: Side view of the combustion chamber showing the region viewed by the intensified camera. This region covers the initial flame formed by the central injector.

multipliers (PM) are placed in front of the second quartz window to record the heat release variations. The sampling rate is 40 kHz. A filter is used to select the UV band corresponding to OH* radiation. The two photo-multipliers are placed at 11 cm from the injection plane. A spatial filter is used to define a small area of observation which roughly measures 10×10 mm^2. The two PM are placed on a vertical line to allow simultaneous detection of fluctuations in the upper and lower parts of the chamber at a distance of 11 cm from the injection plane. One expects to record transverse oscillation of heat release, resulting from the coupling between combustion and acoustic waves. The relative position of the two PM was selected to follow this motion. A photo diode is mounted on the toothed wheel to record the wheel position at each time. Thus, each frame can be accurately linked to the pressure field in the chamber. More information on these diagnostics is available in the previous chapter.

In addition to the previous instruments, a third intensified camera is focused on the central injector element as shown in figure III.6. The optics is a Nikon^{TM}200mm f/2.8 which only transmits light in the visible range. The natural emission of the flames is captured. The CCD matrix features 1024×1024 pixels with a definition of 21 pixels per millimeter. This camera provides a very high spatial definition of the flame radiation close to the injector but the time resolution is very low, as the images are recorded at a rate of 4 Hz.

The flame motion is recorded by a high-speed camera which is slightly out of the view axis but allows to see the injector and the whole chamber. The acquisition rate is equal to 30000 frames per second with a resolution of 256×128 pixels (i.e. 1.5 pixels per millimeter) with common optics, 60 mm f/1.4. Due to the large amount of data recorded by this camera, only 6 seconds of each run can be stored.

The Onera Mascotte team also operates a digital camera to provide real time visual access to the chamber at an acquisition rate of 25 frames per second. This instrument gives information on the quality of the ignition phase, eventual flame/wall interactions and related color changes and quartz

window obscuration due to soot particles, water droplet deposition or window damage. A similar digital camera is used to observe the position of the toothed wheel with respect to the secondary nozzle.

III.2.4 Spectral data processing

Spectral and cross spectral data processing is used to analyze the signals delivered by the pressure sensors and photomultipliers. The spectral densities are calculated by averaging periodograms obtained from M= 200 blocks of N= 2048 points. An overlap of 1/3 of a block is used in these calculations. The sampling frequency is in all cases $f_e = 40$ kHz and the signals are band pass filtered between 500 and 4500 Hz.

III.3 Operating points

The operating points defined in Table III.3 were selected on the following basis :
(1) To augment the coupling level, the global power is increased and distributed over a larger volume through five injector elements. The oxygen mass flow rate reaches 100 g s^{-1} while the methane mass flow rate is varied from 75 to 117 g s^{-1}. This allows to increase the power of the experiment and investigate the influence of mass flow rate on the flame stability.
(2) It is known from many studies of cryogenic combustion that the momentum flux ratio J essentially governs this type of combustion and can be used as a main scaling factor. It is also important to keep the mixture ratio E in the same range of values. To examine the effect of J without changing E one has to change the methane injection diameter d_g from one test to the other, since that would lead to a change of the methane mass flow rate.
(3) An increase of the modulation amplitude can be expected if the ambient pressure in the chamber is augmented. Tests are carried out at 3 MPa and 6 MPa. Most of the tests were completed at 3 MPa, which is below the critical pressure of oxygen (5.04 MPa). Five tests were carried out at 6 MPa to investigate the flame sensitivity when the injection of oxygen is transcritical.
(4) One question raised after the low pressure tests concerned the possibilty of obtaining a strong coupling with a single injector. One wonders whether the coupling requires collective interactions of flames originating from multiple injectors or if the same results can be obtained with an isolated injector. To obtain this complementary information the first hot fire tests were carried out at 1 MPa. Operation with a single injection element was not feasible and these experiments had to be planned with two injectors operating at 1 MPa. The central injectors were blocked to have the largest possible distance between the two flames to keep flow interactions to a minimum.
(5) No attempts were made previously to look at the interaction between coxial jets and transverse modes under high pressure conditions. A cold flow test case was defined at 3 MPa to examine the effect of a strong transverse modulation. For security reasons the system cannot be operated with oxygen and methane. This last reactant was replaced by gaseous nitrogen. The effect of the transverse acoustic modulation on the jet motion was observed by backlighting. This test provides experimental results which can be used to guide numerical simulations. These tests and some numerical calculations will be described in the next chapter.

The previous considerations define the test matrix (see table III.3 and the seven conditions selected for this experimental program). To clarify the presentation, the configurations are divided in three groups :

- The operating points **I5-P30-B**, **I5-P30-C** and **I5-P30-D** are used to investigate the effect of the mixture ratio E and the momentum flux ratio J.
- The operating points **I5-P30-A**, **I5-P60**, **I2-P10** are analyzed independently to study respectively the effects of the low velocity injection, the high chamber pressure and the single element injection.
- The cold flow test **I5-P30-**α is considered in a separate chapter as it serves to guide numerical simulations.

The operating parameters were chosen by extrapolation from what was learned from the previous campaigns. These parameters are summarized in table III.3.
It is important to note at this point the limited number of tests which can be performed sets an important constraint on the experimental program.

III.4 High pressure hot fire experiments

III.4.1 Objectives

This first set of experiments aims at determining the effect of E and J on the combustion stability. Three operating points can be used for this purpose : **I5-P30-B**, **I5-P30-C** and **I5-P30-D**. Operating point **I5-P30-A** was also available but a lower methane injection velocity could be reached and the operating point **C** was preferred to **A**. The only difference between the two points is the methane mass flow decreasing which was 83 g s^{-1} in **I5-P30-A** and only 75 g s^{-1} in **I5-P30-C**.

Previous experiments indicated that low J values generated longer and more receptive flames but no systematic study on the effect of the mixture ratio E had been completed. J characterizes the dynamics of the coaxial flow. For high J the momentum of the gas phase is much higher than that of the liquid phase. This accelerates the liquid jet break-up and subsequent atomization of the liquid phase leading to shorter flames, and improved stability. It was reasoned that by decreasing the velocity ratio between the liquid oxygen and gaseous methane it would be possible to destabilize the system and make it more receptive to acoustic perturbations. The methane to oxygen velocity ratio could not be made smaller than 16.4 (mainly by decreasing the methane injection velocity while keeping a constant oxygen injection velocity of 2.5 m s^{-1}). J is then small compared to usual values encountered in practical engines (above 9 for liquid oxygen / gaseous hydrogen combustion). The influence of J on the flame structure has been observed during the first campaigns and will be confirmed in what follows. The effect of a variation of E is investigated while keeping J constant.

Results obtained for the three operating points are presented without and with modulation. The operating point **B** corresponds to a high J and a low E, **C** is the low J high E point and **D** is the

Test Case	I5-P30-A	I5-P30-B	I5-P30-C	I5-P30-D	I5-P60	I2-P10	I5-P30-α
Fluids	LOx/GCH_4	LOx/GCH_4	LOx/GCH_4	LOx/GCH_4	LOx/GCH_4	LOx/GCH_4	LOx/N_2
Pressure (MPa)	3	3	3	3	6	1	3
Number of Elements	5	5	5	5	5	2	5
LOx Flow Rate ($g.s^{-1}$)	100	100	100	100	90	45	100
LOx Speed ($m.s^{-1}$)	2.5	2.5	2.5	2.5	2.3	2.85	2.53
CH_4 (or N_2) Flow Rate ($g.s^{-1}$)	83	117	75	75	60	40	145
CH_4 (or N_2) Speed ($m.s^{-1}$)	45	64	41	68	28	102	86.3
J ($\rho_{fuel}U_{fuel}^2/\rho_{LOx}U_{LOx}^2$)	6	12	4.8	13	5.6	7.3	33.7
E ($\dot{m}_{LOx}/\dot{m}_{fuel}$)	1.2	0.85	1.33	1.33	1.5	1.12	0.69
d_g (Gas injection diameter) (mm)	5.78	5.78	5.78	4.95	4.95	7	4.95
Number of tests	3	3	4	4	5	3	3

Tab. III.3: Operating points for fundamental investigations

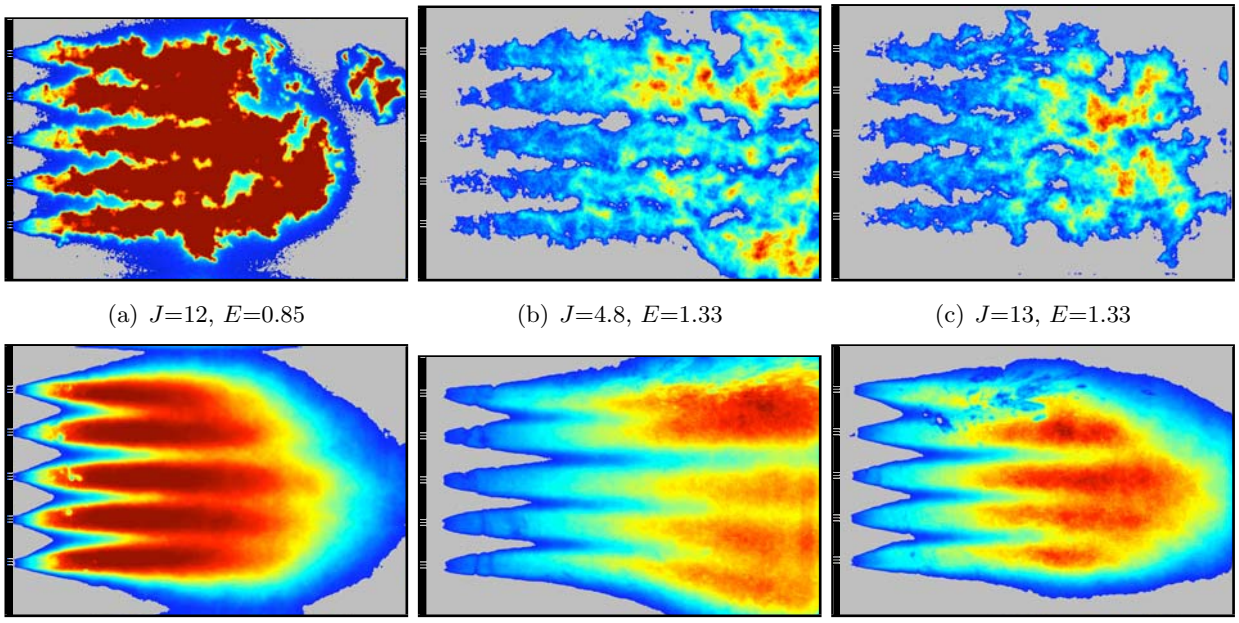

(a) J=12, E=0.85 (b) J=4.8, E=1.33 (c) J=13, E=1.33

(d) J=12, E=0.85 (e) J=4.8, E=1.33 (f) J=13, E=1.33

Fig. III.7: Instantaneous and averaged OH emission for modulation free operating points **I5-P30-B** (respectively (a) and (d)), **I5-P30-C** (respectively (b) and (e)), **I5-P30-D** (respectively (c) and (f)).*

high J high E point. These points are reached by varying the methane mass flow rate and the gas injection diameter d_g.

III.4.2 Modulation free hot fire tests

III.4.2.1 Spatial analysis of the flame structures

Differences between the operating points are conveniently observed by comparing instantaneous OH* emission distributions. These maps provide the general combustion pattern, flame locations and structures. Figure III.7 shows instantaneous and averaged OH* emission respectively for the **B**, **C** and **D** operating points. The instantaneous image of the **B** operating point is of low quality. This test was the first in the series and the global emission of the flame was surprisingly high. Details about the flame structure cannot be observed due to saturation of the intensified CCD detector. This operating point was not tested a second time because it was not considered crucial and it would have been necessary to cancel another operating condition to double it. This image gives relevant information about the flame position at low E value and this remains a useful test in the study.

The three operating points feature three different flame structures.
(1) At high J and low E (**I5-P30-B**), atomization is effective because the velocity differential is large. Mixing and combustion is intense producing compact flames. Combustion takes place close to the injection plane and the flames are contained in the visualization window. Flame lengths are homogeneous and combustion is well stabilized. The expansion angle of the flame is equal to 14.3° which is relatively high compared to what is observed in other cases. Flame interactions occur close to the injector, at about 15 oxygen diameter d_l.

(2) At low values of J and high E (**I5-P30-C**) the flames are longer. For a low value of J, the velocity differential is reduced atomization is delayed and the combustion process is distributed over a longer distance. The flames extend beyond the window right boundary and they cannot be observed entirely. Mutual interactions take place at about 40 d_l. Close to the injector, the expansion angle is equal to 9° and it increases progressively with the distance from the injector. The flames only close on the downstream end of the chamber. The characteristic time of the combustion process is augmented and its value approches that of the typical acoustic period. One expects that the flames will be more receptive to external acoustic perturbations.
(3) The third operating point, at high J and E values (**I5-P30-D**), is intermediate between the two previous cases. The flames are compact, their expansion angle is constant and equal to 10°, mutual interaction occurs at 22 d_l and the flames close right after the visualization window boundary. The five flame lengths have similar values. Due to the saturation at operating point **B**, it is difficult to compare the flame lengths for different values of E but the flame shape is comparable. Figure III.7(f) illustrates one of the difficulties of this experiment. The top flame is not correctly visualized because soot particles were deposited on the window during the ignition process. This seriously deteriorates the image quality.

For operating points **I5-P30-C** and **I5-P30-D**, the central injection element is observed using the second intensified camera. The two operating points have different J but the same E. These images show the initial flame stabilization and they can be used to compare the distances of interaction between adjacent flames.

Figure III.8 shows the instantaneous and averaged OH* emission for these two operating points in the absence of modulation. The interaction zone depends on the operating point. For low J values (C), the flames are longer and the interaction point is moved downstream at 11 d_l in the averaged frame. When J increases, the flames are shorter and the interaction point is located at 8 d_l. One interesting point here is to notice that the expansion angle at the injection is identical whatever the operating point. This angle is equal to 14° for the two cases. However by modifying the momentum ratio, the flames evolve differently. For $J = 4.8$ (C) the atomization is delayed, and the flames remain close the oxygen liquid core. The initial expansion angle decreases quickly to 12° and this moves the interaction point downstream. In contrast, when J increases, the atomization efficiency increases. The expansion angle remains constant and the adjacent flames interact earlier. The injection dynamics strongly modify the flame structure even in the early part of the flame. After only 5 d_l the flame structure is different between the two operating points.

Instantaneous frames of OH* emission indicate that point **B** seems to be more interesting. It is not the most sensitive to external perturbations but the long flames expand significantly when modulated. This was already observed with the three element injector combustor operating at 1 MPa. These conditions provided the strongest and most coherent coupling between heat release and pressure fluctuations.

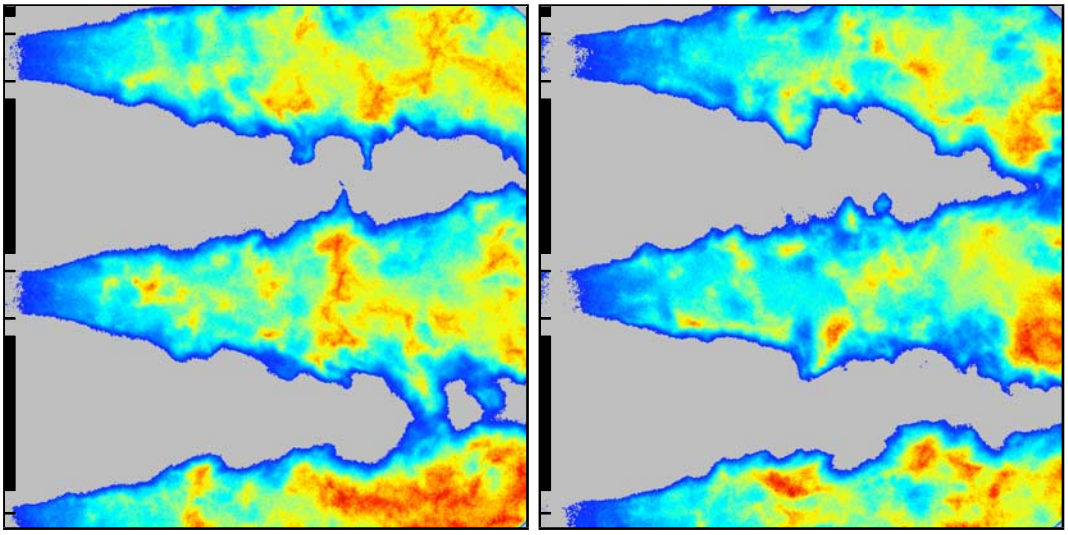

(a) $J = 4.8$, $E = 1.33$ (b) $J = 13$, $E = 1.33$

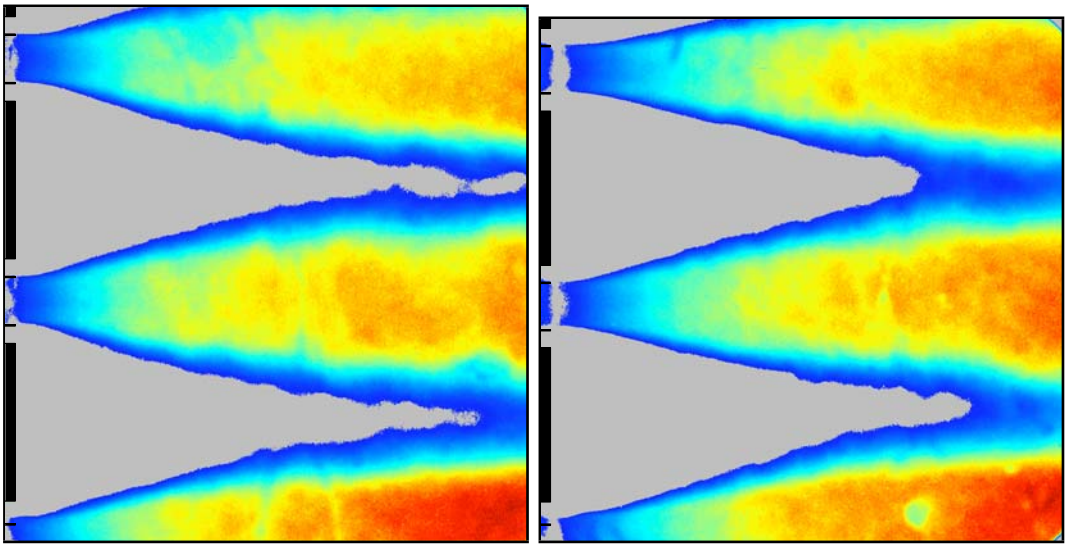

(c) $J = 4.8$, $E = 1.33$ (d) $J = 13$, $E = 1.33$

Fig. III.8: Instantaneous (top) and averaged (bottom) OH emission without external acoustic modulation for operating points I5-P30-C (a and c) and I5-P30-D (b and d).*

	I5-P30-B	I5-P30-C	I5-P30-D
C 1	41°	3°	41°
C 2	38°	4°	35°
C 3	54°	9°	54°
C 4	52°	0°	45°
C 5	82°	27°	93°

Tab. III.4: Phase difference between the five pressure transducer signals and the top photomultiplier at the coherent frequency around 2.1 kHz for the three operating points I5-P30-B, I5-P30-C, I5-P30-D.

III.4.2.2 Temporal and spectral analysis of the flames

It is next important to examine the spectral content of the photomultiplier and pressure transducers signals, see if there are common components and determine phase relations by calculating cross spectral densities and coherence functions. This study is first carried out in the absence of external modulation. The data obtained in previous low pressure tests was treated in this way but no correlation was found between the various signals indicating that combustion was developing in a natural fashion and remained insensitive to the possible resonances associated with the chamber eigenmodes. This is not quite so in the present experiments where power spectral and cross spectral densities of the signals show multiple correlated components which are analyzed in what follows.

As in previous tests, pressure sensors are flush mounted in the upper and lower walls and the two photo-multipliers are vertically aligned and observe two regions located above and below the combustor central plane. Figure III.9 shows the coherence between the first pressure transducer placed in the top upstream wall and the first photomultiplier focused on the top part of the chamber for the three different operating points. Four peaks are visible in the three diagrams in the high frequency range. The corresponding frequencies are around 1600, 2100, 3000 and 4000 Hz with slight variations with respect to the operating points. Only the 3 and 4 kHz peaks do not vary at all. By changing the photomultiplier/pressure transducer couple, one obtains essentially identical coherence functions. The coherence is particularly strong around 2100 Hz. An examination of the signals delivered by the photomultipliers also indicates that the signals are nearly in phase (Figure III.10) but that they are dominated by a low frequency component around 500 Hz. Phase relations between the five pressure sensors and the PM are summarized in table III.4. These values correspond to the spectral component around 2100 Hz. One finds that for operating point **C** the phase difference between the PM and the pressure sensors is near zero but the perturbations levels remain small and the combustor remains stable.

One may try to find the source of the common frequency components observed in these various tests and for this examine the most logical possibilities :

- The natural noise radiated by the combustion process excites the acoustic modes of the cavity

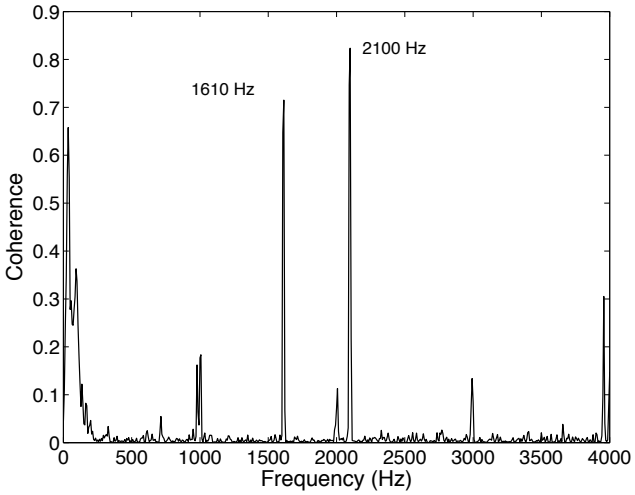

(a) $J = 12$, $E = 0.85$

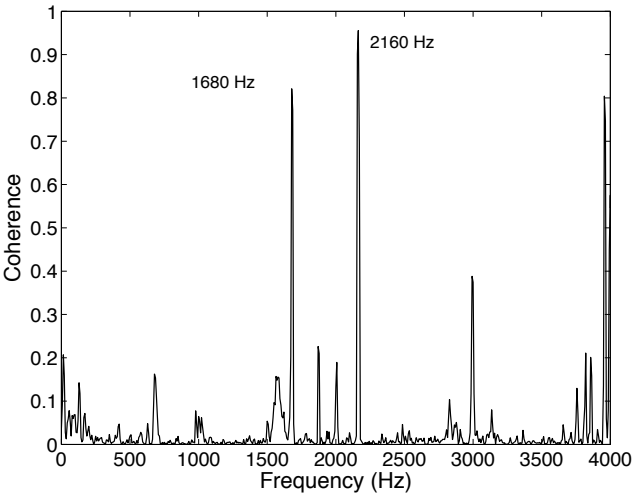

(b) $J = 4.8$, $E = 1.33$

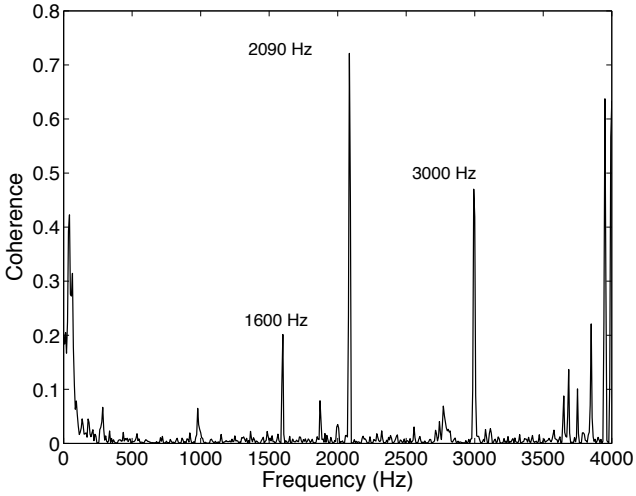

(c) $J = 13$, $E = 1.33$

Fig. III.9: Coherence between photomultiplier 1 (top) and pressure transducer 1 (top upstream) for the three different operating points in the absence of external modulation : (a) I5-P30-B, (b) I5-P30-C, (c) I5-P30-D.

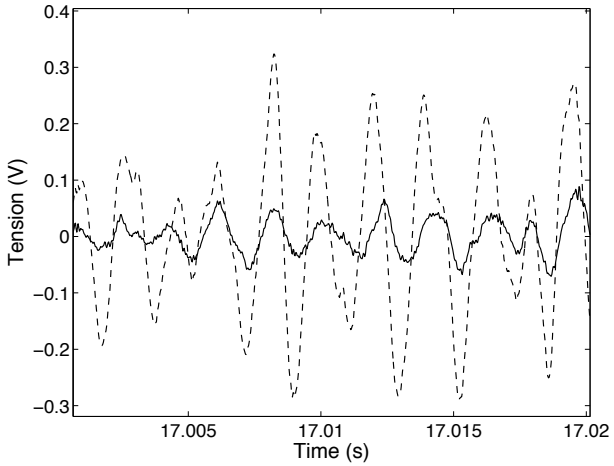

Fig. III.10: Photomultiplier 1 (bold) and photomultiplier 2 (dashed line) signals for the I5-P30-C operating point. Signals are in phase and this is observed during the other test cases as well.

generating coherent components in the pressure and heat release signals. However, the pressure fluctuation level at the common frequencies are quite low and do not appear in the power spectral densities of the pressure sensors which are dominated by lower frequencies. It is also found from the study of the acoustic response of the chamber (see the next subsection) that the modal frequencies are not far but sufficiently different from the values identified in the present section to be eliminated. Also, the phase relations established between the pressure sensors and photomultipliers around 2100 Hz do not correspond to those which are expected in the case of the first transverse mode. It is therefore reasonable to consider that the coherent components observed in the absence of modulation do not result from a coupling with the eigenmodes of the chamber.

- The common frequency components might be associated with the same turbulent fluctuations induced by the high speed injection of reactants. The use of five elements increases the global turbulent fluctuation level in the chamber. The frequencies should be influenced by the injection parameters. However these frequencies do not change significantly while injection conditions are notably modified. Between operating points **C** and **D** the methane injection velocity is divided by 3 but the frequencies remain essentially the same. It is thus reasonable to discard this second possibility.

- The coupling between the combustion chamber and the injection cavities may generate strong fluctuations. This is investigated in a following section.

In conclusion, the naturally developing flames feature coherent components in the high frequency range but these components are weak and cannot be related to the chamber eigenmodes or to characteristic fluctuations in the associated with the injection process.

III.4.3 Linear frequency sweep modulation

Acoustics of the combustion chamber depends on the temperature level and distribution in the chamber. It is then important to identify the eigenfrequencies and eignemodes for each operating point. This is accomplished as in the low pressure experiments by making use of a linear frequency sweep applied by accelerating the toothed wheel from 0 to 4000 rpm. This yields a linearly varying modulation frequency which is used as input to the system. The pressure signals are used as output and the eigenfrequencies are determined by extracting resonant conditions from short time Fourier transform analysis. This method works well when the system is perfectly homogeneous and in a steady state. We will see in what follows that the turbulent fluctuations and specifically those of temperature complicate the process. These fluctuations are in the present case more intense because the power has been augmented and they also affect a larger volume because the system now comprises five injectors. This has consequences which were not expected at the beginning of this investigation but deserve special consideration (see also the theoretical model developed in Chapter VI.2.1 to investigate effects of fluctuations on the sharpness of resonance).
Figure III.11 shows the pressure signals delivered by sensor 1 recorded during the linearly modulated tests and the short time Fourier transform analysis of thess signals presented as time/frequency maps. The data correspond to the three operating points I5-P30-B, I5-P30-C and I5-P30-D. Resonant peaks are observed at different instants in the time domain waveforms. Each peak corresponds to a maximum power level in the time/frequency diagram which is used to identify the corresponding frequency.

Each resonant peak features a finite bandwidth and the identification of the eigenfrequencies is perturbed by the presence of additional resonant spots in the sidebands. It is here useful to recall that numerical simulations carried out in the first chapter feature three resonant peaks in the range of frequencies under consideration : the first peak corresponds to the longitudinal mode, the second peak is related to a mode coupling the chamber and the auxiliary nozzle, the third peak pertains to the first transverse mode. The latter two modes should correspond to the strongest peaks in the signal and in the short time Fourier transform maps. However, figure III.11 indicates that the identification is not straightforward. The response is never sharp and each resonance features a relatively large bandwidth. The five sensors also feature different evolutions during the same test. Additional peaks appear in some of the signals. The resonant peaks are then identified by comparing the five pressure signals to determine the three most amplified peaks and correlate the eigenfrequencies with those expected from the simulation. For each operating point, three eigenfrequencies are obtained and gathered in table III.5.

Each resonant peak displayed in the time/frequency diagram has to be identified by analyzing phase differences between the five pressure sensors. Close-up views of the temporal signal are plotted to purpose around the resonance time to simultaneously observe the five pressure signals. For example, one expects that The first transverse mode will be such that top three pressure signals will be out of phase with the two bottom sensors. This is clearly visible in tests carried out without combustion. However under hot fire conditions the temperature in the chamber fluctuates and this complicates the phase analysis. Figure III.12 shows the five pressure signals pass-band filtered around the resonant frequency and plotted as a function of time to obtain a close-up view. The even numbered pressure

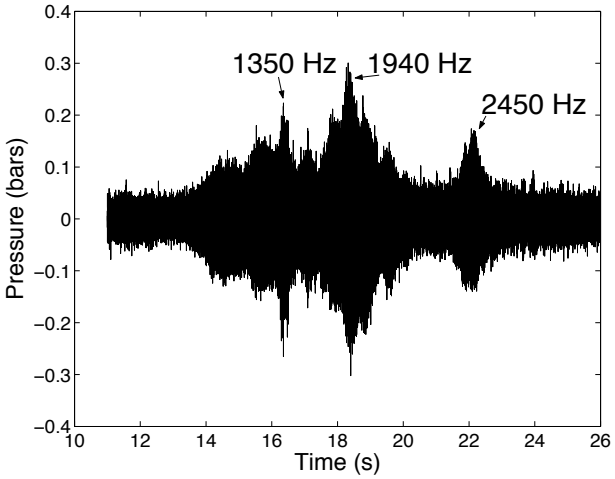

(a) $J = 12$, $E = 0.85$ (I5-P30-B)

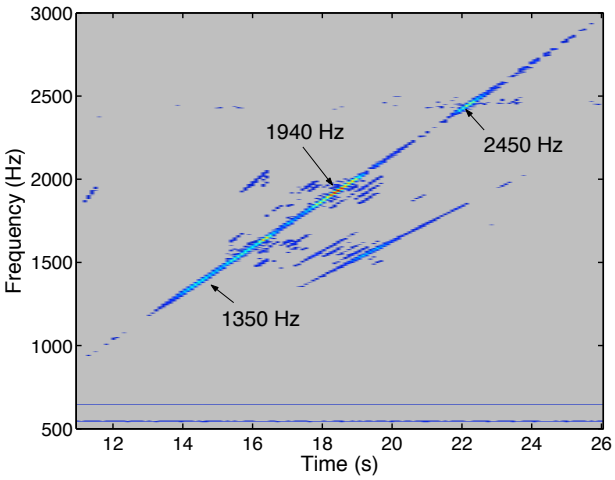

(b) $J = 12$, $E = 0.85$ (I5-P30-B)

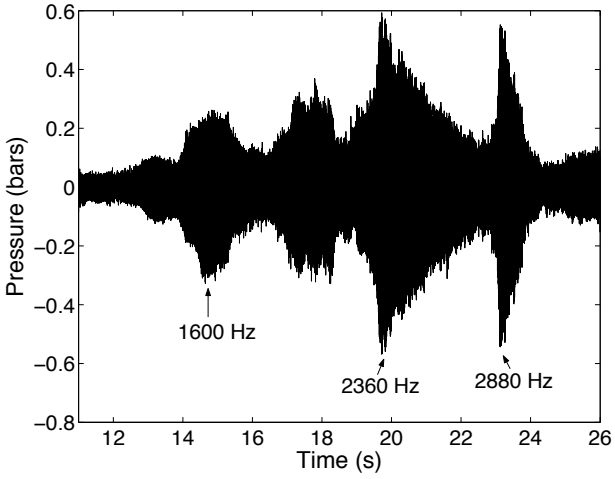

(c) $J = 4.8$, $E = 1.33$ (I5-P30-C)

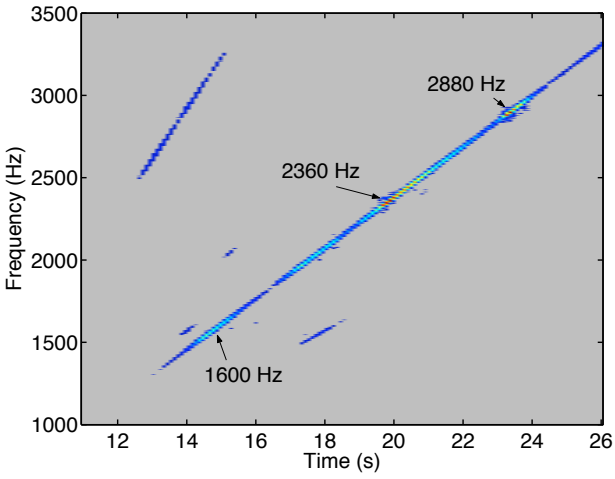

(d) $J = 4.8$, $E = 1.33$ (I5-P30-C)

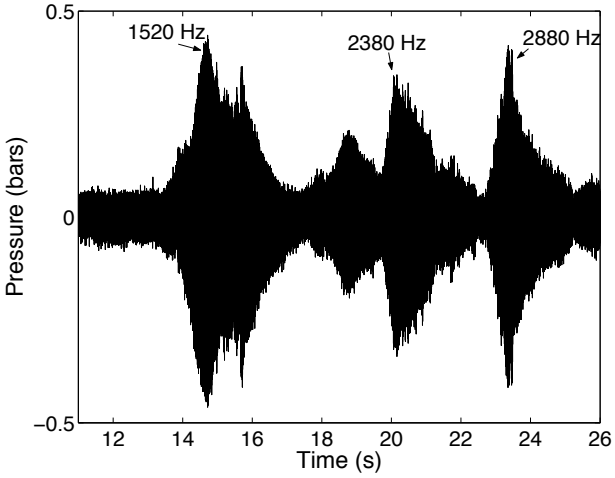

(e) $J = 13$, $E = 1.33$ (I5-P30-D)

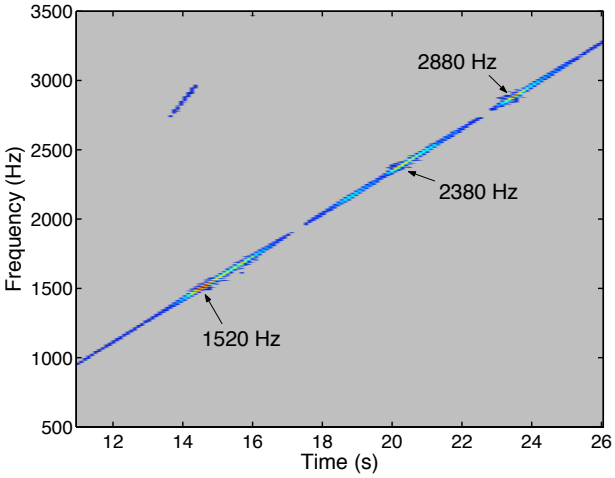

(f) $J = 13$, $E = 1.33$ (I5-P30-D)

Fig. III.11: Pressure signals and short Time Fourier transform analysis for a linear frequency sweep. The data correspond to three different operating points I5-P30-B, I5-P30-C and I5-P30-D.

Operating point	1st eigenfrequency	2nd eigenfrequency	3rd eigenfrequency
I5-P30-B	1350 Hz	1940 Hz	**2450 Hz**
I5-P30-C	1600 Hz	**2360 Hz**	2880 Hz
I5-P30-D	1520 Hz	**2380 Hz**	2880 Hz

Tab. III.5: Eigenfrequencies obtained experimentally for the three operating points I5-P30-B, I5-P30-C and I5-P30-D. The frequencies chosen for the continuous modulation tests are marked by boldface characters.

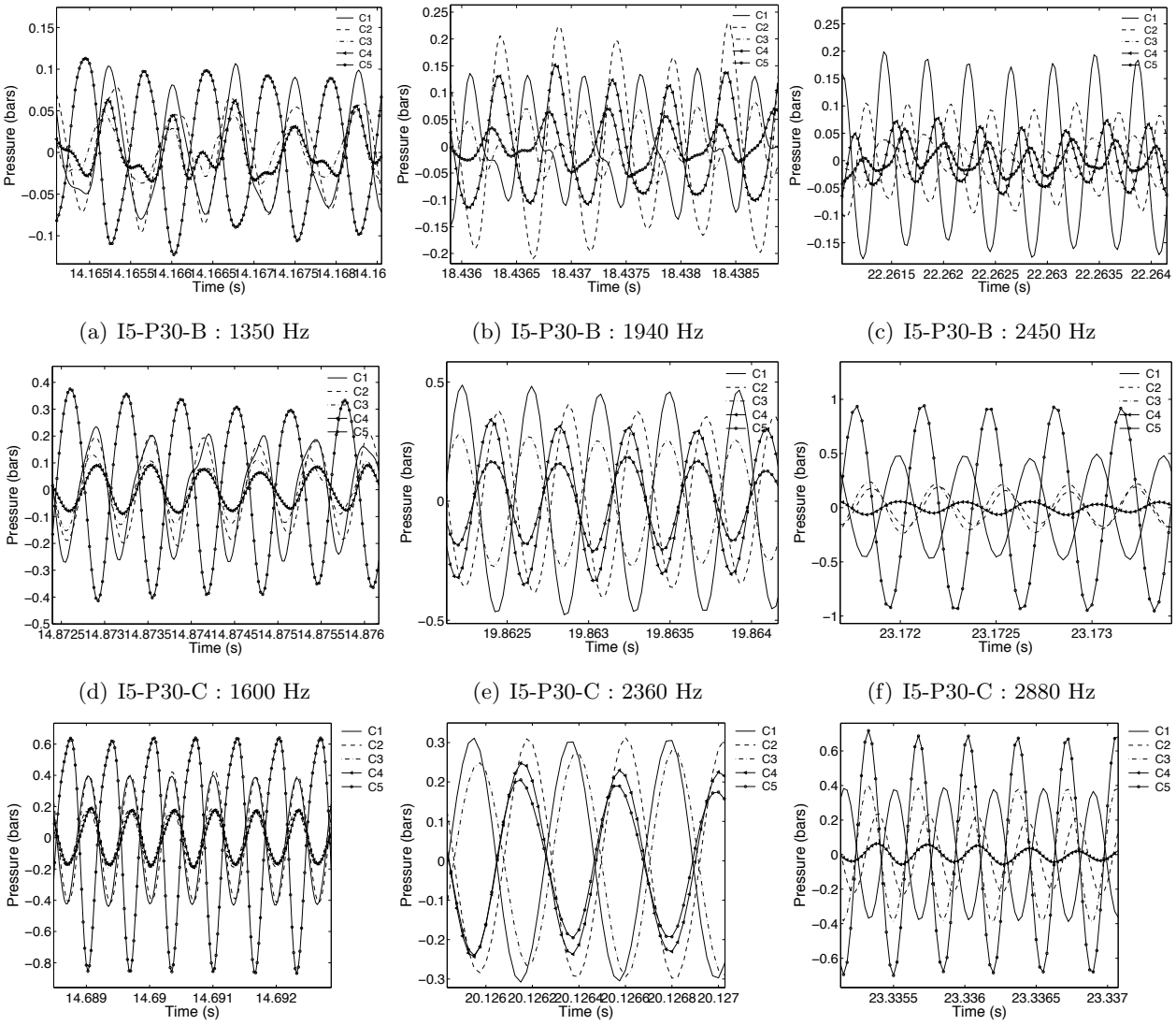

(a) I5-P30-B : 1350 Hz (b) I5-P30-B : 1940 Hz (c) I5-P30-B : 2450 Hz

(d) I5-P30-C : 1600 Hz (e) I5-P30-C : 2360 Hz (f) I5-P30-C : 2880 Hz

(g) I5-P30-D : 1520 Hz (h) I5-P30-D : 2380 Hz (i) I5-P30-D : 2880 Hz

Fig. III.12: Signals delivered by the five pressure sensors at the different eigenfrequencies for each operating point.

transducers are located on the top wall of the chamber while the odd numbered at placed on the bottom wall. One first notices that the second and third eigenfrequencies for operating points **C** and **D** are close to each other. The eigenfrequencies are mainly determined by the temperature distribution in the chamber which directly depends on the mixture ratio. These two operating points have the same mixture ratio and experiments confirm that they have similar eigenfrequencies.

For all the operating points, the first resonance is close to the expected eigenfrequency of the first longitudinal mode of the chamber. The signals of the four first transducers are rigorously in phase. Only the fifth transducer, located at the end of the chamber, has a phase difference equal to 180° with respect to the other sensors.

Further signal analysis, indicates that the second peak is close to the first transverse mode. For the three operating points, the phase difference between the first four sensors are in good agreement with the transverse mode structure. Sensors C1 and C3 are in phase and have a phase difference equal to 180° with respect to the pressure transducers C2 and C4. The last pressure sensor delivers a signal which is in phase with C2 and C4. This is a significant difference with the classical phase relationship of the first transverse mode. During tests carried out without combustion, the three top sensors are perfectly out of phase with the two bottom sensors. Here, this phase anomaly of the last pressure transducer is probably due to the position of the sensor with respect to the flame. When flames are compact (operating points **B** and **D**), the last pressure sensor faces burnt gases and does not directly face the flames. The temperature in the area of the last sensor is definitely lower than that existing in the vicinity of the four other sensors. Under these conditions it is difficult to strictly identify the eigenmode. The frequency of this mode and the phase between the first four sensors tend to show that this mode is the first transverse acoustic mode.

The phase differences between the pressure sensor signals obtained for the third eigenfrequency are even more difficult to interpret. This peak corresponds theoretically to the first transverse mode. The phases do not agree with this assumption. There is no obvious relationship between the different sensors and it is difficult to determine the corresponding modal structure. However this gives relevant information about the influence of the temperature distribution on the acoustics. Operating points **C** and **D** have the same mixture ratio ($E = 1.33$) which leads to the same average maximum temperature but the flow dynamics are markedly different. The eigenfrequencies are nearly identical but the phases between the pressure signals differ. This is so because the temperature distributions corresponding to these two points are notably different and this distorts the modal structure inside the chamber. The three pressure signal analysis cannot be used to prove that this resonant peak corresponds to the first transverse mode. However if one analyzes the phase differences between sensors facing each other, one finds that they are out of phase by 180°. Indeed, the pressure signals recorded by C1 and C2 are never in phase, and their phase difference is most of the time close to 180°. The same observation can be done for sensors C3 and C4. Thus the pressure signals on the two sides of the chamber are always out of phase and this tends to show that a transverse motion is effectively generated in the chamber at the frequency of the third peak. There is however an anomaly since the pressure sensors on the same side are not in phase.

To conclude, it appears that the eigenfrequencies cannot be rigorously identified under hot fire conditions even with the combination of short time Fourier analysis, phase difference determination and numerical simulation. The pressure distributions do not correspond exactly to those expected. A transverse motion is certainly generated in the situations associated with the second and third peaks. It is then probable that the modal structure is influenced by other factors than those considered up to now. One aspect which is seldom considered is the presence of temperature fluctuations over a large volume in the chamber. This modifies the response of the system which cannot be considered to be in a steady state. The phase relations between the pressure signals is obviously not easy to interpret and this is probably due to the presence of these fluctuations. Progress must be made on the problem of modal identification when the system is highly variable.
This could be obtained for example by simulating the three dimensional reactive flow using large eddy simulations and analyzing the acoustic eigenmodes at different instants in time. This issue is also examined in Chapter VI.2.1 but with a simplified model equation.
In the absence of a definitive answer, it was decided to use the third eigenfrequency (2450 Hz) in the continuous wave test for operating point **B**. This choice is mainly based on the theoretical analysis. The third eigenfrequency correspond to what was expected and the phase relation between the pressure signals is close to that of the first transverse mode. The second eigenfrequency (2360 and 2380 Hz) were respectively selected for operating points **C** and **D**. The last eigenfrequency found in these experiments is too high compared to that predicted numerically. Phase differences between the top and bottom sensors for the second eigenfrequencies suggested that the transverse motion prevailed at these values.

III.4.4 Continuous wave modulation at a single frequency

The previously selected frequencies are now used to examine the system response to an external modulation.

Influence of the mixture ratio E and the momentum flux ratio J on the flame structure
In the following experiments a constant frequency wave is applied to the system during the twenty seconds of the hot fire test. Figures III.13 and III.14 respectively show typical instantaneous OH* emission images and average images with and without modulation for the three operating points. Figures III.15, III.16, III.17 provide a set of four instantaneous frames of OH* emission for the operating points **B**, **C** and **D**.

The difference between the two operating points **B** and **D** is the value of E. A decrease of the mixture ratio reduces the flame length but the flame geometry remains the same. Flames are compact and close inside the viewing window. When modulated, the flame length is reduced even further. Based on the average frames, the flame length decreases by about 20%. Atomization is improved by the pressure waves crossing the chamber leading to shorter flames. The global power remaining almost the same in spite of the lateral leak, the heat release rate per unit volume is increased. The acoustic modulation clearly changes the geometry of the reactive zone and creates a asymmetric combustion structure. The bottom flames are shorter than the top ones. The heat release is consequently more intense in the lower part of the chamber, close to the injector.

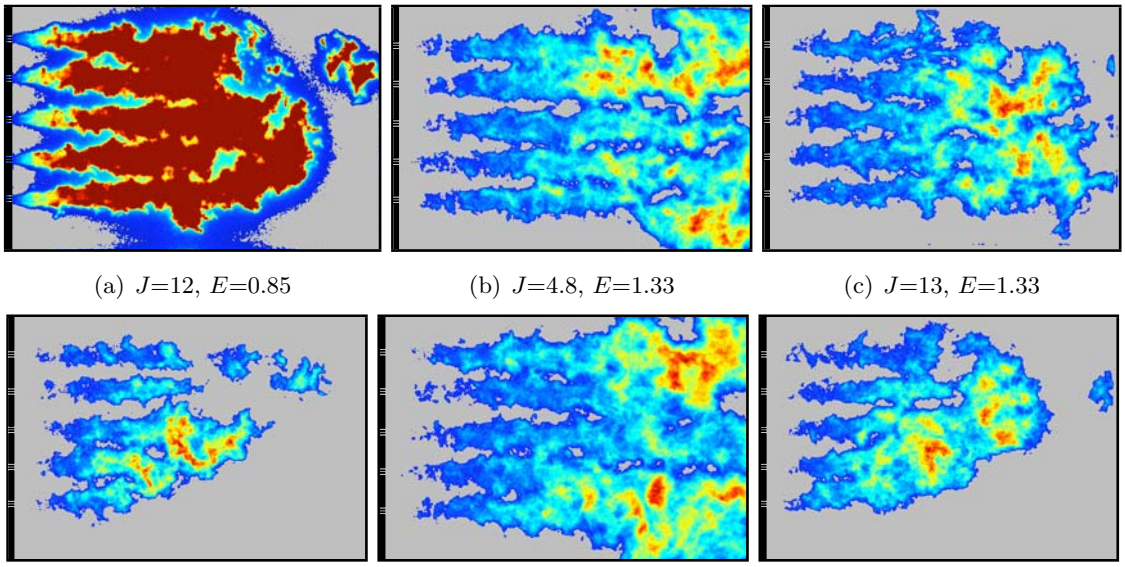

(a) J=12, E=0.85 (b) J=4.8, E=1.33 (c) J=13, E=1.33

(d) J=12, E=0.85 (e) J=4.8, E=1.33 (f) J=13, E=1.33

Fig. III.13: Instantaneous OH emission for non-modulated (top) and modulated (bottom) tests at different operating points : (a,d) I5-P30-B at 2450 Hz, (b,e) I5-P30-C at 2360 Hz, (c,f) I5-P30-D at 2380 Hz.*

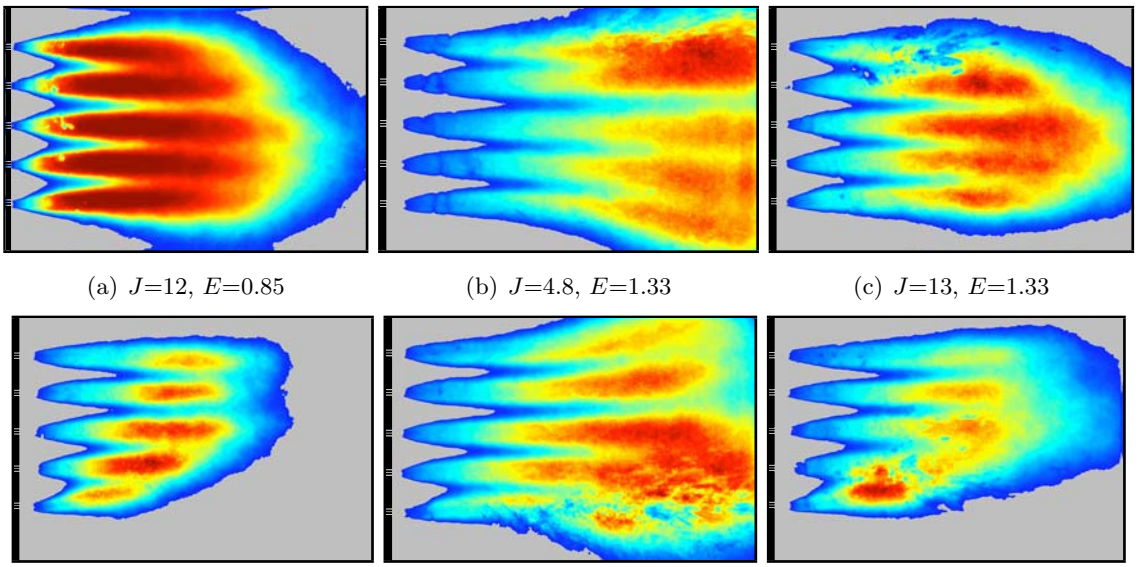

(a) J=12, E=0.85 (b) J=4.8, E=1.33 (c) J=13, E=1.33

(d) J=12, E=0.85 (e) J=4.8, E=1.33 (f) J=13, E=1.33

Fig. III.14: Average OH emission for non-modulated (top) and modulated (bottom) tests at the three operating points : (a,d) I5-P30-B at 2450 Hz, (b,e) I5-P30-C at 2360 Hz, (c,f) I5-P30-D at 2380 Hz.*

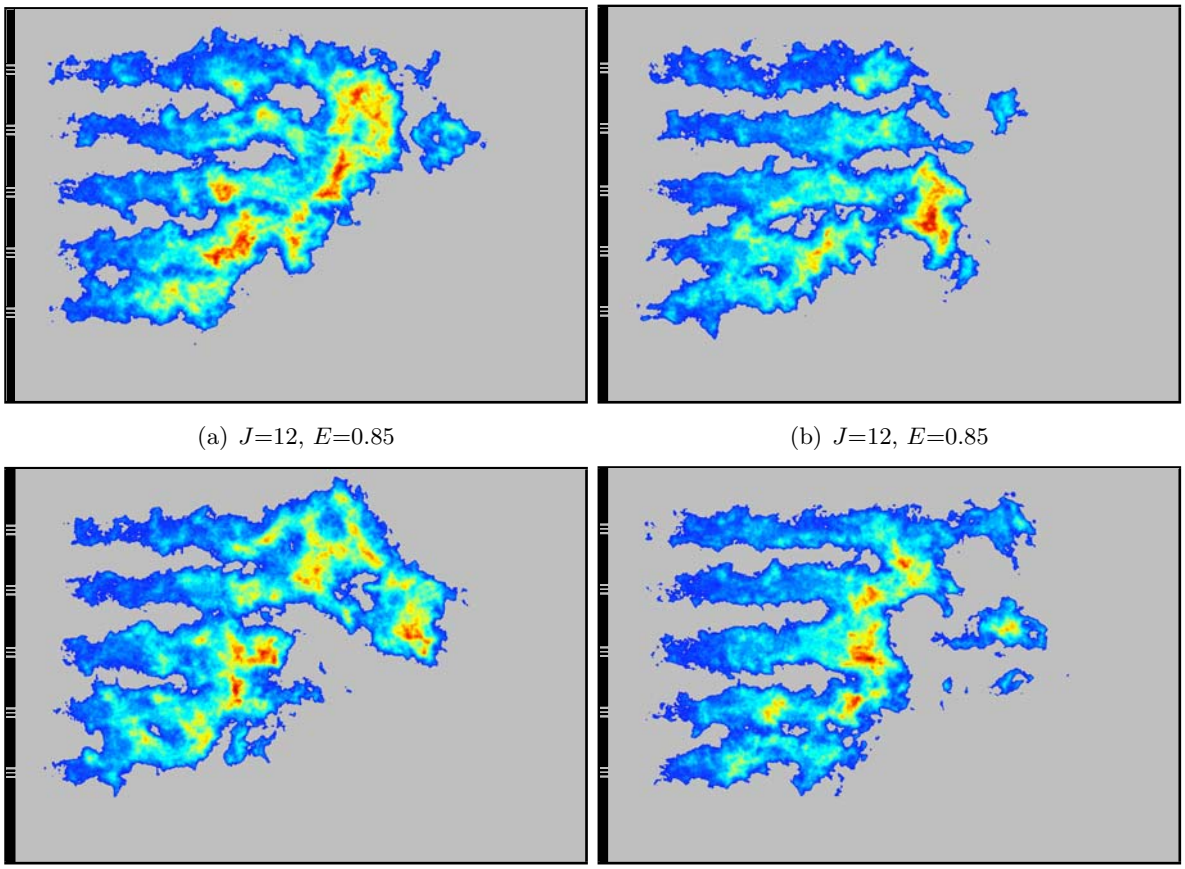

(a) J=12, E=0.85 (b) J=12, E=0.85

(c) J=12, E=0.85 (d) J=12, E=0.85

Fig. III.15: Set of four instantaneous OH emissions for the operating points* ***I5-P30-B*** *modulated at 2450 Hz.*

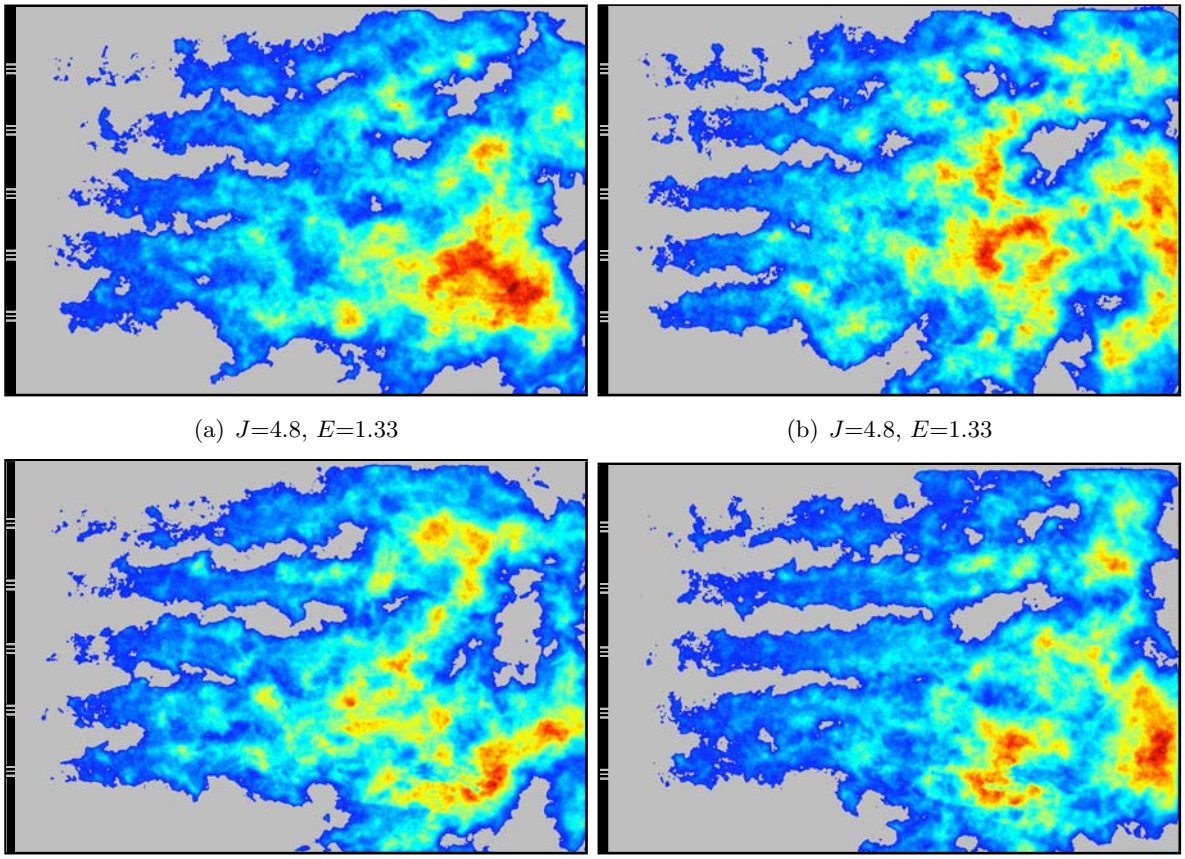

(a) J=4.8, E=1.33 (b) J=4.8, E=1.33

(c) J=4.8, E=1.33 (d) J=4.8, E=1.33

Fig. III.16: Set of four instantaneous OH emission images for the operating point* ***I5-P30-C*** *modulated at 2360 Hz.*

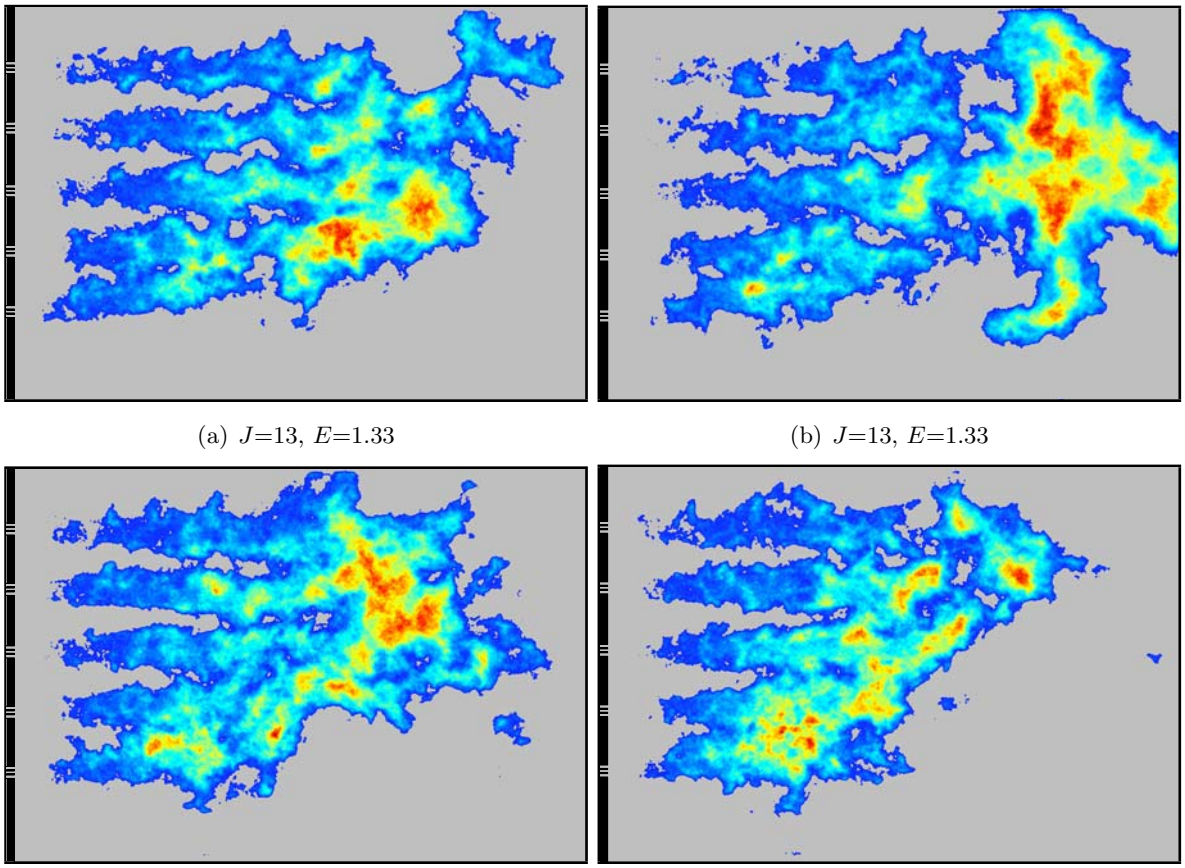

(a) J=13, E=1.33 (b) J=13, E=1.33

(c) J=13, E=1.33 (d) J=13, E=1.33

Fig. III.17: Set of four instantaneous OH emission images for the operating point* ***I5-P30-D*** *modulated 2380 Hz.*

Keeping the mixture ratio constant (operating points **C** and **D**), the longest flames are obtained for low values of the momentum flux ratio (point **C**). Without modulation, the flame geometries are significantly different and the response to transverse acoustic modulation varies with J. For the short flames obtained at point **D**, $J = 13$, the symmetry of the reaction zone is broken and the flame length is reduced by the modulation. When J is lower (point **C**), the flame structure remains globally identical to that observed without modulation. The expansion angle increases in the downstream part going from 9° without modulation to 14.5° with modulation. This tends to reduce the flame length and the distance from the injection plane to the first flame interactions by about 10 %. The top position of the modulator does not seem to modify the flame symmetry. The most intense reactive zone, which was located on the upper part of the reactive zone (between the first and the second jet) without modulation is now located in the lower part, around the fourth flame. The mixture ratio E seems to have no influence on the response, modification of the reaction zone is identical for high and low values of this ratio.

In all cases, the modulation acts on combustion in an asymmetrical fashion. The flame lengths are reduced and heat release rate is increased in the bottom part of the chamber. These findings could be interpreted as follows :

- The position of the modulator on the top of the chamber breaks the symmetry of the system. The modulation may be more intense in the lower part of the chamber and increase the heat release per volume unit by augmenting the turbulence and the vaporization process thus reducing the flame length in this region.
- The transverse wave established in the chamber influences the steady mass flow rates delivered by the different injectors. It is known that a single cavity feeds the five elements with oxygen and another cavity delivers gaseous methane to these units. Thus a pressure differential between the top and bottom parts of the chamber could create a differential in mass flow rates between the top and bottom elements. In this latter case, a coupling should be observed between the oxygen or methane cavity and the combustion chamber. This is investigated in the next section.

The different flame structures observed through the instantaneous OH* emission images reflect differences in operating conditions. The other diagnostics are less easy to analyze because they do not provide a clear coupling mechanism like that found in the low pressure tests. In the following paragraph we only consider the signals obtained at point **I5-P30-C**. This corresponds to the longest flames in the modulation free case and to the maximum expansion of the reaction zone when the modulation is applied to the system. The OH* distribution is close to that recorded at low pressure with the three element injection head. This proved to be a receptive configuration and it led to a strong coupling between acoustics and combustion. The analysis performed in what follows cannot strictly be transposed to the other operating point but most of the phenomena described are also observed for the operating points **B** and **D**.

Analysis of the operating point I5-P30-C

In the linear frequency sweep tests, the eigenmodes appeared as high amplitude pressure signals at the various eigenfrequencies. By modulating the system at the selected eigenfrequencies, the pressure

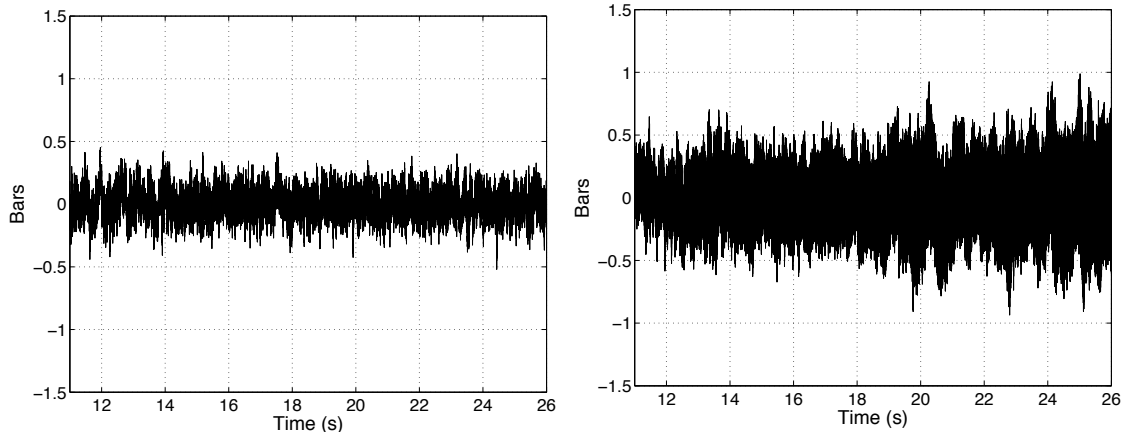

(a) (b)

Fig. III.18: Pressure signals for non-modulated (a) and modulated (b) tests for the operating point I5-P30-C : J=4.8 and E=1.33.

amplitude was expected to reach at least 10% of the mean pressure. Figure III.18 shows the pressure signals recorded with and without external modulation for the operating point **C**.
Without modulation, the amplitude of the pressure signals does not depend on the operating point. The peak-to-peak pressure is equal to 0.1 MPa which already represents 3.3 % of the average chamber pressure. This has considerably increased with respect to the first experiments carried out at 1 MPa. With three elements at 1 MPa, the peak-to-peak pressure amplitude was equal to 0.2 % of the average chamber pressure. By augmenting the number of elements and the chamber pressure, the natural level of oscillations due to turbulence and high speed injection increased quite sigificantly. Most of the energy is contained in the low frequency range and no high frequencies components appear in the power spectral densities. It is however possible to correlate pressure and the heat release signals as shown previously in section III.4.2.2 but the amplitude associated to these components remains low.

The external modulation provides acoustic energy to the system. This increases the pressure fluctuations. The coupling between the pressure waves and combustion also amplifies the pressure fluctuations (driving process). When modulated, the pressure signal amplitude reaches 8 % of the average chamber pressure. This amplification is not as significant as expected. The level of pressure fluctuations is already naturally high. Interactions between acoustics and combustion are observed but the modulation amplitudes remain at levels observed previously. The most amplified response is obtained for operating point **D** with a level of the same order of magnitude as in previous experiments.
Second, the spectral content of the pressure signal is similar to that recorded during the non-modulated test where all the energy is contained in the low frequency range (below 500 Hz), except for a narrow band component at the modulation frequency as shown in figure III.19. When the pressure signal is high-pass filtered at 1 kHz, a single peak remains at the modulation frequency. The phase between the pressure sensors changes during the test. At the beginning of the modulation, the phase corresponds to what was observed in the frequency sweep modulation test. Then the phase difference evolves as can be seen in Figure III.20. This is completely new and differs from what was observed in the low pressure tests. The presence of the high frequency transverse motion progressively modifies the

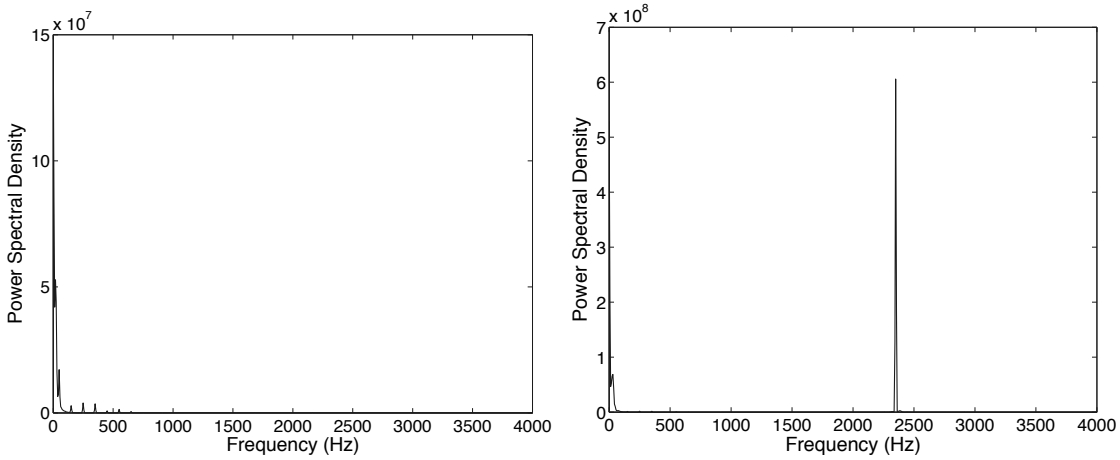

(a) Modulation free

(b) Acoustic modulation at 2360 Hz

Fig. III.19: Power spectral density of the pressure signal recorded by sensor C3 for the operating point ***C*** *without (a) and with (b) external modulation at 2360 Hz. The original pressure signal is first high-pass filtered at 1 kHz.*

pressure distribution in the chamber.

The previous data lead to the following remarks. First, the coherence function between the photomultipliers and pressure signals features strong peaks in the high frequency range even without external modulation. At the same time, the pressure signal amplitude is naturally high. This has not been observed during the previous experiments. Second, when the modulation is activated, the symmetry of the combustion structure is broken. This was observed in the low pressure experiments with the three injection elements combustor. It was already indicated that the pressure waves established in the chamber could influence the mass flow rates.

In view of these observations it is worth examining the flow dynamics in the cavities distributing the propellants to the injection units. Two cavities respectively feed oxygen and methane to the five elements. For the first time, transducers are located in these cavities and signals are recorded with the same sampling rate as the chamber pressure. The signal recorded in the oxygen and methane cavities are respectively shown in figures III.21 and III.22. The signal amplitude is increased by a factor of five when the modulation is activated and the amplitude reached during the tests are quite large. The peak to peak pressure is equal to 4.5 MPa which is more than the chamber pressure.

A typical power spectral density of these signals is plotted in figure III.23.

A relevant piece of information is provided by the coherence function between the pressure signals in the cavities and in those detected in the chamber (figure III.24). The first pressure transducer C1 is used in these calculations but the coherence functions obtained with the other transducers are similar. The coherence between pressures in the methane cavity and in the chamber is stronger than that obtained between the oxygen cavity and the chamber. Methane is gaseous while oxygen is liquid. This can surely explain the difference in coherence amplitude between the two cavities. The strongest

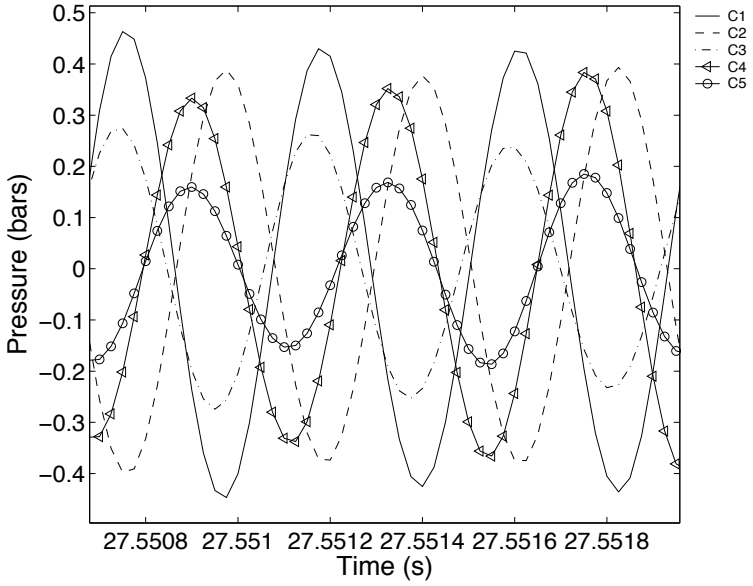

Fig. III.20: Five pressure signals during the modulation of the operating point ***C*** *at 2360 Hz.*

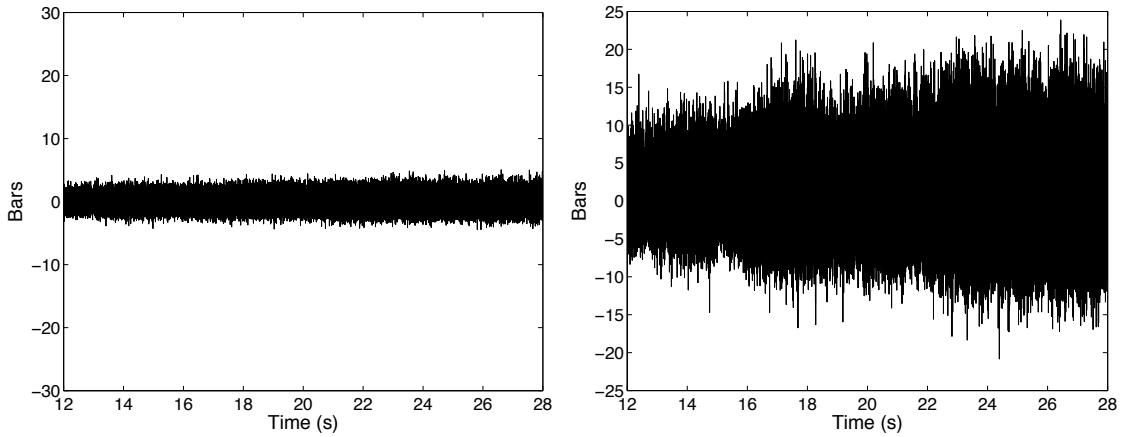

(a) Modulation free

(b) Modulation at 2360 Hz

Fig. III.21: Pressure signal in the liquid oxygen cavity, feeding simultaneously the five elements, without (a) and with external modulation applied in the main combustion chamber at 2360 Hz.

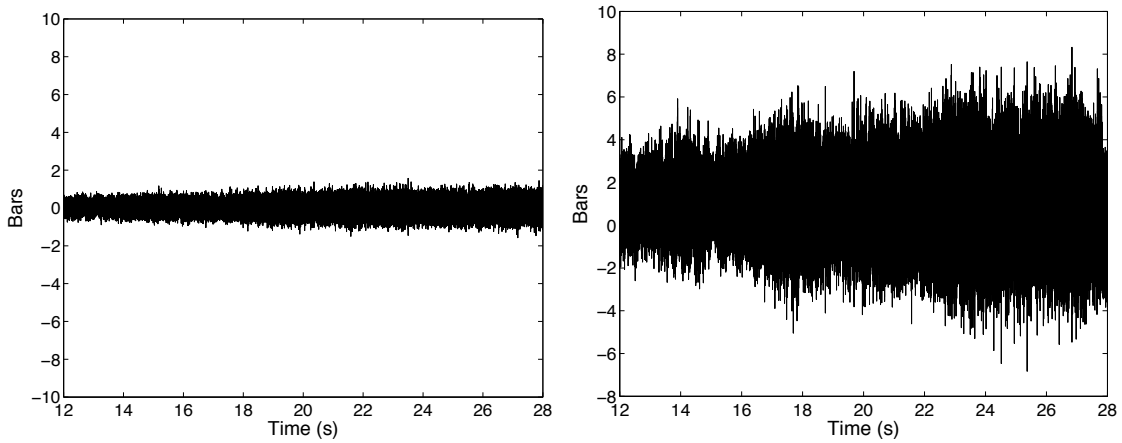

(a) Modulation free (b) Modulation at 2360 Hz

Fig. III.22: Pressure signal in the methane cavity, feeding simultaneously the five elements, without (a) and with external modulation applied in the main combustion chamber at 2360 Hz.

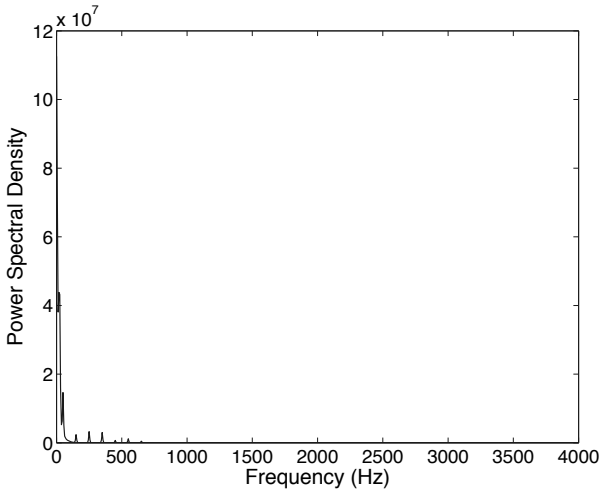

Fig. III.23: Typical power spectral density of the pressure signals in the oxygen cavity without modulation.

coherence are observed in the low frequency range. There is no continuity in the spectrum but regular coherent frequencies are detected. Beyond 1.5 kHz two peaks are noticeable. Their frequency is slightly modified when the acoustic modulation is on. Without modulation the two frequency components are at 1680 Hz and 2160 Hz. These frequencies appeared clearly in the coherence between the pressure signals in the chamber and the photomultiplier signals. Then, there is a coupling between the pressure fluctuations in the methane cavity and combustion occurring in the chamber. The pressure fluctuations observed in the cavity directly influence the heat release in the chamber. When the combustion chamber is externally modulated at a frequency of 2360 Hz, a small level of coherence is observed between the pressure in the chamber and in the methane cavity. The amplitude of the pressure variations in the methane cavity shows that a large amount of the acoustic energy provided to the system through the modulator is transmitted to the methane cavity. The same phenomenon is observed in the oxygen cavity but the coherence between the two pressure oscillations is lower. However, the amplitude of the pressure oscillations in the oxygen cavity is also considerably increased and it appears that the pressure fluctuation in the combustion chamber are transmitted to the liquid oxygen cavity.
It is now worth examining the photomultiplier signals. A detailed view of the waveforms are displayed in Figure III.25. The modulation frequency contains most of the power and a single peak appears in the spectral density. For operating point I5-P30-C the two PM are in phase. The coherence function between the pressure signal recorded by the first sensor C1 and heat release provided by PM1 is shown in figure III.26. The dominant peak appears at the modulation frequency but it is competing with other high frequency components. Coherence induced by the coupling with the injection head is quite strong. The signals are coherent at the modulation frequency and at several other frequencies. The coherence is high at the modulation frequency but no information can be extracted from the phase relation because the phase evolves during the test and no systematic analysis can be done. The acoustic power injected by the modulator is not sufficiently high to organize the pressure distribution in the chamber and dominate the heat release pattern. The phase difference deduced from cross spectral analysis is therefore not meaningful.

The high speed camera records natural light emission in the visible range at a rate of 30 000 frames per second. The effect of the external modulation is clearly observable. The flow dynamics is modified and the transverse motion can be clearly identified. Different techniques have been tried to extract in still figures the motion observed in the film but without success. A few snapshots cannot represent the phenomena which are easily perceived dynamically in the film. The high speed film clearly shows reaction zone oscillations when the system is submitted to a continuous wave modulation, but the turbulence and the flow motion make really hard the identification of the source of the motion. The motion observed depends on the structure size and location. A global decrease of flow velocity is also observed. When the modulation is on, the structures still move downstream but their convection velocity is lower than that found in the absence of modulation.

III.4.5 Conclusions on the 3 MPa hot fire tests

Effects of external modulation are observable but their amplitude is lower than the one obtained in the low pressure tests. The modulation frequency is present in the spectral density and the pressure

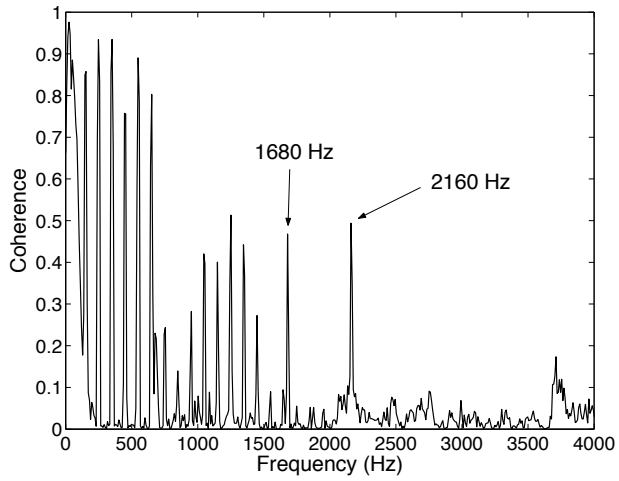

(a) Methane/C1 - Modulation free

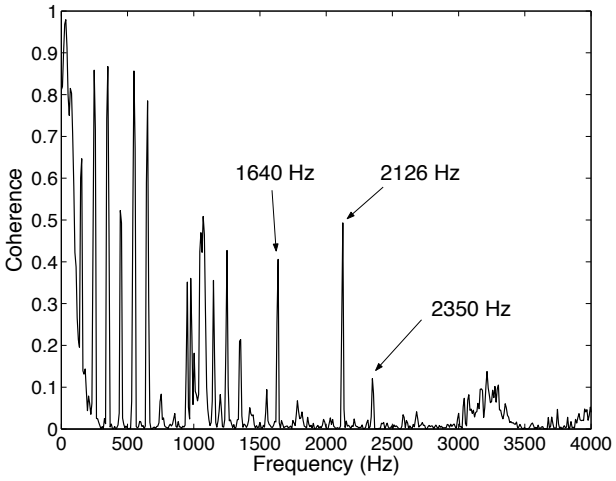

(b) Methane/C1 - Modulation at 2360 Hz

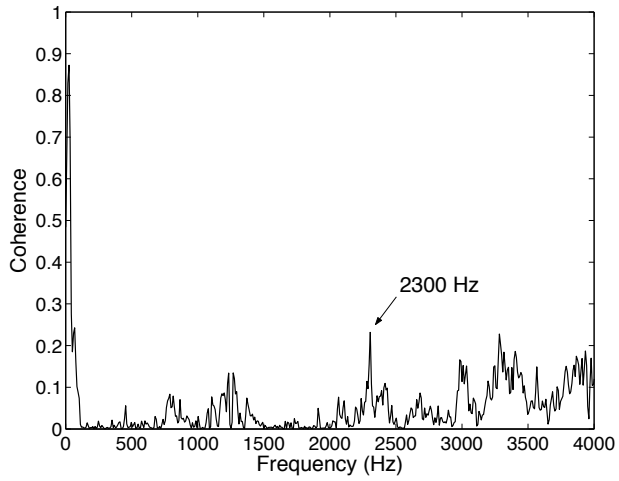

(c) Oxygen/C1 - Modulation free

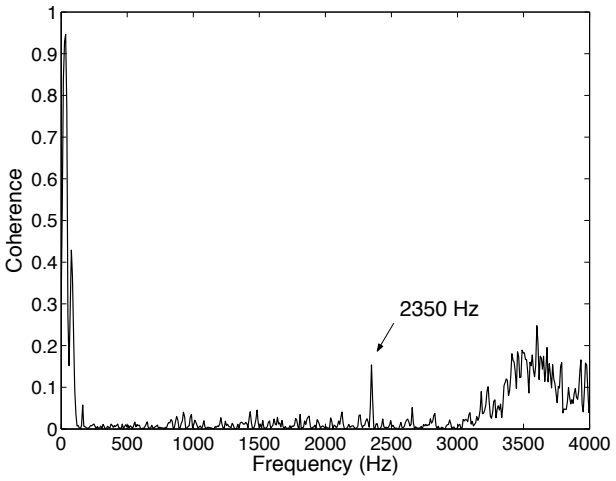

(d) Oxygen/C1 - Modulation at 2360 Hz

Fig. III.24: Coherence between the high-pass filtered pressure signals at 1 kHz in the oxygen (a, b) and methane (c, d) cavities and the first top pressure signal in the combustion chamber without (a, c) and with (b, d) modulation at 2360 Hz.

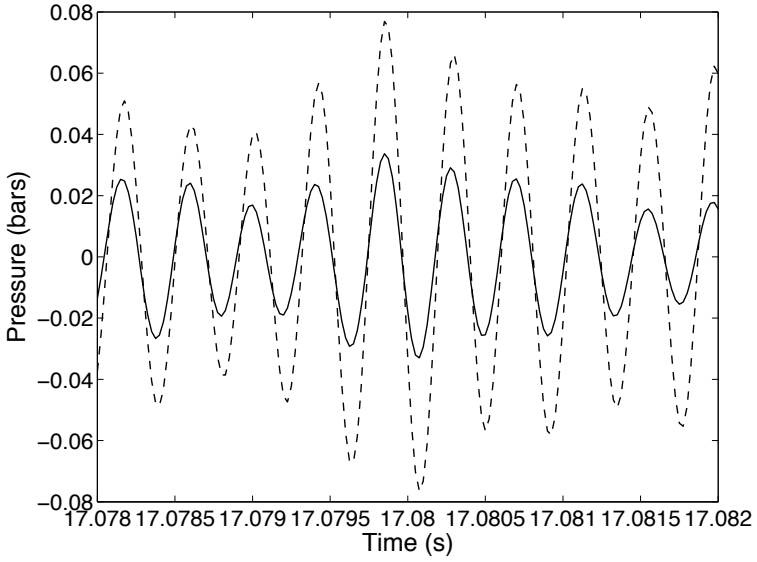

*Fig. III.25: Signals recorded by the two photomultipliers for the point **I5-P30-C** when modulated at 2360 Hz.*

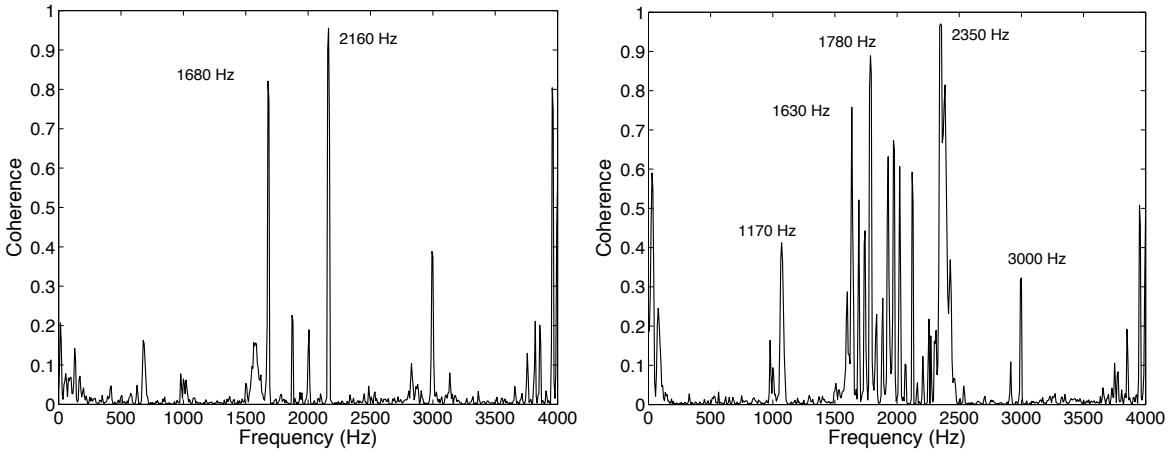

(a) Modulation free

(b) Acoustic modulation at 2360 Hz

*Fig. III.26: Coherence between photomultiplier 1 (top) and pressure transducer 1 (top upstream) without (a) and with modulation (b) for the point **I5-P30-C**.*

Chamber pressure	$\dot{m}_{CH_4}$	U_{CH_4}	$\dot{m}_{LOx}$	U_{LOx}	E	J	d_l	d_g
6 MPa	60 g s^{-1}	28 m s^{-1}	90 g s^{-1}	2.3 m s^{-1}	1.5	5.6	2.9 mm	4.95 mm

Tab. III.6: Characteristic dimensions and injection parameters for the 6 MPa hot fire tests.

signals and heat release fluctuations are coherent. Combustion is modified by the modulation but many competitive phenomena complicate the situation and its interpretation. A coupling with the injection system is observed. High amplitude pressure oscillations are recorded in the two cavities feeding oxygen and methane. The pressure signals recorded in these cavities are dominated by low frequency components but a strong coherence is observed with the pressure oscillation induced in the chamber at the modulation frequency. The turbulence intensity is augmented with the increased pressure and power released in the chamber. This is visible in the elevated levels of pressure fluctuations recorded when the chamber operates in the absence of external excitation. Since the background level is higher, the modulation level required to obtain an acoustically dominated flow is also higher and less easy to achieve in the present configuration. One problem which was not considered at the beginning of this research is that the resonance sharpness is diminished by the fluctuations in temperature, which are naturally present in the flow. The linear sweep tests clearly indicate that the response covers a broader band as if the damping levels were enhanced. It is less easy to identify the modal eigenfrequencies. Correspondingly this reduces the level, which can be reached when the system is excited by a continuous wave at one of the modal frequencies. The fluctuations in the system are usually not taken into account but they clearly influence the acoustical response and may have an important impact in practice. This issue and its consequences should be considered more carefully (an initial analysis is developed in Chapter VI).

III.5 6 MPa hot fire experiments

III.5.1 Test conditions

Three hot fire tests are carried out with an average chamber pressure equal to 6 MPa. These tests aim at :

- Studying the effect of a pressure increase on the modulation amplitude. The exit diameter of the transverse modulation nozzle is the same as the one used in the previous set of experiments at 3 MPa. Thus, 25% of the total flow rate is now evacuated by the modulator.
- Investigating the flame behavior when oxygen is modulated in a transcritical state. The critical pressure of oxygen is 5.04 MPa so it is injected in a transcritical state, the pressure being above the critical value and the temperature below the critical temperature ($T_c(LOx) = 154$ K).

The combustor configuration is the same as in previous tests but the main nozzle diameter has been reduced. The chamber comprises five element injector fed by liquid oxygen and gaseous methane. Characteristic dimensions and injection parameters are gathered in table III.6. The mixture ratio E and the momentum flux ratio J are chosen to maximize the flames sensitivity to external modulation. The mixture ratio E is above 1 and J does not exceed 6. In this case, the flames are long and receptive to acoustic perturbations. To obtain these values of J and E the external diameter of each injection

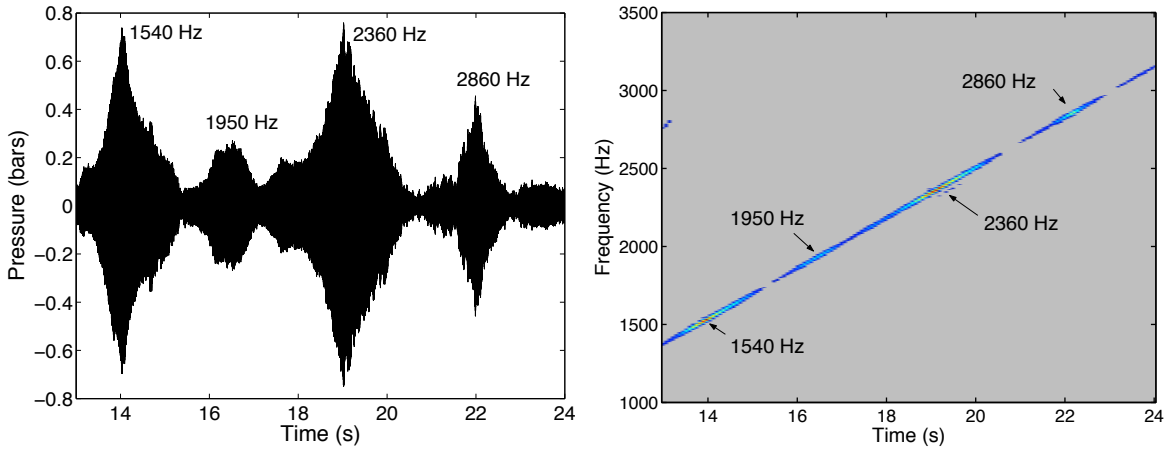

(a) (b)

Fig. III.27: Pressure signal (C3) recorded during the frequency sweep modulation of the 6 MPa test (a) and the corresponding short time Fourier transform (b).

element has been reduced. The gaseous methane annulus has an external diameter of 4.95 mm which is the minimum value which can be used in conjunction with the liquid oxygen posts. For smaller diameters, the distance between the oxygen lip and the external part of the element would be too small to allow a suitable positioning of the injection head.

After a modulation free test, which will be commented in the next section, the combustion chamber is modulated with a linear frequency sweep between 0 and 3500 Hz. Resonance is observed around four different frequencies at 1540, 1950, 2360 and 2860 Hz. The phase between the pressure sensors is used to characterize the eigenmodes. Figure III.28 shows the five pressure signals around the 2360 Hz frequency. The phase difference between the signals does not strictly correspond to the first transverse mode but it is the closest. Pressure signals from sensors C1 and C3 are in phase and have a large phase difference with C2 and C4 which are also in phase. The pressure distribution corresponding to this mode features high transverse velocities in the chamber. This mode is selected for the continuous wave modulation test described below.

III.5.2 Continuous modulation at 2360 Hz : Results

Pressure signals without and with the external modulation are shown in figure III.29. The amplitude of the pressure fluctuations reaches 1.6 % of the average chamber pressure in the absence of modulation. External modulation only generates fluctuations equal to 3 % of the chamber pressure. The difference between the modulated and modulation free tests is low. When the chamber pressure is increased, the effect of the external modulation does not rise correlatively.

Figure III.30 shows the instantaneous and average OH* emission images. Without external modulation, flames do not close in the visualization window and the expansion angle is relatively small. It is equal to 7°. The modulation does not induce strong modification of the flame structure. As observed during the previous experiments at different chamber pressure, the flame length is reduced and the

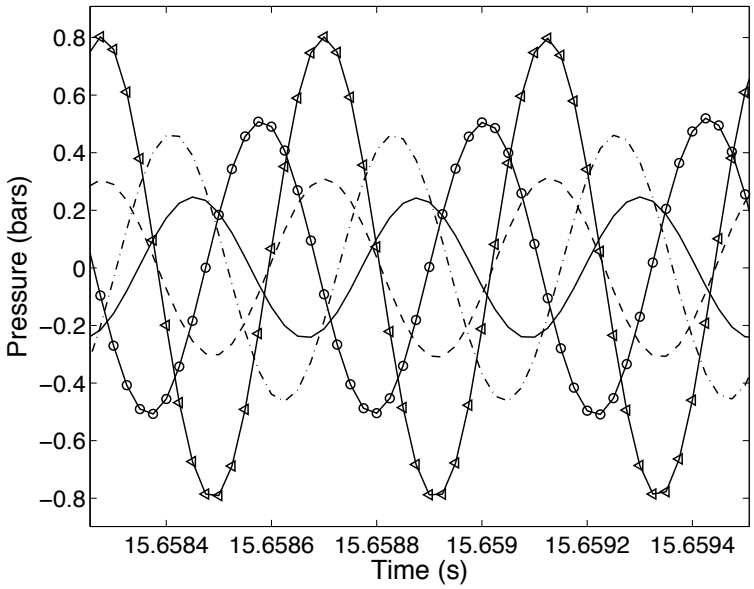

Fig. III.28: Five pressure signals at the eigenfrequency equal to 2360 Hz : (-) C1, (–) C2, (-.-) C3, (△) C4, (○) C5.

lower part of the reaction zone becomes more intense. The expansion angle does not change. The symmetry of the reaction zone is slightly perturbed, the bottom flame is shorter than the four others. Areas between the flames do not have the same intensity. Some interaction regions are changed by the acoustic modulation.

The coherence function calculated between pressure and heat release fluctuations reveals an interesting phenomenon shown in figure III.31. Without modulation, a strong coherence level is found at the first transverse eigenfrequency. At 2360 Hz, coherence is almost equal to 1 in the absence or in the presence of modulation. This means that pressure and heat release oscillations occur at this frequency. The phase between these quantities is not constant and increases during the test. Spectral densities with and without modulation feature high frequency peaks.

The continuous wave test does not yield a high level of oscillation. The level obtained is weaker than the value which could be expected from the linear frequency sweep. As a consequence the turbulent velocity fluctuations remain dominant and the flow is not controlled by the acoustic perturbations. The injected acoustic energy is definitely not high enough to reorganize the flow and the related combustion process.

One may wonder why the acoustic modulation does not increase at least like the chamber pressure. Theoretically this should be obtained but the levels observed are much lower. This may be due to competing phenomena, which reduce the relative level of modulation : as the chamber pressure is increased the turbulent energy per unit volume is augmented and the rate of reaction becomes more intense. This in turn increases the turbulence intensity which gives rise to higher levels of pressure fluctuations in the natural flow. The temperature fluctuations are enhanced reducing the resonance

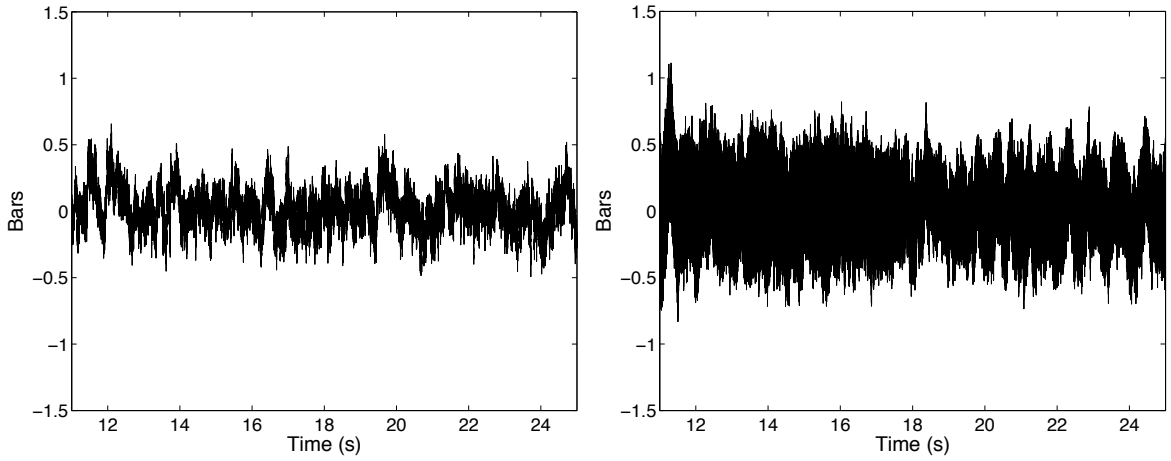

(a) Modulation free test (b) Modulation at 2360 Hz

Fig. III.29: Pressure signals without (a) and with modulation (b) at 2360 Hz.

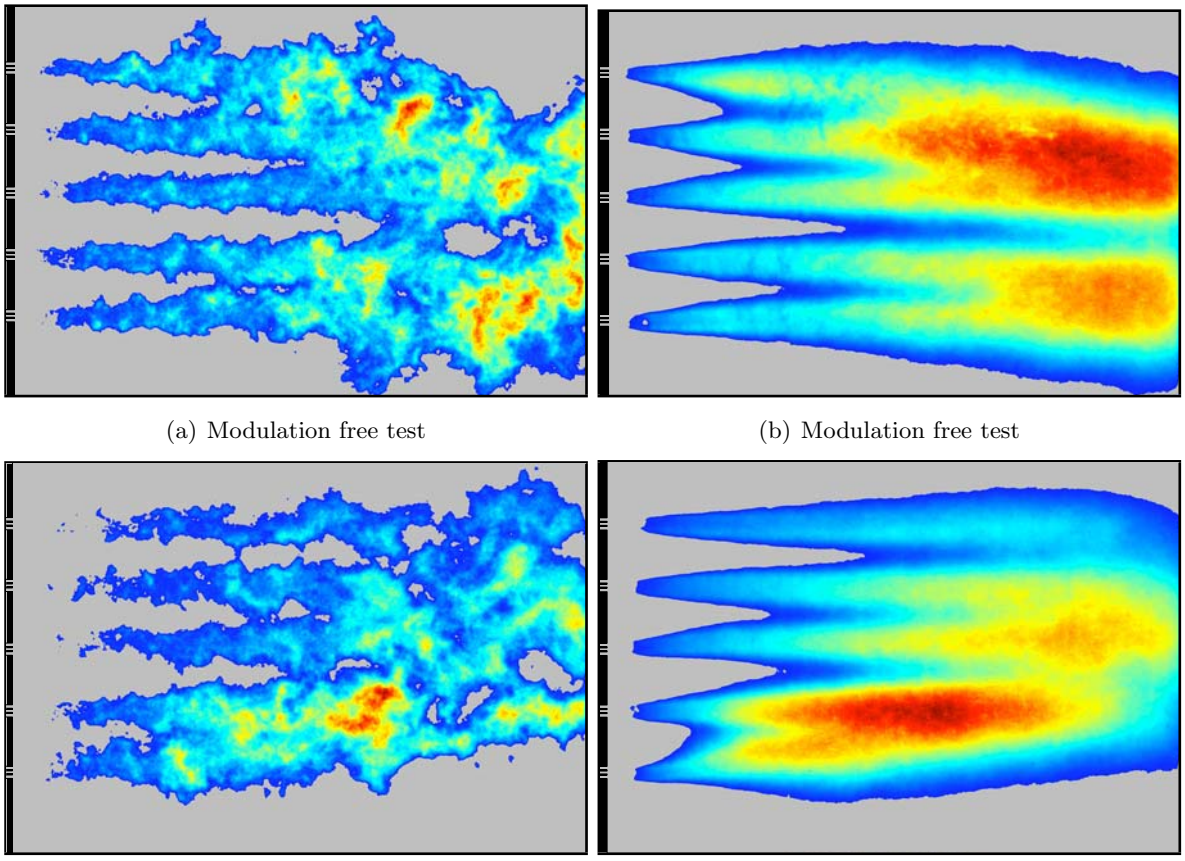

(a) Modulation free test (b) Modulation free test

(c) Modulation at 2360 Hz (d) Modulation at 2360 Hz

Fig. III.30: Instantaneous and average OH emission images without (a, b) and with modulation (c, d).*

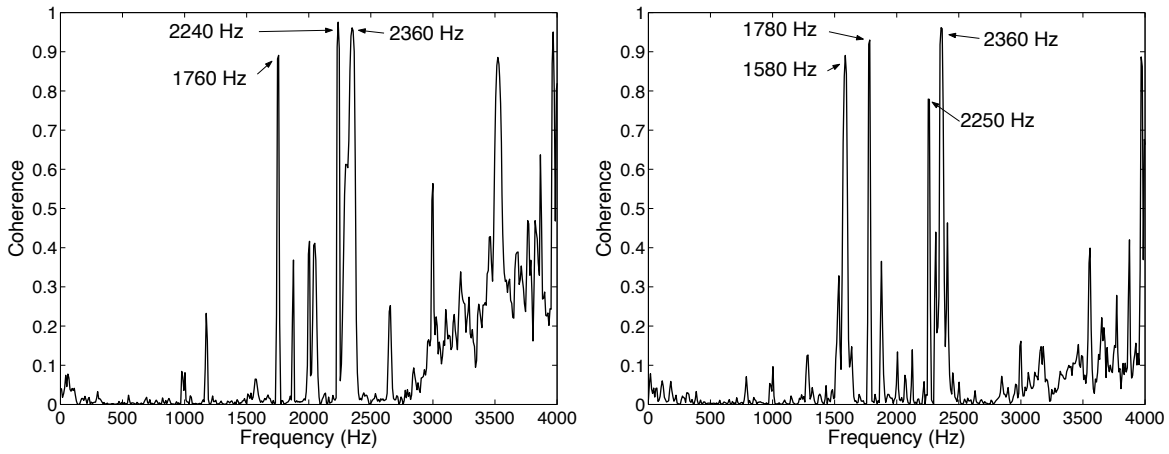

(a) Modulation free test

(b) Modulation at 2360 Hz

Fig. III.31: Coherence between the first photomultiplier and the first pressure sensor without (a) and with modulation (b).

Chamber pressure	$\dot{m}_{CH_4}$	U_{CH_4}	$\dot{m}_{LOx}$	U_{LOx}	E	J	d_l	d_g
1 MPa	37 g s^{-1}	94.5 m s^{-1}	47 g s^{-1}	3 m s^{-1}	1.27	5.7	2.9 mm	7 mm

Tab. III.7: Characteristic dimensions and injection parameters for the double flame low pressure tests.

sharpness and acting as an effective additional damping mechanism in the system. It is also possible that the rotating wheel becomes less effective when the pressure in the chamber is augmented because the inertia of the mass of gases in the auxiliary nozzle is augmented.

III.6 Acoustic modulation of two flames at 1 MPa

The previous set of experiments carried out with three element injector at 1 MPa has provided relevant information on the coupling between acoustics and combustion. Important modifications of the flame structure were induced by the external modulation. However, it was not possible to say if the mecanism required collective interactions between the different flames or if it could be obtained with an isolated injector. It was then decided to examine this question by performing an additional test at 1 MPa with an isolated injector.

However due to practical constraints it was not possible to use a single element. This is because the mass flow rate cannot be reduced below a certain limit. The low J value at 1 MPa could not be achieved without operating with at least two injectors.
The experiment was then designed by blocking the three central injectors. Two flames are stabilized in this case, one at the top of the chamber and one at the bottom essentially avoiding flame interactions. Three tests are carried out in this configuration to determine the acoustics of system and to compare modulated and modulation free tests. Injection parameters are gathered in table III.7.

The frequency sweep test reveals three eigenfrequencies at 1580, 2240 and 2830 Hz as shown in figure III.32. The five pressure signals are plotted in figure III.33 around the 2240 Hz modulation time. The

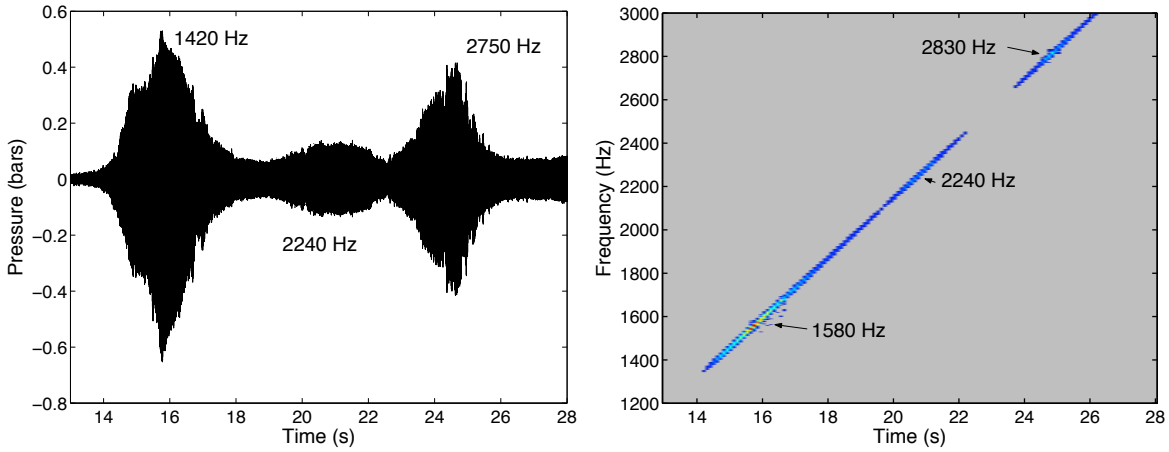

(a) (b)

Fig. III.32: Pressure signal recorded during the frequency sweep modulation of the two flame test (a) and the corresponding short time Fourier transform (b).

phase between the sensors is well determined. The top sensors C1 and C3 have a phase difference of 180° with the bottom sensors C2 and C4. Only the top downstream sensor C5 is exactly in phase with the two bottom sensors. This is very close to the first transverse eigenmode and continuous modulation test is carried out at this frequency.

As in the previous experiments, the difference of pressure levels between non-modulated and modulated tests is not high enough to consider that the level of oscillation is sufficient. Pressure amplitudes are almost identical for the two tests but modifications of the reaction zone can be observed with the intensified cameras.

Figure III.35 shows instantaneous and average OH* emission with and without acoustic modulation. The modulation free test shows that the configuration does not generate symmetric flames. The wall modifies the flow, moving the flame towards the chamber center. Flames are not symmetrical but spread around the axis of the injection element. This is perturbing diagnostics. When modulated, the bottom flame intensity increases and the two flames are moved upwards. A large recirculation zone is observed in the bottom part of the chamber and reactive recirculating gases interacts with the flame front.

Geometry is clearly not well adapted to the study but the interaction between heat release and acoustic is strong. The coherence between pressure and photomultiplier signals is nearly equal to 1 at the modulation frequency and this is strong enough to dominate the dynamics of the jets.

This test is not fully conclusive because the system is aerodynamically perturbed. It is however possible to conclude that a strong interaction also occurs with an isolated injector.

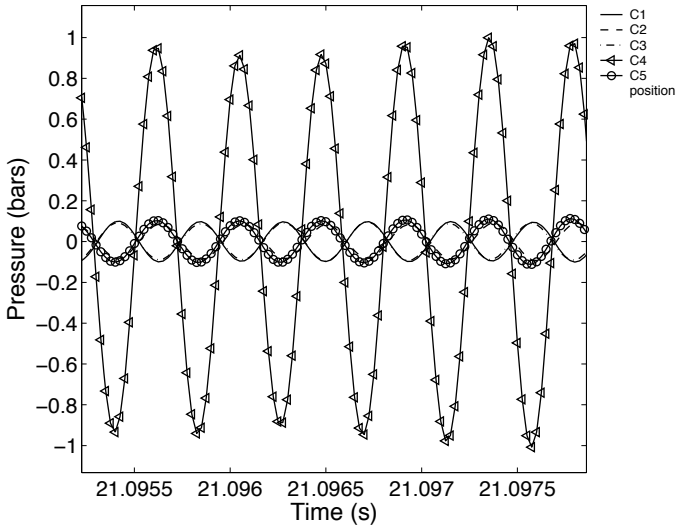

Fig. III.33: Five pressure signals at the eigenfrequency equal to 2240 Hz.

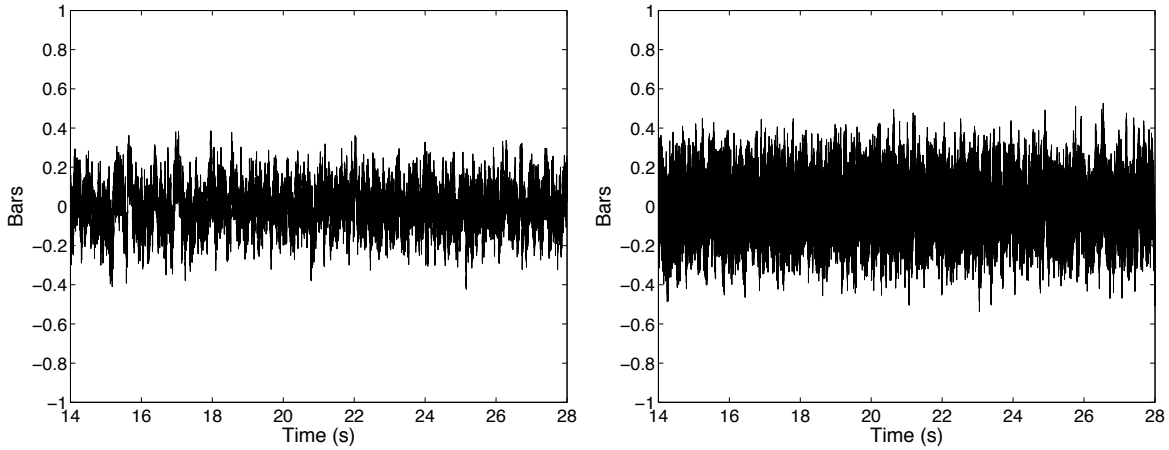

(a) Modulation free test

(b) Modulation at 2240 Hz

Fig. III.34: Pressure signals without (a) and with modulation (b) at 2240 Hz.

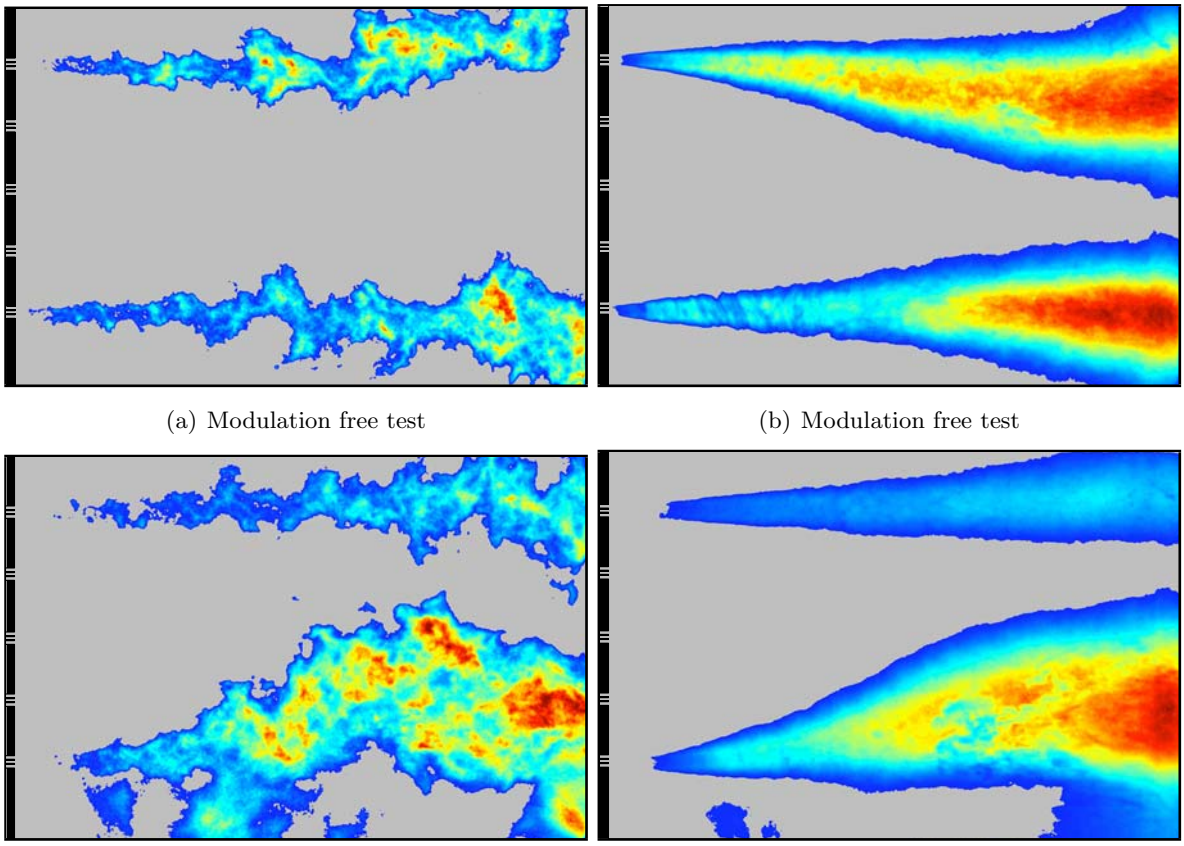

(a) Modulation free test (b) Modulation free test

(c) Modulation at 2240 Hz (d) Modulation at 2240 Hz

Fig. III.35: Instantaneous and average OH emission without (a, b) and with modulation (c, d).*

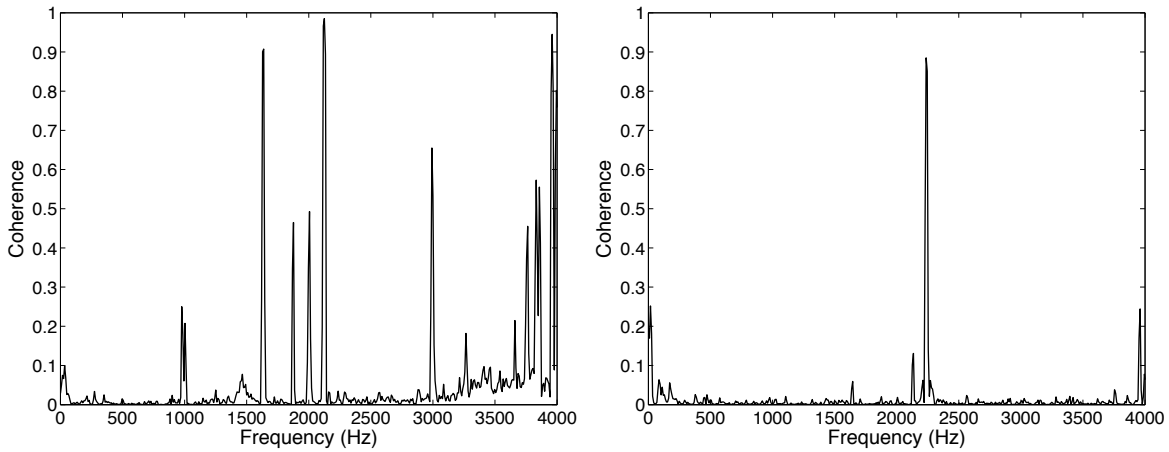

(a) Modulation free test (b) Modulation at 2360 Hz

Fig. III.36: Coherence between the first photomultiplier and the first pressure sensor without (a) and with modulation (b).

III.7 Conclusion

The second series of experiments carried out in the Mascotte test facility is analyzed in this Chapter. The data correspond to a total number of twenty four tests. A large test matrix was used to explore new operating pressures and many pending issues. One objective was to find the most suitable experimental conditions. Systematic hot fire tests were planned to extract the relevant parameters and unravel the mechanisms leading to the high frequency instabilities.

A new five element injector was designed and tests were carried out at 3 MPa to examine the influence of the two dimensionless parameters E and J on the flame sensitivity to acoustics. The increase in chamber pressure led to a decrease in the relative acoustic modulation amplitude. High levels of modulation were obtained but it was not possible to have pressure fluctuations exceeding 10 % of the mean chamber pressure. In contrast, the fluctuating turbulent velocities generated high levels of pressure oscillations competing with the external modulation. The temperature fluctuations were also stronger and this reduced the resonance sharpness, a mechanism which was not forseen at the beginning of this program but which may have important consequences.
Three configurations with different couples of mixture ratio and momentum flux ratio were tested. The influence of these parameters on the flame expansion rate and length was observed and quantified.

The chamber pressure was then increased to cross the critical pressure of oxygen. Tests were carried out at 6 MPa and flame structures were observed with and without modulation. The relative levels of oscillation were insufficient to obtain a flow governed by the acoustic modulation.

Finally, tests at 1 MPa were carried out with two operating injectors separated by a large distance. This was intended to see if the coupling between a transverse mode and combustion could be obtained in the absence of flame interactions. The level of oscillation was not very high but a visible interaction was obtained indicating that a coupling between the transverse mode and an isolated injector was possible.

These various tests indicate that the modulation amplitude constitutes the limiting factor. The resonance sharpness determines the response level of the system and it is influenced by the temperature fluctuations associated with the turbulent combustion process. It is clear that these fluctuations must be taken into account if one wishes to analyze the modal response under hot fire conditions. It is also apparent that augmented levels of modulation will not be obtained with the current toothed wheel modulator. A new configuration is needed of the type considered in Appendix B. This new set up designated as Very High Amplitude Modulator (VHAM) might be able to overcome the current limitations and allow futher investigation of many of the pending issues.

Part 2 : Numerical Simulations

Chapter IV

Interactions between coaxial jets and acoustic modes : experiments and simulations

Résumé

Les interactions entre des ondes acoustiques transverses et des jets coaxiaux non-réactifs sont étudiées numériquement et expérimentalement. Expérimentalement, trois injecteurs coaxiaux sont utilisés pour alimenter la chambre de combustion en oxygène liquide et azote gazeux à une pression de 3 MPA. Une tuyère auxiliaire est située sur le dessus de la chambre et sa sortie est périodiquement obstruée par une roue dentée en rotation afin de générer des ondes de pression transverse de grande amplitude dans la chambre. Le couplage entre les ondes acoustiques et les jets diphasiques est observé par rétroéclairage et imagerie rapide. Numériquement, des simulations aux grandes échelles sont effectuées pour observer la dynamique de jets gazeux coaxiaux oxygène/méthane. Des ondes de pression transverses sont générées numériquement afin de comparer le comportement des jets avec et sans modulation. Le forçage acoustique perturbe fortement les jets comme observé expérimentalement, la longueur du dard central d'oxygène est diminuée et le mélange des réactifs est amélioré. Une analyse spectrale des signaux temporels permet de qualifier la réceptivité des jets aux perturbations extérieures.

Abstract

Interactions between transverse acoustic waves and non-reactive coaxial jets are experimentally and numerically investigated. Experimentally, a three coaxial element injector is used to inject liquid oxygen and gaseous nitrogen in a high pressure (3 MPa) chamber. A secondary nozzle located on the top of the chamber is periodically blocked by a rotating toothed wheel to generate high amplitude transverse pressure waves in the chamber. The coupling between the acoustic waves and the liquid and gas streams is observed by backlighting and high speed imaging. Numerical calculations are carried out in an LES framework to examine the dynamics of coaxial gaseous oxygen and methane injection. Transverse pressure waves are generated numerically allowing a comparison between species mixing in the absence or in the presence of an external modulation. It is found that the reactant jets are wrinkled by acoustic forcing as in the experiment and that this reduces the central oxygen core and enhances reactant mixing. Spectral analysis is also carried out to examine the receptivity of the flow to the external modulation.

IV.1 Introduction

High frequency instability constitutes one of the most difficult problems in liquid rocket propulsion. The phenomenon is often observed during transients or when steady operation is perturbed by a pressure spike. Instability has serious consequences because of the extreme power densities characterizing liquid rocket engines (LRE). A small amount of the energy released in the system is sufficient to feed a large amplitude oscillation in the combustion chamber. Instabilities in the high frequency range are the most destructive because they intensify the heat fluxes to the chamber walls and injection backplane leading to a rapid erosion and destruction of these elements. Data gathered over many years of development of liquid rocket propulsion provides an empirical basis for solving this problem when it is encountered. This is however not sufficient if one wishes to understand the mechanisms and devise tools for prediction of possible instability and stability margin rating. Hot fire tests indicate that a strong coupling is involved between combustion and the eigenmodes of the chamber. For the current engine sizes, oscillations typically occur at frequencies of the order or above 1 kHz generating very high amplitude levels. The most powerful coupling involves transverse modes which in cylindrical combustion chambers are of azimuthal or radial type.

The present study is part of a global project which aims at developing predictive tools for combustion instabilities based on an understanding of the fundamental mechanisms. One idea explored here is to examine the role of the multiple reactant streams interacting with an acoustic mode. It is already known from some fundamental studies by Schuller et al. (2002, Schuller et al. (2003) that the interactions between adjacent flame fronts or between a flame and a wall constitute a powerful source of instabilities. In liquid rocket engines, propellants are fed into the chamber through a large number of injectors which are closely packed and these separate streams may interact. The coupling between a transverse acoustic motion and the reaction layers formed by each of these units may also effectively induce unsteady heat release rates which may in turn constitute sources of instability. This justifies the multiple injector geometry adopted in the present experiments as well as that used in the numerical simulations. A multiple injector combustor (MIC) has been manufactured to recreate on a model scale the high pressure conditions prevailing in real engines. In standard tests, the chamber is fed with liquid oxygen and gaseous hydrogen or methane. These reactants are introduced through a set of coaxial elements. Hot fire tests have been performed with a three element injector system at 1 MPa and are described by Richecoeur et al. (2006). More recent experiments have been carried out with a five element backplane at 3 and 6 MPa. Experiments reported in what follows concern the effect of transverse acoustic waves in this configuration but under cold flow conditions where the coaxial injectors are fed with liquid oxygen and gaseous nitrogen jets. This situation investigated experimentally motivates the numerical simulations reported in this article.

At this point it is worth briefly reviewing the possible mechanisms and the relevant literature dealing with this topic. The interaction between propellant injection and chamber eigenmodes may take various routes :

- The pressure fluctuation in the chamber induces a dynamical response of the injection system giving rise to a perturbation of the propellant mass flow rates. This is usually characterized

by an acoustic impedance. In the coaxial injector case one should in fact consider impedances of the oxidizer and fuel streams separately because the characteristics of these two streams are usually quite distinct.

- The presence of an acoustic oscillation in the chamber can influence the liquid jet break-up process and subsequently modify atomization. This will have an effect on the droplet size distribution in the spray.
- Droplet vaporization may be enhanced by the acoustic oscillation giving rise to a modulation in the available reactant in the gaseous phase.
- Large amplitude acoustic oscillations induce velocity fluctuations. When the resonant mode is transverse to the propellant streams this will enhance mixing between reactants. If the injectors are closely packed, this may lead to interactions between adjacent jets.

Some of these items are considered in the previous literature (Philippart and Moser 1988; Muss and Pieper 1988; Ierardo et al. 2001; Bazarov and Yang 1998; Chehroudi et al. 2003; Conrad et al. 2004; Vingert et al. 1995; Janardan et al. 1979). Some of the recent experiments carried out by Oschwald et al. (2006) on single jets under sub- and transcritical conditions indicate that coupling with a strong acoustic wave perturbs the natural evolution of the liquid oxygen stream, accelerating vaporization and increasing the spatial dispersion of the liquid droplets. Other experimental studies on water jets at ambient conditions submitted to high amplitude acoustic perturbations (Blaisot et al. 2004) feature some remarkable modifications of the jet structure. The case of multiple jets originating from coaxial elements and submitted to a transverse acoustic oscillation is less well documented but it comes closer to the situation which prevails in a real engine. It is thus natural to examine this case under high pressure conditions. It is also logical to use liquid oxygen to feed the various injectors. For cold flow experiments the outer stream should not be reactive and gaseous nitrogen is used for that purpose.

In the experiments, liquid oxygen at 80 K and gaseous nitrogen at 288 K are injected through five injectors and the dynamics of the system is investigated at a high chamber pressure (3 MPa) which is still below the critical value of oxygen (5.04 MPa). The elements are vertically aligned and an external modulator is used to generate high amplitude and transverse acoustic waves. Pressure sensors placed in the chamber are used to characterize the acoustic mode generated in this case. Using backlighting and high speed imaging, one finds that the jets oscillate in the transverse direction and that their structure is perturbed by the external forcing.

In the second part of this study, numerical simulations are carried out in a similar geometry but for simplified injection conditions in which the reactant jets are gaseous. These calculations are aimed at the development of large eddy simulation (LES) of high frequency instabilities. The numerical method used to induce a transverse acoustic motion is that developed by Rey et al. (2005). This allows acoustic excitation of flows from the computational domain boundaries. This method is now part of the AVBP[1] simulation code. Sinusoidal pressure waves are injected in the chamber interacting with the flow. The paper reports three dimensional simulations of three adjacent coaxial jets perturbed

[1] AVBP : a LES code for reactive flows, CERFACS

by transverse acoustic waves. Conditions differ from those of the experimental case since the two reactants (methane and oxygen) are gaseous and the temperature and pressure have ambient values. The purpose is to show the effect of acoustic modulations on coaxial jets using LES methods.

IV.2 Experimental investigation of flow/acoustic interactions

Experiments are carried out on the "Mascotte" test facility dedicated to high pressure cryogenic combustion studies (Vingert et al. 2000). This rig may be used to study combustion of liquid oxygen with gaseous or liquid methane at high pressure. This facility has been equipped with a multiple injector combustor in 2000 to study the role of collective interactions in high frequency combustion instabilities (Rey 2004; Rey et al. 2004; Richecoeur et al. 2005). Hot fire runs have been carried out with three element injectors and more recently with five such units at pressures ranging from 1 to 6 MPa. The chamber dimensions are such that the first transverse eigenfrequency under hot fire conditions is around 2 kHz, depending on the pressure and mass flow rates.
The non-reactive test case described in what follows aims at observing the effect of high frequency transverse acoustic modulations on a collection of cryogenic propellant jets.

IV.2.1 Experimental parameters for the study of cryogenic jets behavior

The experimental set-up involves three main elements : a combustion chamber including a cryogenic feed system, five coaxial injectors forming jets inside the chamber, and an external source of modulation to excite one of the transverse modes. The chamber has a rectangular cross section with dimensions equal to $350\times250\times50$ mm^3. The combustor dimensions have been chosen to place the eigenfrequencies under hot fire operation in the frequency range of instabilities in real engines (above 1 kHz). The small spanwise thickness ($l_z = 50$ mm) is such that pressure perturbations are essentially uniform in this transverse direction in the range of frequencies considered in the present investigation. The chamber can sustain mean pressures up to 10 MPa and it is thus possible to operate above the critical pressure of oxygen (i.e. $p_{cr} = 5.04$ MPa). The upper and lower chamber walls are respectively equipped with three and two pressure transducers (namely C1 to C5 in figure IV.1) while the lateral side walls comprise large transparent windows (150×100 mm^2) allowing direct observation of the five backlighted jets.

Under steady operation, the test chamber is naturally stable. There is no dominant frequency in the pressure signals recorded without external modulation. To perturb the system, the modulation has to be generated externally to induce strong oscillations. A secondary nozzle, placed 100 mm from the chamber backplane on the top wall, is used to eject up to 15% of the total mass flow rate fed into the chamber. The nozzle is periodically blocked by a rotating toothed wheel with a diameter of 185 mm comprising fifty 5-mm large teeth regularly distributed around its external border. The real flow rate ejected through the modulation nozzle is less than 7.5% due to the periodic obstruction. With this secondary nozzle, part of the gases is periodically evacuated from the combustor in the cross stream direction. Due to this lateral mass flow fluctuation, the auxiliary nozzle acts as an acoustic source which

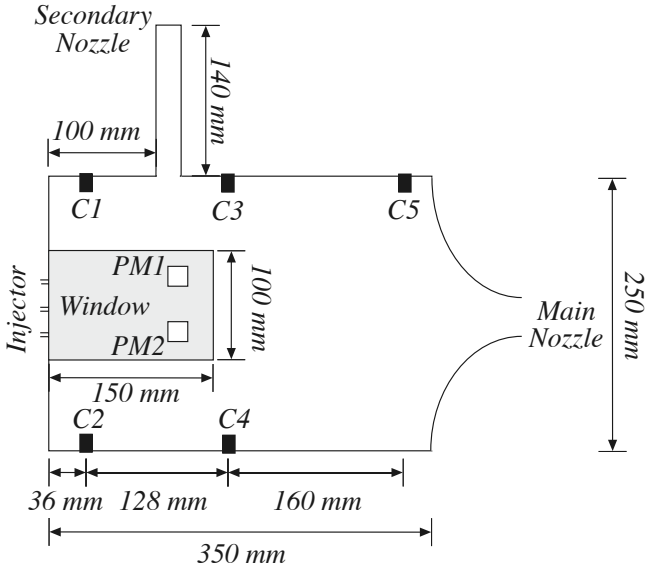

Fig. IV.1: Schematic representation showing the chamber equipped with quartz windows and positions of the five pressure transducers (C1 to C5).

$\overline{p}_{chamber}$	d_{LOx}	d_{N_2}	Injector lip	$\dot{m}_{LOx}$	$\dot{m}_{N_2}$
3 MPa	5.78 mm	7 mm	0.3 mm	100 g s^{-1}	145 g s^{-1}

Tab. IV.1: Injection parameters for the five cryogenic jets at 3 MPa

generates transverse pressure waves in the chamber. The various eigenmodes of the system can be excited by changing the modulation frequency (i.e. the rotation speed of the toothed wheel). This apparatus effectively induces strong well-controlled acoustic oscillations in the chamber (Rey et al. 2004).

In the present experiments the mean chamber pressure is 3 MPa. Gaseous nitrogen and liquid oxygen (80 K) are injected in a subcritical state at flow rates equal to 145 g s^{-1} and 100 g s^{-1} respectively. The injector dimensions and the induced injection velocities are gathered in table IV.1.

IV.2.2 Diagnostics

Pressure transducers and optical diagnostics are used to characterize the acoustic response of the chamber and observe the jet behavior and the direct effect of the modulation on the flow.

Five Kistler pressure sensors (type 701A) are flush mounted in the chamber walls (three in the top walls and two in the bottom ones). Their signals are sampled at a 40 kHz rate. Each pressure sensor has a resonant frequency of 70 kHz which is well above the frequency range of interest. The sensors relative positions are such that the phase between each of these probes can be used to describe the acoustic mode generated in the chamber. Two additional pressure transducers are located on the LOx and N_2 injection lines.

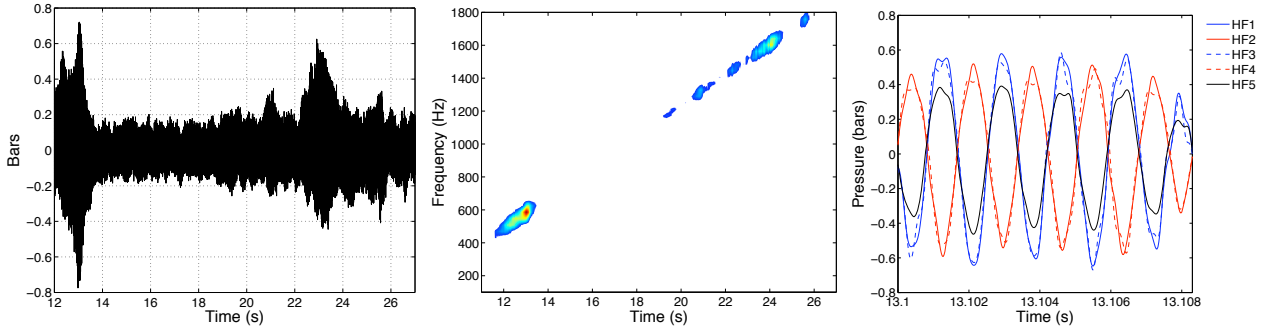

(a) (b) (c)

Fig. IV.2: (a) Pressure signal detected by transducer C3 sampled at 40 kHz during a linear frequency sweep test. (b) Short time Fourier transform of the pressure signal. (c) A close-up view of the signals detected by the pressure transducers showing the phase at the first resonant peak (585 Hz).

The chamber is illuminated from the back by an intense source of white light. Two intensified cameras record instantaneous snapshots. The first covers the whole available window, the sampling rate is 18 Hz with a sensor matrix of 512×512 pixels. The second camera provides close up views of one of the injector element with a sampling rate of 4 Hz and a resolution of 1024×1024 pixels.

A high speed camera operating at 30000 frames per second provides time resolved images of the jet dynamics and interactions. The camera covers the whole window allowing observations of the full development of the jets. The frame rate is high enough to follow turbulent structures in this flow.

IV.2.3 Acoustic mode identification

Three runs are required to investigate the acoustic response. The changing parameter between the three runs is the external modulation applied to the system. The first test carried out without external modulation serves as a reference.
In the second run, the modulation frequency is swept linearly and the excitation frequency is changed continuously from 0 to 2000 Hz at a rate of 90 Hz s^{-1}. The rate of change of this linear sweep was selected by taking into account the frequency response of the system or equivalently the damping characteristics of the system as determined from previous experiments by Richecoeur et al. (2006).
The last run is carried out by exciting the system at the first transverse eigenfrequency deduced from the second test. During this procedure, the first and last runs are used to compare the jet structure without and with modulation, the intermediate test provides the acoustic response in the range of frequencies traversed by the linear sweep.

Two resonant peaks are observed during the frequency sweep as illustrated in figure IV.2(a). Short time Fourier transform analysis of one of the pressure signals is carried out to extract the resonant frequencies. The corresponding time-frequency graph displayed in figure B.4 exhibits two spots which are associated with the two peaks observed in the signal time trace. The corresponding frequencies are respectively 585 Hz and 1600 Hz. By plotting the five signals obtained from the transducers placed at

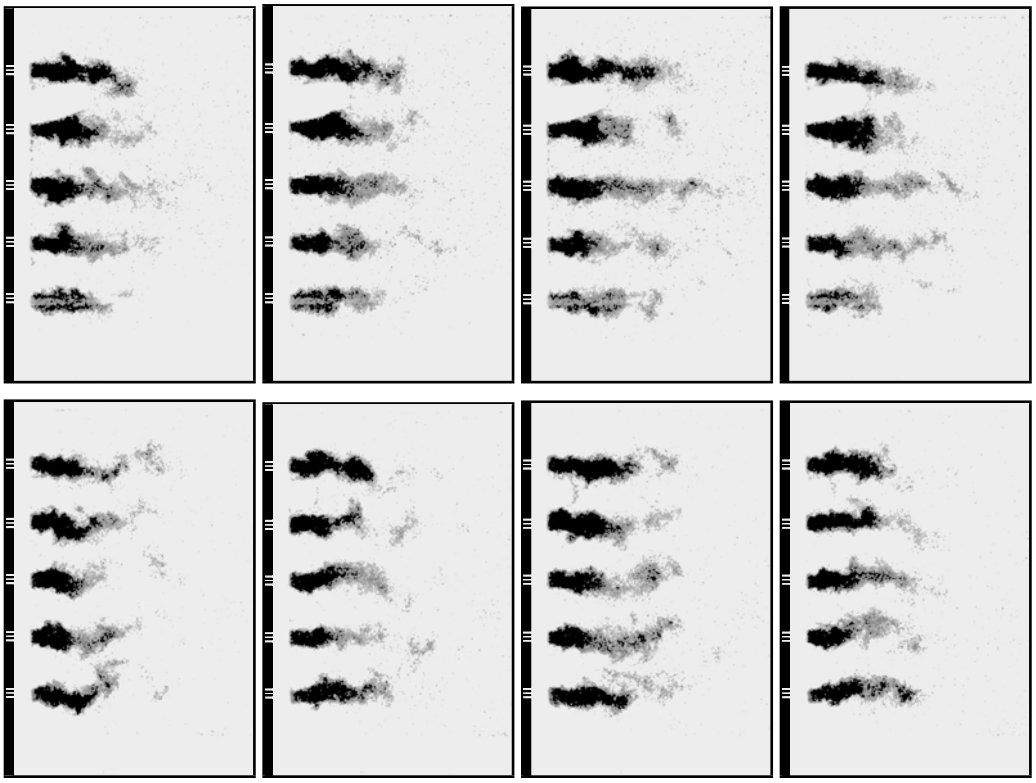

Fig. IV.3: Instantaneous frames for non-modulated (top) and modulated jets (bottom). The transverse modulation is applied at 585 Hz. The injection plane cannot be reached by the light beam and is therefore not viewed in these images. Backlighting begins at 2.8 d_{LOx} from the injection plane.

the chamber walls, the phase can be observed and the spatial characteristics of the acoustic mode are accurately determined. Figure IV.2(c) shows a close-up view of the signals at the time corresponding to the first resonant peak. This shows that the first peak pertains to the first transverse eigenmode. The system is then modulated at this frequency.

IV.2.4 Modulation at the first transverse mode

The system is modulated at the first transverse eigenfrequency. The amplitude of pressure oscillations reaches 0.5 bar (i.e. 1.6 % of the mean chamber pressure). This corresponds to velocity oscillations of 4 m s^{-1}. Figure IV.3 displays light distributions obtained by backlighting. This figure allows a direct comparison between modulated (figures IV.4(a) and IV.4(c)) and the non modulated tests (figures IV.4(b) and IV.4(d)).

The level of acoustic perturbation is strong enough to generate two main effects. The first concerns the structure of each jet, the second is about the collective interaction of the jets.

The visible jet core length is modified as can be seen from average light emission images (figures IV.4(c)-IV.4(d)) which indicate that the modulated core flows are shorter than those found in the naturally developing streams. Figure IV.4 shows a close-up of the central injection element for both

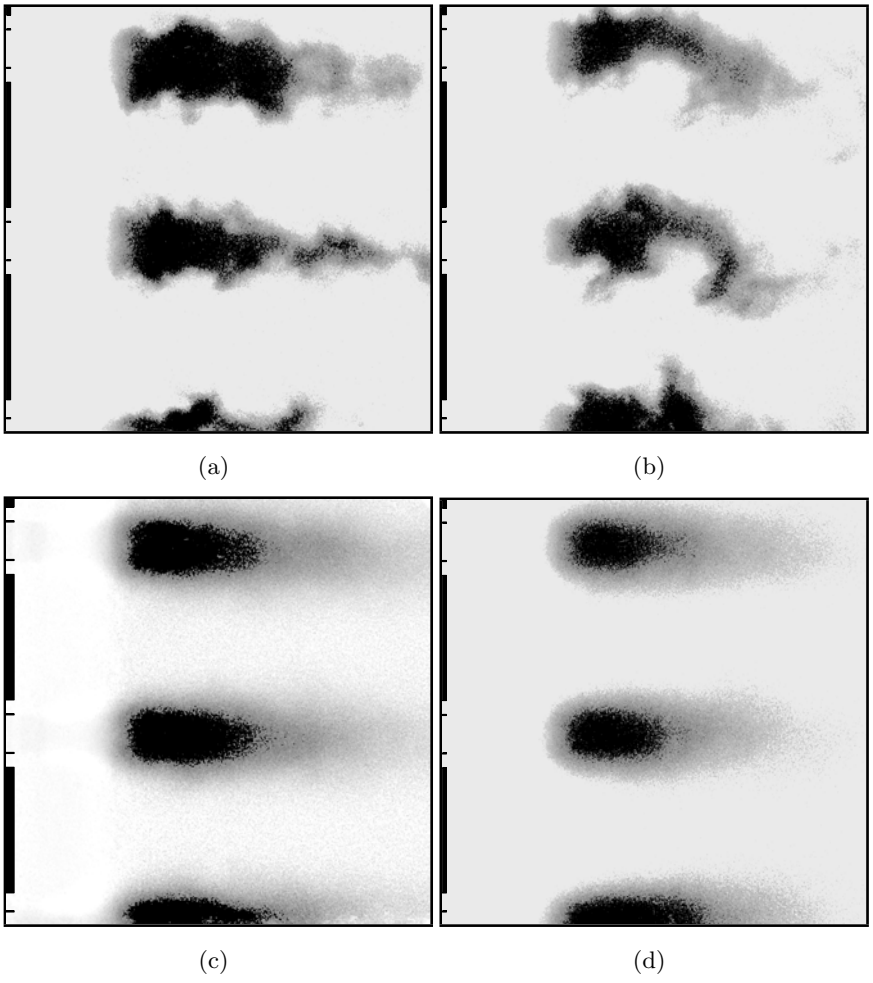

Fig. IV.4: Close-up views of the jet formed by the central injector observed with an intensified CCD camera. Instantaneous frames ((a) and (b)) and average frames ((c) and (d)) for non-modulated (left) and modulated jets (right). The injection plane cannot be reached by the light beam and is therefore not viewed in these images. Backlighting begins at 2.8 d_{LOx} from the injection plane.

the non modulated and modulated tests. This can be used to obtain a quantitative estimate of the length variation of the dense liquid core. The average light distribution has nearly the same shape but the length is modified. This is due to a more effective atomization and dispersion induced by the transverse velocity. When modulated, the atomization process is accelerated by the acoustic perturbation. The vaporization rate is probably accelerated as well and the droplet dispersion is enhanced. As a result the dark region in the light distribution is shorter by about 17%.
Instantaneous images (figures IV.4(a)-IV.4(b)) provide complementary information on this process. Two modifications can be observed in each individual jet when modulated :

- The jet geometry is highly perturbed and features a transverse displacement of the core, induced by the velocity induced by the transverse acoustic mode. A sinusoidal pattern is observed in the instantaneous frames with a periodic inversion of the jet stream curvature.
- The jet is broken into filaments which are periodically detached from the main core. This mechanism of liquid ejection from the core enhances primary atomization and augments the vaporization rate by increasing the amount of exchange surface area. Without modulation the liquid core features instabilities but remains essentially intact until it is broken down and atomized into small droplets. The atomization, leading to the creation of large liquid packages, is not observed in this case while it is quite distinct in the modulated jet situation. Atomization and dispersion are clearly less effective in the natural case than in the modulated case.

The collective behavior of the system is also worth examining. The external modulation generates a field of transverse velocities which globally affects the injected streams. The five jets oscillate at the modulation frequency (i.e. the first transverse eigenfrequency, 585 Hz). There is no phase difference between the jets which all move together. This tends to show that there is little direct interaction between the adjacent streams of dense (liquid) reactant. The distance between the jets is essentially constant and the jet displacement is in the same direction over the whole chamber. One may deduce from this observation that the acoustically induced sloshing motion bring more material in the upper and lower sides of the chamber and that this takes place periodically. The upper part is filled with more material during the part of the cycle corresponding to a positive acoustic velocity while the lower part is fed during the part of the cycle corresponding to a negative velocity.

Experimental results are admittedly incomplete but they constitute an initial data set on a process which may well be important for the development of an instability. These data are used in what follows to guide numerical simulation of this configuration.

IV.3 Large Eddy Simulation

The experimental investigation described in the previous section provides useful but incomplete information. It is thus worth trying to examine the process with numerical simulation. The simulations are not intended to represent real conditions. The real experimental conditions are not accurately reproduced in the simulations because this does not seem feasible at this point in time. Since the flow is turbulent and modulated externally by acoustic pressure waves it is natural to develop the numerical calculations in a large eddy simulation (LES) framework. This can be used to examine the dynamics

of coaxial injection. LES tools are now commonly used to investigate gaseous flows. The treatment of gas liquid configurations is much less advanced and much more difficult on the computational level. It is therefore reasonable to examine a situation where the two injected streams are gaseous. This is admittedly an important simplification but it is required in the present context. The cold flow calculations presented in this article form the basis of hot flow simulations and for that reason it was decided to use gaseous oxygen and methane as injected reactants. The present simulations are also carried out at a pressure of 0.1 MPa instead of the 3 MPa used in the experiment, the transverse frequency adopted in the simulations corresponds to that found under hot fire conditions and hence does not match that identified under cold flow conditions (585 Hz). Simulations differ from experiments in the previous choices (liquid oxygen is replaced by gaseous oxygen, nitrogen is replaced by methane, the resonant frequencies are different). In addition, the number of jets is equal to three to reduce CPU time. While these distortions are quite significant, it is nevertheless possible to use transverse pressure waves generated numerically to compare the dynamics of naturally evolving and modulated jets and examine species mixing in the absence or in the presence of an external modulation.

IV.3.1 Numerical Method

Calculations are carried out with the AVBP code developed at Cerfacs. AVBP can be used to calculate turbulent compressible flows using Large Eddy Simulations (LES) on structured or unstructured meshes. Integration schemes ensure a third order precision in space and second order in time (Colin and Rudgyard 2000). LES is well adapted to the problem at hand because the coupling between external modulations and the flow essentially involves the large scale dynamics. The large eddies carry the major part of the turbulent kinetic energy and one may reasonably assume that, in the case of jets modulated by an external acoustic mode, the smaller scale eddies will not be directly influenced by the forcing. The jet dynamics can then be described by the subgrid scale models used in standard LES calculations.

In LES the flow variables are spatially filtered (Aldama 1990; Vreman et al. 1994) :

$$\overline{f(\boldsymbol{x},t)} = \int_{-\infty}^{\infty} f(\boldsymbol{x}',t)G(\boldsymbol{x}'-\boldsymbol{x})\boldsymbol{dx}' \tag{IV.1}$$

where G is a localised filter and $\overline{f(\boldsymbol{x},t)}$ is the filtered value of the variable $f(\boldsymbol{x},t)$. In the description of turbulent multispecies flows, the primary variables are the velocity vector $v_i(\boldsymbol{x},t)$, the species mass fractions $Y_k(\boldsymbol{x},t)$ and the associated quantities, the total energy E and the density $\rho(\boldsymbol{x},t)$, where $E(\boldsymbol{x},t) = e_k + 1/2\ v_i v_i$ and $\rho(\boldsymbol{x},t) = \sum_{k=1}^{N} \rho_k Y_k(\boldsymbol{x},t)$ (e_k being the mixture sensible energy). It is assumed that all constituents follow ideal gas laws, and that the viscous stress tensor, heat flux and species transport follow standard gradient laws. Under the assumption that diffusion coefficients are not influenced by the unresolved fluctuations, molecular transport terms become a function of the filtered field (Poinsot and Veynante 2005). The Navier-Stokes equations are then written in terms of filtered quantities, and are solved in conjunction with a subgrid-scale closure (SGS) (Freiziger 1977; Moin et al. 1991; Sagaut 2001). In the present context, it is convenient to use the Smagorinsky model (Smagorinsky 1963) to express the subgrid scale stress tensor

$$\overline{\tau_{ij}}^t = -\overline{\rho}(\widetilde{v_i v_j} - \tilde{v_i}\tilde{v_j}) \quad \text{(IV.2)}$$

$$= 2\overline{\rho}\nu_t \tilde{S}_{ij} - \frac{1}{3}\overline{\tau_{ll}}^t \delta_{ij} \quad \text{(IV.3)}$$

$$\tilde{S}_{ij} = \frac{1}{2}(\frac{\partial \tilde{v}_i}{\partial x_j} + \frac{\partial \tilde{v}_j}{\partial x_i}) - \frac{1}{3}\frac{\partial \tilde{v}_k}{\partial x_k}\delta_{ij} \quad \text{(IV.4)}$$

In compressible flow situations, it is standard to weight the filter by the density and use Favre filtered quantities like $\tilde{v}_i$ for the velocity vector and $\tilde{S}_{ij}$ for the resolved strain rate tensor. The Smagorinsky model estimates the turbulent viscosity ν_t by :

$$\nu_t = (C_S\Delta)^2\sqrt{2\tilde{S}_{ij}\tilde{S}_{ij}} \quad \text{(IV.5)}$$

where C_S refers to the model constant. The filter characteristic size Δ is calculated as the cubic-root of the cell volume. The SGS species flux is deduced from the SGS turbulent diffusivity, which is expressed as the ratio of the turbulent viscosity by a turbulent Schmidt number. Similarly, the heat diffusivity is expressed with a turbulent Prandtl number.
It is known from previous studies by Pope (2000) that the Smagorinsky model is not the best possible subgrid scale closure for transitional flows (Sagaut 2001) because of its inherent dissipative nature. It is known that transitional flows involve an energy transfer from the subgrid scales to the resolved scales which cannot be represented by this simple SGS model. The reasons underlying the present choice are however that (1) This scheme is easiest to implement on an unstructured grid, (2) The initial developing part in the jet is finely meshed to minimize the contribution of the unresolved scales (3) The flow response is tightly coupled to the large scale dynamics, which is well described in the LES framework and is only weakly influenced by the SGS model. Thus, it is reasonable to consider that the model will yield adequate predictions of energy-containing components in high Reynolds number flows, provided that Δ is well within the inertial subrange.

IV.3.2 Case overview

As indicated at the beginning of this section, the simulations are intended to observe effects of high amplitude transverse modulations on a cold flow multiple jet configuration without precisely reproducing experimental conditions. Three coaxial jets are simulated and their behavior is investigated with and without forcing. The main objective is to analyse the mixing process and the jet interactions when the system is transversally modulated at high frequency ($f > 1$ kHz). The different steps of the simulation follow the process adopted in the the experimental study. The simulation is first developed without transverse modulation. An acoustic modulation is then generated at the first transverse acoustic mode.

This latter is numerically determined by solving the Helmholtz equation for a rectangular cavity. Numerical determination of the modes provides the eigenfrequency and modal structure. The pressure field corresponding to each frequency can then be viewed in three dimensions.

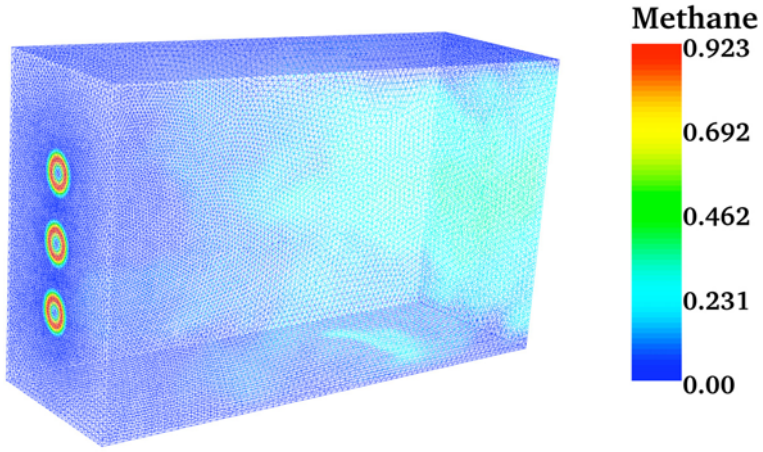

Fig. IV.5: View of the computational mesh (150 mm × 90 mm × 50 mm) colored by the methane mass fraction at injection. The three injection elements are also represented schematically.

IV.3.3 Computational mesh and boundary conditions

The computational domain is a 3D rectangular box of 15 cm × 10 cm × 5 cm, meshed with 10 millions tetrahedric elements corresponding to 950 000 nodes. Experimentally the momentum flux ratio $J = \rho_{CH_4} v_{CH_4}^2 / \rho_{LOx} v_{LOx}^2$ is often used to characterize coaxial injection systems. During the experimental investigations, J was varied between 5 and 12. Because this parameter controls mixing efficiency, numerical simulations are carried out by choosing a value of J equal to 9, which is within the experimental range. The backplane comprises three coaxial element injector which are vertically aligned. The distance between the injector axis is equal to that used in the experiment ($a = 1.7$ cm). For each element, gaseous oxygen is injected through the central channel at a velocity of 25 m s^{-1} while gaseous methane is injected around the oxygen stream at a velocity of 75 m s^{-1}. The selected injection parameters and the mesh size require a time step of 10^{-7} s. An acoustic period corresponds approximately to 5000 time steps.

The boundary conditions are defined to obtain an adequate base flow and suitable acoustic perturbations. On the injection plane, velocity is imposed with artificial turbulent component equal to 8% of the mean velocity. The coaxial elements are not directly meshed, the injection profiles in terms of velocities and species are defined by making use of standard hyperbolic tangent profiles. The outlet is a constant ambient pressure condition. The side walls are no slip boundaries and the acoustic modulation is imposed from the top and bottom walls. These two boundaries are used to modulate the system. Acoustic waves are generated by imposing an oscillating injection velocity around a null value. The injected gas is nitrogen, the tangential injection velocity is null and the normal velocity profiles are given by

$$v_{top}(x, b/2, z, t) = U_0\, A(x)\, \sin(2\pi f t) \quad \text{(IV.6)}$$

$$v_{bottom}(x, -b/2, z, t) = U_0\, A(x)\, \sin(2\pi f t + \phi) \quad \text{(IV.7)}$$

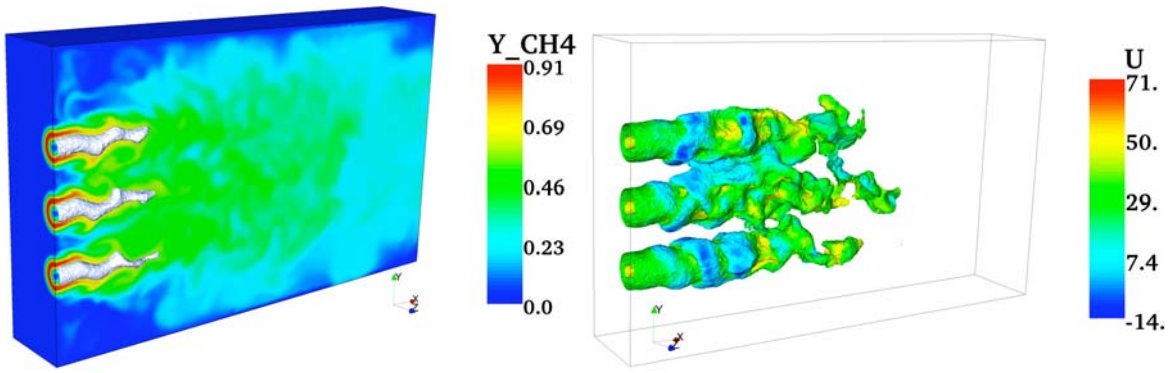

(a) (b)

Fig. IV.6: Three dimensional instantaneous fields with transverse acoustic modulation at 585 Hz. (a): oxygen contour at $y_{\mathbf{Ox}} = 0.3$ on methane field. (b): methane contour at $y_{\mathbf{CH_4}} = 0.4$ colored by axial velocity U

where f is the modulation frequency, b is the transverse dimension of the chamber, U_0 the modulation amplitude, $A(x)$ a shape function used to accommodate the discontinuities at the chamber corners, ϕ is the phase of the velocity profile fluctuations. Two kinds of transverse modulations can be imposed depending on the value of ϕ. When ϕ is null, the modulation mode is varicous, the transverse components have opposite signs. The jets are successively compressed and expanded. When $\phi = \pi$, injection conditions on the two walls are out of phase, the two transverse velocity components have the same sign and induce a sinuous jet motion. This modulation type is adopted in the present simulations. Calculations are carried out for two different modulation amplitudes of 1 and 3 m s^{-1}.

IV.3.4 Results

The simulations aim at demonstrating the feasibility of the calculation and analysing the impact of modulation on mixing. Quantitative comparisons between experiment and simulation are not pursued since the simulation conditions do not correspond to those used in the experiment. The simulation is carried out for gaseous reactants while the experiment uses liquid oxygen. Reference to experiments is made only to validate the global description of the jet response to the acoustic modulation as exemplified in figure IV.6.

IV.3.4.1 Influence of the acoustic modulation on specie mass fractions

Mass fractions of the two reactant streams are used to visualize the flow dynamics and mixing. Spatial distributions of these variables are used to compare the modulated and natural jets. The transverse perturbation is injected trough the lateral walls by generating high amplitude pressure oscillations. Figure IV.7 shows the instantaneous pressure obtained during a modulated test. A transverse mode is excited at 2500 Hz generating a sinusoidal pressure distribution in the chamber. The velocity perturbation displaces the oxygen and methane streams. The jet dynamics is analogous to that observed experimentally. The oxygen mass fraction distribution indicates that (1) the central oxygen core length is reduced and that (2) the oxygen mixes more rapidly with the surrounding flow of

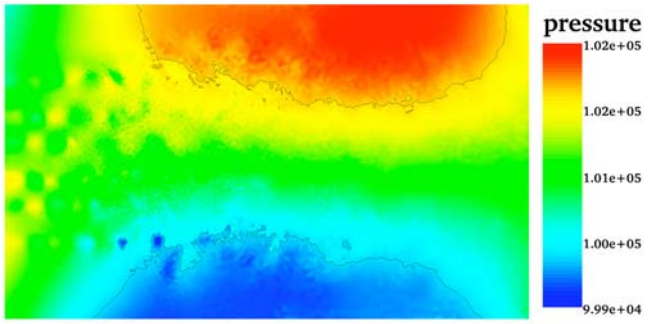

Fig. IV.7: Instantaneous pressure field obtained numerically by inducing fluctuating transverse velocity from the upper and lower walls.

methane.

Figure IV.8 displays methane and oxygen mass fractions for the natural case and for the 1 m s^{-1} modulated case. An increase of the modulation amplitude to 3 m s^{-1} shows only a slight modification of the distribution of reactants in the chamber.

Without modulation (figure IV.8(a) and IV.8(b)), the jet of oxygen mixes at a relatively slow rate with the fast moving methane stream. Oxygen remains bounded inside the co-annular methane stream and oxygen and methane are still well separated over about 7 oxygen diameters. Transition takes place at this stage and mixing is enhanced in the downstream region. The oxygen core length is drastically reduced when the flow is submitted to external modulations. The mass fraction fields are modified to a great extent (figure IV.8(c) and IV.8(d)). The jets are wrinkled by the acoustic motion. Transverse sinusoidal displacements are induced and affect the species distributions. Natural jet oscillations were observed on the downstream part of the chamber without modulations, here these oscillations are visible after only two oxygen diameters. The wavelength is similar for the two species and is approximately equal to a convection velocity U_c divided by the modulation frequency. Here, the frequency is 2500 Hz and the half-sum of the two injection velocities gives a convection velocity $U_c \simeq 50$ m s^{-1} yielding a wavelength $\lambda \simeq 2$ cm. The direct consequence of this wrinkling is a net reduction of the oxygen core length. Methane and oxygen mix at a few centimeters after injection, the oxygen is immediately perturbed and turbulence is enhanced. Figure IV.9 presents the oxygen mass fraction evolution along the central element axis. The oxygen rate of decay is augmented by a factor of two when the jets are modulated but the amplitude of the modulation does not play a significant role in the mixing process. The first amplitude (1 m s^{-1}) is strong enough to destabilize the jets, and mixing is only slightly improved by a further increase of the modulation amplitude. The oxygen mass fraction reaches the same limiting value which is slightly below 0.1 and corresponds to a nearly uniform profile of this specie.

The modulation also affects the co-annular methane stream which expands more rapidly outwards. Turbulence is increased on the external side of the methane flow. This phenomenon has been observed in both reactive and non reactive experimental tests. Under modulation the methane jet expands

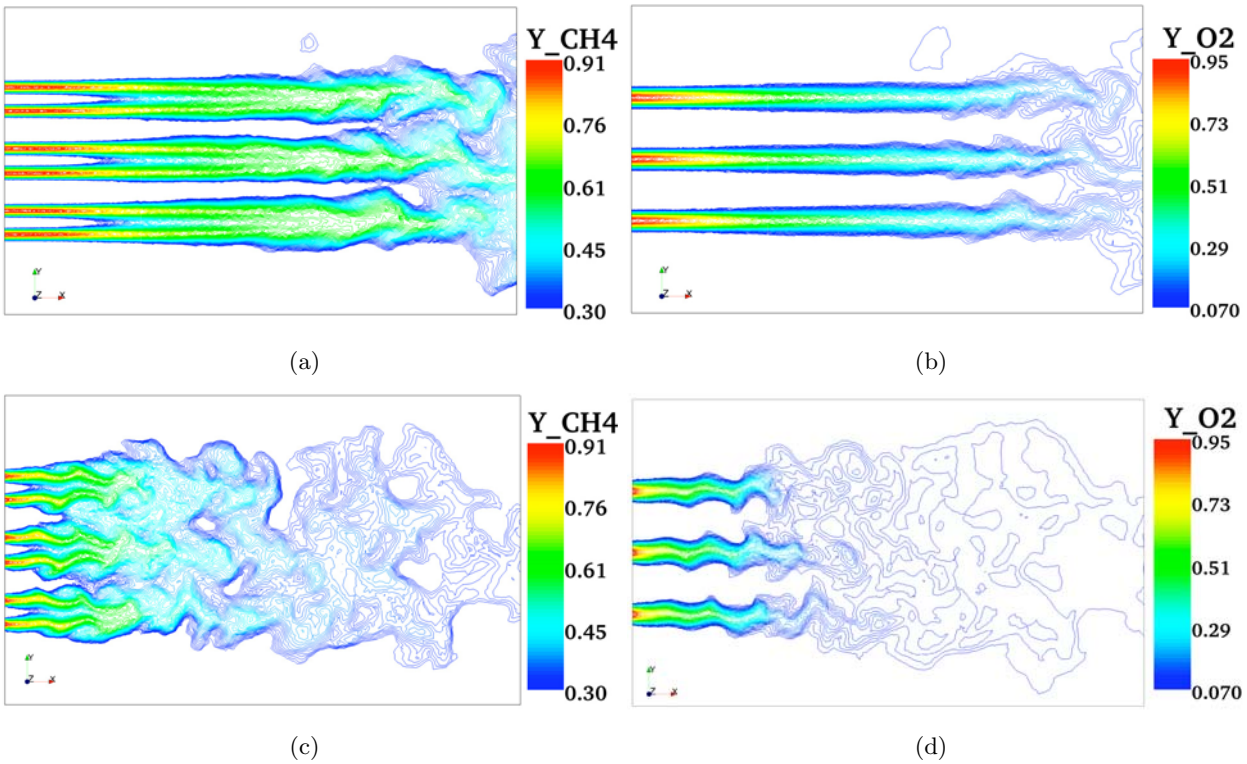

Fig. IV.8: Mass fraction of oxygen (right) and methane (left) in the chamber middle plane (z=0). The natural (top) and modulated (bottom) cases are compared. The modulation is generated by a fluctuating injection velocity on the top and bottom walls. The modulation amplitude is 1 m s^{-1}.

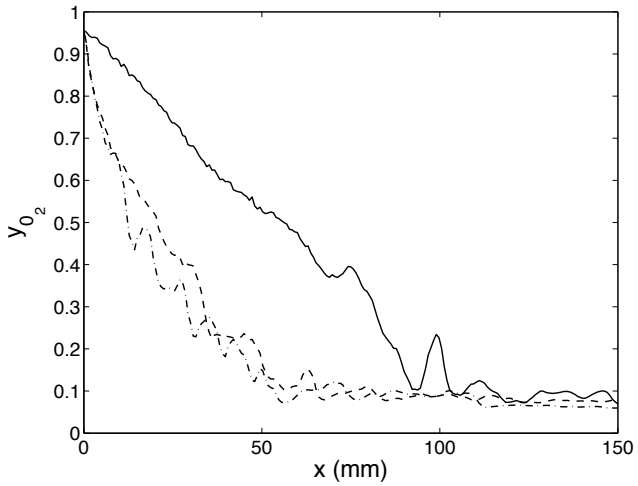

Fig. IV.9: Oxygen mass fraction along the axial line from the injection plane (x=0) to the chamber output (x=150). Natural (continuous line), 1 m s^{-1} modulated (dashed line) and 3 m s^{-1} modulated (dot-dashed line) cases are represented.

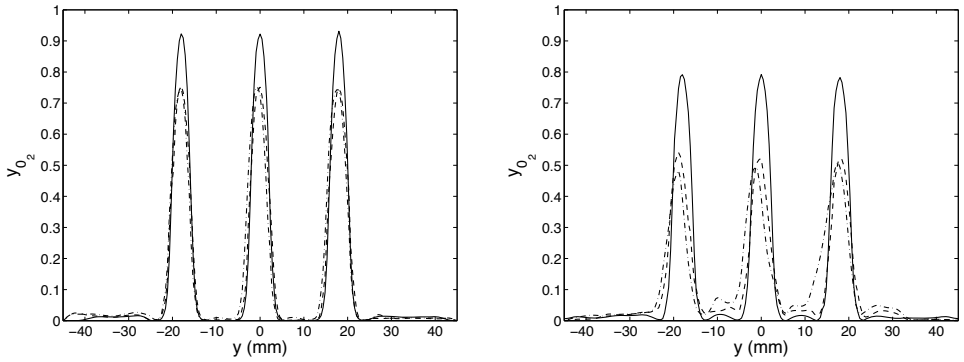

(a) x = 5 mm (d_{O_2}) (b) x = 20 mm ($4d_{O_2}$)

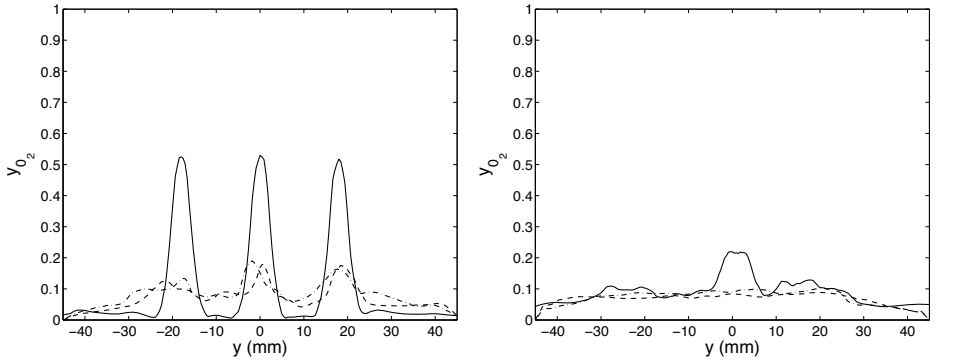

(c) x = 50 mm ($10d_{O_2}$) (d) x = 100 mm ($20d_{O_2}$)

Fig. IV.10: Oxygen mass fraction in different transverse sections. The plot shows natural (continuous line), 1 m s^{-1} modulated (dashed line) and 3 m s^{-1} modulated (dot-dashed line) cases.

more rapidly in response to the augmented level of fluctuation induced by the modulation. The effect on the oxygen is slower. Oxygen is first confined by the methane stream. It is then entrained by the surrounding jet and its mass fraction rapidly diminishes. The same phenomenon of mixing is observed without modulation but the acoustic excitation reduces the characteristic time of the process.

Figure IV.10 displays the oxygen mass fraction in the transverse direction at different distances from the injection plane. The graph shows three cases for each location corresponding to no modulation, 1 and 3 m s^{-1} modulation levels. At a distance of one diameter the oxygen profile significantly differs from that observed in the modulation free case. The oxygen distribution is identical in all cases at a distance of 20 diameters. As already indicated an increase in the modulation amplitude has a minor effect. The 1 m s^{-1} modulation is strong enough to destabilize the jets.

IV.3.4.2 Time evolution

A set of numerical "sensors" placed in the computational domain are used to build time records of all the flow variables. The frequency response of the system is then obtained by summing periodograms calculated by fast Fourier transform methods. The sampling rate is 200 kHz, the number of points in each periodogram is N=2048 and the power spectral density is obtained by summing M= 200 periodograms.
Typical results obtained at a distance x =10 cm from the injection plane and on the chamber axis $y = 0$ are shown in figure IV.11. When modulated, the transverse velocity v at x =10 cm and $y = 0$ is dominated by the 2500 Hz component which concentrates most of the power. This frequency also dominates the power spectral density of the oxygen mass fraction but other frequency bands also show up. Without modulation, two ranges of frequencies are observed in both oxygen mass fraction and transverse velocity spectral densities. The first components represent low frequency fluctuations. Such low frequency components are clearly observed experimentally with and without modulation. The second peak is around 2 kHz. Taking as characteristic flow velocity $U = 80$ m s^{-1} and as characteristic diameter $d = 6$ mm one finds a Strouhal number of 0.15 which is about half that of the preferred mode of a pure free jet (Crow and Champagne 1971). One should however remember that the compound flow formed by each injector with an outer velocity exceeding that existing inside the jet (oxygen is injected at a lower velocity than methane) will not respond like a pure jet. Thus one should not expect to find a maximum at the Strouhal number of 0.3. The frequency components around 2 kHz are however clearly linked to the preferred oscillation frequency of the oxygen/methane compound jet.

One expects a maximum response of this flow if the modulation frequency (i.e. the first transverse eigenfrequency) is of the same order as the natural frequency of the flow. By coupling the transverse acoustic eigenmode and the hydrodynamic frequency of the flow, the external modulation could induce the largest effects on the reactant jets. This is not quite the case here since the modulation frequency is greater than the natural frequency by about 500 Hz.

When modulated, the frequency response of the system is modified. The transverse velocity is logically responding at the modulation frequency. The excitation is obtained by imposing a sinusoidal velocity component in the system. Transverse velocity is directly influenced by the modulation. The mod-

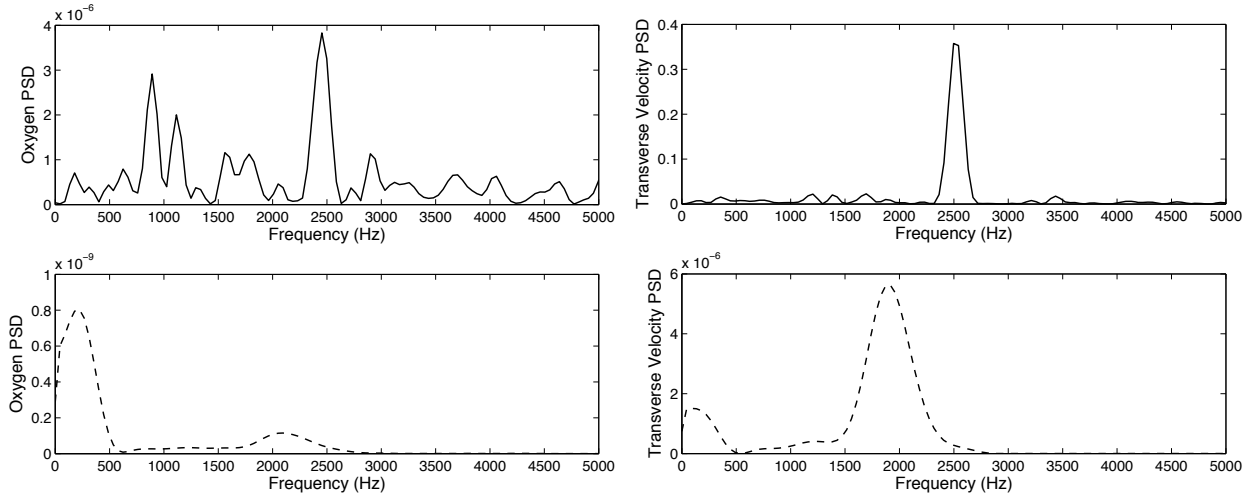

(a) Oxygen mass fraction (b) Transverse Velocity, v

Fig. IV.11: Power Spectral Density (PSD) of oxygen mass fraction and transverse velocity fluctuations observed at x =10 cm from the injection plane. Top: 1 m s^{-1} modulated case. Bottom: natural case.

ulation is strong enough to organize the transverse velocity field and the low frequency components essentially vanish.

The oxygen mass fraction is less influenced by the transverse modulation or at least the oxygen jet response to the modulation does not only occur at the excitation frequency. The highest peak is obtained at 2500 Hz but there are other high amplitude peaks in the response especially around 1 kHz. This tends to show that the oxygen jet is not exclusively organized around the modulation frequency. The acoustic modulation has a direct impact on the low frequency phenomenon and dominates the fluctuations in mass fraction. Similar observations have been made from hot fire test cases. Large scale vortex formation were observed which may correspond to these mid-frequency phenomena.

The modulation has a coupled effect on the species field. It directly modifies the flow by imposing an observable wavelength. The strong transverse velocity injected in the system also seems to decelerate the global flow, the turbulent energy is concentrated in the first part of the combustion chamber which leads to the creation of large structures with characteristic frequencies around 1 kHz but the exact origin of these mid-frequency phenomena is not yet clarified.

IV.4 Conclusion

The coupling between coaxial jets of reactants and a high amplitude transverse acoustic mode is investigated in this article in relation with the problem of high frequency instability. Experiments and numerical simulations are very different but similar phenomena are examined. On the experimental side the flow is characterized with backlighting images and pressure signals detected at the chamber walls. It is shown that the modulation reduces the intact core length of the liquid oxygen stream. The jets feature wrinkles and liquid filaments are ejected from the core. Dispersion of the liquid droplets and mixing are enhanced by the presence of the transverse modulation. The jets originating from the different injectors are set in a sloshing motion and this may periodically feed

separate parts of the chamber with reactive material. Simulations carried out in a simplified configuration in which reactants are in gaseous form complement the experiments. A transverse modulation is introduced numerically and its effect on the jets is examined. Modifications are observed on the coaxial oxygen/methane gaseous jets. Mixing is enhanced by the external acoustics. The velocity and mass fraction variables feature the imposed frequency in their power spectral density. It is also found that the species mass fraction is not exclusively responding at the modulation frequency but contains additional mid-frequency components which have also been observed in modulated hot fire experiments.

Chapter V

Numerical combustion model for turbulent diffusion flames

Résumé

Ce chapitre concerne la modélisation des flammes non prémélangées dans le cadre des simulations aux grandes échelles. Ces simulations représentent une solution idéale pour le développement de modèles prédictifs des instabilités de combustion. A l'heure actuelle, la simulation aux grandes échelles d'un moteur fusée complet n'est pas faisable car plusieurs étapes de modélisation restent à franchir. Des travaux antérieurs ont mis en évidence le caractère non prémélangé des flammes cryotechniques. Un modèle numérique pour cette catégorie de flammes est proposé dans ce chapitre. Le modèle est fondé sur le concept de densité de surface de flamme notamment développé pour les simulations RANS et qui est ici étendu aux simulations aux grandes échelles. Le taux de réaction est décrit analytiquement comme le produit de la densité de surface de flamme et du taux de production par unité de surface. La flamme est localisée autour de la valeur stoechiométrique de la fraction de mélange et le terme source est exprimé en fonction du gradient local de cette variable. La fraction de mélange est transportée par une équation classique de diffusion/convection. Ce modèle est testé sur un cas tridimensionnel où de l'oxygène et du méthane gazeux sont injectés à travers trois éléments coaxiaux à température et pression ambiantes. Un examen des champs instantanés des produits de combustion, de température et de taux de réaction indique que le modèle donne des résultats réalistes.

Abstract

This chapter deals with the numerical simulation of nonpremixed flames in the framework of Large Eddy Simulations (LES). LES is a suitable solution to develop predictive tools for combustion instabilities but at this point, combustion simulations of an entire rocket engine is not feasible. It is known from previous experiments and simulations that cryogenic combustion can be considered to be essentially nonpremixed. The model is therefore defined for this specific mode of combustion. This model is based on the concept of flame surface density exploited in the RANS framework and extended to LES in the present chapter. The reaction rate is analytically described as the product of the flame surface by the reaction rate per unit area. The flame is located at the stoichiometric iso-surface of the mixture fraction. This variable is transported by a classical diffusion/convection equation and the consumption rate is computed from its distribution. A test of this model is carried out in a three dimensional configuration where gaseous oxygen and methane are injected through three coaxial jets at ambient pressure and temperature. Distributions of burnt products, temperature and reaction rates obtained with this model indicate that the model provides realistic results.

V.1 Introduction

Numerical modeling is now widely used in most applications of fluid mechanics. Current efforts in this area are focused on complex flows and specifically those where turbulence plays an essential role. These problems are now considered using large eddy simulation (LES) tools. Much progress has been accomplished in this direction mainly for nonreactive flows but LES is also actively developed for combustion and some spectacular calculations of turbulent flames are already available.

The application of LES in the present context features additional complexities. Calculation of real rocket engines is important but difficult because of the unusual operating conditions. The reactants are pure liquid oxygen associated with hydrogen or methane. The oxidizer is injected in a transcritical state, at a temperature of 80 K and a high pressure exceeding 10 MPa (the critical pressure and temperature of oxygen are 5.04 MPa and 154 K respectively). Heat release rates in typical engines exceed 50 GW m^{-3}. This induces large gradients of temperature. The system also features very large gradients of specific mass and the typical Mach numbers are of the order of 0.2-0.3 in the burnt products. The geometrical complexity is also substantial because propellants are injected by a very large number of units (more than 500 in the Vulcain engine) and this implies a wide range of scales, the largest scale being typically of the order of the chamber diameter while the smallest scale is only a fraction of a single injector diameter. The simulation of a chamber including the physical and geometrical complexity is probably not feasible at this point in time but further improvements in computational power will progressively allow to deal with such problems. It is therefore important and timely to prepare the numerical models which will be needed in this field. The effort has already begun with some remarkable initial LES calculations of transcritical combustion by Oefelein and Yang. A current project is also developed by EM2C in collaboration with Cerfacs to develop LES tools for transcritical combustion. This will be certainly useful for future developments of predictive tools for combustion instabilities. Another area which has been explored by Rey et al. (2005) in his doctoral thesis is the numerical representation of transverse acoustic modulation and application to multiple premixed flames. This effort is pursued in the present chapter which is essentially focused on the development of combustion models applicable to the large eddy simulation of nonpremixed flames. The objective is to develop methods which can be used to simulate interactions between multiple propellant jets and transverse acoustic modes. The modeling effort carried out to complement experimental investigations described previously, uses the knowledge obtained from hot fire tests and prepares future developments of predictive tools for combustion instability.

A step is taken here to devise a relevant description which can be integrated in the large eddy simulation of cryogenic combustion. Since the large eddies are resolved, the interactions between flames and acoustic modes can be simulated and instability mechanism can be examined in great detail. This is attractive but there are many practical difficulties which are gathered below as a list :

- The flame stabilization mechanism constitutes a challenging problem but much has been learnt in recent years from experiments and detailed calculations. A criterion for stabilization near the injector lip was put forward providing conditions in which the flame can be stabilized in the near vicinity of the high speed stream of hydrogen or methane. This criterion is described by Juniper

and Candel (2003) and some experimental verifications are included in Singla et al. (2006b). In essence, it is demonstrated that the flame is well anchored if the flame edge is thinner than the lip size of the liquid oxygen post. The lip size must be sufficiently large so that the flame can be tucked behind it. Numerically, the stabilization process constitutes a big challenge because it involves a physical and chemical complexity but the region of interest has a small scale of the order of a few lip thickness. The quality of flame stabilization may be of importance in the development of combustion instability but this aspect cannot be studied at this point. It is assumed in what follows that the flame is attached to the lip and spreads from this point as a wrinkled sheet. This is obtained by placing a hot point at the lip. This will have to be replaced later on by a more suitable model of the edge flame dynamics.

- The flames formed by cryogenic propellants are essentially nonpremixed. The reaction zone formed where reactants meet in stoichiometric proportions is mainly controlled by turbulent mixing and transport of reactants to the reaction sheet. It is then important to devise suitable representations of the rate of reaction in such nonpremixed flame configurations and in particular develop methods, which will locate the consumption and heat release source terms at the right spatial position. The level of reactant consumption and heat release should also be suitably estimated to obtain the correct flame structure and dynamics and the modeling should be applicable to the highly interacting propellant streams found in practical applications or at the laboratory scale. This chapter focuses on these central items.

- Combustion in liquid rocket engines takes place at elevated pressures. The combustion model should be sensitive to pressure and specifically account for the pressure dependence of the reaction rates. There are some indications on this problem (Juniper et al. 2003) and some unpublished work by L. Pons at EM2C which tend to show that the reaction rate per unit flame area increases like the square root of the pressure. It will be important to examine the effect of pressure on the experimental level and include pressure effects in the combustion models to be used in the LES framework.

- In the real engine some of the reactants are injected as a liquid phase (when the pressure is below critical) and in a transcritical state when the pressure is above critical. In the subcritical case, the two-phase process involves various complications like liquid jet break-up, atomization and vaporization in a dense spray. In the transcritical case, there is a dense jet of oxygen giving rise to large gradients of specific mass. It is then important to treat real gas effects and the corresponding thermodynamics of transcritical fluids. These difficult problems will not be considered in what follows but they will have to be included in comprehensive numerical tools. Some experimental investigations have been carried on the response of coaxial jets to external acoustic modulations and some data concern the transcritical case (Oschwald and Micci 2002). The modeling of cryogenic flames including subcritical and transcritical situations has also been developed for example by Jay et al. (2006) but only in the Reynolds Average Navier-Stokes (RANS) framework.

- Combustion chemistry involves a large number of species and reactants but this cannot be included in all its details. There is a need for reduced models avoiding a full description complex

kinetics. Current LES models use various simplifications to deal with this problem. Most calculations rely on one or two step reactions or tabulated chemistry methods. More elaborate techniques might be needed in the future.

This chapter focuses on the second item in this list. It is concerned with the representation of volumetric reaction terms in the LES framework. It is important at this point to note that methods which are now well established for premixed flames like the thickened flame model cannot be used in the nonpremixed situation. The scaling which applies in the premixed or partially premixed case has no value in the nonpremixed case as shown by Rey (2004).

This chapter aims at presenting and testing an alternative strategy. It is first useful to examine cryogenic flames and discuss the mode of combustion in this situation (section 2). This discussion is based on an analysis of the available experimental data. Some of the models developed in the Reynolds Average Navier Stokes (RANS) framework are considered and their extensions to LES are briefly presented in section 3.
Section 4 describes the model devised to represent the spatially filtered reaction rates. The model is specifically designed to deal with nonpremixed flames and it relies on ideas borrowed from the flame surface density models used in RANS. The filtered flame surface density is derived from the spatial distribution of the mixture fraction gradient and the filtered reaction rate is derived by combining this expression with the local consumption rate.
The last section discusses initial results of simulations in a the multiple jet configuration already envisaged in the cold flow calculations discussed previously in chapter IV. Three coaxial flames are simulated in this geometry.

V.2 Combustion mode in cryogenic flames

To begin with, it is important to examine combustion in cryogenic flames and specifically determine the mode of burning governing this process. This will certainly have physical consequences and it will also determine the modeling effort. At this point, it is worth recalling that some important differences distinguish the premixed and nonpremixed modes of burning. Considering laminar flames, it is known for example that the nonpremixed mode of combustion is controlled by the strain rate (or equivalently the scalar dissipation) applied to the flame. The reaction rate increases with the square root of this quantity at least until extinction conditions are approched. The combustion intensity is low if the strain rate is small. This notably differs from the premixed case where the rate of reaction in laminar flames is essentially determined by the laminar burning velocity, which only weakly depends on the strain rate. It is also possible to show that the effect of pressure is fundamentally different in these two cases. The differences found in the laminar case will certainly influence the turbulent burning rate.

Coaxial elements injector used in liquid rocket engines deliver two separate streams of reactants. Oxidizer is surrounded by a high speed stream of fuel, and the flame is formed between these two reactants. Experiments indicate that reaction takes place in a thin sheet anchored in the vicinity of the oxygen post lip (Juniper 2001). Initial data by Snyder et al. (1997) and more recent experiments clearly indicate that the flame spreads as a thin sheet separating fuel and oxidizer. This is well

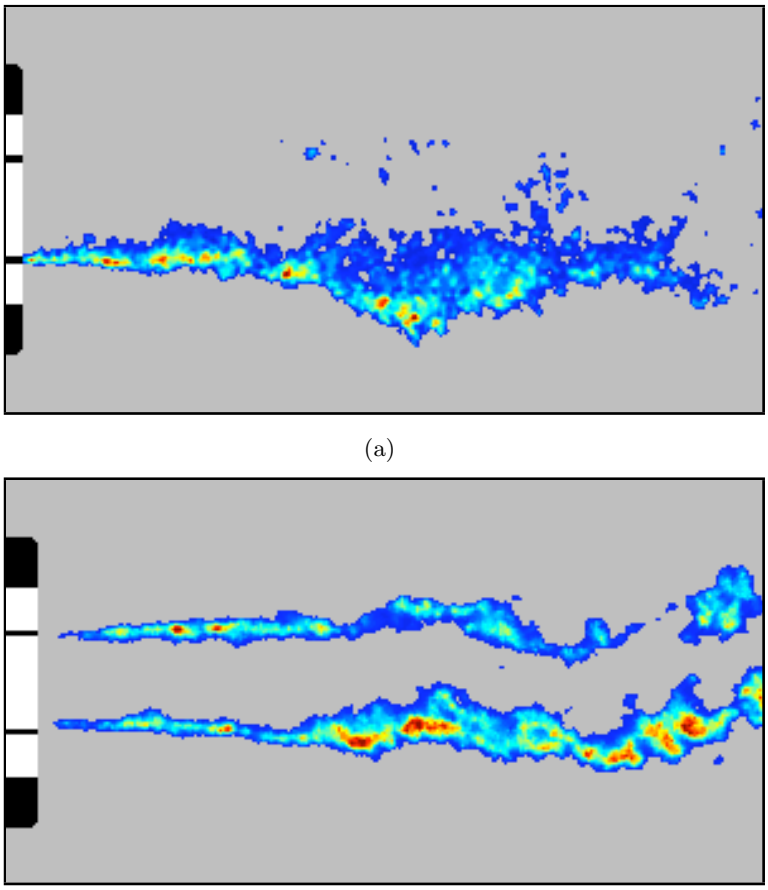

(a)

(b)

Fig. V.1: Laser induced fluorescence images for LOx/GH_2 combustion at 6.3 MPa (a) and for LOx/GCH_4 combustion at 2 MPa (b). (Credits G.Singla).

demonstrated in some remarkable planar laser induced fluorescence images of Singla et al. (2006) for LOx/GH_2 combustion at 6.3 MPa and for LOx/GCH_4 combustion at a lower pressure of 2 MPa (Figure V.1). Close-up views of the flame in the near vicinity of the injector show details of the flame edge and confirm that anchoring takes place near the LOx post lip if the thickness of the flame edge is less than the lip height. The distance between the flame front and the lip does not exceed one lip height showing that there is essentially no premixing region prior to the stabilization point of the flame. The flame spreads from this point on a wrinkled surface and the wrinkling becomes more intense in the downstream region.
Cryogenic flames thus appear as almost perfect examples of nonpremixed combustion. This should be taken into account in any modeling effort of this type of flame. It is specifically important in this context to describe effects of the turbulent flow on the burning rate and make sure that pressure effects will be reflected in the combustion model.

V.3 Combustion modeling of nonpremixed flames

Many models have been developed to describe nonpremixed turbulent flames. Much of this research has been carried out in the Reynolds Average Navier-Stokes (RANS) framework in which the balance equations are averaged and solved together with various turbulence closure schemes. RANS calculations require models describing the turbulent transport of momentum species and energy in combination with models for the mean reaction rates. The RANS framework is however not useful in combustion instability studies because it does not provide the nonsteady heat release which constitutes the driving source of instability.
Modeling of instabilities must therefore rely on Large Eddy Simulations (LES) in which the large scales of turbulence are resolved while the small scales are modeled. This naturally provides the nonsteady reaction rates which play a central role in the problem at hand. It is however important to review some of the RANS ideas because they are readily used to devise LES models. This is only a brief summary of the state of the art which serves to delineate two alternative routes.

We only consider nonpremixed flames and use standard assumptions underlying many nonpremixed turbulent combustion models :

- Specific heats of all species are equal and constant
- Molecular diffusion follows the Fick's law and is identical for all the species
- The Lewis numbers of all species are equal to unity
- The fuel and oxidizer are introduced separately in the respective reference states (T_F^0, Y_F^0) and (T_O^0, Y_O^0)

It is also assumed that the chemistry can be represented by a single-step reaction

$$\nu_F F + \nu_O O \rightarrow \nu_P P$$

and that it is infinitely fast. It is convenient to write this equation in terms of mass

$$F + sO \rightarrow (1+s)P$$

where s designates the mass stoichiometric coefficient

$$s = \frac{\nu_O W_O}{\nu_F W_F}$$

It is also convenient to introduce the global mixture ratio ϕ defined by

$$\phi = s\frac{Y_F^0}{Y_O^0}$$

which compares conditions in the injected propellants to the stoichiometric mass ratio s.
Under these conditions, the species mass fractions and temperature equations can be replaced by a single balance equation for the mixture fraction Z. This quantity is defined as a linear combination of species mass fractions or temperature and species mass fractions.

$$Z = \frac{sY_F - Y_O + Y_O^0}{sY_F^0 + Y_O^0} = \frac{(c_p/Q)(T - T_O^0) + Y_F}{(c_p/Q)(T_F^0 - T_O^0) + Y_F^0} \tag{V.1}$$

Conversely, it can be shown that the temperature and mass fractions are linearly related to the mixture fraction. One also finds that the instantaneous flame location corresponds to the stoichimetric surface

$$Z = Z_{st} = \frac{1}{1+\phi}$$

From this point, two directions can be taken to proceed in the RANS framework :

- The balance of mass and momentum are solved together with transport equations for the turbulent fluxes. Balance equations for mixture fraction ($\widetilde{Z}$) and its variance $\widetilde{Z''^2}$ are used to estimate the mixture fraction probability density function $p(Z)$. The balance equations of temperature and species are no longer needed and the species and temperature are deduced from their expression in terms of the mixture fraction and its probability density function.

- The balance of mass, momentum energy and species are solved together with transport equations for the turbulent fluxes. The mean reaction rates appearing in the temperature and species equations are modeled for example by making use of laminar flamelet libraries.

The first method has the advantage of requiring a modeling of the mean reaction terms but this is also a disadvantage because the burning rate is not available. The second method requires a model for the burning rate and is therefore less straightforward.
Further descriptions of RANS models may be found for example in Poinsot and Veynante (2005).

The large eddy simulation methods devised for nonpremixed combustion follow similar strategies. In contrast with RANS, the large scales of turbulence are resolved while subgrid models are used to represent the smaller scales. The concept of probability density functions can be extended quite naturally to LES models and the spatially filtered species mass fractions and temperature are then deduced from

the mixture fraction using a subgrid scale probability density function $p(Z)$ which can be presumed or transported as proposed for example by Cook and Bushe (1999, Cook (1997, Cook and Riley (1994, Gao (1993, Meneveau et al. (1996, Réveillon and Vervisch (1996).

It is also possible to devise models for the spatially filtered reaction rate. This is perhaps more adequate in the context of combustion instabilities where the unsteady rate of reaction plays an essential role in the process. To obtain an explicit representation it is convenient to use flamelet modeling ideas and specifically those relying on flame surface density concepts. This development is described in the next section.

V.4 A model for the filtered reaction term

The modeling of the filtered reaction term is envisaged in this section. This modeling relies on standard assumptions and borrows ideas from flame surface density concepts developed in the RANS framework and extensively exploited in many practical applications. It is assumed that the chemical kinetics can be described by a single step reaction between fuel (F) and oxidizer (O) generating products (P) :

$$\nu_F F + \nu_O O \rightarrow \nu_P P$$

The instantaneous balance equations for the species mass fractions take the standard form

$$\frac{\partial \rho Y_k}{\partial t} + \frac{\partial}{\partial x_i}(\rho v_i Y_k) = \frac{\partial}{\partial x_i}\left(\rho \mathcal{D} \frac{\partial Y_k}{\partial x_i}\right) + \dot{\omega}_k \tag{V.2}$$

where all species diffusivity have the same value $\mathcal{D}$.
The reaction rates in the species balance equations are all linked to the single step reaction rate $\dot{\omega}$

$$\dot{\omega}_k = W_k \nu_k \dot{\omega}$$

The mixture fraction Z is again defined by

$$\begin{aligned} Z &= \frac{sY_F - Y_O + Y_O^0}{sY_F^0 + Y_O^0} \\ &= \frac{1}{\phi + 1}\left(\phi \frac{Y_F}{Y_F^0} - \frac{Y_O}{Y_O^0} + 1\right) \end{aligned}$$

where ϕ is the global mixture ratio. With these definitions Z is governed by a convective/diffusive balance equation

$$\frac{\partial \rho Z}{\partial t} + \frac{\partial}{\partial x_i}(\rho v_i Z) = \frac{\partial}{\partial x_i}\left(\rho \mathcal{D} \frac{\partial Z}{\partial x_i}\right) \tag{V.3}$$

When this equation is spatially averaged, it provides a filtered mixture fraction $\tilde{Z}$. The filtered flame position is extracted from this field by locating the stoichiometric surface defined by $\tilde{Z} = Z_{st}$ surface.

Considering the local flame structure, it is possible to use the mixture fraction as a variable and show that the internal variables like the temperature and species mass fractions satisfy a set of transport equations taking the remarkably simple form

$$\rho\frac{\partial Y_k}{\partial t} = \dot{\omega}_k + \frac{1}{2}\rho\chi\frac{\partial^2 Y_k}{\partial z^2} \tag{V.4}$$

In this expression χ is the scalar dissipation rate

$$\chi = 2\mathcal{D}\left(\frac{\partial Z}{\partial x_i}\frac{\partial Z}{\partial x_i}\right)$$

These expressions define the local flame structure, the "flamelet", and indicate that this structure is essentially controlled by the scalar dissipation. It is also possible to show that the local consumption of reactants can be expressed in terms of the mixture fraction gradient (Delhaye et al. 1994) :

$$\dot{m}_F = \rho\mathcal{D}\frac{1+\phi}{\phi}Y_F^0|\boldsymbol{\nabla}Z|_{st} \tag{V.5}$$

$$\dot{m}_O = \rho\mathcal{D}(1+\phi)Y_O^0|\boldsymbol{\nabla}Z|_{st} \tag{V.6}$$

The modeling of the combustion process may now involve the following steps.

- The filtered mixture fraction is first calculated by solving the filtered equation for this quantity. This equation has no source term and it is easily solved in the LES framework providing $\widetilde{Z}(x_i,t)$
- The consumption rates for fuel and oxidizer are then deduced from the filtered mixture fraction gradient starting from expressions V.5 and V.6. This provides rates per unit flame surface.
- Consumption rates per unit volume are estimated by multiplying the previous expressions by the filtered flame surface area per unit volume.
- These consumption terms are in principle concentrated in a thin sheet around the flame. Since the grid is coarse, it is important to distribute these source terms for example by making use of a smoothing function. The distribution is defined in the flame neighborhood. This effectively thickens the flame in a fashion which is somewhat analogous to the method used in the premixed case.

The first step is easily completed with a suitable LES code like AVBP. The Navier-Stokes equations are solved in three dimensions together with an equation for the mixture fraction treated as a fictious variable. It is for example possible to use the balance equation for methane, imposing $Z = 1$ in the initial fuel stream and $Z = 0$ in the oxidizer stream and set the reaction term to zero. This gives the instantaneous distribution of filtered mixture fraction $\widetilde{Z}(\boldsymbol{x},t)$.

The second step only involves the filtering of expressions V.5 and V.6 while the third step is treated as an extension of flame surface density models. In the fast chemistry limit considered in this derivation, the flame is infinitely thin and its location in Z-space is $\widetilde{Z} = Z_{st}$ (Peters 1983; Williams 1985) where the stoichiometric mixture fraction Z_{st} is determined by

$$Z_{st} = \frac{1}{1+\phi}$$

It is now possible to express the resolved fuel reaction rate per unit volume. This quantity $\widetilde{\dot{\omega}}_F$ is obtained by taking the product of the consumption rate per unit surface by the filtered flame surface per unit volume :

$$\widetilde{\dot{\omega}}_F = \dot{m}_F \widetilde{\Sigma} \tag{V.7}$$

An exact expression for the flame surface density can be obtained from its definition at the iso-level Z_{st} (Pope 1988)

$$\Sigma = |\boldsymbol{\nabla} Z| \delta(Z - Z_{st})$$

where $\delta(Z - Z_{st})$ is the Dirac-delta function. The filtered expression of the flame surface density is then equal to

$$\widetilde{\Sigma} = \widetilde{|\boldsymbol{\nabla} Z| \delta(Z - Z_{st})}$$

and is modeled by the expression

$$\widetilde{\Sigma} = |\boldsymbol{\nabla} \tilde{Z}|_{st} (1 + \Xi) \tag{V.8}$$

where Ξ is a subgrid scale flame wrinkling factor which accounts for the subgrid flame surface density. Injecting the previous expression for the resolved flame surface density in equation V.7 one finds :

$$\widetilde{\dot{\omega}}_F = \dot{m}_F |\boldsymbol{\nabla} \tilde{Z}|_{st} (1 + \Xi) \tag{V.9}$$

From this expression, it appears that the subgrid wrinkling effectively changes the rate of consumption per unit surface. This is now

$$\dot{m}_F (1 + \Xi) = \rho \mathcal{D} \frac{Y_F^0}{1 - Z_{st}} |\boldsymbol{\nabla} \tilde{Z}|_{st} (1 + \Xi)$$

The principle is to distribute a volumetric rate of reaction which when integrated across the flame yields precisely this value. Let $\dot{\Omega}_F$ designate this volumetric rate of reaction. This distribution must be such that

$$\dot{m}_F (1 + \Xi) = \int_{l_*} \dot{\Omega}_F \; dl \tag{V.10}$$

where the integration is carried out in the direction normal to the resolved flame. This distribution $\dot{\Omega}_F$ is conveniently defined as a function of $\widetilde{Z}$

$$\dot{\Omega}_F = (\dot{\Omega}_F)_{\max} \; f(\widetilde{Z}) \tag{V.11}$$

where $f(\widetilde{Z})$ is a smooth function (typically a Gaussian one) centered on the flame front and such that its integral over $\widetilde{Z}$ equals unity. It is natural to propose

$$f(\widetilde{Z}) = \frac{1}{\sigma \sqrt{\pi}} \exp \left[- \frac{(\widetilde{\mathrm{Z}} - \mathrm{Z_{st}})^2}{\sigma^2} \right] \tag{V.12}$$

Now Equation V.10 may be cast in the form

$$\dot{m}_F (1 + \Xi) = (\dot{\Omega}_F)_{\max} \int_{l_*} f(\widetilde{Z}) \; dl \tag{V.13}$$

One has to express the elementary distance in the normal direction as a function of $\widetilde{Z}$. This can be done by first writing

$$\begin{aligned} d\widetilde{Z} &= \frac{\partial \widetilde{Z}}{\partial x}dx + \frac{\partial \widetilde{Z}}{\partial y}dy + \frac{\partial \widetilde{Z}}{\partial z}dz \\ &= \boldsymbol{\nabla}\widetilde{Z} \cdot \boldsymbol{n}\ dl \end{aligned}$$

The normal vector is given by

$$\boldsymbol{n} = \frac{\boldsymbol{\nabla}\widetilde{Z}}{|\boldsymbol{\nabla}\widetilde{Z}|}$$

which gives

$$d\widetilde{Z} = |\boldsymbol{\nabla}\widetilde{Z}|\ dl$$

This is an exact expression which can be used together with expression V.13 :

$$\dot{m}_F(1+\Xi) = (\dot{\Omega}_F)_{\max} \int_{z_*} \frac{f(\widetilde{Z})}{|\boldsymbol{\nabla}\widetilde{Z}|}\ d\widetilde{Z} \tag{V.14}$$

This provides the exact value of $(\dot{\Omega}_F)_{\max}$ which can be used to determine $\dot{\Omega}_F$ as initially specified in Equation V.11. It is reasonable to consider that $|\boldsymbol{\nabla}\widetilde{Z}|$ in the region of interest can be approximated by $|\boldsymbol{\nabla}\widetilde{Z}|_{st}$. With this approximation, expression V.14 is simplified and yields an explicit value for the maximum reaction rate

$$(\dot{\Omega}_F)_{\max} = \dot{m}_F(1+\Xi)|\boldsymbol{\nabla}\widetilde{Z}|_{st}$$

This provides the distribution

$$\boxed{\widetilde{\dot{\Omega}}_F = \rho\mathcal{D}\frac{Y_F^0}{1-Z_{st}}\frac{1+\Xi}{\sigma\sqrt{\pi}}|\boldsymbol{\nabla}\tilde{Z}|_{st}^2 \exp\left[-\frac{(\tilde{Z}-Z_{st})^2}{\sigma^2}\right]} \tag{V.15}$$

The source term depends only on the resolved mixture fraction. This expression is relatively easy to implement as a source term and has some interesting physical features.
The factor $(\mathcal{D})^{1/2}|\boldsymbol{\nabla}Z|$ may be identified as the square root of the scalar dissipation χ. The scalar dissipation is linearly related to the strain rate and as a consequence the reaction rate is proportional to the square root of the strain rate. The factor $|\boldsymbol{\nabla}\tilde{Z}|(1+\Xi)$ represents the total flame surface density available for combustion. This term contains a subgrid wrinkling factor Ξ which represents the unresolved flame surface area. The gaussian shape is used to center the maximum rate of reaction on the flame sheet and distribute the reaction rate around this iso-surface over a sufficient distance defined by σ in Z-space.

The other species reaction rates $\widetilde{\dot{\omega}}_k$ and the heat release rate are linked to the fuel reaction rate by

$$\begin{aligned} \widetilde{\dot{\omega}}_k &= \frac{\nu_k W_k}{\nu_F W_F}\,\widetilde{\dot{\omega}}_F \\ \widetilde{\dot{\omega}}_T &= -Q\,\widetilde{\dot{\omega}}_F = \sum_{k=1}^{N} \Delta h_{f,k}^0\,\widetilde{\dot{\omega}}_k \end{aligned}$$

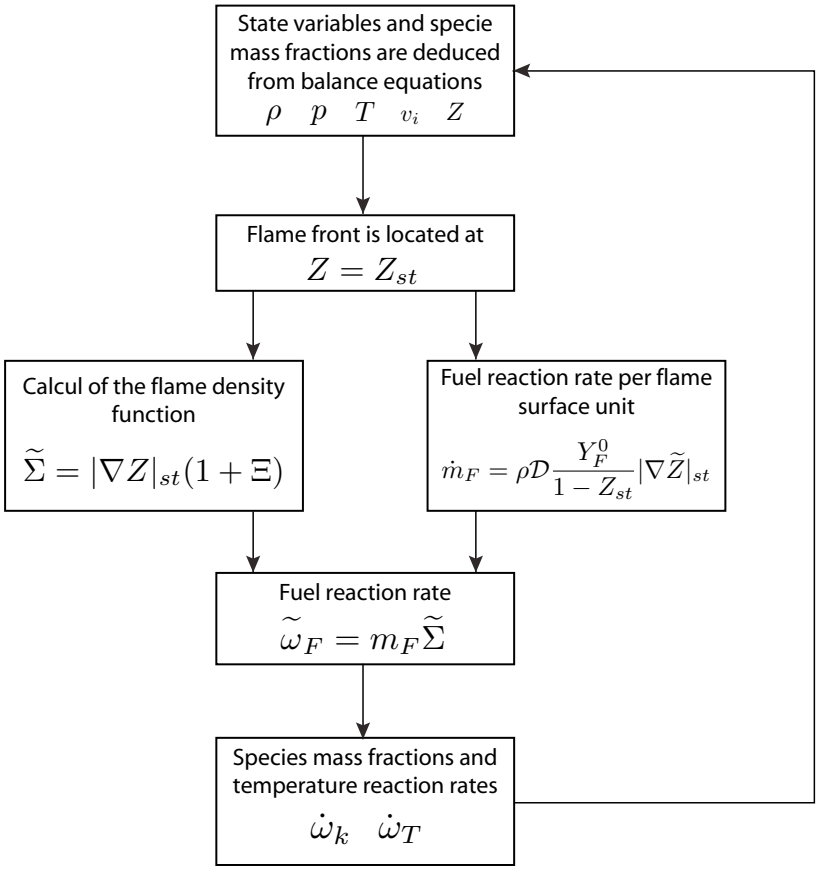

Fig. V.2: Schematic representation of the different elements defining the nonpremixed turbulent flame model.

This procedure defines the source terms in the filtered balance equations for $\widetilde{Y_k}(\boldsymbol{x}, t)$ and $\widetilde{T}(\boldsymbol{x}, t)$. These equations can be integrated on the coarse grid used for the LES. The diagram shown in figure V.2 summarizes the main elements of the model.

Remark

It has been mentionned previously that the fuel reaction rate per unit surface associated with strained diffusion flames scales like the square root of the pressure (Juniper et al. 2003). This property is embedded in the present expression as can be seen from the following rearrangements.
Expression V.15 is first written in the successive forms :

$$\begin{aligned}\widetilde{\dot{\omega}}_F &= \rho\mathcal{D}|\boldsymbol{\nabla}\widetilde{Z}|^2 F(\widetilde{Z}) \\ &= \rho\mathcal{D}^{1/2}|\boldsymbol{\nabla}\widetilde{Z}|\mathcal{D}^{1/2}|\boldsymbol{\nabla}\widetilde{Z}|F(\widetilde{Z}) \\ &= (\rho^2\mathcal{D})^{1/2}|\boldsymbol{\nabla}\widetilde{Z}|\chi^{1/2}F(\widetilde{Z})\end{aligned}$$

One then uses the same reasoning as Juniper et al. (2003) to relate $\rho^2\mathcal{D}$ to a reference value of this product evaluated under reference conditions.

$$\widetilde{\dot{\omega}}_F = (\rho_{ref}^2\mathcal{D}_{ref})^{1/2}|\boldsymbol{\nabla}\widetilde{Z}|\chi^{1/2}F(\widetilde{Z})\left(\frac{p}{p_{ref}}\right)^{1/2}$$

The expression of $\widetilde{\dot{\omega}}_F$ obtained with this model also scales with the square root of the pressure. This is an interesting feature of the model which will have to be tested in the future

V.4.1 An estimate of the wrinkling function Ξ

The influence of the subgrid flame wrinkling is estimated by calculating the experimental oxygen consumption rate per unit surface. This can be accomplished by making use of experimental data gathered for a typical cryogenic jet flame. This estimate does not aim at precisely defining the value of the subgrid wrinkling function. It is merely developed to get an order of magnitude of the strain rate needed to obtain realistic rates of consumption.

The mean oxygen consumption per unit surface is calculated by considering that the flame is cylindrical with a diameter $d_l = 3$ mm and a typical length $l = 25$ cm at a pressure of 1 MPa. Thus

$$\begin{aligned} A_{1\text{MPa}} &= \pi d_l l \\ &= \pi \times 3.10^{-3} \times 0.25 \\ A_{1\text{MPa}} &= 2.35\ 10^{-3}\ \text{m}^2 \end{aligned}$$

At ambient pressure, the oxygen/methane flame will be longer and could extend over a distance $l =$ 70 cm. This yields a new estimate for the flame area

$$A_{0.1\text{MPa}} = 6.6\ 10^{-3}\ \text{m}^2$$

The global oxygen mass flow rate is equal to 50 g s^{-1} for three elements. Thus each flame is fed by $50/3 = 16.6$ g s^{-1}. This gives oxygen reaction rates per unit surface

$$\dot{\omega}_O(1\text{MPa}) = 7\ \text{kg m}^{-2}\text{s}^{-1}$$

$$\dot{\omega}_O(0.1\text{MPa}) = 2.5\ \text{kg m}^{-2}\text{s}^{-1}$$

with

$$\begin{aligned} \dot{\omega}_O &= s\,\dot{\omega}_F \\ &= s\rho\mathcal{D}\frac{Y_{F_0}}{1-Z_{st}}|\nabla Z| \end{aligned} \tag{V.16}$$

It is possible to link the gradient of Z to the scalar dissipation rate and then use a standard expression of this quantity in terms of the local strain rate :

$$\begin{aligned} \chi &= 2\mathcal{D}|\nabla Z|^2 \\ \frac{\epsilon_s}{\pi}\exp(-\eta_{st}^2) &= 2\mathcal{D}|\nabla Z|^2 \end{aligned} \tag{V.17}$$

where ϵ_s is the strain rate and $\eta_{st} = \text{erf}^{-1}\left[(\Phi-1)/(\Phi+1)\right]$. By injecting equation V.16 in equation V.17, one eliminates $|\nabla Z|$ and obtains

$$\dot{\omega}_O = \frac{s\,\rho\mathcal{D}\,Y_{F_0}}{1-Z_{st}}\left(\frac{\exp(-\eta_{st}^2)}{2\mathcal{D}\pi}\right)^{1/2}\epsilon_s^{1/2}$$

Φ	s	Z_{st}	$\mathcal{D}$	ρ	Y_F^0
4	4	0.2	10^{-4} m^2 s^{-1}	2 kg m^{-3}	1

Tab. V.1: Values used for the calculation.

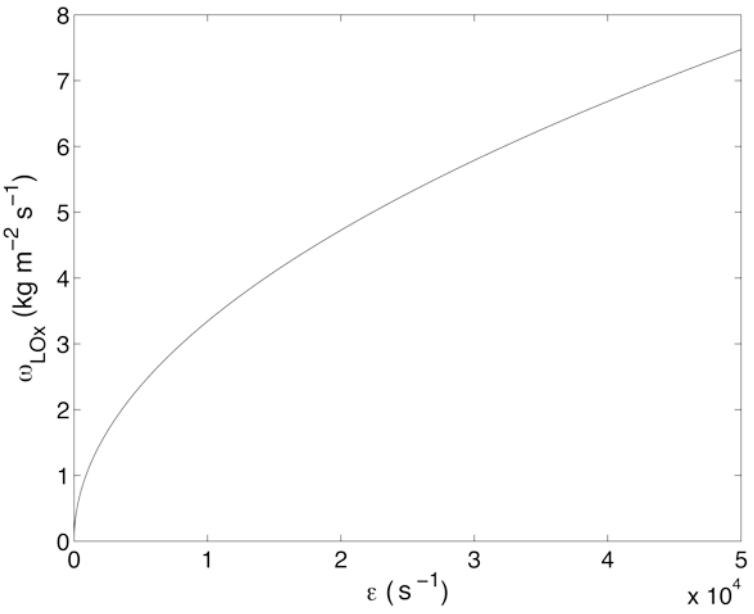

Fig. V.3: Oxygen consumption rate $\dot{\omega}_O$ as a function of the local strain rate. The consumption rate deduced from experiments is estimated to be around 2.5 kg s^{-1} m^{-2}. This would require local strain rates which in the mean should be of the order of 5. 10^3 s^{-1}.

Table V.1 gathers the characteristic values appearing in this expression for liquid oxygen and gaseous methane at ambient temperature.
These values are used to plot the oxygen consumption rate per unit surface as a function of the strain rate (figure V.3).
Comparison between the model and the experimental value of the consumption rate indicates that the strain rate should be of the order of 5 10^3 s^{-1} to get similar values. Since the filtered strain rates calculated numerically are an order of magnitude lower, one may conclude that the wrinkling function should take values of about 10. This indicates that the subgrid flame surface is much larger than the resolved flame surface area. As a first step, this can be compensated by assigning a constant value to the wrinkling factor : $\Xi \simeq 10$.

V.5 Multiple jet simulation

V.5.1 Three dimensional test case

The previous model has been included in AVBP and this plateform is used to solve the Navier-Stokes equations in the LES framework. The first test is carried out in the case of a shear layer formed by

the confluence of a high and low speed streams of reactants. The mesh had a relatively small number of grid points to allow repeated test calculations. These initial calculations were carried out to verify that the model provided reasonable results. This case is not shown for the sake of brevity and we only examine calculations carried out in the multiple jet configuration defined in chapter IV and already explored under cold flow conditions.

V.5.2 Slight modification of the formulation

A slight modification of the formulation is required because the amount of oxygen injected in the chamber is much lower than that required for stoichiometric conditions. Oxygen is the limiting species and will disappear first. Consider the Schvab-Zeldovich coupling function β defined by

$$\beta = sY_F - Y_O$$

In most of the nonpremixed flame simulations fuel is injected in a large amount of oxidizer. The limiting species is the fuel which is provided to the system. Thus β is naturally normalized with respect to the oxidizer to obtain the mixture fraction expression. In the three coaxial jet configuration, oxygen is injected in the middle of the injector and is surrounded by methane. The fuel is in excess and the flame is terminated when the oxidizer is depleted. It is then more convenient to change the respective roles of fuel and oxidizer in the definition of the mixture fraction. A new variable ζ is used instead of Z. This is obtained by normalizing β with respect to the fuel :

$$\zeta = \frac{\beta - \beta_F^0}{\beta_O^0 - \beta_F^0} = 1 - Z$$

The boundary conditions are such that $\zeta = 1$ in pure oxygen and $\zeta = 0$ in pure fuel. The new mixture fraction ζ can be expressed in terms of the species mass fractions

$$\zeta = \frac{Y_O + s(Y_F^0 - Y_F)}{Y_O^0 + sY_F^0}$$

This new expression of the mixture fraction does not modify the source terms since the derivative of Z and ζ are similar. Only the value of mixture fraction at stoichiometry is changed since

$$\begin{aligned} \zeta_{st} &= \zeta(Y_F = 0, Y_O = 0) \\ &= \frac{\phi}{1+\phi} \end{aligned} \tag{V.18}$$

For reaction between oxygen and methane this leads to

$$\zeta_{st} = 0.8$$

V.5.3 Conditions

Non-reactive three dimensional simulations of three oxygen/methane coaxial jets are already discussed in the chapter IV. Jets are injected at ambient pressure and temperature with a momentum flux ratio J similar to that used experimentally. It was shown that the simulations carried out without combustion provided realistic jet spreading. Collective interactions were observed when the jets were

submitted to a transversal modulation.

It is now possible to explore a reactive case. The calculations aim at testing the model in a realistic three-dimensional configuration. There is no reference data for this case because the two propellants are injected in gaseous form while the oxygen is injected in liquid form in the experiments. The purpose is to observe the model for the first time and point out limitations for further improvement. It is already providing encouraging results showing that this simple combustion model may be extremely useful.

Two constants have to be adjusted to tune the reaction rate calculation. First, a gaussian function is used to locate the flame front on the ζ_{st} iso-surface and to distribute the reaction rate on several adjacent cells. The width of this distribution σ is adjustable and depends on the cell size. Here σ=0.15 which means that the reaction is distributed between iso-surfaces ζ_0=0.65 and ζ_f=0.95 with the maximum at ζ_{st}. Second the wrinkling factor Ξ is adjusted to take into account the sub-grid scale quantities. There is no function to estimate the sub-grid scale quantities so Ξ is set to a relatively high value of 25. In future simulations, these constants will be determined automatically but this first run is performed with fixed values chosen after some sytematic calculations of reactive shear layers.

The calculation is carried out with a second order spatial scheme. The time step is equal to 1.17 10^{-7} s. The model ran during 50000 iterations where it reached a constant maximal temperature. By considering the chamber length and the average velocity of the flow, 10000 iterations are needed to balance the fluxes between the input and output boundaries.

V.5.4 Non modulated

Figure V.4 shows the instantaneous distributions of temperature and water source term in the middle plane containing the injectors. The ζ_{st} iso-level is plotted in black. The temperature distribution features large scale eddies in the burnt gases. Collective interactions are induced by the flow motion and temperature fluctuations can be observed locally. The maximum temperature reaches 2250 K and the distribution follows the stoichiometric contour. One should remember that this is a filtered temperature which will be lower than the adiabatic flame temperature which would be found in at the instantaneous flame sheet.
As expected the water reaction rate is located close to the injection plane where the mixture fraction gradient is maximum. The source term follows the ζ_{st} iso-level. Most of the reaction rate is induced by the strong gradient at the inlet but spots of reaction are also observed further downstream. Here, the gradients are presumably generated by the vortices observable on the temperature distribution. The contribution of these spots is limited but a local burning takes place in these dowstream regions. The constant Ξ factor adopted in this simulation probably exagerates the rate of burning near the injection plane.

Because the mixture fraction gradient is very high in the vicinity of the injection plane, the burning rate takes large values in that region. To reduce this problem it was necessary to artificially diminish

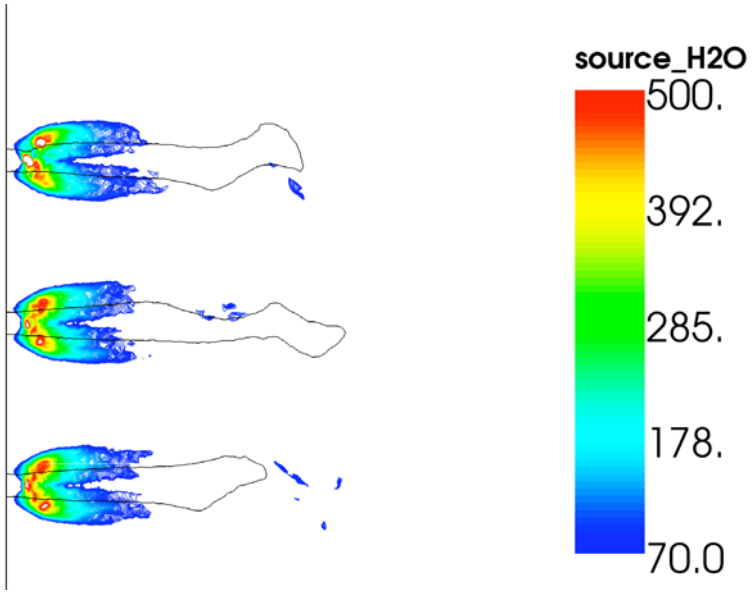

(a)

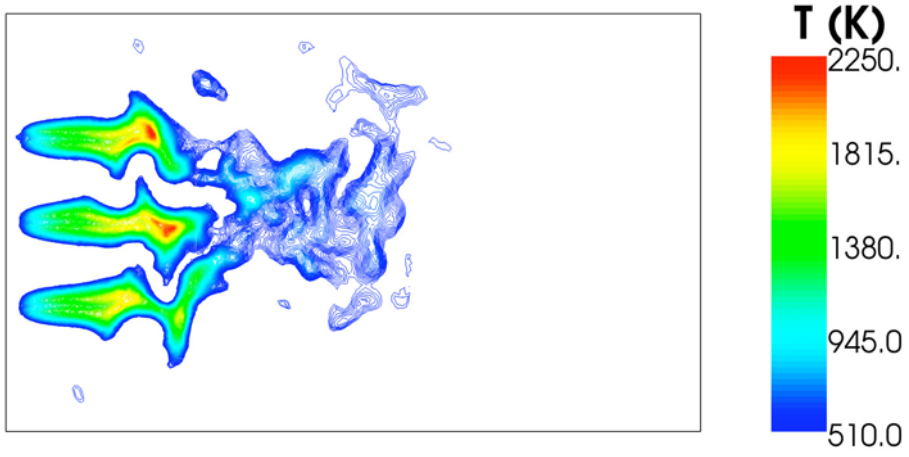

(b)

Fig. V.4: Temperature and water source term distribution. In black, the iso-level corresponding at $\zeta = \zeta_{st}$

the reaction rate near the entrance with a mask and let the flame develop at a distance of $d_i = 4$ mm from the injection plane. This mask induces a strong gradient in the axial direction creating an artificially strong water source term between the stoichiometric lines at the injection. This affects a few cells which do not influence the temperature or water mass fraction distributions. Further work should be directed at improving injection conditions and the treatment of the injector near field. It might be useful to begin the simulation inside the injector to let profiles develop more naturally.

Figure V.5 shows the axial velocity field in the whole computational domain. Combustion induces intense turbulent fluctuations. The domain can be divided in three regions from the injection plane to the outlet. In a first region the injection velocity controls the motion. High velocities are found on the outer boarder of the methane coaxial jets. Oxygen injected at 20 m s^{-1} is rapidly accelerated to 50 m s^{-1} by gas expansion and by entrainment by the methane flow. Expansion in the transverse direction is visible a few centimeters after the injection. In the second part of the domain, the jets merge. Collective interactions take place in the middle of the chamber where the velocity is almost uniform. Smaller scale eddies are generated in the downstream region and some recirculation can be observed. This velocity distribution shows that the flow is highly turbulent. Comparing with the non reactive case, a high level of turbulence is induced by combustion.

The species mass fractions are presented in figure V.6. The methane distribution confirms what is observed on the axial velocity distribution. This species distribution spreads outwards after injection. Without combustion, the methane stream was developing with little perturbation. With combustion one note an expansion angle of a few degrees. The direct consequence of this expansion is the mutual interaction of the jet which is considerably accelerated. After ten oxygen injection diameters, the methane jets interact and small scale structures are created and convected downstream. The methane jet is broken down before the end of the reaction zone materialized by the ζ_{st} iso-contour. The same modification of the oxygen behavior is also visible. The inner oxygen core expands quickly after injection and the jet break-down is accelerated.
Water vapor is mainly created near the end of the flame around the flame front. The reactive spots observed on the temperature distribution produce burnt products from the remaining fresh reactants.

V.5.5 Results of the modulated tests

The numerical simulations aim at observing the effect of a transverse pressure fluctuation on multiple flame configuration. The effect of the modulation on nonreactive jets has been investigated and presented in the previous chapter. Pressure waves increased mixing between the two reactants and generated transverse oscillations of the jets.

In the present simulation, the boundary conditions of the top and bottom walls are changed as indicated in the previous chapter to generate sinusoidal transverse waves in the chamber. The amplitude of the modulation is controlled by the amplitude of the induced velocity which is equal to 1 m s^{-1}. The phase difference between the top and bottom walls is 180° to generate a sinusoidal mode.

The pressure distribution obtained with these boundary conditions is presented in figure V.8. The

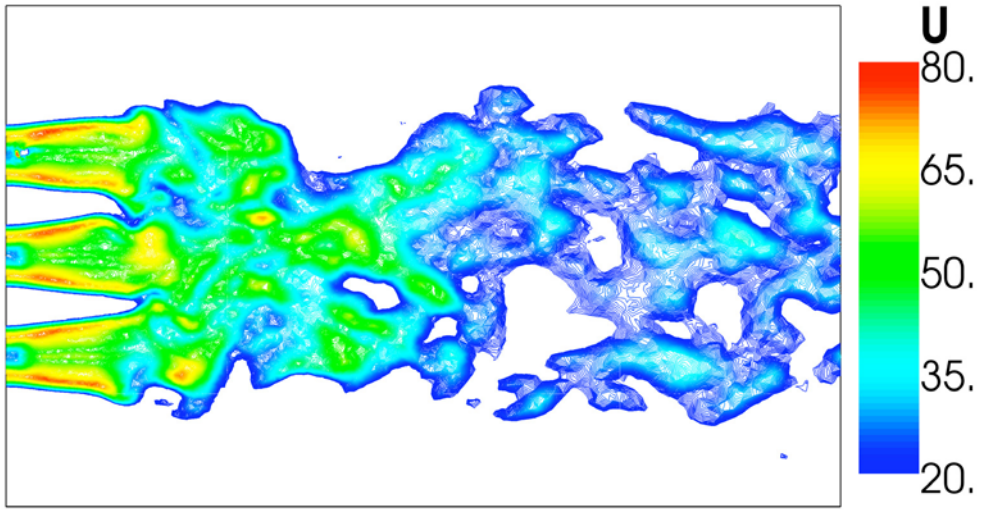

(a) Instantaneous axial velocity field.

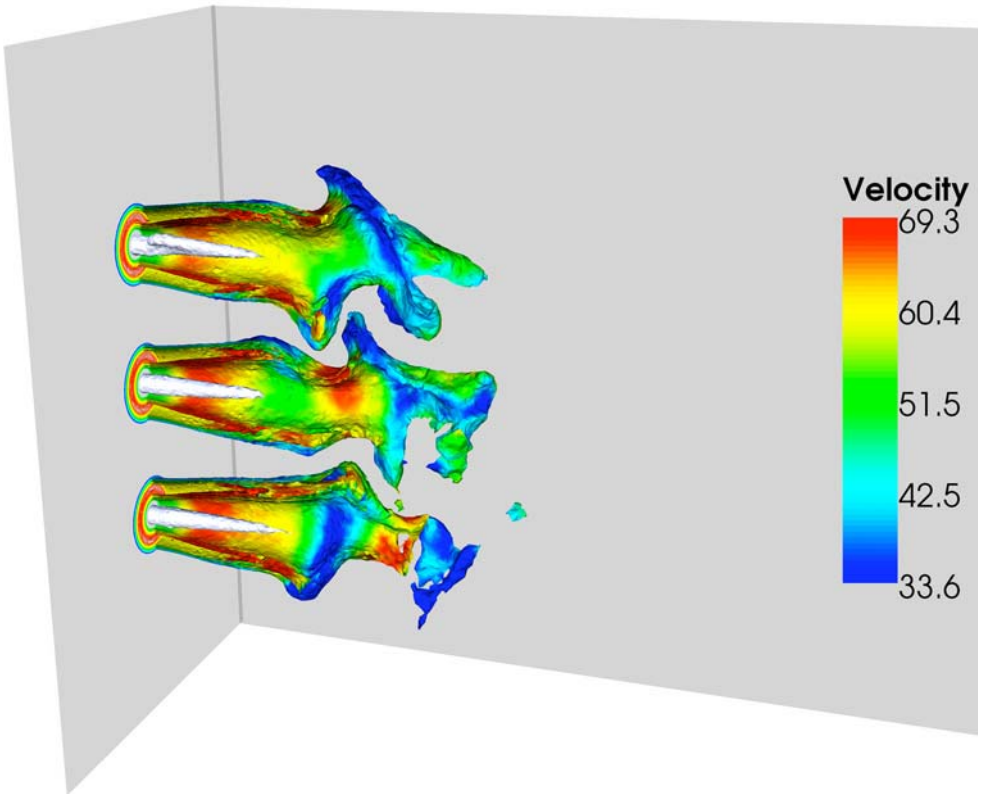

(b) Set of methane mass fractions colored by the velocity magnitude.

Fig. V.5: 2D and 3D visualization featuring the velocity.

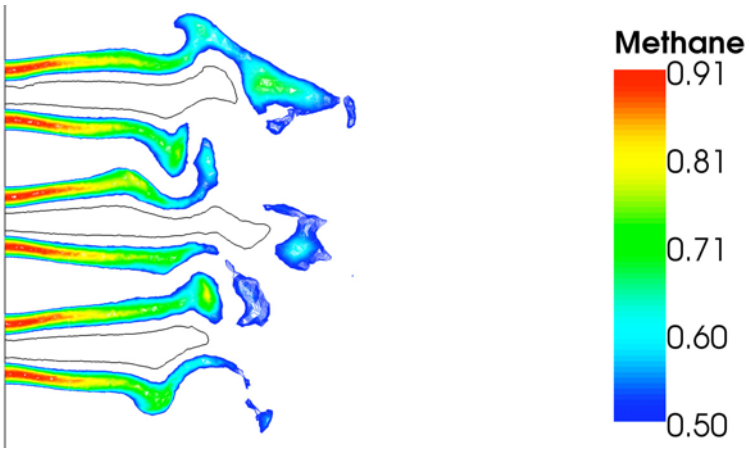

(a) Methane mass fraction, $\widetilde{Y}_{CH_4}$

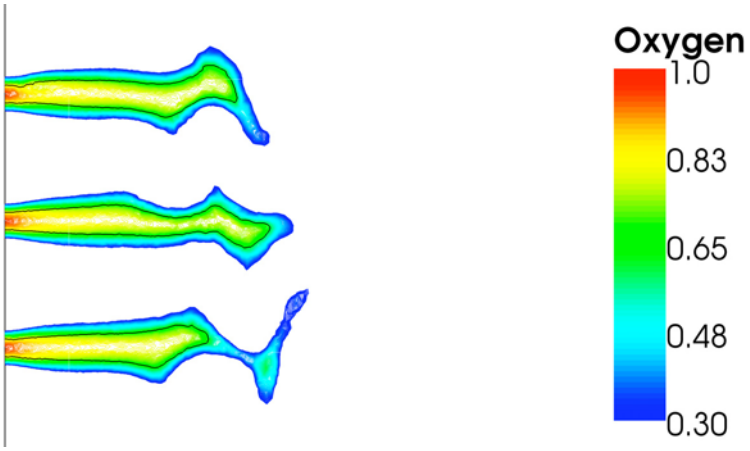

(b) Oxygen mass fraction, $\widetilde{Y}_{O_2}$

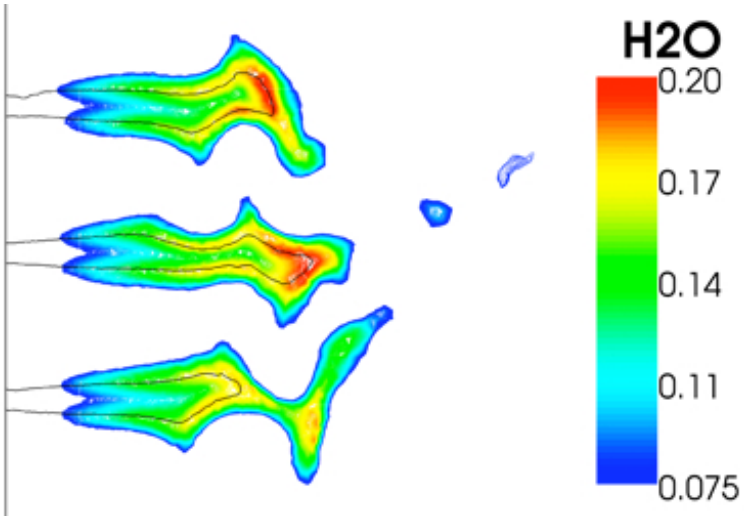

(c) Water mass fraction, $\widetilde{Y}_{H_2O}$

Fig. V.6: Mass fraction of methane, oxygen and water. The ζ_{st} contour is plotted in black.

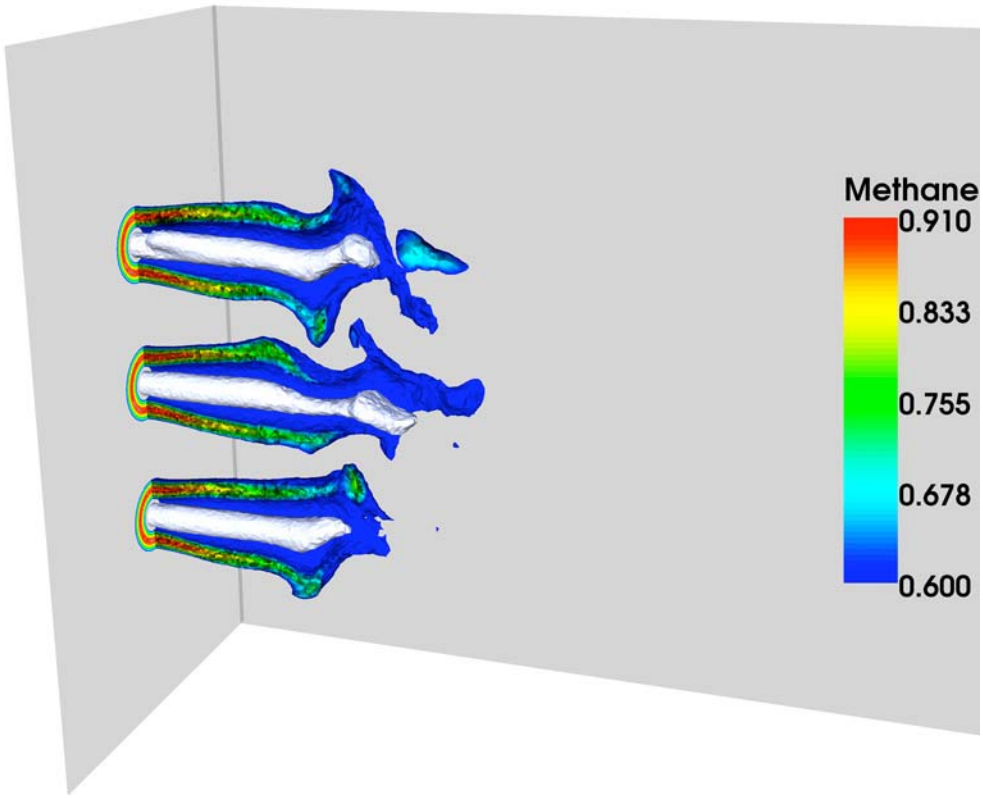

(a) Methane mass fraction surrounding $\widetilde{Y}_{0_2} = 0.7$ iso-level (in white).

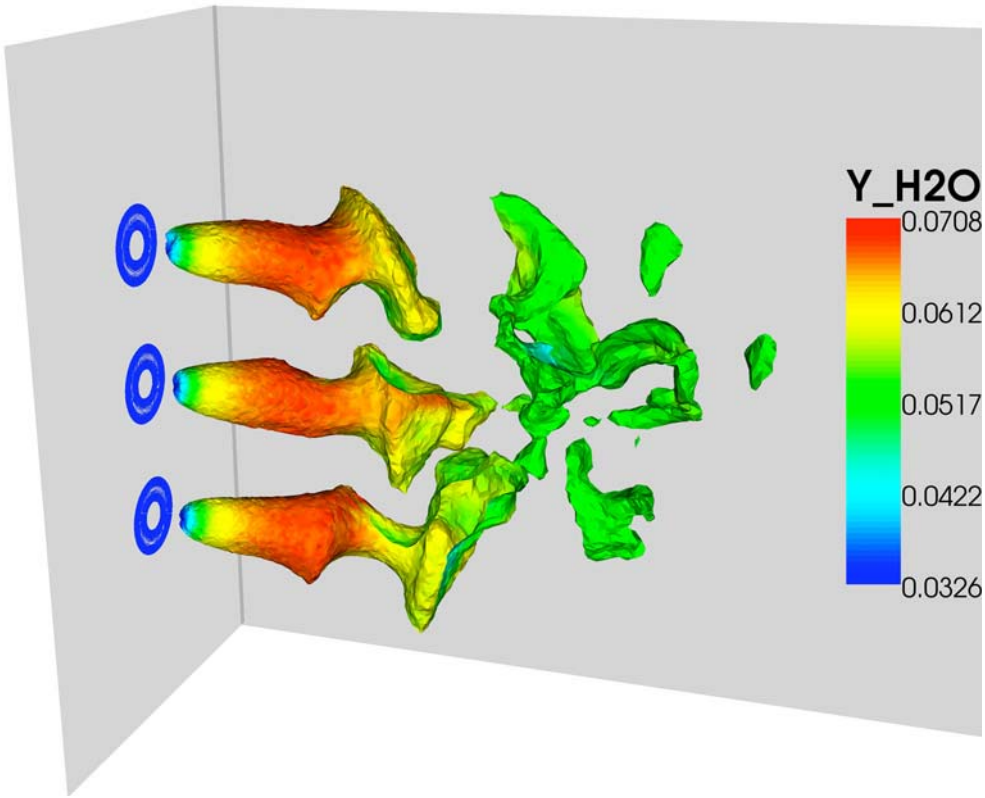

(b) T = 700 K iso-level colored by the water mass fraction.

Fig. V.7: Three dimension visualizations of the three coaxial flames.

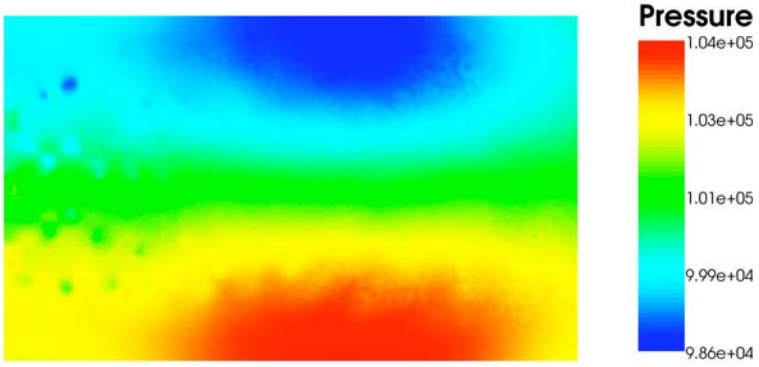

(a)

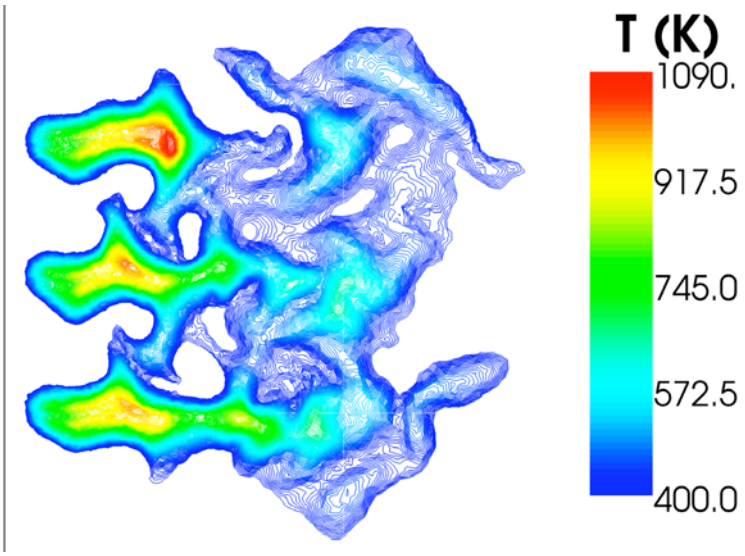

(b)

Fig. V.8: Instantaneous pressure (a) and temperature (b) fields when the three coaxial oxygen/methane flames are transversally modulated at 2500 Hz.

transverse mode is clearly apparent, the top and bottom parts of the chamber being out of phase. In addition, the presence of the jet flames is perceptible close to the injection plane. Vortex formation generates small scale pressure fluctuations. The instantaneous temperature resulting from the modulated combustion is also shown in figure V.8. The maximum temperature is below what is expected. The constant parameters defined in the model have been kept constant with respect to the non modulated case. With the modulation, turbulence is enhanced and its effect on the reaction rate is not reproduced in the model since the wrinkling factor Ξ is constant. In future developments of the model it will be necessary to use a variable wrinkling factor depending on the turbulence level. Temperature distribution features strong interactions between the flames and acoustics. Jets are rapidly interacting and contours feature wavelengths corresponding to the modulation frequency.

These phenomena are confirmed in figure V.9, where the species distributions are displayed in a plane containing the injector axis. Methane jets interact strongly after a few centimeters from the injec-

tion plane and large scale vortices are formed between the jets. The scale of these vortices is of the order of the inter jet distance. Oxygen distribution field features islands of oxygen extending in the cross stream direction which drastically improve mixing. Interactions between oxygen jets is nearly complete after ten injection diameters. Formation of water vapor is also perturbed by the acoustic modulation.

Three dimensional visualizations of these results are presented in figure V.10. The acoustic modulation has a strong effect on the jet dynamics. The characteristic length of mixing is reduced and interactions between the adjacent jets are observable. At this point of development of the combustion model, it may be too early to conclude on any phenomena observed here. However, these simulations provide two interesting informations. First, it is confirmed that LES is adapted to the numerical study of interactions between acoustics and combustion. Flames are significantly distorted by pressure waves and the unsteady properties of the flames may be accurately simulated. Second, these simulations can help to improve the combustion model. Acoustics increases the fluctuation level in the chamber and the model should be able to capture this high level of turbulent fluctuations and its effect on heat release. For further improvements, it will be needed to investigate high frequency instabilities using such simulations. It will then be possible to examine heat release and pressure fluctuations and to look at the details of the coupling mechanism.

V.6 Conclusion

This chapter proposes a nonpremixed flame model for numerical simulations based on the flame surface density concept. Recent cryogenic combustion experiments are reviewed to determine the combustion mode. It is concluded unambiguously that nonpremixed burning prevails in such flames. An analytical description of the reaction rate is derived for this type of conditions and is used to simulate combustion in the case of three coaxial element injector delivering gaseous oxygen and methane. The first test of the model yields encouraging results. Combustion is well localized close to the stoichiometric contour and the description based on the mixture fraction gradient provides reasonable levels of burning rates. The model is attractive because it uses an explicit expression which is physically meaningful. The pressure exponent is imbedded in this expression. The model does not require complex chemistry calculations and no tabulations are needed for the simulation. The model only requires an additional transport equation for the mixture fraction. Initial results for a multiple injection configuration are promising but a number of improvements are needed. It is in particular necessary to devise a scheme which will determine the wrinkling factor and the extent in Z space of the burning rate distribution.

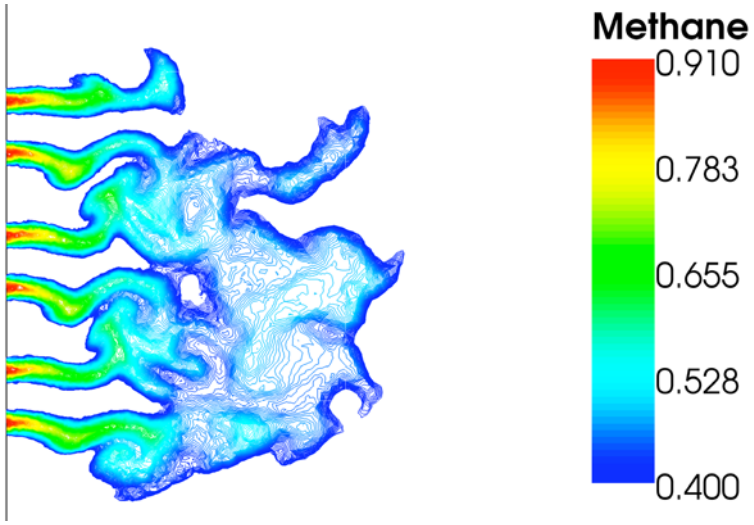

(a)

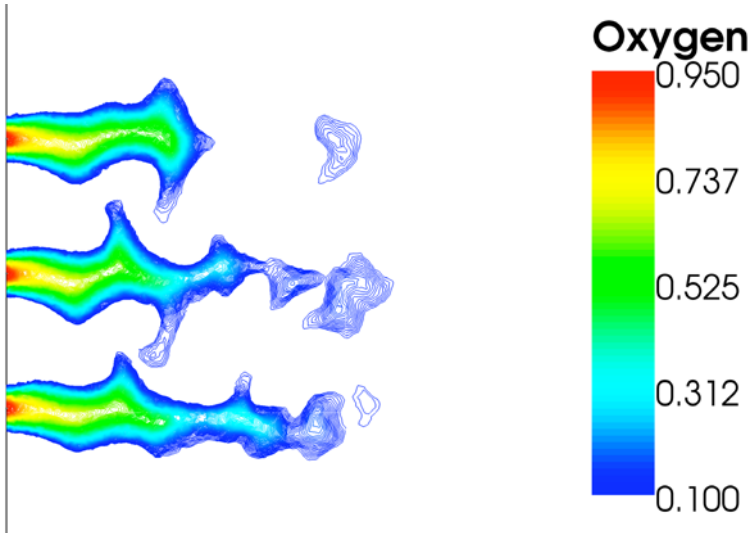

(b)

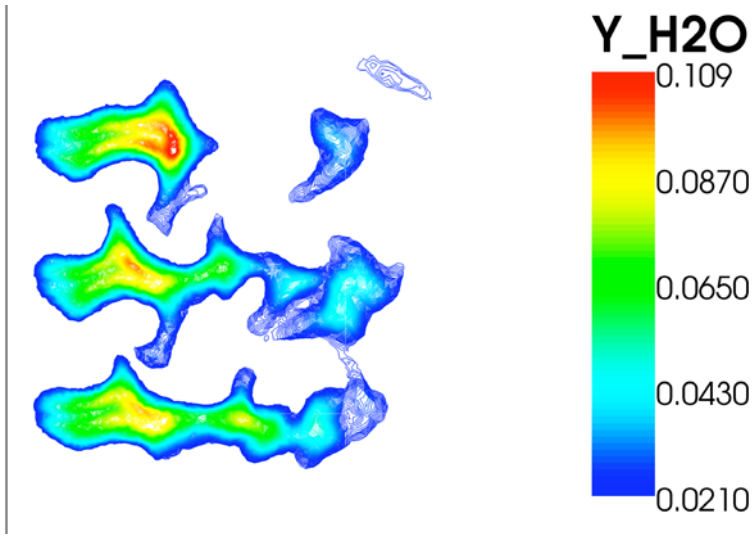

(c)

Fig. V.9: Instantaneous methane (a), oxygen (b) and water (c) mass fraction distribution fields when the three coaxial oxygen/methane flames are transversally modulated at 2500 Hz.

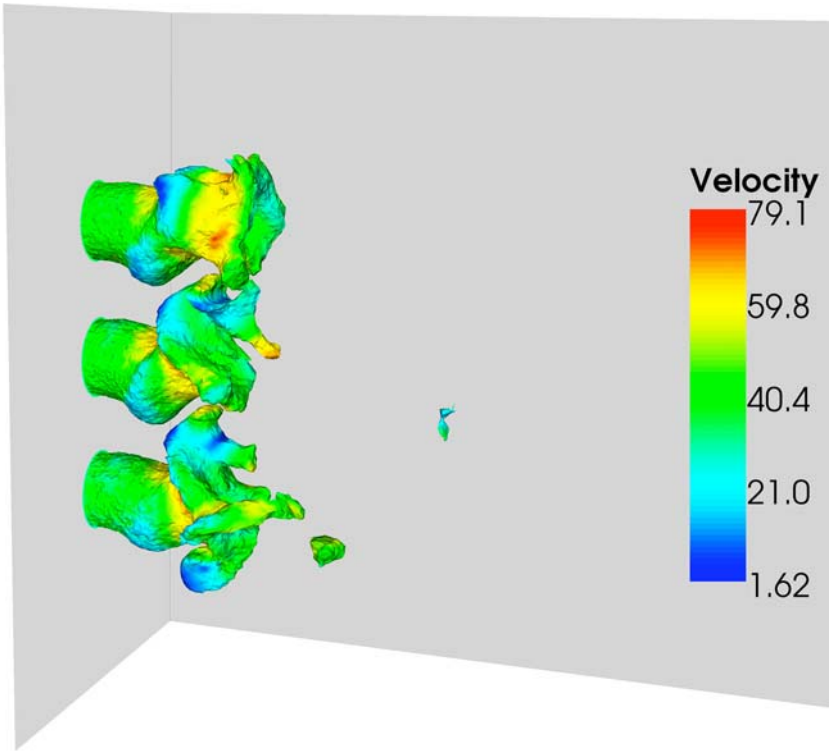

(a) Methane mass fraction Iso-level equal to 0.6 colored by the velocity magnitude.

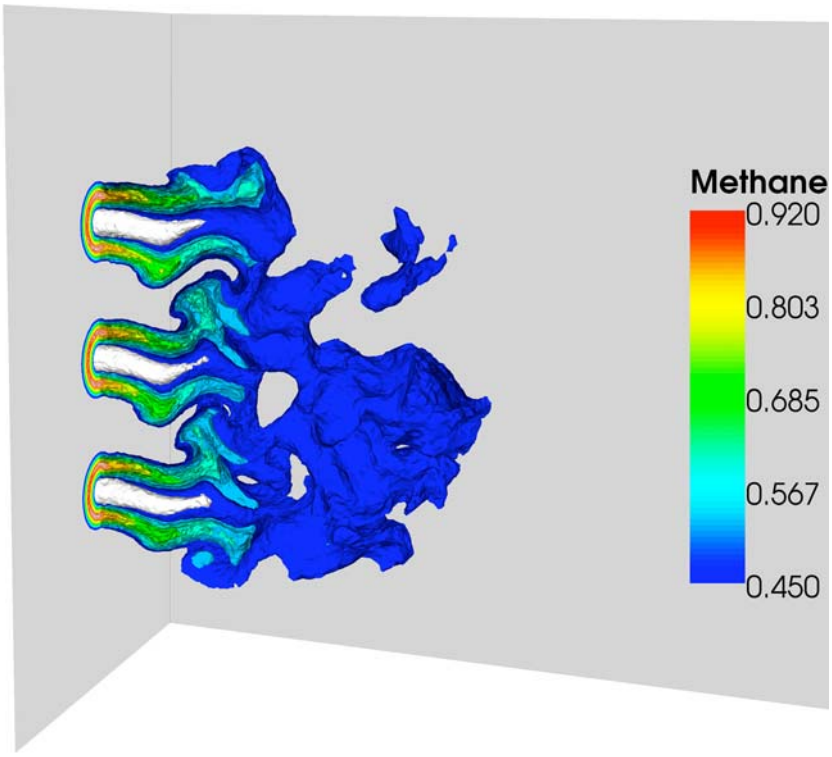

(b) Methane mass fraction surrounding oxygen iso-level equal to 0.6 (in white).

Fig. V.10: Three dimensional visualizations of the three coaxial flames transversally modulated at 2500 Hz.

Chapter VI

Analytical modeling of the acoustic coupling in liquid rocket engine

Résumé

Deux modèles analytiques sont présentés dans ce chapitre. Le premier traite du mécanisme de couplage par la vitesse. Il s'agit de montrer comment les fluctuations de vitesse acoustique peuvent conduire à des fluctuations de dégagement de chaleur qui peuvent à leur tour constituer des sources acoustiques. Ce modèle s'appuie sur les résultats expérimentaux obtenus lors des campagnes sur le banc Mascotte ainsi que sur les travaux réalisés antérieurement sur les instabilités de combustion haute-fréquence des moteurs fusées à propulsion liquide. On utilise notamment des visualisations par film rapide au moyen de fentes transversales pour déduire le comportement spatio-temporel du dégagement de chaleur. Ces visualisations sont ré-interprétées et conduisent à une modélisation du dégagement de chaleur instationnaire dont les fluctuations font intervenir la vitesse transversale retardée d'un délai τ et le signe du gradient de vitesse transverse. Du point de vue des fluctuations de dégagement de chaleur, la chambre de combustion rectangulaire est divisée en deux parties séparées par l'axe de symétrie. Lorsque la fluctuation de dégagement de chaleur est positive du coté supérieur, elle est négative du coté inférieur. Cette situation s'inverse après une demi-période. Ce comportement correspond à ce qui est observé expérimentalement. Cette distribution de dégagement de chaleur prend donc une forme semblable à celle de la pression associée au premier mode transverse. Pour une valeur adéquate du délai τ, le dégagement de chaleur et la pression peuvent être en phase. Dans ce cas, le critère de Rayleigh est positif et la perturbation acoustique est amplifiée. On montre qu'il en est effectivement ainsi au moyen d'une méthode de projection sur les modes de la chambre. La seconde analyse traite des effets des fluctuations de température sur les caractéristiques de résonance d'une cavité. Les expériences ont montré que ces fluctuations pouvaient réduire le niveau de réponse du système. On sait que les fluctuations de température entrainent des fluctuations de la vitesse du son et donc de la fréquence propre du système. Cet effet est représenté au moyen d'une équation différentielle du second ordre avec une fréquence propre fluctuante autour d'une valeur moyenne. Le système est soumis successivement à une modulation linéaire de la fréquence puis à une excitation mono-fréquentielle. On montre qu'en présence d'une fluctuation de la fréquence propre le système se comporte comme si son taux de dissipation acoustique était augmenté. Il est conclu que ce type de mécanisme peut avoir un impact important sur le développement d'oscillations dans les moteurs fusées à liquides.

Abstract

Two analytical models are presented in this chapter. The first model deals with the velocity coupling mechanism for high frequency instabilities. The objective is to show how acoustic velocity fluctuations may lead to heat release fluctuations which may in turn constitute acoustic sources. This model relies on experimental results obtained on Mascotte and on earlier investigations of high frequency instabilities in liquid rocket engines (LRE). High speed films recorded with a tranverse slit are specifically used to characterize the space time evolution of heat release in the chamber. These visualizations are reinterpreted to extract a model for the nonsteady heat release which involves the transverse velocity delayed by a time τ and the sign of the transverse velocity gradient. In terms of heat release the rectangular chamber can be subdivided in two parts separated by the symmetry axis. When the heat release fluctuation is positive in the upper part of the chamber, it is negative in its lower part. This situation is reversed after one half period. This corresponds to what is observed experimentally. The heat release distribution takes a shape which is similar to that of the pressure associated with the first transverse mode. For adequate values of the delay τ the heat release and pressure may be in phase. The Rayleigh criterion is satisfied and the acoustic perturbation is amplified. It is shown that this is effectively the case by projecting the pressure field on the normal modes of the system. The second analysis deals with effects of temperature fluctuations on the resonance characteristics of a cavity. It is known from experiments that this can reduce the response level of the system. It is known that temperature fluctuations induce fluctuations in the speed of sound which in turn perturb the eigenfrequency of the system. This effect is investigated with a second order differential equation featuring an eigenfrequency which fluctuates around its mean value. The system is then successively modulated with a linear frequency sweep and at a single frequency. It is shown that when the eigenfrequency fluctuates, the system behaves as if it had an augmented level of dissipation. It is concluded that this mechanism could have an important impact on the development of oscillations in liquid rocket engines.

VI.1 Introduction

Modeling of combustion instabilities has been developed over many years of research and is best exemplified by the sensitive time lag concept devised about 50 years ago (Crocco et al. 1958). Much of the modeling activity relied on early experiments which were either carried out on full scale engines or on intermediate scale systems. Very few smaller scale experiments were carried out and in all cases the instrumentation and data acquisition were quite limited. The modeling question is here reconsidered by first revisiting some of the earlier experiments and in particular those of Tischler and Male or by making use of the experimental data obtained on Mascotte by Rey et al. (2004, Richecoeur et al. (2006).

In the first analytical study described in this chapter we specifically consider the velocity coupling mechanism for high frequency instabilities. It is intended to see how acoustic velocity fluctuations may drive heat release fluctuations which may in turn become acoustic sources generating pressure modes. The model is based on experimental data obtained on Mascotte and specifically on the phase relations established in the low pressure tests. The model also relies on results from earlier investigations of high frequency instabilities in liquid rocket engines (LRE). In the early days many visualizations were based on high speed films recorded with a tranverse slit. These can be used to characterize the space-time evolution of heat release in the chamber. These visualizations are revisited and reinterpreted to extract a model for the nonsteady heat release. In its present form the model involves the transverse velocity delayed by a time τ and the sign of the transverse velocity gradient.

Considering a rectangular chamber geometry similar to that of the MIC, it is shown that the resulting heat release distribution can be subdivided in two parts separated by the symmetry axis. When the heat release fluctuation is positive in the upper part of the chamber, it is negative in its lower part. This configuration is reversed after one half period. This corresponds to what is observed experimentally. The heat release distribution takes a shape which has some similarity with that of the pressure associated with the first transverse mode. For suitable values of the delay τ the heat release and pressure may be in phase. The Rayleigh criterion is satisfied and the acoustic perturbation is amplified. It is shown that this is effectively the case by projecting the pressure field on the normal modes of the system determining the evolution of the modal amplitude. The model is formulated in section VI.2.1. The coupling term is then used in section VI.2.2 to see if it can drive instabilities and to define the ranges of delays which can lead to instability.

The second analysis focuses on a different aspect of combustion instabilities. The aim is to estimate effects of fluctuations on the resonance characteristics of a system. This analysis is motivated by results of the high pressure tests, which clearly indicated that the level of resonance was diminished in a situation where the level of fluctuation was intensified. This aspect is apparently not well documented in the previous literature neither on the experimental nor on the theoretical side. In studies of acoustic instabilities, the resonance of the system is usually calculated by assuming a constant temperature (as was done for example in Chapter I) or by taking into account the mean temperature distribution in the chamber as first proposed by Laverdant et al. (1986). Effects of temperature fluctu-

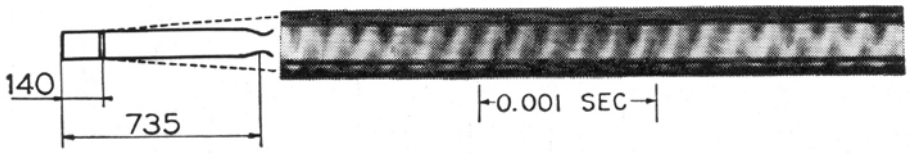

Fig. VI.1: Streak film of a spiral mode of oscillation observed through a slit located at 14 cm from the injection plane. The oscillation frequency is 6000 Hz. (from Tischler and Male (1956))

ations on the resonance characteristics of a cavity are usually neglected often without any justification.

It is known from experiments carried out at high pressure (see Chapter I) that this can be a possible cause for the reduced response level of the system. Theoretical analysis have been performed by Clavin et al. (1994) and Burnley and Culick (2000). It is known that temperature fluctuations induce fluctuations in the speed of sound which in turn perturb the eigenfrequencies of the system. This effect is investigated on a simplified level with a second order differential equation featuring an eigenfrequency ω_0 which fluctuates around its mean value (section VI.3.2). It is then possible to induce various types of fluctuations and see how the system responds. This is accomplished in section VI.3.3 by successively applying a linear frequency sweep and a single frequency modulation. It is shown that when the eigenfrequency fluctuates, the system behaves as if it had an augmented level of dissipation. This leads to the important conclusion that fluctuations inside the chamber could have a notable impact on the development of oscillations in liquid rocket engines.

VI.2 Heat release model based on the velocity gradient

VI.2.1 Description of the model

To begin with, it is worth revisiting some of the early experiments on high frequency instability and in particular that of Tischler and Male (1956). The objective is to reinterpret what was observed and devise a coupling model for velocity coupled heat release oscillations. The experiment was carried out on a 10-cm diameter 1-m long model scale rocket engine equipped with a slit. A video camera recorded the light intensity through the transverse slit placed in a section at 14 cm from the injection plane. Figure VI.1 presents the light observed when a 6 000 Hz transverse mode is set-up in the chamber. The experiment shows that the luminous zone moves across the chamber in a helical way. The oscillation in the chamber is coupled by the first transverse acoustic mode. Under these conditions, energy is released periodically in the upper and lower sides of the chamber. The frequency of positive excursions of heat release in the upper part of the chamber coincides with the oscillation frequency. This is also true for the lower part. When heat release fluctuation is positive in the upper part, it is negative in the lower part. The situation is reversed at each half period.
It is then natural to infer that positive heat release fluctuations occur at the same frequency as the transverse velocity variations. During one half period the velocity is oriented in the upper direction while during the second part of the period it is directed towards the lower side of the chamber. This idea can now be used to devise an analytical model.

It is first worth recalling that the coupling model which is proposed in this section aims at showing how velocity fluctuations may give rise to heat release fluctuations which will in turn give rise to acoustic sources eventually leading to instability. The model is established in a simplified framework where the pressure field inside the chamber is governed by a wave equation :

$$\frac{1}{c^2}\frac{\partial^2 p_1}{\partial t^2} - \nabla^2 p_1 = \frac{\gamma - 1}{c^2}\frac{\partial q_1}{\partial t} \tag{VI.1}$$

The right hand side features the nonsteady rate of heat release $\partial q_1/\partial t$. The central issue is to express this term as a function of perturbations in the chamber. One may infer from the reexamination of Tischler and Male (1956) and from experimental results obtained in the low pressure tests that the rate of heat release term follows the acoustic velocity in the transverse direction. It will be assumed for simplicity that this term is proportional to this velocity. Very large velocity fluctuations directed upwards will lead to an accumulation of reactants in the upper part of the chamber. These reactants will burn at a later instant in time. Similarly large excursions of velocity in the negative direction will bring reactants in the lower part of the chamber and these will burn again after a certain delay.
It is then assumed that the nonsteady heat release term is proportional to the transverse velocity perturbation but it is important to include a delay τ in order to take into account a phase between the energy release and the wave oscillation. Thus the heat release is proportional to $v_1(y, t-\tau)$.

Based on the photograph in Fig.VI.1, the heat release location in the chamber may be assumed to be correlated with the velocity direction. Considering an instant in time where the transverse component of the velocity is positive in a cross section. Reactants are displaced towards the top side of the chamber and the heat release will take place in that region. This will also induce a reduction of reactants in the lower side and consequently a negative fluctuation in heat release. Inversely, when the transverse component of the velocity is negative, the heat release will become positive in the lower part of the chamber and negative in the upper side. Consequently the sign of the heat release has to depend on the sign of the gradient of the transverse velocity :

$$\frac{\partial q_1}{\partial t} = \beta \,\mathrm{sign}\left[\frac{\partial v_1}{\partial y}(y, t-\tau)\right] v_1(y, t-\tau) \tag{VI.2}$$

In the previous expression β designates an interaction index.
The pressure in the chamber can be approximated by $p_1(y,t) = A(t)\cos(ky)\cos(\omega t + \phi)$ where A and ϕ are slowly varying functions of time. The transverse velocity v_1 is obtained from momentum equation

$$\rho_0 \frac{\partial v_1}{\partial t} + \frac{\partial p_1}{\partial y} = 0 \tag{VI.3}$$

Using Equations VI.2 and VI.3 and the expression of $p_1(t)$, one may determine an analytical expression of the heat release. It is interesting to see how this compares with the experiments of Tischler and Male (1956). To simplify the calculation one may consider a 2D duct with the same dimensions as used by Tischler and Male (1956) where a 6 000 Hz transverse acoustical mode is set-up. Under these conditions, the evolution with respect to time of the heat release in a transverse section deduced from expression VI.2 is displayed in Fig.VI.2.

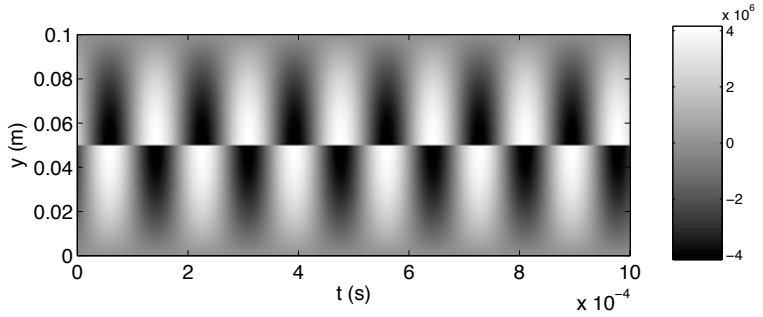

Fig. VI.2: Time evolution of nonsteady heat release represented as a streak film taken through a transverse slit through a rectangular 2D combustor.

The pattern obtained in this way is clearly similar to the data shown in Fig. VI.1. When a 6000 Hz transverse mode is set-up in the chamber, six periods are observed during 1 ms in both cases. The positive heat release takes place alternately in the upper and then in the lower part of the chamber, forming a sinusoidal space-time distribution. The analytical expression adopted for the heat release (Eq.VI.2) renders the phenomenon observed experimentally and this gives confidence in the initial assumption about the space-time heat release model.

VI.2.2 Analysis of velocity coupling

From hereon the analysis may be developed in a standard way. The objective is to determine how the pressure amplitude evolves in the chamber when the coupling model is used to describe the nonsteady rate of heat release.
For this, it is convenient to use an expansion in terms of eigenmodes

$$p_1 = p_0 \sum_{n=1}^{\infty} \eta_n(t) \Psi_n(x)$$

where Ψ_n are such that $\nabla^2 \Psi_n + \left(\omega_n^2/c^2\right) \Psi_n = 0$ and $\eta_n(t)$ designates the amplitude of the n-th mode. The chamber has a transverse size a and the first transverse eigenmode has the form $\Psi_1(y) = \cos(ky)$ where $k = \pi/a$. Considering that the eigenmodes are orthogonal, Eq.VI.1 can be written

$$\frac{d^2\eta_n}{dt^2} + \omega_n^2 \eta_n = \frac{\gamma - 1}{p_0 \Lambda_n} \int \frac{\partial q_1}{\partial t} \Psi_n \, dV \tag{VI.4}$$

where $\Lambda_n = \int \Psi_n^2 \, dV$. From Eq.VI.2 and after integration of the source term in Eq.VI.4, one finds

$$\frac{d^2\eta_1}{dt^2} + \omega_1^2 \eta_1 = \alpha \, A(t) \sin[\omega(t - \tau) + \phi(t)] \tag{VI.5}$$

$$\eta_1(t) = A(t) \cos[\omega t + \phi(t)] \tag{VI.6}$$

with $\alpha = 2\beta(\gamma - 1)/(p_0 \Lambda_1 \rho_0 \omega)$
To determine the pressure evolution in the chamber and obtain stability conditions, the amplitude $\eta(t)$ has to be evaluated from Eq.VI.5 and VI.6. It is convenient to consider that the amplitude and phase

vary on a time scale which is much smaller than the period of oscillation and examine the evolutions of $A(t)$ and $\phi(t)$ with respect to time. One applies in this analysis the two time methods or more precisely the averaging techniques which are extensively used to examine nonlinear oscillations.
Differentiation of Eq.VI.6 gives

$$\frac{d\eta}{dt} = \dot{A}\cos(\omega t + \phi) - A\dot{\phi}\sin(\omega t + \phi) - A\omega\sin(\omega t + \phi)$$

It is standard to assume that $\dot{A}\cos(\omega t + \phi) - A\dot{\phi}\sin(\omega t + \phi) = 0$. A second differentiation of Eq.VI.5 yields the following system

$$\left\{ \begin{array}{rcl} \dot{A}\cos(\omega t + \phi) - A\dot{\phi}\sin(\omega t + \phi) & = & 0 \\ \dot{A}\sin(\omega t + \phi) + A\dot{\phi}\cos(\omega t + \phi) & = & -\frac{\alpha}{\omega}A\sin\left[\omega(t-\tau) + \phi\right] \end{array} \right.$$

Taking the average of the previous system over a period of oscillation yields first order differential equations for $A(t)$ and $\phi(t)$

$$\begin{array}{rcl} \dot{\phi} & = & \dfrac{\alpha}{2\omega}\sin(\omega\tau) \\ \dfrac{dA}{dt} & = & -\dfrac{\alpha}{2\omega}\cos(\omega\tau)A(t) \end{array} \qquad \text{(VI.7)}$$

One may then deduce the pressure amplitude :

$$\eta(t) = B\,\exp\left(-\frac{\alpha}{2\omega}\cos(\omega\tau)t\right)\cos\left(\omega t + \frac{\alpha}{2\omega}\sin(\omega\tau)t\right) \qquad \text{(VI.8)}$$

Stability is easily deduced from Eq.VI.7 which determines the evolution with respect to time of the amplitude. The rate of growth will be positive if $\cos(\omega\tau) < 0$ or equivalently if $\omega\tau \in [\pi/2; 3\pi/2]$ modulo 2π, the system will be unstable. This last situation is illustrated in Fig.VI.3. It is also possible to confirm this result by recombining Eq.VI.6 and Eq.VI.5 to obtain a differential delayed equation

$$\frac{d^2\eta(t)}{dt^2} + \frac{\alpha}{\omega}\frac{d\eta(t-\tau)}{dt} + \omega^2\eta(t) = 0 \qquad \text{(VI.9)}$$

This equation can then be solved numerically. The calculation is carried out in a configuration similar to the present experiment. The first transverse mode is set-up at 3330 Hz. The pressure evolves as predicted in the analytical treatment (see Fig.VI.3).
The model devised in this chapter clearly shows that a velocity coupling is possible. This takes however a somewhat unusual form because it depends on the delayed transverse velocity perturbations and on the sign of the gradient of this velocity. This last dependence reflects the physical phenomenon by which reactants are accumulated alternately in one side or in the other side of the chamber. The model provides a nonsteady rate of heat release which is similar to that observed in some early experiments of combustion instability in liquid rocket engines and it has been verified analytically and numerically that it can lead to an unstable growth of oscillations for certain ranges of delays.

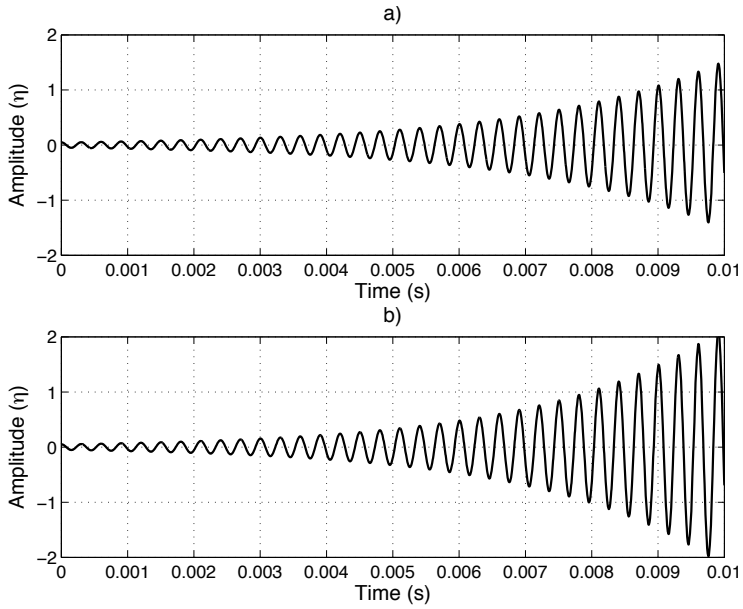

Fig. VI.3: Pressure signal deduced from the velocity coupled model. The signal is plotted as a function of time for $\omega\tau = \pi$: (a) numerical solution , (b)analytical solution.

VI.3 Influence of fluctuations on resonance characteristics

VI.3.1 Introduction

This section now focuses on the effects of fluctuations on resonance characteristics of a system. This question is not often discussed in the literature and not well documented. It is motivated by observations of the response in the high pressure experiments. Hot fire tests carried out with the five element injector feature modulation levels lower than those expected from an extrapolation of the low pressure tests. The modulator has been improved and the total mass flow rate passing through the secondary nozzle was equal to 25% of the global mass flow rate, which is the maximum value ever tested. This however did not generate pressure amplitudes commensurate with the improved operating conditions. It was considered that the reduced response amplitude could be due to the augmented level of temperature fluctuation in the high pressure hot fire experiments. It is not possible to measure the intensity of these fluctuations but it has been found that the pressure fluctuation level in the absence of external modulation was much higher than that found in the low pressure experiments. Without modulation, the level of pressure fluctuations reaches 2% of the mean chamber pressure. Spectral analysis of the pressure signals again in the absence of modulation shows that there is a level of coherence between the pressure fluctuations and heat release fluctuations. The system is characterized by intense and coherent turbulent fluctuations and it was hypotesized that this could lead to a reduced level of resonance. This possibility is generally not considered in the literature perhaps because the intensity of temperature fluctuation in a real engine is lower than that existing in the multiple injector combustor. In an engine, the injectors cover the full backplane in a showerhead arrangement and they produce an essentially uniform temperature distribution with turbulent fluctuation around a mean value. In the present multiple injector configuration, the five injectors are placed in the center of the cavity and

there is a large contrast of temperature between the flame region and the surroundings. One then expects that the fluctuations will be much more pronounced. Whatever the reason, it is worth looking at the effect of fluctuations. The objective is to see how these fluctuations modify the resonance properties.

VI.3.2 Dynamical system model

To do this, a dynamical model is devised in which the eigenfrequency fluctuates. The system is then submitted to a frequency sweep and a continuous modulation.
The dynamics of the chamber oscillations are represented by a second order differential equation

$$\frac{d^2x}{dt^2} + 2\omega_0\zeta\frac{dx}{dt} + \omega_0^2 x = G(t)$$

where $2\omega_0\zeta = \alpha$ is the damping coefficient, ω_0 is the system angular frequency and $G(t)$ is the external modulation exciting the system. This second order equation may replaced by a first order differential system. A couple of variables (X, Y) is defined as

$$\begin{cases} X = x \\ Y = \dfrac{dx}{dt} \end{cases} \tag{VI.10}$$

The second order differential equation is now equivalent to the first order differential system :

$$\begin{cases} \dfrac{dX}{dt} = Y \\ \\ \dfrac{dY}{dt} = -2\zeta\omega_0 Y - \omega_0^2 X + G(t) \end{cases} \tag{VI.11}$$

The damping coefficient α is linked to the resonance bandwidth Δf of a second order system by the relation $\Delta f = \alpha/\pi$. Experimentally, the damping coefficient α was found approximately equal to 220 s^{-1} giving a resonance bandwidth of about 60 Hz.

The idea here is to consider that the eigenfrequency of the system f_0 is not constant but fluctuates around a mean value F_0 at a frequency f_1. Then the eigenfrequency changes with respect to the time following the expression

$$f_0 = F_0(1 + \epsilon\cos(2\pi f_1 t))$$

where ϵ represents the amplitude of the fluctuations. So,

$$\omega_0 = 2\pi F_0(1 + \epsilon\cos(2\pi f_1 t))$$

VI.3.3 Results of simulations

Two different modulations are generated to simulate the experimental test procedure. In the first calculation a linear frequency sweep is used as input to the model. The frequency increases linearly from 0 to 3500 Hz with a growth rate equal to 100 Hz s^{-1}. Like in the experiment, this can be used

α	f_0'	f_1	p	A
220 s^{-1}	2800 Hz	500 Hz	100 Hz s^{-1}	500 s^{-2}

Tab. VI.1: Values of the parameters used to solve the first order differential system representing the acoustic response of the combustion chamber.

to determine the eigenfrequency by processing the response by short time Fourier transform analysis. In the second calculation, the excitation is a continuous wave modulation (CW) at the mean system eigenfrequency F_0. This gives two different expressions for $G(t)$:

$$\begin{cases} G(t) = A\sin(\pi p t^2) \\ G(t) = A\sin(F_0 t) \end{cases}$$

Table VI.1 gathers the values of the different parameters used in the numerical simulations. In the linear frequency sweep case, the system operates over a period of 35 s which represents the length of an experimental test. Two different values of ϵ are chosen corresponding to the ideal system behavior ($\epsilon = 0$, no fluctuations of the eigenfrequency) and the naturally perturbed system ($\epsilon = 0.05$, 5% of amplitude fluctuation around the mean eigenfrequency).
The response of the system to a linear frequency sweep is shown in figure VI.4 with the corresponding short time Fourier transform. The system is sampled at a rate of 20 kHz and the short time Fourier transform is performed with 1024 points per block and an overlap of one half.

For $\epsilon = 0$, the system eigenfrequency is equal to 2800 Hz so the resonant peak is expected 28 s after the beginning of the modulation. The resonance amplitude is significant and occurs at the eigenfrequency. The damping coefficient α controls the peak shape giving the expected frequency bandwidth ($\Delta f =$ 60 Hz). This corresponds to what is observed without combustion in the chamber. The resonance is strong enough and the eigenfrequency can be easily identified.

For $\epsilon = 0.05$, the eigenfrequency of the system is oscillating around 2800 Hz at a frequency equal to 500 Hz. The frequency excursion is approximately equal to 280 Hz. The system response to the frequency sweep modulation changes drastically. First, the response covers a broader frequency range and several peaks are identified. Two of the peaks at 2720 Hz and 2880 Hz have about the same amplitude. Additional smaller peaks are also observed. Second, the maximum amplitude is 1.10^{-4} which is only 62% of the peak value obtained for $\epsilon = 0$. This phenomenon represents to some extent what was found experimentally. The simulations indicate that the response bandwidth is not controlled exclusively by the damping coefficient and that the fluctations act somewhat like an additional dissipation. Because the peak is broadened, it is less easy to extract the eigenfrequency. For a system featuring multiple eigenfrequencies one expects that fluctuations will mix the resonances further complicating the modal identification.

It is now worth considering the system response to a continuous wave modulation. The frequency is fixed at 2800 Hz. The system output signals without and with fluctuations are shown in figure VI.5. The top subfigure displays the output signal plotted over a long time interval. In the two cases, the

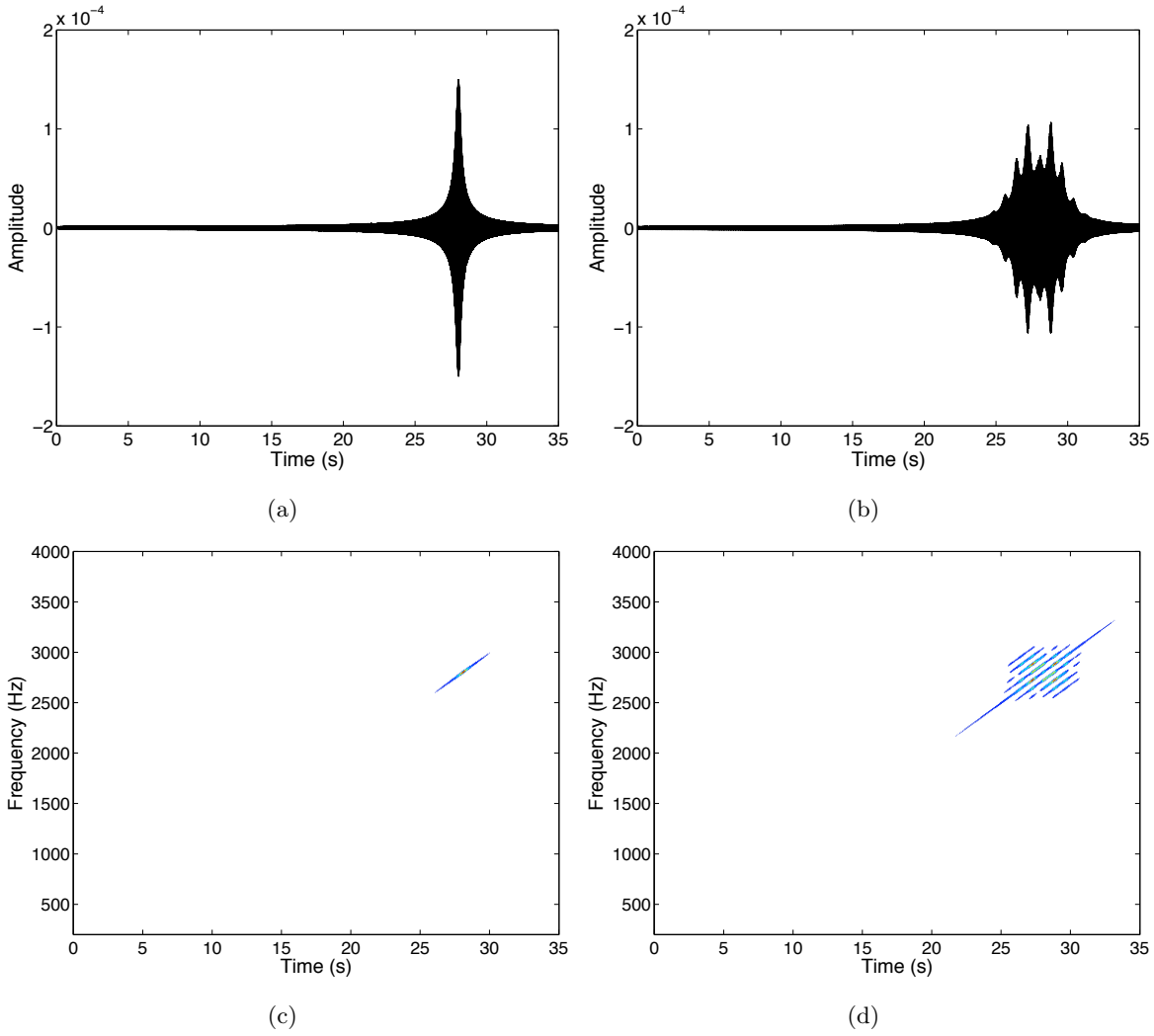

Fig. VI.4: System response to a frequency sweep modulation. (a) The frequency is constant and the fluctuation amplitude is $\epsilon = 0$, (b) The eigenfrequency is perturbed with a level of fluctuation $\epsilon = 0.05$. (c) and (d) Short time Fourier analysis of the signal delivered by the system in cases (a) and (b) respectively.

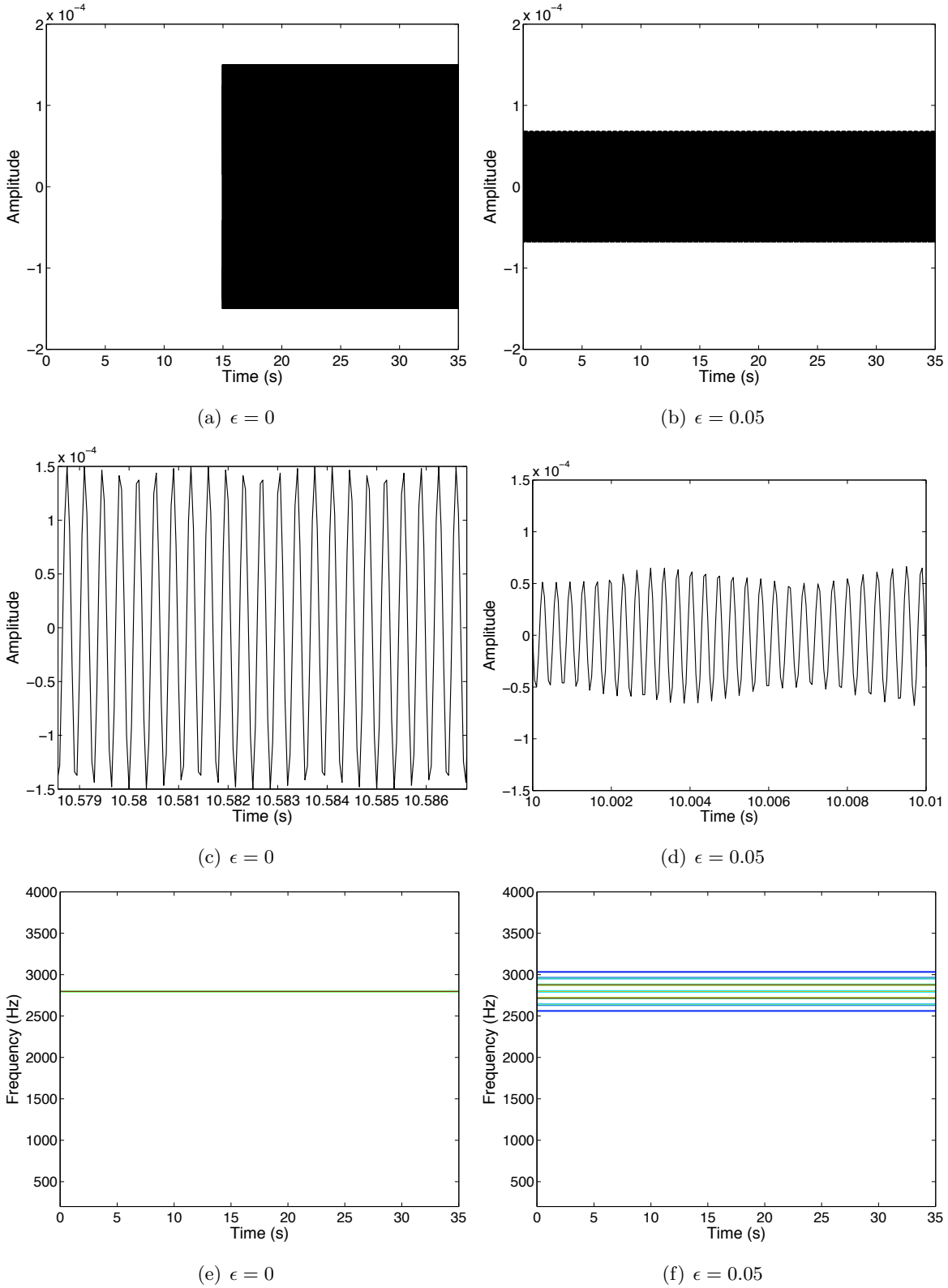

(a) $\epsilon = 0$ (b) $\epsilon = 0.05$

(c) $\epsilon = 0$ (d) $\epsilon = 0.05$

(e) $\epsilon = 0$ (f) $\epsilon = 0.05$

Fig. VI.5: System response to a continuous wave modulation at a fixed frequency F_0 =2800 Hz without (a and c, $\epsilon = 0$) and with eigenfrequency fluctuations (b and d, $\epsilon = 0.05$). (e) and (f) give the corresponding short time Fourier transform maps.

signal does not fluctuate significantly. The amplitude is constant but the response amplitude for $\epsilon = 0$ is about twice that observed for $\epsilon = 0.05$. This shows that the presence of fluctuations reduces the output amplitude for the same input level.

A close-up view of this response is also shown in figure VI.5. When $\epsilon = 0.05$, the low frequency which can be observed in the signal response is equal to 500 Hz and corresponds to the frequency of the fluctuation. The small low frequency oscillation observed in the case where $\epsilon = 0$ is due to the moderate sampling rate which is not quite sufficient to describe the oscillation at 2800 Hz. The sampling rate should be increased to avoid this phenomenon but this would significantly increase the cost of the calculation without bringing more significant information.

The short time Fourier transform maps corresponding to the constant frequency modulation are plotted in the last subfigures of figure VI.5. This confirms that when $\epsilon = 0.05$ the response of the system to a continuous modulation at a given frequency does not feature a single frequency. Subfrequencies around the main frequency are also found and the amplitude of the response is lower than that found for $\epsilon = 0$.

VI.3.4 Theoretical analysis of the effect of fluctuations

It is interesting to examine the effect of fluctuations from a theoretical point of view. The model problem is again defined by the differential equation

$$\frac{d^2x}{dt^2} + 2\omega_0\zeta\frac{dx}{dt} + \omega_0^2 x = G(t) \tag{VI.12}$$

where $G(t) = G_0\cos(\omega t)$. One assumes that ω_0 fluctuates around a mean value and that it may be expressed as

$$\omega_0 = \bar{\omega_0}\left[1 + n(t)\right] \tag{VI.13}$$

where $n(t)$ only features low frequency oscillations (frequencies lower than $f_0 = \omega_0/2\pi$. To examine this problem it is convenient to use the method of averaging which was already exploited in the analysis of velocity coupled instabilities.

The signal $x(t)$ is first written in terms of an amplitude $A(t)$ and a phase $\Phi(t)$:

$$x(t) = A(t)\cos[\omega t + \Phi(t)]$$

The amplitude and phase are slowly varying functions of time. Taking the time derivative of $x(t)$ one obtains

$$\frac{dx}{dt} = -A\sin(\omega t + \Phi) + \dot{A}\cos(\omega t + \Phi) - A\dot{\Phi}\sin(\omega t + \Phi) \tag{VI.14}$$

At this point one may impose the standard condition

$$\dot{A}\cos(\omega t + \Phi) - A\dot{\Phi}\sin(\omega t + \Phi) = 0 \tag{VI.15}$$

This simplifies equation VI.14 :

$$\frac{dx}{dt} = -A\sin(\omega t + \Phi) \tag{VI.16}$$

One may now calculate the second derivative of x with respect to time :

$$\frac{d^2x}{dt^2} = -A\omega^2\cos(\omega t+\Phi) - \dot{A}\omega\sin(\omega t+\Phi) - A\dot{\Phi}\omega\cos(\omega t+\Phi) \qquad \text{(VI.17)}$$

It is now possible to express the original differential equation VI.12 in terms of A and Φ. One obtains after some rearrangements :

$$\begin{aligned} -\dot{A}\omega\sin(\omega t+\Phi) - A\dot{\Phi}\omega\cos(\omega t+\Phi) &= A(\omega^2-\omega_0^2)\cos(\omega t+\Phi) \\ &\quad +2\zeta\omega_0\omega A\sin(\omega t+\Phi) + G_0\cos(wt) \qquad \text{(VI.18)} \end{aligned}$$

Using the standard condition VI.15, one obtains a linear system and it is a simple matter to deduce expressions for $\dot{A}$ and $A\dot{\Phi}$. Designating by B the right hand side of equation VI.18

$$B = A(\omega^2-\omega_0^2)\cos(\omega t+\Phi) + 2\zeta\omega_0\omega A\sin(\omega t+\Phi) + G_0\cos(wt) \qquad \text{(VI.19)}$$

one finds

$$\dot{A} = \frac{1}{D}\begin{vmatrix} B & -\omega\cos(\omega t+\Phi) \\ 0 & -\sin(\omega t+\Phi) \end{vmatrix} = -\frac{B}{D}\sin(\omega t+\Phi)$$

and

$$A\dot{\Phi} = \frac{1}{D}\begin{vmatrix} -\omega\sin(\omega t+\Phi) & B \\ \cos(\omega t+\Phi) & 0 \end{vmatrix} = -\frac{B}{D}\cos(\omega t+\Phi)$$

where the determinant is given by

$$D = \begin{vmatrix} -\omega\sin(\omega t+\Phi) & -\omega\cos(\omega t+\Phi) \\ \cos(\omega t+\Phi) & -\sin(\omega t+\Phi) \end{vmatrix} = \omega$$

One obtains in this way

$$\begin{aligned} \dot{A} &= -\frac{A}{\omega}\left[(\omega^2-\omega_0^2)\cos(\omega t+\Phi) + 2\zeta\omega_0\omega\sin(\omega t+\Phi)\right]\sin(\omega t+\Phi) \\ &\quad -\frac{G_0}{\omega}\cos(\omega t)\sin(\omega t+\Phi) \end{aligned}$$

and

$$\begin{aligned} A\dot{\Phi} &= -\frac{A}{\omega}\left[(\omega^2-\omega_0^2)\cos(\omega t+\Phi) + 2\zeta\omega_0\omega\sin(\omega t+\Phi)\right]\cos(\omega t+\Phi) \\ &\quad -\frac{G_0}{\omega}\cos(\omega t)\cos(\omega t+\Phi) \end{aligned}$$

Before averaging, it is convenient to replace products of sines and cosines by sums :

$$\begin{aligned} \dot{A} &= -\frac{A}{\omega}\left[(\omega^2-\omega_0^2)\frac{\sin 2(\omega t+\Phi)}{2} + \zeta\omega_0\omega(1-\cos 2(\omega t+\Phi))\right] \\ &\quad -\frac{G_0}{\omega}\frac{\sin\Phi+\sin(2\omega t+\Phi)}{2} \end{aligned}$$

and

$$\begin{aligned} A\dot{\Phi} &= -\frac{A}{\omega}\left[(\omega^2-\omega_0^2)\frac{1+\cos 2(\omega t+\Phi)}{2} + \zeta\omega_0\omega\sin 2(\omega t+\Phi)\right] \\ &\quad -\frac{G_0}{\omega}\frac{\cos\Phi+\cos(2\omega t+\Phi)}{2} \end{aligned}$$

One may now integrate over a period of oscillation $T = 2\pi/\omega$. Since ω_0 contains low frequency components terms like

$$\int_0^{2\pi/\omega} (\omega^2 - \omega_0^2) \cos 2(\omega t + \Phi) dt$$

essentially vanish. The averaging process yields

$$\dot{A} = -A\zeta\omega_0 - G_0 \frac{\sin\Phi}{2\omega} \quad \text{(VI.20)}$$

$$A\dot{\Phi} = -A\frac{(\omega^2 - \omega_0^2)}{2\omega} - G_0 \frac{\cos\Phi}{2\omega} \quad \text{(VI.21)}$$

Equations VI.20 and VI.21 constitute a system of two differential equations which is solved numerically to obtain the amplitude $A(t)$ and the phase $\Phi(t)$ of the system response to external modulation. The eigenfrequency frequency follows the equation VI.13 :

$$\begin{aligned} \omega_0 &= \overline{\omega_0}\,[1 + n(t)] \\ &= 2\pi f_0\,[1 + \epsilon\cos(2\pi f_1 t)] \end{aligned}$$

with f_0=2800 Hz and f_1=100 Hz. When ϵ is set to 0, the system has a constant eigenfrequency equal to f_0. The fluctuation is activated with ϵ=0.05. This corresponds to a temperature fluctuation equal to 10% around the mean value. Initial solutions are assigned by taking values of the order of magnitude of the steady solution, $A(t_0) = 2$ and $\Phi(t_0) = 0$. The transient being short, the initial values have little influence on the long time behavior. The time duration of the calculation (t_f =0.05 s) corresponds to a few low frequency periods.

Figure VI.6 shows the phase Φ and the amplitude A with respect to the time. When $\epsilon = 0$, the amplitude rapidly reaches unity and stays constant. The phase follows the same behavior, reaching $-\pi/2$ and remains at that value. This leads to a sinusoidal signal $x(t) = A(t)\cos(\omega t + \Phi(t))$ corresponding to the response of a system to external modulation in the absence of eigenfrequency fluctuations. When $\epsilon = 0.05$, the amplitude does not tend to a constant value. It is oscillating around an averaged value of 0.81 at a frequency equal to 200 Hz which is exactly twice the low frequency fluctuations of the eigenfrequency. The variations of the eigenfrequency strongly modifies both the mean value and the temporal behavior of the response amplitude. The phase is also modified by the eigenfrequency fluctuations. The average value of the phase remains equal to $-\pi/2$ but large sinusoidal oscillations around this value are observed at a frequency equal to f_1=100Hz. Variations of the phase between the different transducers have been observed experimentally. This model may explain the origin of such phase fluctuations.

To conclude, the variations of the eigenfrequency due to a fluctuating local temperatures modifies the response of the system to an external modulation. The average value of the amplitude decreases and both the phase and the amplitude are oscillating at low frequencies.

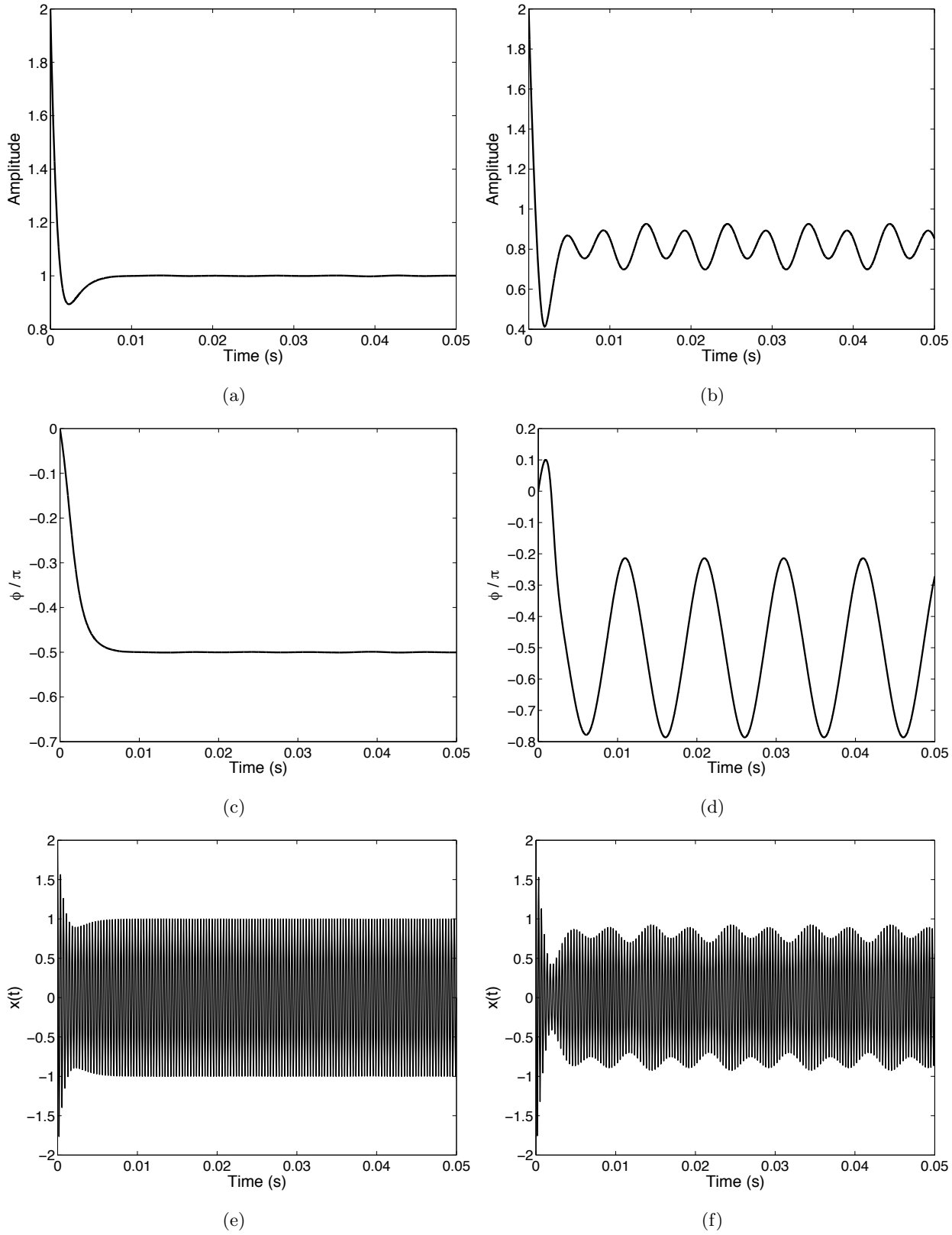

Fig. VI.6: Amplitude (a, b), phase (c, d) and temporal response (e, f) of the system without (a, c, e) and with (b, d, f) continuous modulation.

VI.4 Conclusion

This chapter describes two models of interest in combustion instability. The first model is devised to represent velocity coupling. The model relies on a novel expression for the nonsteady rate of heat release. The model expression involves the delayed transverse velocity perturbations and the sign of the gradient of this velocity. It is shown that the nonsteady rate of heat release is similar to what was observed in some early experiments of combustion instability in liquid rocket engines. This model is explored analytically and numerically and it is shown that it can lead to an unstable growth of oscillations for certain ranges of the delay parameter.
The second model is devised to examine the effect of fluctuations on the resonant response of a system. This is motivated by experimental observations under hot fire conditions indicating that the response is less pronounced. The system is represented as a second order differential equation and it is excited by linear frequency sweeps and continuous wave modulations. Two different cases are studied. In the first case, the eigenfrequency of the system is fixed and kept constant. In the second case, the eigenfrequency oscillates around a mean value.

Results of simulation obtained for this dynamical model confirm what was observed experimentally. When the eigenfrequency of system is fluctuating, the identification of the resonant peak is less easy. The system output amplitude is also lower in the presence of fluctuations.

This indicates that turbulent fluctuations generated by combustion inside the chamber influence the resonant properties and may reduce the reponse to an external modulation, a fact which was not understood at the beginning of this investigation. The eigenfrequencies are less easy to determine and the response is weaker. The resonant response under hot fire conditions is not as sharp as that found under cold flow conditions in the absence of temperature fluctuations. This model shows that it is important to consider the level of fluctuation when one examines the acoustic response of a combustion chamber a fact which has been essentially overlooked up to now.

Conclusions

Work described in this document has focused on the interactions between multiple flames and transverse modulations with application to the analysis of high frequency instabilities. Cryogenic hot fire tests were carried out on a multiple injector combustor (MIC) specifically designed to allow such investigations. The geometry was defined to obtain a good separation between longitudinal and transverse modes of the combustor. It had some of the features of a rocket engine and in particular included between three and five coaxial injectors. The objective of experimental investigations carried out on this model scale combustor was to generate data on coupling phenomena similar to those observed in liquid rocket engines.

On the experimental level one series of experiments was carried out on the Mascotte testbed operating in the low pressure range at 0.9 MPa. Modal identification was carried out systematically. The experimental frequencies were compared with results of calculations based on the three dimensional code MESA-3D. The 3D numerical simulation of the acoustic modes allows a better understanding of the Mascotte testbed acoustic response. The coupling between the main chamber and the secondary nozzle generates an additional mode at a frequency which lies between these of the first longitudinal and the first transverse modes. This numerical analysis was experimentally confirmed and it allowed a suitable identification of the modes observed during the hot fire tests.

A systematic investigation showed that a strong coupling could be induced under certain conditions (essentially by varying the gas injection velocity) and that it was possible to gather precious indications on the phenomenon. These results were generated after a careful optimization of the modulation wheel used to generate transverse pressure fluctuation in the combustor. A new wheel and an improved set-up was developed. The modulation was applied to 15 % of the main mass flow rate which is ejected trough the secondary nozzle. The nozzle is periodically blocked by a toothed wheel to generate acoustic waves in the chamber. The relative position of the nozzle and the rotating wheel is a key parameter to obtain a high level of pressure fluctuation and this parameter has been carefully adjusted in the hot fire tests.

Injection conditions were varied to determine injection parameters leading to the strongest coupling between combustion and acoustic fluctuations. The methane flow rate was successively equal to 50, 70 and 100 g s^{-1}. Gaseous methane was injected at 280 K and at a lower temperature of 180 K. The highest pressure fluctuation levels were obtained for low injection velocity at 280 K. When modulated

at the first transverse mode eigenfrequency (i.e. 2345 Hz), the root mean square pressure reached 7.5 % of the mean chamber pressure. The maximum pressure amplitude observed was about 0.9 bar peak-to-peak, but high amplitude pressure fluctuations were not sustained without the modulating wheel.

The combustion response to the external modulation is characterized by three phenomena : (1) the flame front expansion, (2) the increase of the heat release and (3) the spreading rate and velocity of the convected reactive structures. Expansion has been characterized by using instantaneous OH* emission images. The expansion angle is found to be doubled. The emitted light intensity also increases significantly, the intensity of the OH* radical emission increases by a factor 3. This is a strong indication that the volumetric heat release is augmented. It was also found that the heat flux to the wall is augmented as indicated by a rapid increase of the wall temperature. High speed camera records showed modification of the reactive spot sizes, their subsequent consumption and their convection velocity in the flow. A transverse motion is clearly observable in the high speed film. The analysis of phase relations between pressure signals detected at the wall and heat release deduced from light emission indicated that these two quantities have essentially the same spatial structure.
These initial experiments have provided indications on effects of injection parameters but the respective influence of the mixture ratio E and momentum flux ratio J on the stability remained to be elucidated. The interactions between pressure fluctuations and combustion have been observed by optimizing the test conditions and by a systematic variation of the operating parameters but much more data are required.

The second experimental program carried out in the intermediate and high pressure range was a logical follow-up of the tests already carried out at low pressure. One conclusion of the previous tests was that it was worthwhile to increase the number of jet flames. This would give a more suitable distribution of heat release in the combustor. The configuration would then be closer to typical engine injector arrangements. This geometrical change was possible because the injection head had to be improved to avoid the leaks which had previously led to the destruction of the previous head.

A new injection head was designed and manufactured. This system was used in the high pressure experiments. The combustor was operated with the same oxygen flow rate per injector and as a consequence the power released was increased by 65% in this configuration. The new backplane with 5 injectors allows a better representation of the highly packed uniformly distributed injection arrangement of real engines. Optical diagnostics were used as in previous experiments to examine the flame dynamics. Intensified cameras provided the spatial modifications generated by the external modulation. The temporal evolution of the combustion process submitted to external modulation was obtained with the high speed camera. This camera was operated to visualize the full chamber. Results obtained at the intermediate pressure of 3 MPa featured characteristics similar to those found at low pressure but it was also noticed that the resonance characteristics of the system were modified and the response to external modulation was weaker. At the same time the level of pressure fluctuations in the absence of modulation (the natural noise level) was augmented. This led to the conclusion that temperature fluctuations were increased and this diminished the sharpness of the resonance. A few

cold flow tests were also carried out at a pressure of 3 MPa by injecting liquid oxygen and gaseous nitrogen. The resonance was in that case quite sharp and it was possible to image the jet motion induced by the transverse mode.

Experiments carried out on the multiple injector combustor were complemented with simulations. These are carried out in the LES framework which offers a compromise between the cost and precision of the description. LES is well suited to the analysis of acoustic coupling with combustion. Calculations were first focused on the cold flow case but in the case of gaseous injection. It was possible to examine the collective motion induced by transverse oscillations and to quantify the mixing enhancement induced by the periodic modulation. A model was then proposed to deal with the nonpremixed flames prevailing in cryogenic combustion. The filtered burning rate is calculated explicitely from the mixture fraction variable and it is distributed in the vicinity of the flame. The RBR (reconstructed burning rate) model was introduced in the AVBP code and some initial calculations were carried out. Results indicate that the model could be used to study the interaction between acoustics and combustion.

The influence of high frequency external modulation on reactive jets and multiple shear layers has been numerically examined. The transversally modulated reactive jet behavior was compared with an experiment carried out at EM2C on a multiple injector nonpremixed combustor. Multiple shear layers interacting with acoustic modulation feature a coalescence of the larger scale vortices which takes place successively in the top and in the bottom part of the modeled chamber, and is synchronized by the external excitation.

A theoretical model was proposed to describe observed transverse instabilities. The model features the role of velocity through a new interaction term involving the transverse velocity perturbation and its direction. This model assumes that the coupling between the modulations and the interactions are linear which means that the combustion instabilities and the external modulations are linked phenomena occurring at the same frequency. Another model was considered to analyze effects of temperature fluctuations on the resonance characteristics of the system. Direct simulations and an amplitude-phase representation deduced by applying the method of averaging indicated that the sharpness of resonance was reduced and the response level was diminished.

Perspectives

Research described in the present report has led to progress in the understanding of the mechanisms involved in high frequency instabilities. However, there are still many open questions and they deserve to be the subject of further consideration. Since the problem is so complex, the effort should be carried out in a combined manner at the experimental level and in the domains of simulation and modeling. In terms of experiments, the new injection head including five injectors has been used in high pressure hot fire tests described in this document. The objective of future experiments will be to explore in a more systematic fashion the high pressure range (6 MPa). Tests carried out up to now have only allowed to demonstrate their feasibility. This range of pressures deserves further exploration since in this situation the pressure exceeds the critical pressure of oxygen (5.04 MPa) and the coupling involves in this case a propellant injected under transcritical conditions. For this new series of hot fire tests, it will be necessary to solve the problem of the level of modulation that can be reached in the system. It has been observed that the amplitudes generated under high chamber pressure conditions were lower than what was expected. To this purpose, one should plan to improve the toothed wheel modulator and its specificied dimensions and mechanical positioning.
It is also proposed to change the general configuration of this system. The new arrangement imagined to this purpose is designated as VHAM (VHAM: Very High Amplitude Modulator). In its principle, this system is conceived to modulate the total mass flow rate injected in the chamber by making use of an arrangement in which two nozzles are blocked alternately. This may allow to generate the levels of modulation of the order of 25 % of the mean pressure. Such very high levels of fluctuations are typically observed in self-sustained instabilities. The VHAM should allow to reach coupling conditions in the very large amplitude range where nonlinear effects become important. In this situation the high frequency unsteady motion will dominate the other types of fluctuations. It will be necessary to perform systematic hot fire tests to find conditions of maximum receptivity of flames to external perturbations. It would also be interesting to pursue cold flow studies to examine the effect of transverse oscillations on the injected streams of propellants. Here again it would be timely to operate in the high pressure transcritical regime. This might give results which could be useful for validation of large eddy simulations in which the transcritical (real gas) behavior of propellants is taken into account.

At the simulation level, the development of a combustion model deserves to be consolidated by further calculations and improvements of various sub-models. It will then be possible to launch realistic calculations of the coupling between transverse modes and cryogenic combustion. One might use to this purpose current developments carried out in a separate project associating EM2C and CERFACS.

On the modeling side, the two problems envisaged in the present work deserve further and more complete exploration. It would be interesting to introduce the coupling model in a multidimensional simulation code. The other problem concerning effects of temperature fluctuations on the resonance sharpness has been treated in an elementary way. It would be possible to envisage a more realistic modeling which would allow a better estimation of turbulence effects on the development of instabilities.

The final objective of all these additional investigations is the development and demonstration of predictive methods for high frequency combustion instabilities which could be used in engineering design and analysis of liquid rocket engines.

Conclusions

Les travaux décrits dans ce document sont centrés sur les interactions de flammes multiples avec des modulations acoustiques transverse en vue d'une application à l'analyse des instabilités à haute fréquence des moteurs fusées à propulsion liquide. Les essais en combustion cryotechnique prévus sur la chambre à injection multi-injecteurs (MIC) sont spécifiquement conçus pour permettre ce type d'investigation. La géométrie de ce système a été définie pour permettre une bonne séparation des modes longitudinaux et transverses. La chambre recrée de façon évidemment partielle les conditions qui existent dans les moteurs fusées et elle est notamment équipée de plusieurs injecteurs. L'objectif des études expérimentales menées sur cette configuration était de fournir des donnée sur des phénomènes de couplage semblables à ceux observés dans des moteurs réels.

Sur le plan expérimental, une première série d'essais a été réalisé sur le banc Mascotte de l'ONERA muni de la chambre multi-injecteurs (MIC) fonctionnant dans la gamme des basses pressions (0.9 MPa). L'identification modale a été réalisée de façon systématique. Les fréquences propres expérimentales ont été comparées à des calculs tri-dimensionnels effectués avec le code MESA-3D. Les simulations numériques des modes acoustiques ont permis de mieux comprendre la réponse acoustique du système. Le couplage entre la chambre principale et la tuyère secondaire utilisée par le modulateur fait apparaître un mode supplémentaire entre le premier mode longitudinal et le premier mode transverse propres à la chambre. Cette analyse numérique a été confirmée expérimentalement et elle a permis une identification plus fiable des modes observés au cours des essais à feu.

Une étude systématique a montré qu'un couplage fort pouvait être induit dans certaines conditions (ce résultat a été obtenu en faisant varier les conditions d'injection de l'ergol gazeux) et il a été possible de rassembler des indications précieuses sur ce phénomène. Ces résultats ont été obtenus après une optimisation de la roue utilisée pour la modulation. Un nouveau système avec un meilleur ajustement mécanique a été conçu et mis en oeuvre. la modulation a été appliquée au débit ejecté par la tuyère secondaire qui représente 15 % du débit masse principal. Cette tuyère est bloquée de façon périodique par la roue tournante. La position relative de la roue et de la tuyère secondaire est apparue comme un des paramètres clés pour obtenir des niveaux de fluctuation de pression élevés et cette position a été ajustée au plus près durant les essais.

Diverses conditions d'injection ont été testées pour déterminer les valeurs des paramètres conduisant au couplage le plus fort entre l'acoustique et la combustion. Le debit masse de méthane a été fixé

successivement à des valeurs de 50, 70 and 100 g s^{-1} avec des températures d'injection de 280 K et 180 K. Les niveaux de fluctuation les plus élevés ont été obtenus pour des vitesses d'injection faibles et une température proche de l'ambiante.En présence d'une modulation à la fréquence du premier mode transverse (i.e. 2345 Hz), le niveau de fluctuation atteint 7.5 % de la pression chambre. Le niveau maximum observé était d'environ 0.9 bar crête-crête. Ce niveau de fluctuation ne pouvait être soutenue sans l'action de la roue de modulation.
La réponse à l'excitation externe est caractérisée par trois phénomènes : (1) le taux d'expansion de la flamme, (2) l'augmentation du dégagement de chaleur volumétrique et (3) le taux d'expansion et la vitesse de convection des structures réactives. Le taux d'expansion a été caractérisé au moyen d'images du rayonnement du radical OH*. L'angle d'expansion est doublé. L'intensité de l'émission de ce radical augmente aussi de façon significative d'un facteur 3. Cela montre que le taux de combustion volumètrique est aussi plus important. Une autre indication vient des observations de la température de paroi qui augmente rapidement. Les visualisations à grande vitesse par caméra rapide montrent une modification des structures réactives. la vitesse de convection de ces structures est notablement réduite. Un mouvement transverse est clairement observé dans les films à grande vitesse. Les relations de phase entre les signaux de pression détectés au niveau des parois et le dégagement de chaleur déduit de l'observation de l'émission de lumière indiquent que ces deux quantités possèdent des structures spatiales semblables.
Les expériences réalisées dans le cadre de ce travail ont donné des indications sur les effets de paramètres d'injection mais l'influence respective du rapport de mélange E et du rapport des débits de quantité de mouvement J sur la stabilité reste à élucider. Les interactions entre les fluctuations de pression et la combustion ont pu être étudiées en optimisant les paramètres d'essais mais des données supplémentaires étaient nécessaires.

La deuxième série d'essais, principalement réalisée dans des gammes de pression intermédiaire et élevée constitue une suite logique des essais à basse pression. Une des conclusions de ces essais avait été qu'il fallait augmenter le nombre d'injecteurs, ceci pouvait permettre d'obtenir une distribution plus uniforme du dégagement de chaleur dans la chambre. Une configuration comportant plus d'injecteurs serait aussi plus proche des géométries de fond de chambre des moteurs fusées. Ce changement était aussi possible car la tête d'injection devait être améliorée pour éviter les fuites qui avaient conduit à plusieurs reprises à des incidents en cours d'essais et à sa destruction finale.

Une nouvelle tête d'injection comportant cinq injecteurs au lieu de trois a été conçue et réalisée par l'ONERA et ce nouveau système a été utilisé dans tous les essais de la deuxième série. Chaque injecteur était alimenté avec le même débit masse d'oxygène liquide que lors de la campagne précédente avec comme conséquence une augmentation de 65 % de la puissance dégagée. La nouvelle tête devait ainsi permettre une meilleure représentation du fond de chambre des moteurs fusées avec une augmentation de la puissance volumique dégagée dans la chambre. Des méthodes d'imagerie numérique étaient installés pour examiner la dynamique des flammes et analyser les modifications associées à la modulation externe. L'évolution temporelle était obtenue à partir d'une caméra rapide observant la totalité de la chambre. Les résultats d'essais à 3 MPa sont généralement semblables à ceux trouvés à plus basse pression mais il a aussi été noté que les caractéristiques de résonance du système étaient

modifiées et que la réponse à la modulation appliquée était plus faible. Dans le même temps le niveau des fluctuations de pression en l'absence de modulation (le bruit de combustion naturel) était augmenté. Ces observations nous ont conduits à conclure que l'intensité des fluctuations de température avait augmenté et que cela avait réduit la finesse de la résonance.
Quelques essais à froid ont aussi été réalisés à une pression de 3 MPa en injectant de l'oxygène liquide et de l'azote gazeux. La résonance était dans ce cas très marquée et il était possible d'observer le mouvement collectif des jets d'oxygène en présence de la modulation acoustique transverse.
Les expériences réalisées sur la chambre multi-injecteurs ont été complétées par des simulations. Les calculs sont effectués dans le cadre de la SGE qui offre un bon compromis entre le coût et la précision. La SGE est bien adaptée à l'analyse du couplage acoustique avec la combustion. Les calculs ont d'abord porté sur un cas à froid en présence d'une injection purement gazeuse. Il a été possible d'examiner le mouvement collectif induit par des oscillations transverses et de mesurer l'augmentation du mélange qui résulte de la modulation. Un modèle a été proposé pour traiter la combustion non-prémélangée qui prévaut dans le cas des flammes cryotechniques. Le taux de combustion filtré est calculé de façon explicite à partir de la fraction de mélange et il est distribué au voisinage de la flamme. Ce modèle a été introduit dans le code AVBP et des premiers calculs encourageants ont été réalisés. Les résultats montrent que le modèle peut être utilisé pour étudier les interactions entre l'acoustique et la combustion dans des configurations comportant plusieurs flammes.

Un modèle théorique a été proposé pour décrire les instabilités transverses. Ce modèle fait intervenir la vitesse au travers d'un terme d'interaction impliquant les perturbations de vitesse transverse et leur direction. Ce modèle suppose que le couplage entre les fluctuations acoustiques et la combustion instationnaire se fait de façon linéaire ce qui implique que les oscillations de combustion et celles du champ acoustique sont des phénomènes liés ayant la même fréquence. Le modèle permet de retrouver la structure spatiale du dégagement de chaleur observée dans des expériences antérieures sur des oscillations auto-entretenues à haute fréquence. Un autre modèle a été étudié pour analyser les effets de fluctuations de température sur les caractéristiques de résonance du système. Des simulations numériques et une analyse en amplitude-phase fondée sur les méthodes de moyenne indique que la finesse de la résonance est effectivement réduite et que la réponse est diminuée.

Perspectives

Les travaux qui viennent d'être décrits ont permis de progresser dans la connaissance des mécanismes qui interviennent dans le développement des instabilités haute-fréquence. Cependant un certain nombre de questions restent ouvertes et méritent d'être traitées. Comme le problème est complexe, l'effort doit être mené de façon combinée au niveau expérimental et dans les domaines de la simulation numérique et de la mondélisation. Sur le plan expérimental, le nouveau système d'injection comporte cinq éléments et une première série d'essais a été réalisée. Les résultats sont décrits dans ce document. L'objectif pour les essais à venir sera d'explorer la gamme des paramètres accessibles de façon plus sytématique notamment dans le domaine des hautes pressions (6 MPa). Les essais réalisés aux pressions élevées ont simplement permis de démontrer la faisabilité. Ce domaine mérite d'être exploré car dans cette situation la pression est supérieure à la valeur critique pour l'oxygène (5.04 MPa) et le couplage implique dans ce cas un ergol injecté dans des conditions transcritiques. Pour mener ces essais il faut au préalable résoudre le problème du niveau de modulation acoustique du système. On a vu que les amplitudes obtenues dans la gamme des hautes pressions étaient plus faibles que celles qui pouvaient être espérées. A cet effet, il faudrait d'une part améliorer encore la roue de modulation et son dimensionnement. Il faut aussi changer la configuration générale du système. La nouvelle disposition imaginée a été désignée sous le nom de VHAM (VHAM : "Very High Amplitude Modulator"). Dans son principe ce système est conçu pour moduler la totalité du débit masse qui passe dans la chambre de combustion en utilisant un arrangement dans lequel on bloque deux tuyères de façon alternée. On doit pouvoir ainsi augmenter le niveau de modulation pour atteindre des valeurs de l'ordre de 25 % de la pression moyenne. Ces niveaux d'amplitude très élevés sont typiquement ceux que l'on observe dans le cas d'instabilités auto-entretenues. Le VHAM devraient permettre d'atteindre les conditions d'un couplage entre les modes transverses et la combustion dans le domaine des amplitudes très élevées, c'est à dire dans un domaine où les effets non-linéaires seront importants. Dans cette situation le mouvement instationnaire haute-fréquence dominera les autres types de fluctuations. Il restera alors à réaliser des essais systématiques permettant de trouver les conditions dans lesquelles les flammes sont les plus sensibles aux perturbations externes. Il serait aussi intéressant de poursuivre les travaux déjà réalisés à froid pour étudier l'effet des oscillations transverses sur les jets d'ergols. Là encore, il serait crucial d'étudier des conditions d'injection transcritiques. Ces résultats pourraient être très utiles à la validation de simulations aux grandes échelles avec une prise en compte du comportement transcritique des ergols.

Au niveau de la simulation, le développement du modèle de combustion mérite d'être consolidé par des

calculs supplémentaires et l'amélioration de certains sous-modèles. Il sera alors possible d'effectuer des calculs réalistes du couplage entre les modes acoustiques transverses et la combustion d'ergols cryotechniques. On utilisera à cet effet les développement d'outils de simulation aux grandes échelles qui sont actuellement menés en parallèle dans le cadre d'un autre projet de recherche regroupant le CERFACS et EM2C.

Au niveau de la modélisation, les deux problèmes envisagés dans le présent travail méritent d'être explorés d'une façon plus complète. Il serait possible d'introduire le modèle de couplage dans un code de simulation multidimensionnelle. L'autre problème, celui des effets des fluctuations de température sur les caractéristiques de résonance, a été traité ici au moyen d'un modèle élementaire. On pourrait envisager une modélisation plus réaliste pour mieux estimer les effets de la turbulence sur le développement des instabilités.

L'objectif final des travaux envisagés pour la suite est la mise au point de méthodes de prévision des instabilités de combustion, utilisables dans la chaîne de conception des moteurs à ergols liquides.

Bibliography

Air Liquide (2002). *Gas Encyclopedia*. Elsevier / L'Air Liquide.

Aldama, A. A. (1990). *Filtering techniques for turbulent flow simulations*. New York, Springer.

Anderson and V. Yang (1995). *Liquid Rocket Engine Combustion Instability*, Volume 169. AIAA, Washington.

Barrère, M. and J. Corbeau (1963). *Combustion And Propulsion - Fifth AGARD Colloquim*, Chapter Les instabilités de combustion dans les fusées à propergol liquide, pp. 637–692. Oxford: Pergamon Press.

Bazarov, V. G. and V. Yang (1998). Liquid-propellant rocket engine injector dynamics. *Journal of Propulsion and Power 14*(5), 797–806.

Blaisot, J. B., C. Dumouchel, F. Baillot, and G. Boisdron (2004, September). Interaction between an air assisted jet and an acoustic field. In *19th Annual European Conference on Liquid Atomisation and Sprays Systems, ILASS*, Nottingham (UK).

Bogolioubov, N. and I. Mitropolski (1962). *Les méthodes asymptotiques en théorie des oscillations non linéaires.* Paris: Gauthier-Villars.

Breisacher, K. J. and R. J. Priem (1988). Analysis of 5 kHz combustion instabilities in Methane/LOx combustion chambers. Technical report, NASA - 25th JANNAF Combustion Meeting.

Burnley, V. S. and F. E. Culick (2000). Influence of random excitations on acoustic instabilities in combustion chambers. *AIAA Journal 38*(8), 1403–1410.

Candel, S. (1992). Combustion instabilities coupled by pressure waves and their active control. *Proceedings of the Combustion Institute 24*, 1277–1296.

Candel, S. (2003). Combustion dynamics and control: Progress and challenges (Hottel Lecture). *Proceedings of the Combustion Institute 29*, 1–28.

Candel, S., G. Herding, R. Snyder, P. Scouflaire, C. Rolon, L. Vingert, M. Habiballah, F. Grisch, M. Péalat, P. Bouchardy, D. Stepowski, A. Cessou, and P. Colin (1998). Experimental investigation of shear-coaxial cryogenice jet-flame. *Journal of Propulsion and Power 14*, 826–834.

Candel, S., M. Juniper, G. Singla, P. Scouflaire, and C. Rolon (2006). Structure and dynamics of cryogenic flames at supercritical pressures. *Combustion Science and Technology* (178), 161–192.

Candel, S. and T. Poinsot (1987). A tutorial on acoustics. Technical report, Ecole Centrale Paris, Châtenay-Malabry.

Chehroudi, B., D. Davis, and D. Talley (2003). Initial results from a cryogenic coaxial injector in an acoustic field. *AIAA Paper 2003-1339*.

Cheuret, F. (2005). *Instabilités thermo-acoustiques de combustion haute-fréquence dans les moteurs fusées*. Ph. D. thesis, Université de Provence - Aix-Marseille I.

Clavin, P., J. S. Kim, and F. A. Williams (1994). Turbulence-induced noise effects on high-frequency combustion instabilities. *Combustion Science and Technology 96*(1-3), 61–84.

Colin, O. and M. Rudgyard (2000). Development of high-order Taylor-Galerkin schemes for unsteady calculations. *Journal of Computational Physics 162*(2), 338–371.

Conrad, T., A. Bibik, D. Shcherbik, E. Lubarsky, and B. T. Zinn (2004). Control instabilities in liquid fueled combustor by modification of the reaction zone unsing smart fuel injector. *AIAA Paper 2004-4029*.

Cook, A. W. (1997). Determination of the constant coefficient in scale similarity models of turbulence. *Physics of Fluids A 9*(1485-1487).

Cook, A. W. and W. K. Bushe (1999). A subgrid-scale model for the scalar dissipation rate in non-premixed combustion. *Physics of Fluids A 11*, 746–748.

Cook, A. W. and J. J. Riley (1994). A subgrid model for equilibrium chemistry in turbulent flows. *Physics of Fluids A 6*, 2868–2870.

Crocco, L. and S.-I. Cheng (1954). High frequency combustion instability in rockets with distributed combustion. pp. 865–879.

Crocco, L., J. Grey, and D. T. Harrje (1958). On the importance of the sensitive time lag in longitudinal high-frequency rocket combustion instability. *Jet Propulsion 28*(12), 841–843.

Crow, S. C. and F. H. Champagne (1971). Orderly structure in jet turbulence. *Journal of Fluid Mechanics 48*(3), 547–591.

Culick, F. E. and V. Yang (1995). Overview of combustion instabilities in liquid-propellant rocket engines. *Liquid Rocket Engine Combustion Instability 169 Progress in Astronautics and Aeronautics*, 3–37.

Delhaye, B., D. Veynante, S. M. Candel, and H. H. Minh (1994). Simulation and modeling of reactive shear layers. *Theoretical and computational fluid dynamics 6*(2-3), 67–87.

Fisher, S., F. Dodd, and R. Jensen (1995). *Scaling Techniques for Liquid Rocket Combustion.* "Liquid Rocket Engine Combustion Instability", pp. 545-564, Vol.169 - AIAA, Washington.

Freiziger, J. H. (1977). Large eddy simulations of turbulent flows. *AIAA Journal 15*(9), 1261–1267.

Gao, F. (1993). A large-eddy simulation scheme for turbulent reacting flows. *Physics of Fluids 5*, 1282–1284.

Harrje, D. and F. Reardon (1972). Nasa SP-194. *Liquid Propellant Rocket Combustion Instability*.

Herding, G., R. Snyder, C. Rolon, and S. Candel (1998). Investigation of cryogenic propellant flames using computerized tomography of OH emission images. *Journal of Propulsion and Power 13*, 146–151.

Herding, G., R. Snyder, P. Scouflaire, C. Rolon, and S. Candel (1996). Flame stabilization in cryogenic propellant combustion. *Proceedings of the Combustion Institute 26*, 2041–2047.

Ho, C. M. and P. Huerre (1984). Perturbed free shear layers. *Ann. Rev. Fluid Mech. 16*, 365–424.

Hussein, H. J., S. P. Capp, and W. K. George (1994). Velocity measurements in a high-reynolds-number , momentum-conserving, axisymmetric, turbulent jet. *Journal of Fluid Mechanics 258*, 31–75.

Ierardo, N., A. Accettura, A. Congiunti, F. Cuoco, C. Bruno, and E. Giacomazzi (2001). LOx-HC : Current Status and Modeling of Supercritical Injectors. *IAF-01-S.3.07*.

Janardan, B. A., B. R. Daniel, W. A. Bell, and B. T. Zinn (1979). Measurements of reactive gaseous rocket injector admittances. *Combustion Science and Technology 20*(5-6), 185–193.

Jay, S., F. Lacas, and S. Candel (2006). Combined surface density concepts for dense spray combustion. *Combustion and Flame 144*, 558–577.

Jensen, R. J., S. E. Claflin, and H. Dodson (1990). Liquid oxygen/methane combustion instability investigation. Technical report, Rocketdyne Division - Rockwell International.

Juniper, M. (2001). *Structure et stabilisation des flammes cryotechniques*. Ph. D. thesis, Ecole Centrale Paris.

Juniper, M. and S. Candel (2003). Edge diffusion flame stabilization behind a step over a liquid reactant. *Journal of Propulsion and Power 19*(3), 332–341.

Juniper, M., N. Darabiha, and S. Candel (2003). The extinction limits of a hydrogen counterflow diffusion flame above liquid oxygen. *Combustion and Flame 135*(1-2), 87–96.

Juniper, M., A. Tripathi, P. Scouflaire, C. Rolon, and S. Candel (2000). Structure of cryogenic flames at elevated pressures. *Proceedings of the Combustion Institute 28*, 1103–1109.

Kalmykov, G. P. and S. V. Mossolov (2000). Liquid rocket engines working on oxygen + methane for space transportation systems of the XXI century (on the results of scientific and experimental studies). *IAF-00-S.2.10*.

Kendrick, D., G. Herding, P. Scouflaire, C. Rolon, and S. Candel (1998). Effet du retrait sur la stabilisation des flammes cryotechniques. *Comptes Rendus de l'Académie des Sciences 326*(Série IIb), 111–116.

Kendrick, D., G. Herding, P. Scouflaire, C. Rolon, and S. Candel (1999). Effects of a recess on cryogenic flame stabilization. *Combustion and Flame 118*, 327–339.

Laverdant, A. M., T. Poinsot, and S. M. Candel (1986). Mean temperature-field effect on acoustic mode structure in dump combustors. *Journal of Propulsion and Power 2*(4), 311–316.

Lawhead, R. B. (1961). Photographic studies of combustion processes in liquid propellant rockets. In *Proceedings of the Combustion Institute*, Volume 8, pp. 1140–1151.

Lieuwen, T. and V. Yang (2005). *Combustion instabilities in gas turbine engines. Progress in Astronautics and Aeronautics*, Volume 210. AIAA, Washington.

McManus, K., T. Poinsot, and S. Candel (1993). A review of active control of combustion instabilities. *Progress in Energy and Combustion Science 19*, 1–29.

Meneveau, C., T. Lund, and W. Cabot (1996). A lagrangian dynamic subgrid-scale model of turbulence. *Journal of Fluid Mechanics 319*, 353.

Moin, P., K. Squires, and S. Lee (1991). A dynamic subgrid scale model for compressible turbulence and scalar transport. *Physics of Fluids A 3*, 2746–2757.

Muss, J. A. and J. L. Pieper (1988). Performance and stability characterization of LOx/Hydrocarbon injectors. *AIAA Paper 88-3133*.

Nottin, C. (2002). *Développement de méthodes de prévision des instabilitiés de combustion dans les foyers prémélangés*. Ph. D. thesis, Ecole Centrale Paris.

Oefelein, J. C. and V. Yang (1993). Comprehensive review of liquid-propellant combustion instabilities in F1 engines. *Journal of Propulsion and Power 9*(5), 657–677.

Oefelein, J. C. and V. Yang (1998). Modeling high-pressure mixing and combustion processes in liquid rocket engines. *Journal of Propulsion and Power 14*(5), 843–857.

Ongoren, A. and D. Rockwell (1988). Flow structure from an oscillating cylinder - part 2: Mode competition in the near wake. *Journal of Fluids Mechanics 191*, 225–245.

Oschwald, M. and M. M. Micci (2002). Spreading angle and centerline variation of density of supercritical nitrogen jets. *Atomization and Sprays 12*(1-3), 91–106.

Oschwald, M., J. J. Smith, R. Branam, J. Hussong, A. Schik, B. Chehroudi, and D. Talley (2006). Injection of fluids into supercritical environments. *Combustion Science and Technology 178*(1-3), 49–100.

Pempie, P., T. Frohlich, and H. Vernin (2001). LOx/Methane and LOx/Kerosene high thrust engine trade-off. *AIAA Paper 2001-3542*.

Peters, N. (1983). Local quenching due to flame stretch and non-premixed turbulent combustion. *Combustion Science and Technology 30*, 1.

Philippart, K. D. and M. D. Moser (1988). Stability analyses of liquid oxygen/methane injectors using current available analytical tools. *AIAA Paper 88-2851*.

Poinsot, T. and D. Veynante (2005). *Theoretical and numerical combustion*. Philadelphia, PA: R. T. Edwards.

Pope, S. (1988). The evolution of surfaces in turbulence. *Int. Journal Eng. Sci. 26*, 445.

Pope, S. B. (2000). *Turbulent flows*. Cambridge, UK: Cambridge University Press.

Réveillon, J. and L. Vervisch (1996). Response of the dynamic LES model to heat release induced effects. *Physics of Fluids A 8*, 2248–2250.

Rey, C. (2004). *Interactions Collectives dans les Instabilités de Combustion Haute Fréquence. Application aux Moteurs Fusées à Ergols Liquides*. Ph. D. thesis, Ecole Centrale Paris.

Rey, C., S. Ducruix, and S. Candel (2002). Transverse acoustic forcing of a reacting mixing layer. In *9th International Conference on Numerical Combustiion*, Sorrento, Italy.

Rey, C., S. Ducruix, and S. Candel (2005, Feb). A method for the transverse modulation of reactive flows with application to combustion instability. *Combustion Theory and Modelling 9*(1), 5–22.

Rey, C., S. Ducruix, F. Richecoeur, P. Scouflaire, L. Vingert, and S. Candel (2004). High frequency combustion instabilities associated with collective interactions in liquid propulsion. *AIAA Paper 2004-3518*.

Rey, C., S. Ducruix, P. Scouflaire, and S. Candel (2002). Analysis of high frequency instabilities associated with collective interactions. In *7th French-German Colloquium on Liquid Propulsion*, pp. 17–18.

Richecoeur, F., P. Scouflaire, S. Ducruix, and S. Candel (2005, July). Experimental investigation of high frequency combustion instabilities. In *20th ICDERS*, Montreal, Canada.

Richecoeur, F., P. Scouflaire, S. Ducruix, and S. Candel (2006). High frequency transverse acoustic coupling in a multiple injector cryogenic combustor. *Journal of Propulsion and Power 22*(4), 790–799.

Sagaut, P. (2001). *Large eddy simulation for incompressible flows*. New York, Springer.

Schuller, T., D. Durox, and S. Candel (2002). Dynamics of and noise radiated by aperturbed impinging premixed jet flame. *Combustion and Flame 128*, 88–110.

Schuller, T., D. Durox, and S. Candel (2003). Self induced combustion oscillations of laminar premixed flames stabilized on annular burners. *Combustion and Flame 135*, 525–537.

Singla, G. (2005). *Etude des flammes cryotechniques oxygène liquide / méthane à haute pression*. Ph. D. thesis, Ecole Centrale Paris.

Singla, G., P. Scouflaire, C. Rolon, and S. Candel (2005). Transcritical oxygen/transcritical or supercritical methane combustion. *Proceedings of the Combustion Institute 30*, 2921–2928.

Singla, G., P. Scouflaire, C. Rolon, and S. Candel (2006a). Planar laser induced fluorescence of OH in high pressure cryogenic LOx/GH2 jet flames. *Combustion and Flame 144*, 151–169.

Singla, G., P. Scouflaire, C. Rolon, S. Candel, and L. Vingert (2006). OH PLIF and emission imaging in high pressure cryogenic LOx/Methane flames. *Journal of Propulsion and Power in press*.

Singla, G., P. Scouflaire, J. C. Rolon, and S. Candel (2006b). Flame stabilization in high-pressure LOx/GH_2 and GCH_4 combustion. *Proceedings of the Combustion Institute 31*.

Smagorinsky, J. (1963). General recirculation experiments with the primitive equations. I. The basic experiments. *Monthly Weather Review 91*, 99–164.

Snyder, R., G. Herding, C. Rolon, and S. Candel (1997). Analysis of flame patterns in cryogenic propellant combustion. *Combustion Science and Technology 124*, 331–370.

Takahashi, F. and V. R. Katta (1999). Stability-limit predictions of methane jet diffusion flames. *AIAA Paper 99-2781*.

Tamura, H., F. Ono, A. Kumakawa, and N. Yatsuyanagi (1987). LOx/Methane staged combustion rocket combustor investigation. *AIAA Paper 87-1856*.

Tamura, H., H. Sakamoto, M. Sasaki, M. Takahashi, T. Tomita, and W. Mayer (1995). An experimental study on the stability characteristics of the LOx/Methane rocket combustor. *AIAA Paper 95-2359*.

Tischler, A. O. and T. Male (1956). Oscillatory combustion in rocket-propulsion engines. *Gas Dynamics Symposium*, 71–81.

Trouvé, A., S. Candel, and J. W. Daily (1988). Linear stability analysis of inlet jets and shear layers. *24th Joint Propulsion Conference, AIAA Paper 88-0149, Boston, Massachusetts (1988).*

Vingert, L., P. Gicquel, D. Lourme, and L. Ménoret (1995). *Liquid Rocket Engine Combustion Instability*, Volume 169, Chapter Coaxial Injector Atomization, pp. 145–190. AIAA.

Vingert, L., M. Habiballah, P. Vuillermoz, and S. Zurbach (2000, October). Mascotte, a test facility for cryogenic combustion research at high pressure. In *51st International Astronautical Congress*, Rio de Janeiro.

Vreman, B., B. Geurts, and H. Kuerten (1994). Realizability conditions for the turbulent stress tensor in large eddy simulations. *Journal of Fluid Mechanics 278*, 351–362.

Williams, F. A. (1985). *Combustion Theory*. Menlo Park: Addislon-Wesley.

Wygnanski, I. and H. Fiedler (1969). Some measurements in the self-preserving jet. *Journal of Fluid Mechanics 38*, 577–612.

Zikikout, S., S. Candel, T. Poinsot, A. Trouvé, and E. Esposito (1986). High-frequency combustion oscillations produced by modes selective acoustic excitation. In *Proceedings of the Combustion Institute*, Volume 21, pp. 1427–1434.

Zurbach, S., J.-L. Thomas, P. Vuillermoz, L. Vingert, and M. Habiballah (2002). Recent advances on LOx/Methane combustion for liquid rocket engine injector. *AIAA Paper 2002-4321*.

Appendix A

Laboratory Scale Experiments

Abstract

The experiments presented in this part have been carried out at EM2C laboratory with the help of two engineering students Catherine Lasfille and Nicolas Routaboul of Ecole Centrale during their third year project. The following section based on their report is written in French. The objective is to analyze the coupling between two cavities separated by a perforated plate. The configuration idealizes what is found in a liquid rocket engine where the LOx dome and the chamber are connected by a shower head arrangement of injectors. Acoustic coupling of two cavities through a perforated separation is investigated in this simplified geometry. The number of holes and their diameter has been varied. The coupling is observed for a large number of holes in the chamber and the eigenmodes are described.

Résumé

L'expérience présentée dans cette annexe a été réalisée par deux élèves ingénieurs de l'Ecole Centrale, Catherine Lasfille et Nicolas Routaboul, dans le cadre de leur projet de synthèse de troisième année. Le chapitre est basé sur le rapport de projet qu'ils ont rédigé et est ainsi écrit en français. L'objectif est d'étudier le couplage entre deux cavités séparées par une plaque perforée. Cette configuration idéalise celle qui existe dans les moteurs fusées à liquide, dans lesquels le dôme LOx et la chambre sont reliés par un ensemble d'injecteurs disposés en pomme de douche. La couplage des deux cavités est réalisé par le biais d'une plaque perforée. Le nombre et le diamètre des trous est varié. Un couplage fort est observé lorsque le nombre de trous est suffisamment grand.

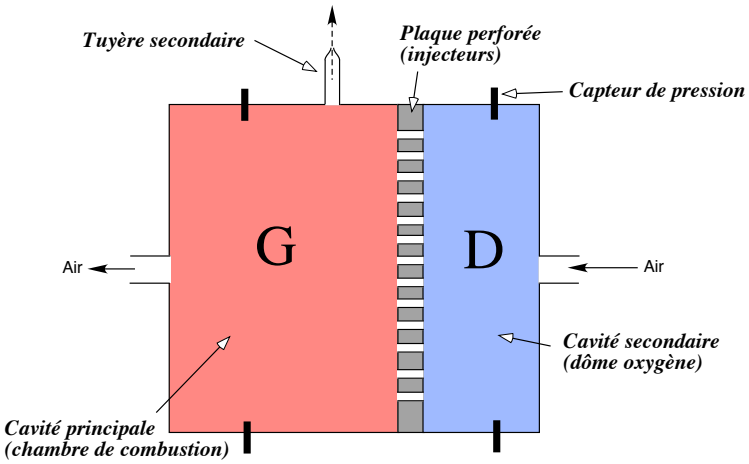

Fig. A.1: Schéma du boîtier expérimental utilisé

A.1 Introduction

Le programme de recherche dans lequel s'inscrit ce projet vise à reproduire certains des phénomènes qui peuvent intervenir dans l'apparition des instabilités de combustion haute fréquence dans les moteurs fusées à liquides. On cherche plus particulièrement à étudier le couplage acoustique entre le dôme d'injection oxygène et la chambre de combustion. Le moteur sera alors modélisé par 2 cavités séparées par une plaque perforée représentant la tête d'injection. L'expérience proposée est représentée schématiquement sur la figure A.1.
Grâce à une tuyère placée sur une face latérale de la cavité en aval de la plaque et obturée de manière périodique, on génère des oscillations de pression dans la partie représentant la chambre. Les fluctuations ainsi créées par cette excitation seront préférentiellement transverses. Le but est de mesurer la réponse en pression dans la cavité amont afin d'analyser l'éventuel couplage. Pour cela, on place des capteurs de pression dans chacune des cavités. On considère que le phénomène est réversible, c'est-à-dire que l'on pourra assimiler le comportement en amont causé par l'instabilité forcée à la situation qui provoque les instabilités dans la chambre de combustion en fonctionnement normal. On envisage ici les modes acoustiques en l'absence de combustion. La combustion amplifie mais ne modifie pas la structure des modes. On estime donc qu'une étude à froid du couplage acoustique entre les 2 cavités est représentative du comportement acoustique du système avec la combustion. Il faut cependant noter que les pertes de charge dans les injecteurs sont différentes de celle que l'on va établir dans la plaque perforée. L'expérience permet cependant de voir s'il y a couplage entre les cavités dans le cas d'une modulation transverse. On va donc chercher à travers cette expérience à retrouver expérimentalement les fréquences de résonance théoriques et vérifier que les modes d'excitation apparaissent dans le dôme oxygène.

Modes	1L	$1T_y$	2L
Frequences (Hz)	966	1691	1932

Tab. A.1: Dimensions du boîtier et fréquences des modes propres calculées analytiquement

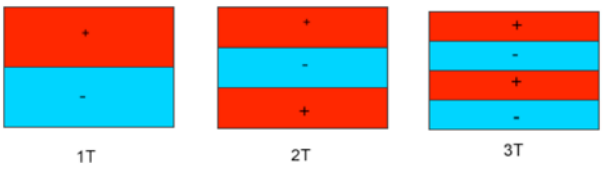

Fig. A.2: Champs de pression instantanés correspondants aux 3 premiers modes transverses

A.2 Protocole expérimental

A.2.1 Calcul des fréquences théoriques

Pour déterminer les domaines de fréquences dans lesquels les acquisitions seront effectuées, il est nécessaire de connaître les fréquences de résonance théoriques. On utilise pour cela l'équation d'Helmholtz. Les dimensions de la cavité G sont : $100\times175\times60$ mm^3 et les fréquences propres et les structures modales sont rassemblées respectivement dans le tableau A.1 et la figure A.2
Les modes transverses (1T, 2T, 3T...) ont des structures différentes. La pression du mode 1T est maximale sur une face et minimale sur l'autre. Pour le mode 2T, la pression est maximale (respectivement minimale) sur chacune des deux faces et elle passe par un minimum (respectivement un maximum) au milieu de la chambre. Le mode 3T présente les mêmes conditions aux limites en pression que le mode 1T.

A.2.2 Montage

Le dispositif est composé des éléments suivants :

- La boîte en acier composée de deux cavités représentant le dôme d'injection (D) et la chambre de combustion G du moteur. L'interface est une plaque percée de 3 ou 60 trous. La grande cavité est équipée de deux tuyères, l'une principale dans l'axe de l'écoulement, l'autre secondaire perpendiculairement à l'écoulement. Quatre bossages permettent de placer des capteurs de pression : on dispose de deux points de mesures dans la cavité avale et deux points de mesures dans la cavité amont.

- La roue excitatrice : cette roue dentée (50 dents) est placée au contact de la tuyère secondaire. Elle est entrainée par un moteur asynchrone. La roue bloque de façon périodique la tuyère secondaire.

- Les capteurs : la pression dans les cavités est mesurée â l'aide de capteurs de pression haute fréquence. La pression ambiante dans la boîte est mesurée à l'aide d'un manomètre. Cette pression relative peut être ajustée entre 0.5 et 3.5 bars.

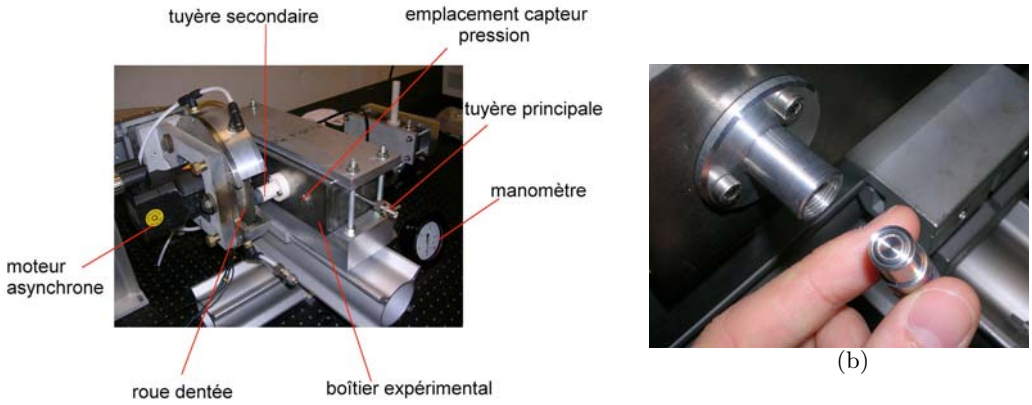

Fig. A.3: (a) Agencement des éléments de l'expérience - (b) Capteur de pression différentielle Kistler

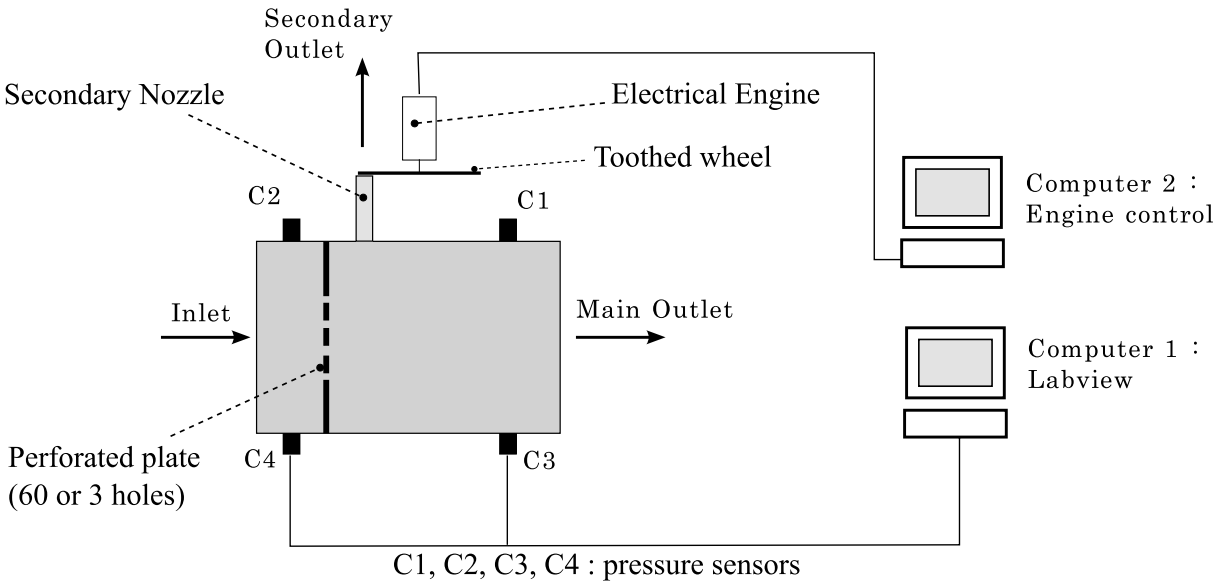

Fig. A.4: Schéma du dispositif expérimental

La figure A.3(a) présente l'agencement des différents éléments. La roue excitatrice doit être au contact de la tuyère secondaire, cependant la tuyère est trop courte et la place laissée entre le dispositif d'excitation et la boîte empêche d'installer l'un des deux capteurs de pression de ce côté. On ne pourra avoir que trois mesures simultanées. Pour avoir les deux mesures dans une même cavité qui indiqueront la phase, le montage expérimental sera modifié.

La chaine d'acquisition et de commande sont représentées sur le schéma de la figure A.4. Le programme Matlab de commande du moteur est installé sur le premier ordinateur. Ce programme permet de choisir le mode de fonctionnement de la roue : une rampe en fréquence ou une fréquence constante. Les signaux analogiques issus des capteurs sont traités au moyen d'une carte d'acquisition puis sur un deuxième ordinateur. On utilise le logiciel Labview pour piloter la cadence et la durée d'acquisition.

A.2.3 Acquisition

Connaissant les fréquences propres théoriques, les premières acquisitions sont effectuées en imposant une rampe en fréquence. La pente de cette rampe est de 100 Hz s^{-1} et la fréquence augmente linéairement jusqu'à une valeur maximale de 2 kHz. Au delà de 100 Hz.s^{-1}, la résonance n'a pas le temps de s'établir dans la chambre rendant son identification impossible. Selon le théorème de Shannon, pour observer un phénomène à une fréquence de 2 kHz, la fréquence d'acquisition minimale est de 4 kHz. L'acquisition est faite à une fréquence de 8192 Hz ou 16384 Hz car si une fréquence supérieure est utilisée le temps d'acquisition disponible devient trop court. Le but de ces acquisitions avec une rampe en fréquence est de déterminer la fréquence pour laquelle l'amplitude de l'oscillation de pression est maximale. On cherche notamment à caractériser les ondes transverses 1T et déterminer expérimentalement la fréquence de résonance de ce mode. Une excitation monofréquentielle à la fréquence déterminée pour ce mode permet de caractériser le comportement acoustique du système et surtout de savoir dans quelles conditions le mode 1T est capable de se propager de la cavité G vers la cavité amont D. Pour les expériences à fréquence fixe, la fréquence d'acquisition peut être maximale car une durée d'acquisition de 2 secondes est suffisante (contrairement à la rampe qui nécessite 16 secondes d'essai). La pression moyenne relative a été fixée à 1 bar (la pression est donc de 2 bar au niveau de l'alimentation) et la fréquence d'acquisition est prise égale à 32kHz.

A.2.4 Traitement

Le traitement numérique des signaux de pression est effectué à l'aide de MATLAB. Quatre programmes différents sont utilisés:

- Affichage : affiche les signaux bruts.
- Filtrage passe-bas : les signaux acquis sont filtrés pour éliminer les composantes haute fréquence.
- Spectre : Pour la rampe, un graphe donnant la fréquence en fonction du temps est tracé. L'amplitude de l'oscillation est représentée sur une échelle de couleurs. Le but est de visualiser la fréquence pour laquelle l'amplitude de la pression est maximale. La fréquence de résonance apparaît en rouge.
- Périodogramme : Lorsque la commande du moteur correspond à une valeur fixe, on calcule la densité spectrale de puissance au moyen de la méthode des périodogrammes.

A.3 Acquisition et Résultats

A.3.1 Acquisition sans excitation

Afin de comparer les signaux obtenus lors d'une excitation avec la roue dentée, on réalise une première acquisition de l'amplitude de la pression en l'absence d'excitation.
On observe un signal dont l'amplitude varie entre -0.003 et 0.003 bar. Une fréquence prédominante apparaît dans le spectre aux environs de 75 Hz (Fig.A.5).

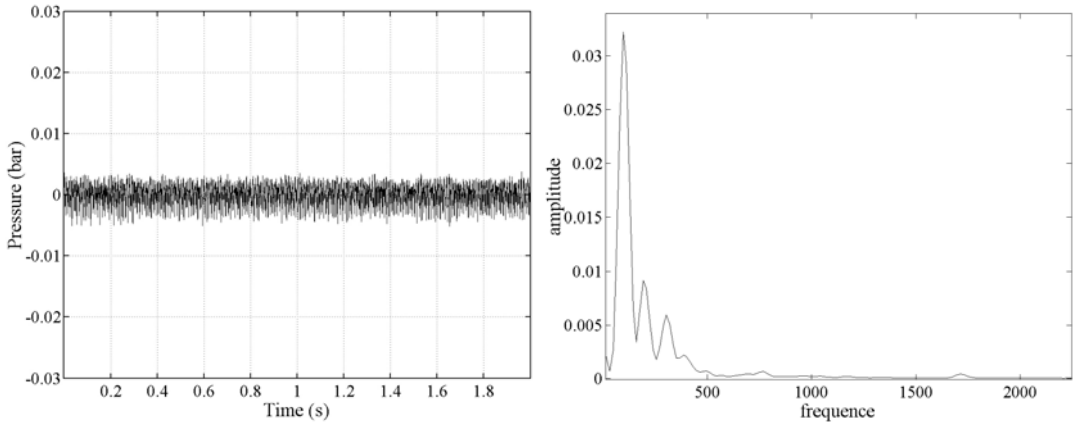

(a) (b)

Fig. A.5: Amplitude des oscillations dans la grande cavité sans excitation avec une fréquence d'acquisition de 16384 Hz (a) et son spectre (b)

A.3.2 Plaque de 60 trous

Plusieurs acquisitions ont été effectuées en faisant varier les paramètres (pression moyenne, fréquence d'acquisition, filtre numérique...).
Une évolution typique de la pression mesurée pendant un test durant lequel la chambre est soumise à une modulation de fréquence linéairement croissante est présentée Fig.A.6. Le signal bleu représente la pression mesurée par le capteur C3 et le signal rouge la pression mesurée par le capteur C4. Pour plus de clarté un offset de 0.05 bar a été ajouté entre les deux signaux, ainsi seule l'amplitude des oscillations est à observer. Les deux signaux ont une amplitude du même ordre de grandeur (0.01bar) sur la majeure partie de l'acquisition puis à environ 11 secondes, l'amplitude de la pression augmente de la même façon dans les deux cavités. La résonance est observée à deux fréquences relativement proches. L'amplitude des oscillations est doublée (0.02 bar). L'objectif est de connaître les fréquences correspondant à ces résonances. On utilise à cet effet une analyse temps-fréquence en accumulant des densités spectrales de puissances calculées sur des durées brèves.
La modulation linéaire en fréquence est retrouvée entre 8 et 12 secondes de l'acquisition (la pente est bien de 100Hz par seconde). Un doublet de fréquences pour lequel l'amplitude des oscillations de pression atteint un maximum est mis en évidence. Il correspond à des fréquences de 1720 et 1770 Hz. L'amortissement moyen d'une cavité rectangulaire combiné à une modulation fréquentielle à 100 Hz s^{-1} permet d'identifier le pic de résonance avec une précision voisine de 60 Hz. D'autre part, la transformée de Fourier effectuée sur 1024 points est précise à 50 Hz environ. Il s'agit donc probablement d'une seule et même résonance qui se situe entre les deux fréquences de 1720 et 1770 Hz. La fréquence du premier mode transverse calculée analytiquement est de 1691 Hz, le pic de résonance dans la grande cavité (environ 1750 Hz) correspond donc à ce mode.
Le même doublet de fréquences est retrouvé dans la petite cavité (Fig.A.7). Le mode 1T est donc parfaitement transmis de la grande à la petite cavité à travers la grille perforée de 60 trous.

L'excitation au moyen d'une rampe a permis de déterminer expérimentalement la fréquence de résonance

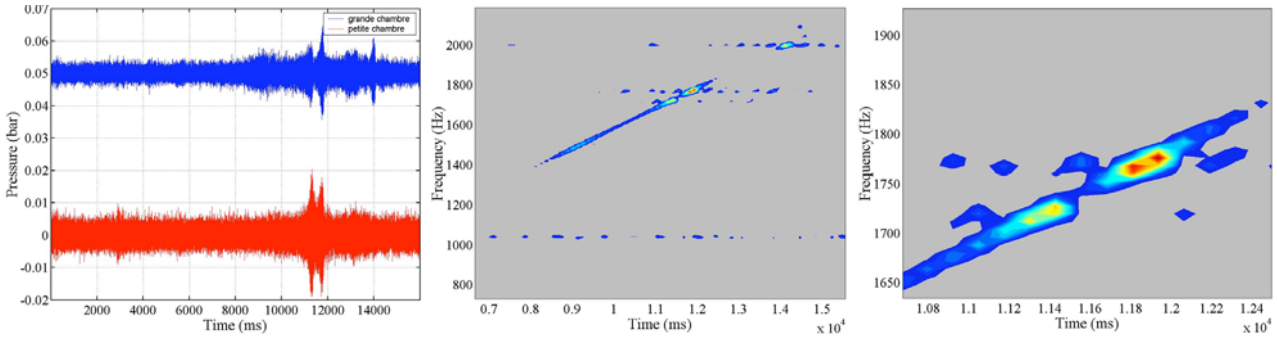

(a) (b) (c)

Fig. A.6: Amplitude des oscillations dans les 2 cavités au cours d'une excitation en rampe (100 $Hz.s^{-1}$) avec une fréquence d'acquisition de 8192 Hz (a) et la Transformée de Fourier du signal de pression dans la grande cavité (b) lors de la modulation linéaire en fréquence (c : zoom sur les pressions de forte amplitude). On utilise ici la plaque perforée à 60 trous.

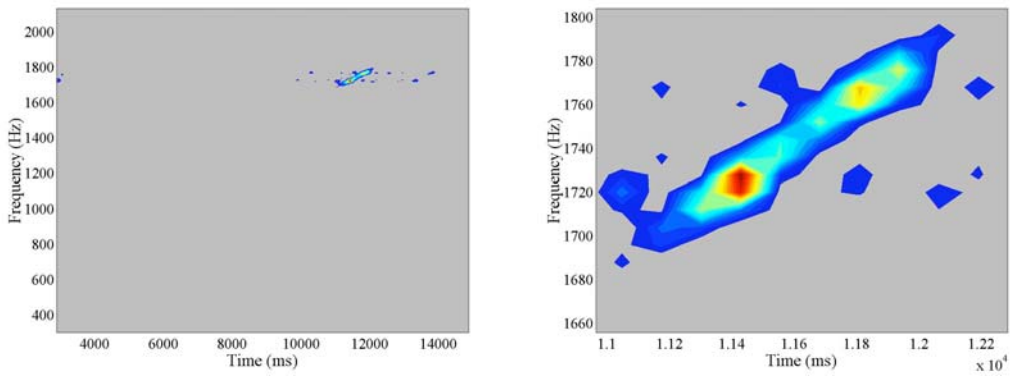

Fig. A.7: Transformée de Fourier du signal de pression dans la petite cavité (capteur C4) lors de la modulation linéaire en fréquence (à droite son zoom sur les pressions de forte amplitude)

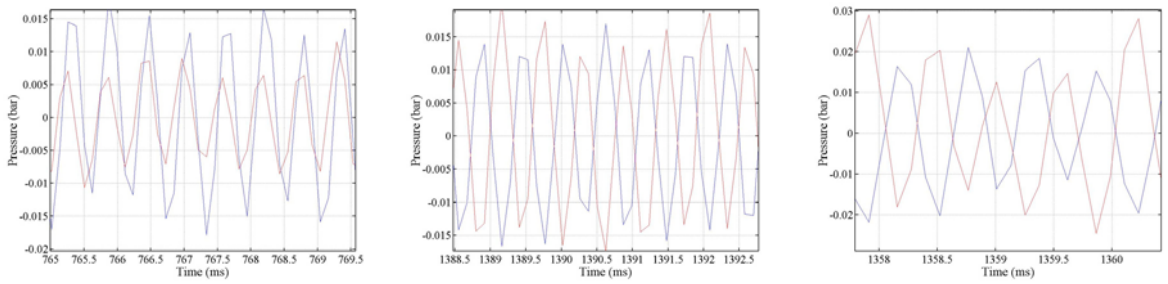

(a) (b) (c)

Fig. A.8: Amplitude des signaux de pression pour une fréquence d'acquisition de 8 kHz et une pression moyenne de 1 bar. a: signaux C3 et C4 (même face), b: signaux C1 et C3 (grande cavité et face opposée), c: signaux C2 et C4 (petite cavité et face opposée)

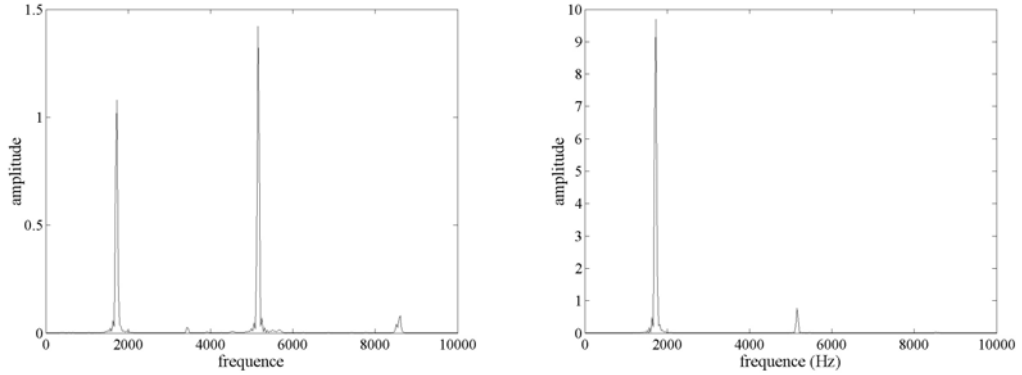

(a) (b)

Fig. A.9: Spectre du signal pour une fréquence d'acquisition de 32 kHz. a: grosse cavité (capteur C3), b: petite cavité (capteur C4)

du mode 1T. Une excitation à cette même fréquence est maintenant utilisée pour de caractériser le comportement acoustique du système. Pour cela, on observe la phase et le spectre des signaux.
Pour vérifier que le mode acoustique à 1720 Hz (ou à 1770Hz) correspond bien à un mode transverse, on représente les signaux issus des différents capteurs (Fig.A.8). Si ce mode correspond bien à un mode transverse (1T,3T...), les deux signaux doivent être en opposition de phase lorsque les capteurs sont placés l'un face à l'autre (Fig.A.8(b)-A.8(c)) et en phase lorsque les capteurs sont placés sur la même face de la boîte (Fig.A.8(a)). Les deux signaux sont bien en phase, ce qui confirme la théorie. Cependant un léger retard de phase de 0.1 ms du signal de la petite cavité est observé.
Les deux signaux sont bien en opposition de phase que ce soit pour la petite ou pour la grande cavité. Le mode acoustique observé est bien un mode transverse. Remarque : Les signaux ne sont pas parfaitement sinusoïdaux car la fréquence d'acquisition est relativement faible (8192 Hz) par rapport à la fréquence du mode transverse observé (1T).
En utilisant les périodogrammes, les spectres des signaux sont obtenus dans les deux cavités (Fig.A.9). Deux pics sont observés dans chaque cavité, le premier à 1750 Hz et le second à 5350 Hz. Ces fréquences correspondent aux modes transverses 1T et 3T respectivement. Des différences apparaîssent entre les

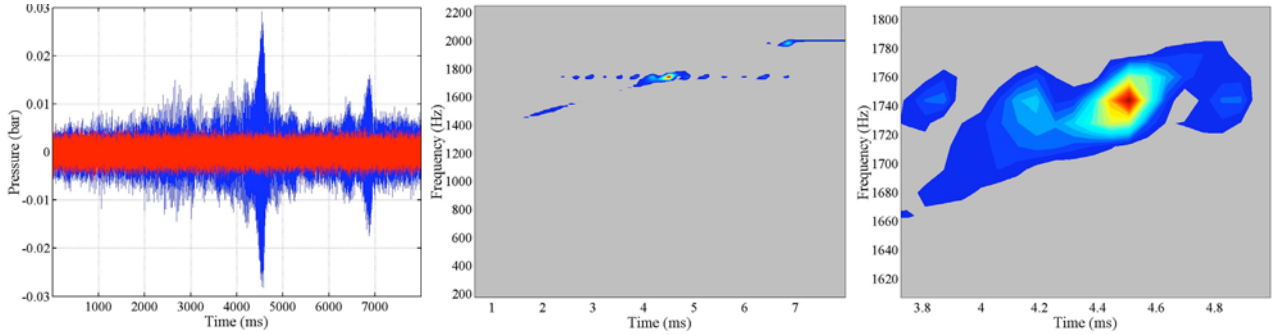

(a) (b) (c)

Fig. A.10: Amplitude des oscillations (gauche) dans les 2 cavités (bleu capteur C3 et rouge capteur C4) et la transformée de Fourier du signal de pression (au milieu et à droite) dans la cavité aval au cours d'une excitation en rampe (100 $Hz.s^{-1}$) pour la plaque perforée comportant trois trous avec une fréquence d'acquisition de 16384 Hz et une pression moyenne de 3 bars

deux cavités. L'amplitude du mode 3T de la petite cavité est plus faible que celle du mode 1T (amplitude de 10 pour le 1T et de 1 pour le 3T) alors que ces modes sont d'amplitude comparable dans la grande cavité (amplitude de 1 pour le 1T et de 1.5 pour le 3T). De plus la somme des amplitudes du spectre pour la petite cavité est bien supérieure à celle dans la grande cavité (11 dans la petite et 2,5 dans la grande). Ces différences d'amplitude ne sont pas un résultat global, d'autres acquisitions avec des paramètres différents (pression moyenne, différence de pression entre les cavités) présentent un mode 3T prépondérant. Le signal d'excitation obtenu par la roue fait apparaître la fréquence fondamentale mais il excite aussi des modes supérieurs et notamment le mode 3T. Ce résultat est inattendu mais néanmoins cohérent au vu de la structure semblable de ces deux modes. On trouve essentiellement des modes impairs dans les conditions utilisées pour ces expériences (1T, 3T et 5T). Les deux modes transverses présents par excitation dans la grande cavité sont aussi observés dans la petite et cela malgré la présence de la plaque de 60 trous.

A.3.3 Plaque comportant 3 trous

Les mêmes acquisitions ont été effectuées sur la boîte avec la plaque perforée de 3 trous.

Les signaux de pression obtenus pour une excitation en rampe sont tracés sur la figure A.10. Le signal bleu représente la pression mesurée par le capteur C3 et le signal rouge la pression mesurée par le capteur C4. Les deux signaux ont une amplitude de même ordre de grandeur (0.005 bars). Cependant une différence majeure apparaît, le signal dans la grande cavité (bleu) donne un pic de résonance alors que le signal de la petite cavité reste identique durant les 8 s d'acquisition. Lors d'une acquisition sans excitation (roue immobile), le signal dans la petite cavité reste d'ailleurs identique. La pression dans la petite cavité est donc peu affectée par l'excitation (sans excitation, l'amplitude est de 0.03 bar). L'objectif est de connaître la fréquence correspondant à cette résonance de la grande cavité.
Le résultat dans la grande cavité avec la plaque à 3 trous est comparable à celui obtenu avec la plaque à 60 trous, le mode 1T est retrouvé à 1750 Hz.

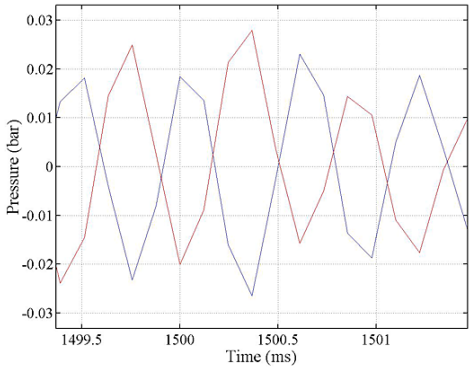

Fig. A.11: Signaux détectés par les capteurs C1 (bleu) et C3 (rouge) à gauche et transformée de Fourier du signal de pression dans la cavité amont lors de la modulation à 1720 Hz pour la plaque perforée de 3 trous

De même qu'avec la plaque à 60 trous, la fréquence d'excitation est prise égale à 1720 Hz (mode 1T). Pour vérifier que le mode acoustique à 1720 Hz correspond bien à un mode transverse on représente les signaux dans la grande cavité (Fig.A.11). Pour un mode tranverse 1T, les deux signaux doivent être en opposition de phase lorsque les capteurs sont placés l'un face à l'autre (C1 avec C3). Cette propriété est bien observée. Le mode acoustique dans la grande cavité est bien un mode transverse.

Avec la plaque comportant 3 trous les modes 1T et 3T sont excités dans la cavité G. Par contre, le mode transverse n'est plus observé dans la petite cavité et il n'émerge pas du bruit.

A.4 Influence des paramètres

A.4.1 La fréquence d'acquisition du signal

Le mode 1T (1700 Hz) est bien détecté avec une fréquence de 8 kHz A.12. Par contre les modes 3T (5100 Hz) et 5T (8500 Hz) ne peuvent être détectés avec une fréquence d'acquisition aussi faible (conformément au théorème de Shannon). Pour les mesures effectuées, la fréquence d'acquisition de 32kHz a été retenue car elle permet d'obtenir plus d'informations sur le contenu spectral des signaux.

A.4.2 Les niveaux de pression dans la cavité

On trouve ici les amplitudes mesurées dans la grande cavité pour des pressions moyennes différentes. L'amplitude des signaux augmente avec la pression moyenne: 0.02 bar pour une pression relative de 1 bar et 0.03 bar pour une pression de 2.5 bar.
Les spectres restent identiques : la pression moyenne ne modifie pas le comportement fréquentiel de la chambre. Les acquistions peuvent donc être faites avec différentes pressions moyennes sans que les

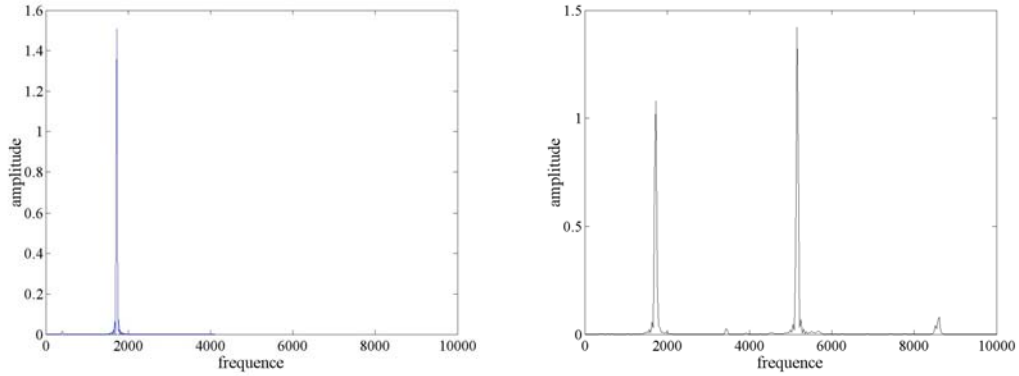

(a) (b)

Fig. A.12: Spectre du signal avec le capteur dans la grosse cavité et avec une fréquence d'acquisition de 8 kHz (a) et 32 kHz (b)

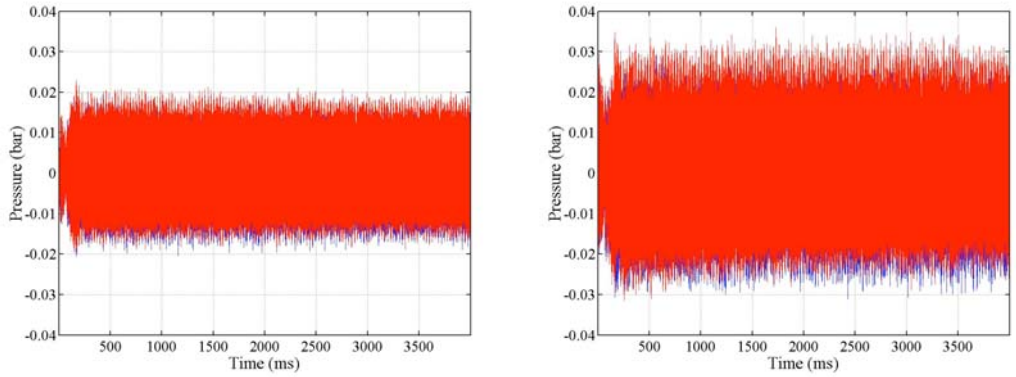

(a) (b)

Fig. A.13: Amplitude des signaux avec les capteurs dans la petite cavité avec une fréquence d'acquisition de 8 kHz et une pression moyenne de 1 bar (a) et de 2.5 bars (b)

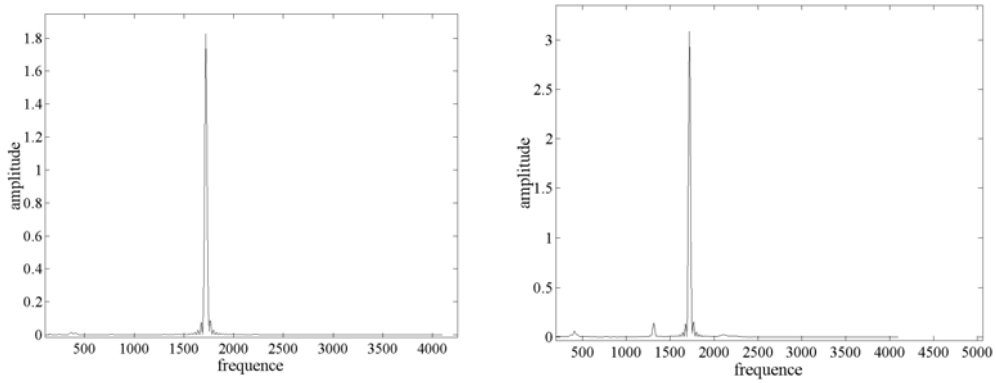

(a) (b)

Fig. A.14: Spectre du signal avec le capteur dans la petite cavité avec une fréquence d'acquisition de 8 kHz, une pression moyenne de 1 bar (a) et 2.5 bars (b)

fréquences de résonance soient modifiées.

A.5 Conclusion et perspectives

L'objectif était de mettre en évidence le couplage de deux cavités séparées par une plaque perforée lors d'une excitation d'un mode transverse dans la grande cavité. Les résultats montrent que les modes transverses remontent facilement lorsque la porosité du système séparant les deux cavités est grande (ici 60 trous) alors qu'ils sont difficilement identifiables lorsque cette porosité est faible (plaque à 3 trous). Le rapport surface perforée-surface totale pour chaque plaque apparaît comme un paramètre de contrôle du couplage. Lorsque ce rapport est grand, le couplage est facilement réalisé. Pour la plaque à 3 trous, ce rapport est de 0.35% alors qu'il est de 7% pour la plaque à 60 trous. Les rapports faibles empêchent donc le couplage des cavités, les oscillations transverses ne peuvent pas remonter dans la petite cavité. Néanmoins, il est nécessaire de compléter l'étude avec des systèmes plus représentatifs de la réalité et en faisant varier la surface des orifices d'une façon plus systématique. Les pertes de charges au passage de la plaque perforée peuvent elles aussi représenter un élément critique pour la remontée des oscillations de pression. Une amélioration de cette étude consisterait à faire varier les pertes de charge induites par la plaque (au moyen de diaphragmes par exemple). L'existence d'un couplage acoustique entre deux cavités a été montrée. Le couplage entre le dôme d'injection et la chambre de combustion d'un moteur fusée est donc possible. La configuration étudiée est cependant assez différente de celle qui existe en pratique, les pertes de charges dans la plaque perforée et dans la tête d'injection ne sont pas comparables. Une simulation numérique du comportement acoustique des deux cavités lors d'une excitation sur un mode transverse serait intéressante à réaliser. En effet les paramètres tels que les pertes de charge ou la surface perforée seraient alors facilement modifiables.

Appendix B

Evolution of the Mascotte facility : Very High Amplitude Modulator (VHAM)

B.1 Introduction

The test configuration employed on Mascotte has provided some remarkable results. However significant differences between combustion in real engines and the flow in the model scale system can be pointed out. The challenge for the next years will be to set up experiments which will come closer to the combustion process taking place at the engine scale and which will exhibit stronger perturbations in the combustor.
The coupling between the chamber acoustics and the combustion dynamics controls the high frequency instability process. It will be important to work on the two controlling processes : chamber acoustics and combustion.
The chamber acoustics is well understood and it is now possible to determine the chamber eigenfrequencies and eigenmodes but these predictions must be compared with experiments. The modulation wheel can be effectively used to study this aspect by sweeping the frequency in a linear fashion and observing the modal structure with the pressure sensor placed on the upper and lower chamber wall. The effects of acoustics on combustion has been featured but efforts have to focus on the creation of more realistic combustion conditions. This means that heat release in the combustion chamber has to take place on a larger part of the chamber to obtain a more homogeneous distribution.

One of the control parameters is the ratio σ between the oxygen injection surface and the total surface of the injection head. In practical cases, even with five injectors, this ratio is relatively small (1.96 10^{-3}). For such low σ values, the combustion process is influenced by the presence of recirculation regions at the top and bottom parts of the chamber. The flame expansion observed with three modulated jets may not be representative of the real behavior due to the geometrical configuration adopted for injection. In terms of fluid mechanics and heat release distribution one would like to improve the surface ratio parameter σ. This ratio can be doubled by using 16 injectors with an oxygen diameter of 2 mm. (This direction is apparently that taken by the Penn State team working in the REAP2

framework. Their combustor will be equipped with a 16 injector backplane. However, Penn State does not envisage an external modulation of the type considered in the present document.) The injectors could be equally distributed in the chamber height to create a 1D shower-head with 1.5 cm between the adjacent injectors. To keep the same injection velocity ($\simeq$ 3 m s^{-1}), the total flow rate of oxygen would have to be increased to about 180 g s^{-1}, which is not far from the available capacity of the Mascotte test bench. Slight modifications of the test bench are needed or hot fire tests have to be performed on another test facility like P8. The increase of the global power and a more homogeneous distribution of heat release is of fundamental interest for the study of self-sustained oscillations.

The pressure fluctuations obtained during the hot fire tests have allowed a suitable description of the combustion response to acoustic perturbations but self-sustained instabilities could not be trigerred. This type of phenomenon is intimately related to the phase between heat release and pressure fluctuations but it is also conditioned by the losses in the chamber. Without external modulation, the high pressure oscillations vanish. Only the effect of acoustics on combustion can be observed, the feedback loop (namely the influence of periodic heat release on pressure fluctuations) is not observable.
The modulation generated by the toothed wheel is well adapted to the analysis of the first type of process. The fluctuation levels reached with this modulator are high enough to modify combustion at a given frequency. However, the next step is to generate self-sustained oscillations to observe the global motion of the flames in their own acoustic field. This will be possible by increasing the power release to counterbalance the losses.

It may also be useful to improve the modulation tool. The mass flow trough the secondary nozzle cannot be increased without bound and its main drawback is its non-symmetric position in the chamber. By doubling the nozzle ie by plugging an additional unit at the bottom wall, the amplitude of the modulation could be increased while generating a symmetric pressure fluctuation. The idea is to use two modulators with toothed wheels synchronized and out of phase to excite the system from the top and the bottom sides of the chamber. This would strongly favor the odd order modes and in particular the 1T mode.
Another configuration might consist in eliminating the central nozzle and placing two nozzles oriented in the axial direction on the upper and lower sides of the chamber. The flow would be blocked by a single rotating wheel. The number of teeth would be odd to allow the periodic blockage of the upper and lower nozzles. Synchronization would be obtained without effort in this new geometry. The whole flow could be blocked in this situation allowing the strongest possible external excitation.

These new configuration of the multiple injector combustor designated as MIC-16-2LM or MIC-16-2AM with 16 injectors and two modulation nozzles would combine an increased power release, an augmented surface ratio and an enhanced pressure fluctuation level. These modifications could create a more realistic experiment leading to a better understanding of the fundamental coupling mechanisms controlling HF instabilities.
It is also possible to imagine an intermediate configuration which would use MIC-5 and be terminated with the new double nozzle geometry periodically blocked by the same wheel. The various possibilities are summarized in Table B.3

Designation	Injection units	Modulator nozzles	Modulator wheels	Main nozzle
MIC-3-1LM	3	1 lateral	1	central
MIC-5-1LM	5	1 side	1	central
MIC-5-2AM	5	2 axial	1	
MIC-16-2LM	16	2 lateral	2	central
MIC-16-2AM	16	2 axial	1	

Tab. B.1: Possible injector and modulator configurations

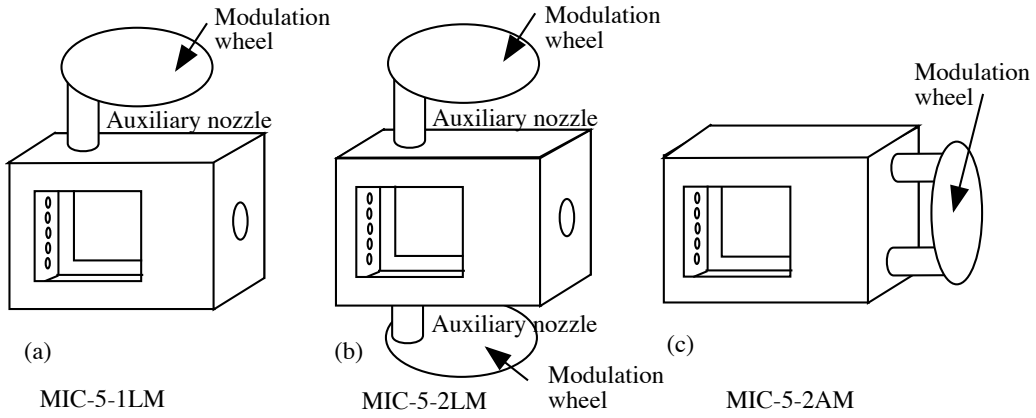

Fig. B.1: Multiple injector combustor equipped with various numbers of auxiliary nozzles and modulators.

It is apparent that there is an important progress can be made with the proposed double nozzle single wheel modulator (Figure B.1) designated from here on as the VHAM. This could already be adapted on the present MIC providing a sizable gain in the perturbation intensity.

B.2 Theoretical analysis of the chamber acoustic behavior

The Very High Amplitude Modulator is intended to generate strong acoustic perturbations. In this configuration, 100% of the stream is modulated, to be compared with the 15% of the three jet configuration. This will obviously increase the pressure fluctuations. It has been shown during the previous hot fire test campaign that the acoustic coupling between the main part of the combustion chamber and the secondary nozzle, situated at the top of the chamber, generates additional acoustic mode in the frequency range of modulation. Numerical and experimental studies were used to to determine the structure of the additional modes and their frequency. This kind of preliminary study is carried out in what follows in the case of the VHAM configuration. The eigenfrequencies of the system are calculated analytically by solving the Helmholtz equation. A numerical simulation is then carried out to account for coupling effects between the main part of the chamber and the two axial modulation nozzles. A reduced-size chamber has been manufactured for preliminary cold flow tests under modulation. Thus the eigenfrequencies and the mode structures can be examined and compared with those

Modes	1L	1T	1T1L	2L	1T2L	2T
Analytical Frequencies (Hz)	850	1214	1482	1700	2089	2428
Numerical Frequencies (Hz)	953	1257	1528	1734	2095	2550
Experimental Frequencies (Hz)	950	1240	1535	x	2180	x

Tab. B.2: Eigenfrequencies of the chamber calculated analytically (first row), numerically (second row) and determined experimentally (third row).

predicted analytically and numerically. If one assimilates the configuration to a rectangular box the eigenfrequencies are given by :

$$f = c/2 \left[(n/L)^2 + (m/h)^2 + (p/l)^2 \right]^{1/2}$$

where L, h and l are respectively the length, height and thickness of the chamber. By changing the value of the integers n, m, p, one obtains the different resonant frequencies. The previous expression does not account for the existence of the two axial exhaust nozzles. The coupling between the main part of the chamber and the two additional cavities can not be predicted in a sample manner. The chamber is assimilated to a rectangular box with L=200 mm, h=140 mm, l=50 mm. Because the spanwise dimension is small it is not necessary to examine higher mode numbers in that direction. The acoustic behavior of the chamber can be considered as two dimensional in the range of frequencies studied (i.e. less than 3 kHz). The sound speed is taken equal to 340 m s^{-1} and the calculated frequencies can be compared with the values observed experimentally. Theoretical estimates of the eigenfrequencies are given in the first line in table B.2. The chamber dimensions have been chosen to obtain eigenfrequencies above 1 kHz for the transverse modes.

B.3 Experiments

B.3.1 Experimental setup

The experimental test of the VHAM is carried out on the small chamber described previously. Air at ambient temperature is injected in the chamber through the back plane. On the opposite end, the two axial nozzles are periodically blocked by a rotating toothed wheel. The wheel periodically blocks the upper or lower nozzles, the difference of phase is equal to π : when one nozzle is blocked, the other one is open. The modulation frequency can be adapted by changing the rotation speed of the wheel. In this configuration, the stream passing through the chamber is entirely modulated, amplifying the acoustic level. The objective of the present study is to (1) Estimate the amplitude of the pressure fluctuations obtained when the system is externally modulated at the first transverse frequency, (2) Understand the acoustic behavior of the system and evaluate the influence of the two nozzles on the structure of the pressure field. As observed during hot fire tests, the coupling between the cavities composing the system may strongly modify the acoustic behavior of the chamber. The chamber features transverse modes above 1 kHz to simulate the high frequency coupling. The nozzles have a length equal to one half of the chamber length. Figure B.2 presents the different components of the experimental setup. Four pressure sensor positions are located near the four corners of he chamber. Pressure is measured by Kistler high-frequency sensors similar to those used in the Mascotte test bench. Only

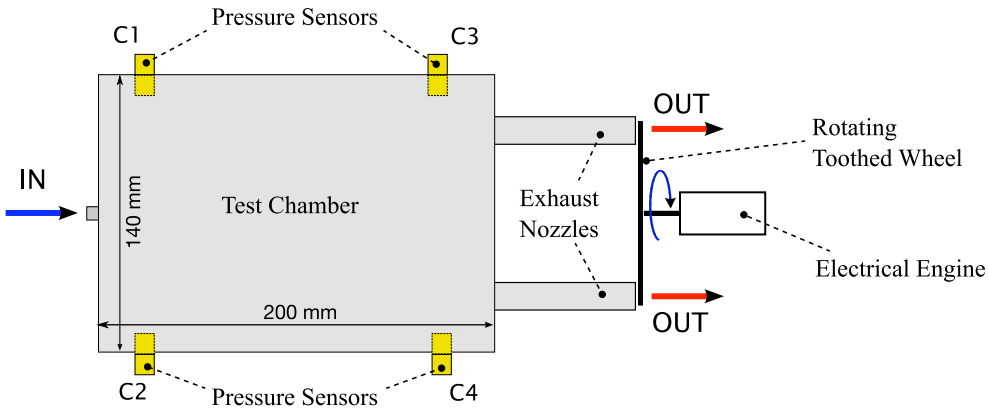

Fig. B.2: Schematic representation of the experimental test chamber equipped with a Very High Amplitude Modulator (VHAM)

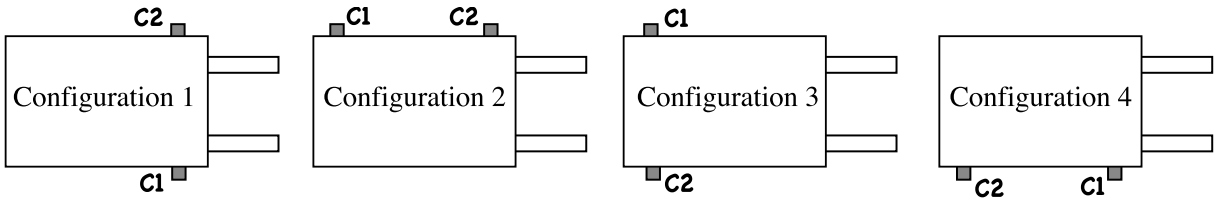

Fig. B.3: Schematic views nof the different positions of the pressure sensors depending on the configuration

two sensors were available so the different tests have been carried out with four different configurations corresponding to different positions of the pressure transducers shown schematically in figure B.3. The pressure signals are acquired at a sampling frequency of 32 kHz. The acquisition board does not include sample and hold units and there is a small delay between the two channels. This delay has been measured by delivering the same sinusoidal signal to the two channels simultaneously. The delay measured during these tests is equal to $15\mu s$. This represents less than 3% of the period of typical acoustic signals recorded in this experiment and it is not taken into account in what follows.

B.3.2 Experimental results

The experimental procedure is similar to that used during the hot fire tests. For each configuration (i.e. for each position of the sensors) four tests have been carried out. The first test aims at determining the eigenfrequencies by modulating the system at different frequencies and observing the occurrence of resonance. The modulation wheel is linearly accelerated and the modulation frequency varies from 0 to 2500 Hz at a constant rate equal to 120 Hz.s^{-1}. Results are quite similar for each configuration. The graph in Fig.B.4(a) shows the filtered signals recorded by the two pressure transducers in configuration 1. Three resonance peaks emerge well above the background noise. The Fast Fourier Transform (FFT) of this signal (Fig.B.4(b)) yields the frequency at which the peaks appear. The three peaks observed in the signal are represented by three spots in the spectrogram. The three frequencies of these peaks are 1240 Hz, 1535 Hz and 2180 Hz. These values are gathered in Table B.2 to compare them with analytical frequency estimates. During the experiments, the resonance is perceptible since the phenomenon generates chamber structural vibrations when the modulation frequency reaches an

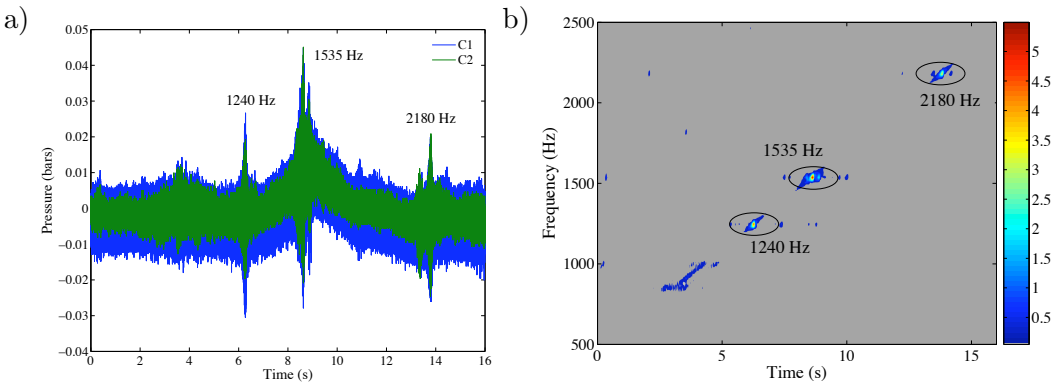

Fig. B.4: Filtered pressure evolution in the chamber during a frequency sweep modulation test (left) and the corresponding spectral map (right).

eigenfrequency. At this point, the corresponding structure of the pressure field cannot be determined. Three additional tests are carried out for each configuration in order to (1) Measure the amplitude of the pressure fluctuations generated by the resonance of the system submitted to a constant frequency modulation and (2) Determine the pressure fields by analyzing the phase differences between the pressure transducers in the different configurations.

During the single frequency modulation tests, the mean pressure in the chamber is stabilized at 1.8 bars. This pressure is relative to the atmospheric pressure. At this pressure, the effect of the modulation on the stream is characterized by a strong noise emission at the modulation frequency. At 1240 Hz, the amplitude of the signals reaches 3% of the mean pressure. Compared to the amplitude reached during the hot fire tests this level can be relatively small. Combustion and higher level of pressure in the chamber seem to have a strong effect on the resonance amplitude. The pressure variations recorded in the four different configurations are plotted in Fig.B.5. Without precisely calculating the phase difference between the sensors, the signals are either in phase or in phase opposition. When the sensors are on the same side of the chamber, the signals are in phase. When the sensors are placed on the opposite sides, the pressure features a phase difference equal to π. It is clear that 1240 Hz corresponds to the first transverse mode which is the most interesting in the case of high frequency instabilities. However, Figure B.4(a) shows that the resonance of the system is not the strongest at 1240 Hz but that the highest amplitude is reached at 1535 Hz.

The pressure signals obtained when the system is modulated at 1535 Hz are plotted in Fig.B.6. The four graphs represent the signals recorded by the two pressure transducers in the four different configurations. The phase difference between the signals is not as clear as in the previous case. In the four configurations, the signals are out of phase, the phase difference is always close to π. These phase relations tend to show that the eigenmode has a transverse and longitudinal structure. An additional configuration with pressure sensors placed on a diagonal of the chamber would have confirmed this diagnostic. The numerical simulations presented in the next section confirm that the resonance at 1535 Hz corresponds to a 1T1L mode. The linear modulation test indicates that the most amplified resonance occurs at the frequency of the coupled mode 1T1L. The coupling between the two nozzles and the chamber may be the cause of this strong amplification. By changing the length of the nozzles, one mode may be preferred with respect to the other. Additional experiments are needed in this

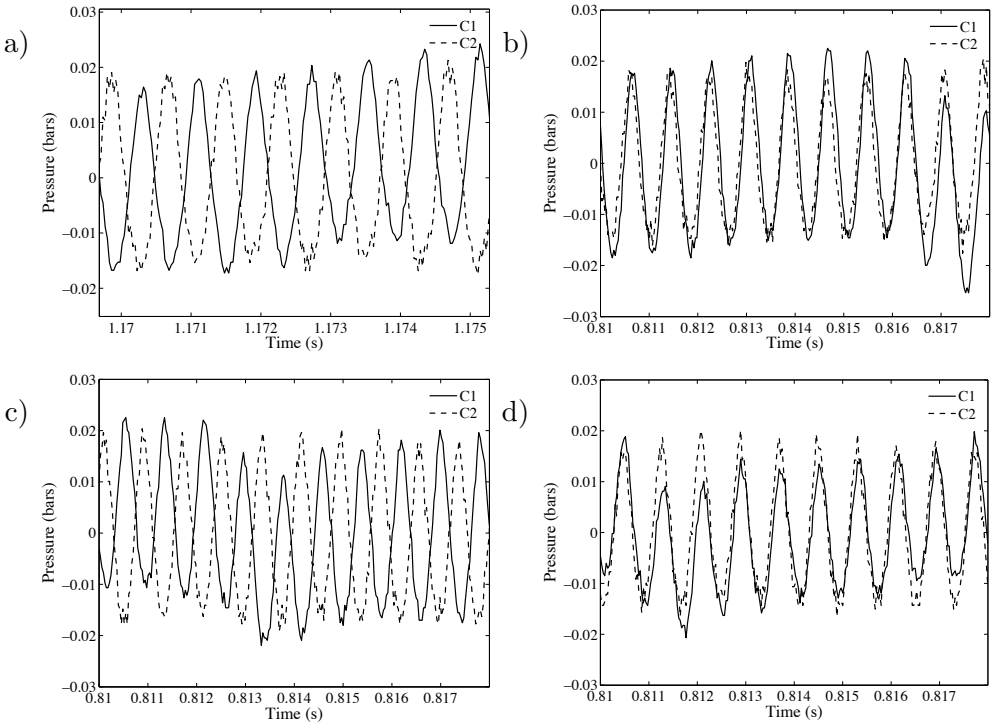

Fig. B.5: Evolution of the signals recorded by sensors C1 and C2. The modulation frequency is 1240 Hz. Configuration 1 to 4 respectively from a) to d).

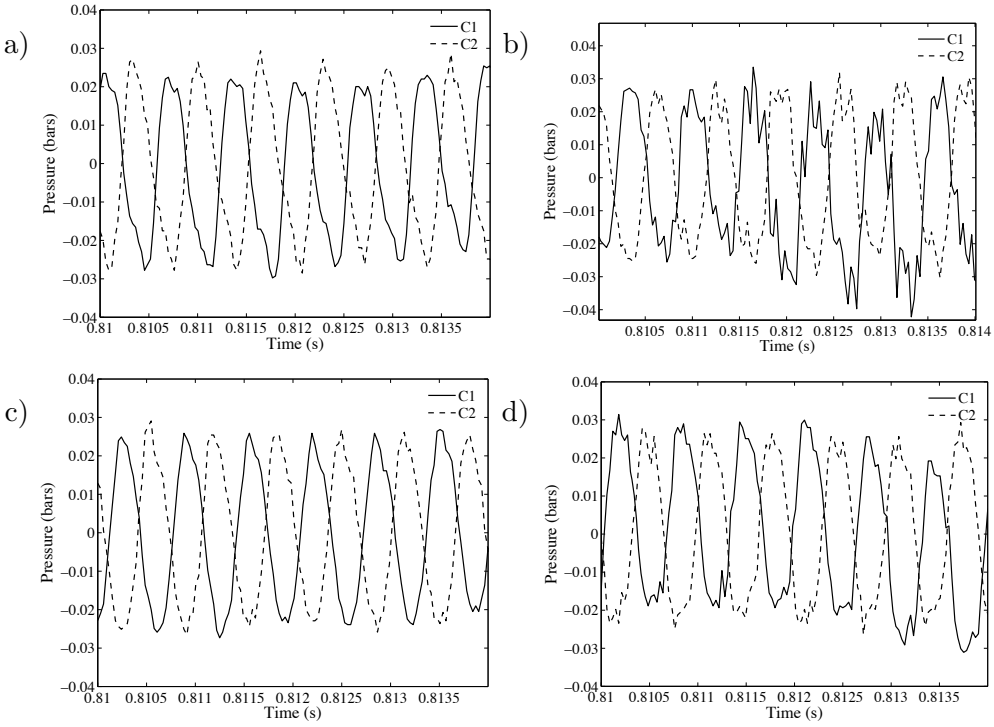

Fig. B.6: Evolution of the signals recorded by sensors C1 and C2 when modulated at 1535 Hz. Configuration 1 to 4 respectively from a) to d).

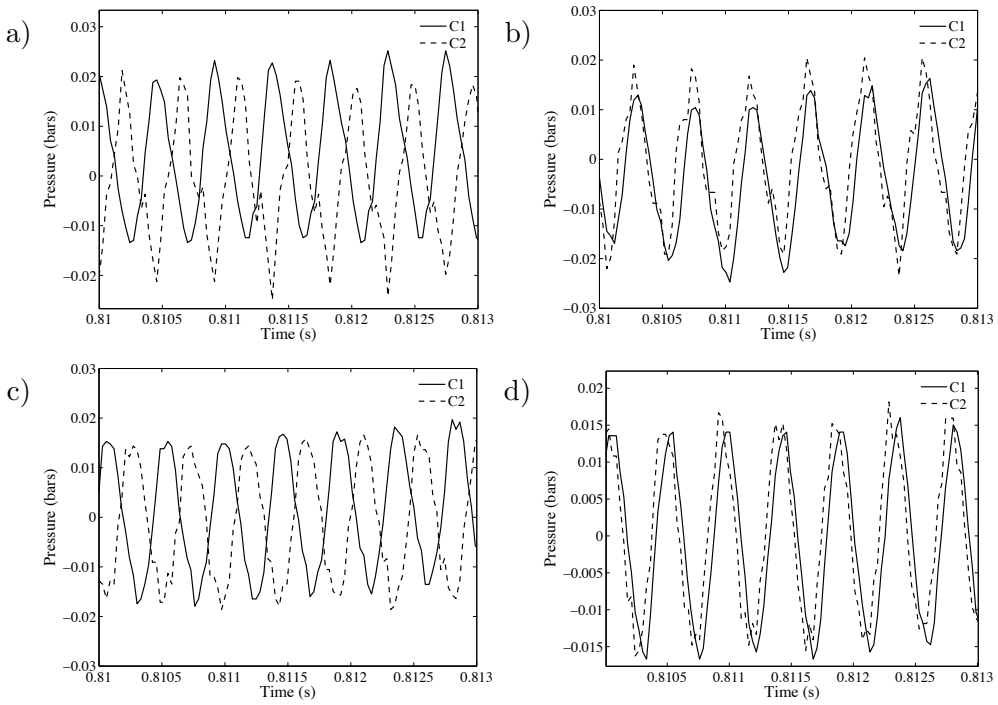

Fig. B.7: Evolution of the signals recorded by sensors C1 and C2 when modulated at 2180 Hz. Configuration 1 to 4 respectively from a) to d).

direction.

The third peak which has been detected during the frequency sweep test is at 2180 Hz. This peak has an amplitude similar to that of the first transverse mode and the phase relations between the pressure signals are also similar. These signals are presented in Fig.B.7. The phase difference between the sensors is close to what has been observed for the first transverse mode. The sensors situated on the same side of the chamber are in phase whereas when they are in front of each other the phase difference is equal to π. These phase differences characterize the eigenmode 1T2L. Once again, the position of the nozzles tends to generate a coupling mode between the transverse and the longitudinal modes. Analytical estimates of the eigenfrequencies helps to determine the structure of these modes and provides useful indications on the nature of the eigenfrequencies detected experimentally.

Figure B.8 summarizes all the phase differences which have been measured at the different modulation frequencies and different configurations. This confirms that the 1T and 1T2L eigenmodes have similar structures when the pressure is recorded at the four corners of the chamber.

In the configuration used to generate acoustic perturbations on Mascotte, the lateral nozzle constitutes a cavity and the coupling between the chamber and this element modifies the eigenmode structure. The combustion chamber and secondary nozzle have their own eigenmodes the coupled cavities give rise to additional acoustic modes. Here the coupling between the main chamber and the nozzles does not give rise an additional mode but favors modes with a longitudinal component.

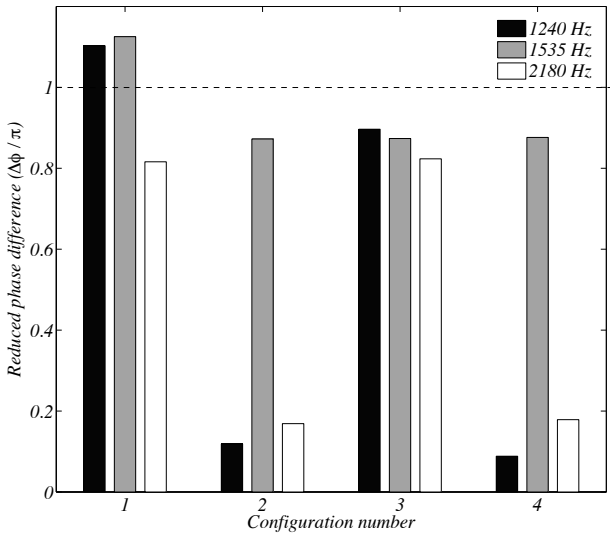

Fig. B.8: Reduced phase difference ($\Delta\Phi_{C1C2}/\pi$) between the two sensors depending on the sensor configuration and modulation frequency.

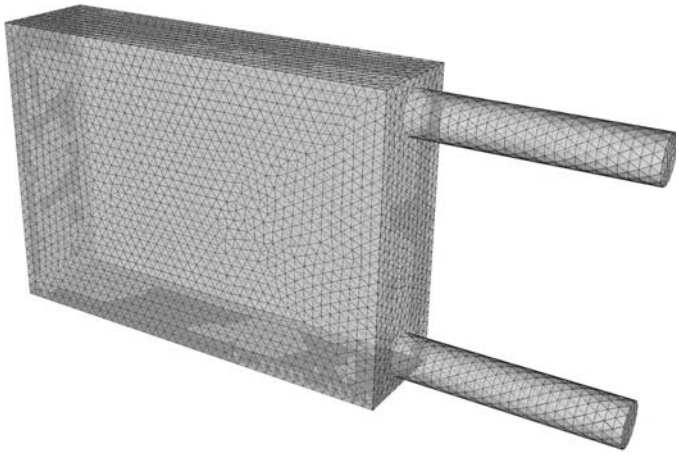

Fig. B.9: Tetrahedral mesh of the Very High Amplitude Modulator created for acoustic numerical simulation

B.4 Numerical determination of the chamber eigenmodes

The analysis carried out in this section is performed with the acoustic code AVSP. This tool is designed to obtain eigenfrequencies of complex systems and the corresponding pressure fields in three dimensions. The whole chamber is meshed with tetrahedral cells (Fig.B.9) and the Helmholtz equation is solved. The impedance of the nozzles may be taken into account but, in this simulation, all the boundaries are considered as walls. Von Neumann (rigid wall) boundary conditions are used in these calculations, $\boldsymbol{\nabla} p_1 \cdot \mathbf{n} = 0$ where $\mathbf{n}$ designates the normal to the boundary. This is only an approximation for the nozzle exhaust surfaces but it gives results which suitably match the experimental data.

Frequency values close to those observed experimentally can be obtained with the simulation. The geometry of the pressure field has been previously deduced from the phase between the different pres-

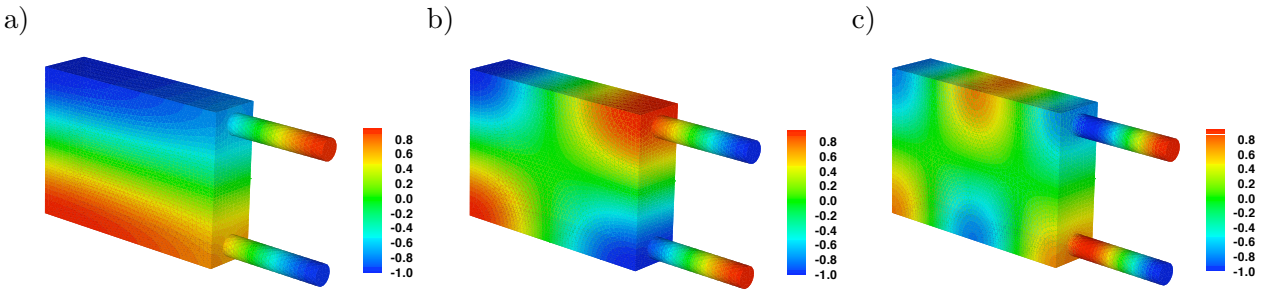

Fig. B.10: Normalized pressure fields for the three main eigenfrequencies of the system (a: 1257 Hz (1T), b: 1528 Hz (1T1L), c: 2095 Hz (1T2L))

sure sensors around the chamber. These deduced pressure fields can be compared with the numerical simulation. The eigenfrequencies obtained numerically are gathered in Table B.2. The first transverse mode features a corresponding frequency of 1257 Hz. This mode was experimentally observed at 1240 Hz. Figure B.10(a) shows the pressure field and the acoustic structure of this mode. The phase between the top and bottom parts of the chamber is equal to π. This field shows that a coupling with the two axial nozzles remains possible in this configuration since a phase difference can be observed between the beginning and the end of the nozzles. Experimental results indicate that the coupled mode first transverse first longitudinal is the most amplified. The structure of this 1T1L mode is displayed in Fig.B.10(b). Finally, the third eigenfrequency determined numerically corresponds to the 1T2L mode. This structure is displayed in Fig.B.10(c).

The numerical simulations confirm the identification of the system eigenmodes. The frequencies calculated numerically match those measured experimentally. The pressure field corresponding to each frequency confirms the acoustic structure of each eigenmode deduced from the phase difference between the four pressure transducers used during the experiment. These numerical simulation are useful for a precise description of the acoustic behavior of a complex system. While the system geometry is relatively simple, the coupling between the different cavities constituting the chamber complicates the prediction of eigenfrequencies. Attention has to be focused on possible coupled modes. The coupling is essential to amplify the pressure fluctuations. At the junction between two cavities, the value of the pressure in the nozzle has to match the pressure in the chamber to generate a strong acoustic fluctuation. In Fig.B.10, the value of the pressure is the same at the boundary between the main part of the chamber and the nozzles. This may be due to a well chosen nozzle length. In this case, the length of the two axial nozzles is half of the length of the chamber. This value seems to provide the required conditions for generation of a high level of modulation. A systematic study of the effect of the length of the nozzles is in progress and may be crucial for the design of the VHAM to be used on the Mascotte facility.

Appendix C

Fluid and acoustic interactions test simulations with Fluent 6.1

The main purpose of the numerical part of the thesis is to simulate transverse interactions between flames and acoustic modes. Before using the AVBP simulation code it was decided to see if such processes could be simulated with the version 6.1 of *Fluent*. Indeed Fluent is so commonly used in industry that it is worth examining this possibility. Numerical and analytical solutions are compared for a basic case where acoustics is the driving phenomenon.

C.1 Test configuration

The test problem geometry is a closed rectangular cavity where the first longitudinal eigenmode is taken as initial condition. Theoretically the cavity eigenmodes must be sustained at a constant level, so the evolution of pressure and velocity can be predicted analytically as exact solutions of the Helmholtz equation. Comparison between numerical and analytical solutions will show if *Fluent* can be used to deal with flow perturbations.

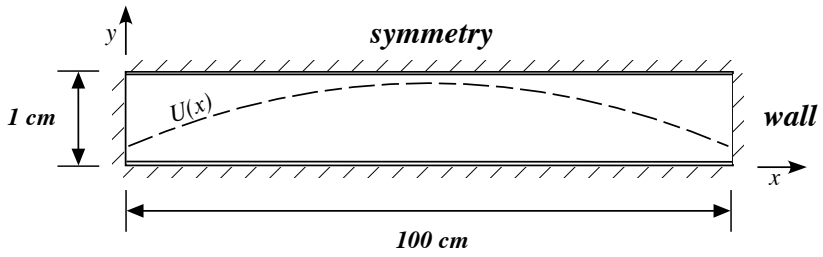

Fig. C.1: Schematic of the close rectangular cavity meshed for acoustic test with Fluent 6.1. The dashed line shows the initially imposed sinusoidal velocity profile U(x,0) corresponding to the first longitudinal eigenmode.

Figure C.1 shows the dimensions of the mesh used for these numerical simulations. The cavity is one meter long, one centimeter large. A fine mesh comprises 9000 cells, a coarser mesh features 4500 cells. These meshes are relatively fine since they feature 18 and 9 cells per centimeter respectively. Sensors are located at the entrance ($x = 0$), at one third ($x = 0.3l$), at two thirds ($x = 0.6l$) and at the exit

of the cavity ($x = l$) to record the pressure and velocity evolutions.

To get the first longitudinal mode in the cavity the initial axial velocity component is written like $U(x) = U_0 \sin(x\pi/l)$ (c.f. Fig.C.1) so the velocity is equal to zero at the cavity boundaries whereas it is maximum at the center. The initial pressure perturbation is equal to zero in the whole cavity. The amplitude of the velocity is chosen equal to 0.5 m.s^{-1}. This should induce a pressure amplitude equal to $\rho_0 cU$=205 Pa.

C.2 Analytic resolution

The complex expression of the pressure is given by $p(x,t) = \Psi(x)e^{-i\omega(t-\tau)}$ where

$$\Psi(x) = A\cos\left(\frac{n_x\pi x}{L_x}\right)\cos\left(\frac{n_y\pi y}{L_y}\right)$$

and

$$\omega^2 = c^2\pi^2\left[\left(\frac{n_x}{L_x}\right)^2 + \left(\frac{n_y}{L_y}\right)^2\right]$$

In the present case, only the first longitudinal mode is considered ($n_x = 1$, $n_y = 0$) and $L_x = 1$ m so $\Psi(x) = A\cos(\pi x)$. The real part of the pressure is then $p(x,t) = A\cos(\pi x)\cos\left[\omega_{(1,0)}(t-\tau)\right]$ with $\omega_{(1,0)} = c\pi$. Since at $t = 0$, the pressure has to vanish in the cavity, $c\pi(-\tau) = \pi/2$ thus $\tau = -1/2c$. The pressure expression is

$$p(x,t) = A\cos(\pi x)\cos\left[c\pi\left(t+\frac{1}{2c}\right)\right] \quad \text{(C.1)}$$

$$= -A\cos(\pi x)\sin(c\pi t) \quad \text{(C.2)}$$

The momentum equation gives the relation between the velocity and the pressure variations

$$\rho_0\frac{\partial v}{\partial t} + \frac{\partial p}{\partial x} = 0$$

thus

$$v(x,t) = B\sin(\pi x)\sin\left[c\pi\left(t+\frac{1}{2c}\right)\right] = B\sin(\pi x)\cos(c\pi t) \quad \text{(C.3)}$$

with A and B linked by the relation $A = \rho_0 cB$. If B is taken equal to 0.5 m.s^{-1}, $A = 205$ Pa, and the variations of the pressure and the velocity may be plotted with respect to the time (c.f. Fig.C.2 and C.4).

C.3 Numerical simulation

Several tests were performed changing the parameters for the numerical simulation of the oscillating motion in the closed cavity. The 'inviscid' model is chosen in order to solve the Euler equations. The best results are obtained for a coupled explicit unsteady simulation. Coupled solution is of importance since acoustic motion can only be modeled if the velocity and pressure are solved simultaneously. The time step has to be given explicitly (Δt is calculated from the size Δx with the formula

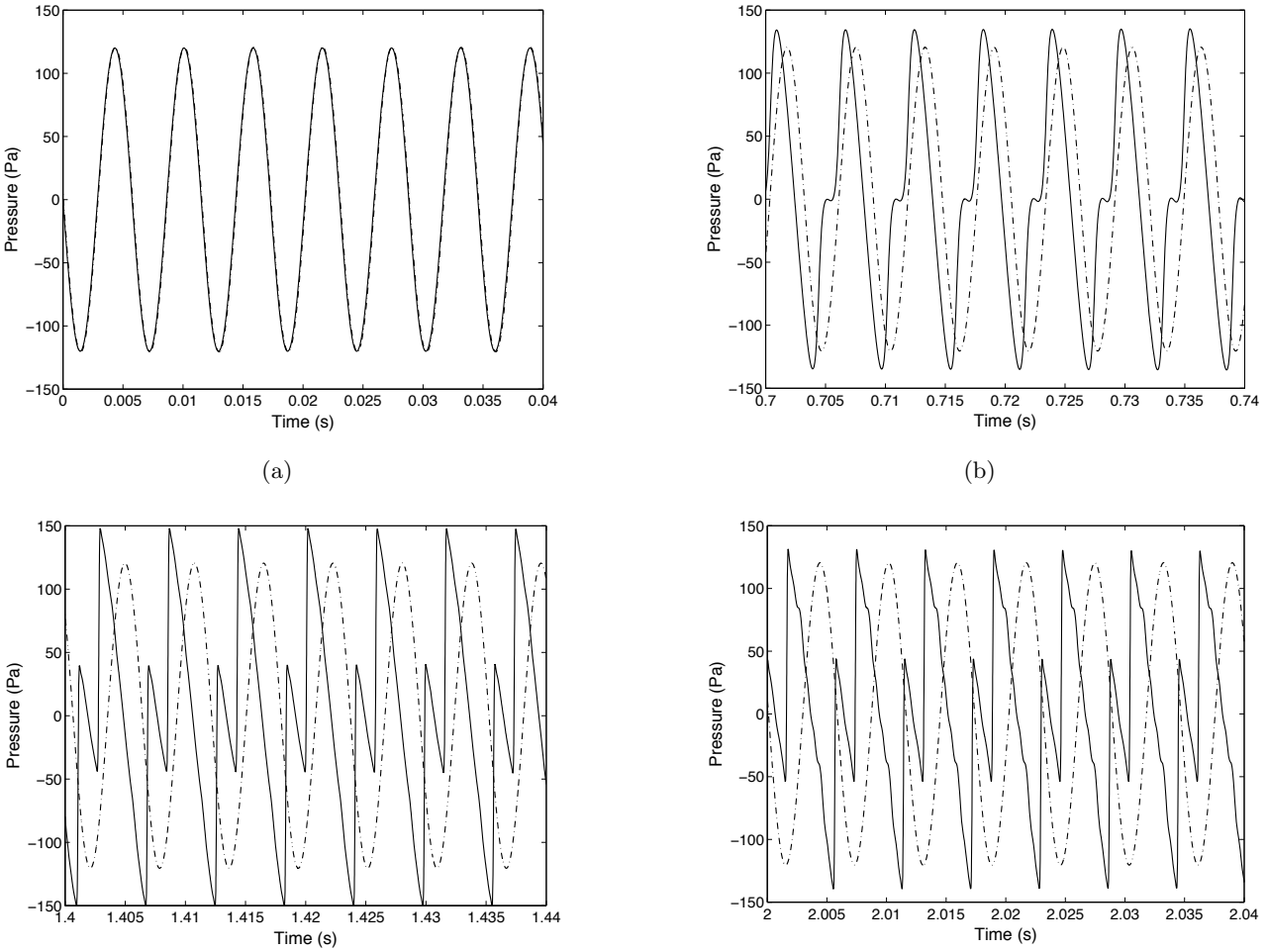

Fig. C.2: Numerically (-) and analytically (- -) calculated pressure in a closed cavity plotted as a function of time in an axial section located at x=0.3l.

$\Delta t = CFL(\Delta x/U)$ where CFL has to be adjusted).

Solution of acoustic fluctuations with *Fluent* does not provide the expected results. Figures C.2 and C.4 show the evolutions of pressure and velocity at a position $x = 0.3l$ as a function of time. During the twenty first oscillations, the evolutions of both pressure and velocity follow the analytical expressions accurately whereas after one hundred oscillations, the amplitude and phase progressively differ from their nominal values. The pressure and velocity become highly nonlinear and differ from the analytical model. Spectra of the pressure and velocity signals presented in Fig.C.3 and C.5 indicate that the numerical solution generates harmonics of the fundamental frequency. Indeed, the eigenfrequency f_0 is given by

$$f_0 = \frac{\omega_0}{2\pi} = \frac{c\pi}{2\pi} = \frac{c}{2} = 173.5\,Hz$$

and is the only visible frequency during the first instants whereas harmonics appear later in the simulation.

The signal distortion and dissipation observed in this case indicate that the code cannot be used

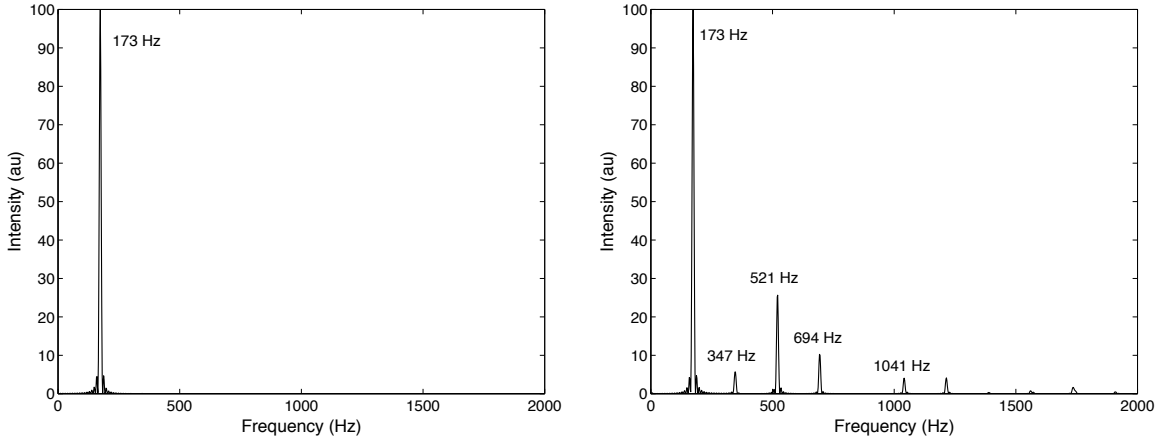

(a) (b)

Fig. C.3: Spectral density of the pressure calculated numerically for $t \in [0; 0.1]$ (a) and $t \in [2; 2.1]$ (b).

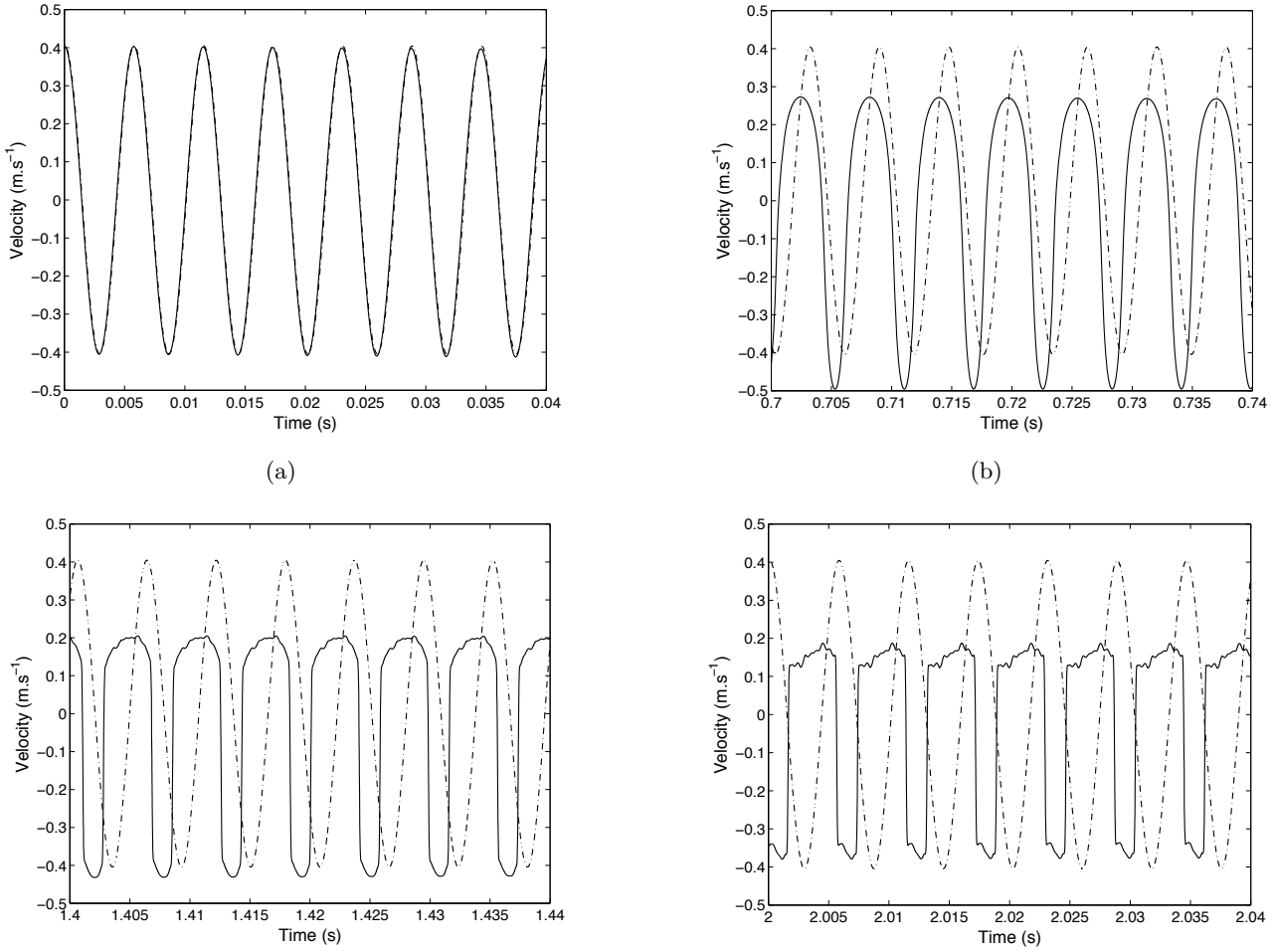

(a) (b)

(c) (d)

Fig. C.4: Velocity calculated numerically (continuous line) and analytically (dashed line) in a closed cavity for different times at x=0.3l.

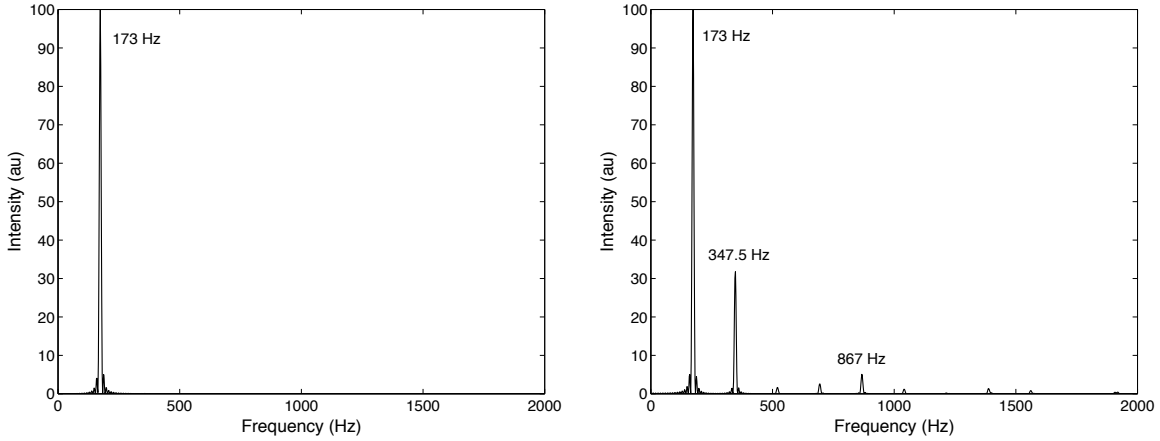

(a) (b)

Fig. C.5: Spectral density of the velocity calculated numerically for $t \in [0; 0.1]$ *(a) and* $t \in [2; 2.1]$ *(b).*

effectively to study interactions between acoustics and combustion.